REPORT DOCUMENTATION PAGE

Form Approved OMB No. 0704-0188

1. REPORT DATE *(DD-MM-YYYY)*	2. REPORT TYPE	3. DATES COVERED *(From – To)*
29-07-2004	Final Report	01-Feb-02 - 01-Feb-04

4. TITLE AND SUBTITLE

Surface Microwave and Surface Pulsed-Periodic Discharges in Supersonic Flow

5a. CONTRACT NUMBER
ISTC Registration No: 2248p

5b. GRANT NUMBER

5c. PROGRAM ELEMENT NUMBER

6. AUTHOR(S)

Professor Valery Shibkov

5d. PROJECT NUMBER

5d. TASK NUMBER

5e. WORK UNIT NUMBER

7. PERFORMING ORGANIZATION NAME(S) AND ADDRESS(ES)

Moscow State University (MSU)
Faculty of Physics
Moscow
Moscow 119992
Russia

8. PERFORMING ORGANIZATION REPORT NUMBER

N/A

9. SPONSORING/MONITORING AGENCY NAME(S) AND ADDRESS(ES)

EOARD
PSC 802 BOX 14
FPO 09499-0014

10. SPONSOR/MONITOR'S ACRONYM(S)

11. SPONSOR/MONITOR'S REPORT NUMBER(S)
ISTC 01-7032

12. DISTRIBUTION/AVAILABILITY STATEMENT

Approved for public release; distribution is unlimited.

13. SUPPLEMENTARY NOTES

14. ABSTRACT

This report results from a contract tasking Moscow State University (MSU) as follows: The contractor will develop methods of creation of plasmas of different types of gas discharges near the surface of Aerodynamic models and in the boundary layers. Also, the contractor will develop modes of internal and external fuel ignition of propane-air and hydrogen-air mixtures. He will develop methods of analysis of plasma properties in plasma regions near the surface. The following experimental work will be done in supersonic air flow (M<2) at pressures between 1 and 200 Torr: a) measurement of variation of the displacement thickness of boundary layer at creation of surface microwave and surface transversal pulse-periodical discharges on a flat plate; b) measurement of plasma parameters of a flame formed in a supersonic flow at internal and external fuel ignition with the help of the microwave discharges. A theoretical analysis of the obtained results will also be delivered. Recommendations for using of microwave surface and volumetric discharges for supersonic aerodynamics will be worked out.This Project consists of two tasks, 1) Task 1 is devoted to investigation of large-area plasma of surface discharge with the purpose of elucidating the interrelationship of electrodynamical, gasdynamical and kinetical properties of plasma of surface discharge. Such information is of paramount importance for practical application of gas surface discharge in supersonic aerodynamics; 2) Task 2 will be devoted to investigation of application of the surface and volumetric freely localized microwave discharges both for internal and external ignition in supersonic flows of combustion such as air-propane, and air-hydrogen mixtures.

15. SUBJECT TERMS
EOARD, Physics, Plasma Physics & Magnetohydrodynamics

16. SECURITY CLASSIFICATION OF:			17. LIMITATION OF ABSTRACT	18, NUMBER OF PAGES	19a. NAME OF RESPONSIBLE PERSON
a. REPORT	b. ABSTRACT	c. THIS PAGE			WAYNE A. DONALDSON
UNCLAS	UNCLAS	UNCLAS	UL		19b. TELEPHONE NUMBER *(Include area code)* +44 (0)20 7514 4299

MOSCOW STATE UNIVERSITY

Department of Physics

Final Scientific Report
of ISTC Project #2248p

Surface microwave and surface transversal pulsed-periodic discharges in supersonic flow

(From 1 February 2002 to 31 January 2004 for 24 months)

Dean of Physical Department of MSU V.I. Trukhin

ISTC Project #2248p Manager V.M. Shibkov

March 2004

This work was supported financially by the European Office of Aerospace Research and Development (EOARD) and performed under the contract to the International Science and Technology Center (ISTC), Moscow

CONTENTS

DENOTATIONS LIST

Chapter II

M – flow Mach number

T_v - vibrational temperature

T_g - gas temperature

λ - microwave wavelength

ω – electromagnetic field frequency

τ - pulse duration

T - period of repetition of pulses

f - pulse repetition frequency

Q - pulse period-to-pulse duration ratio

W_p - pulsed microwave power

W_m - mean microwave power

p – air pressure

s - waveguide section

s - nozzle exit section

s – section of aerodynamical channel

U – voltage

i - discharge current

d_1 - outlet diameter of cylindrical nozzle

d_2 - diameter of critical cross section of cylindrical nozzle

d – diameter of electric hydraulic valve

L_1 and L_3, - thermocouple

L_2 - ionization lamp.

V_i - valves

p_o – air pressure into high-pressure air receiver

p_g – pressure into high-pressure propane-butane receiver

h - depth of a rectangular cavity

L - length of a rectangular cavity

b - width of a rectangular cavity

dm_{air}/dt - the second mass consumption of air

dm_{gas}/dt - the second mass consumption of gaseous fuel (propane-butane mixture)

V_c - volumes of the discharge chamber

V_{r_air} - volumes of air high pressure reservoir

V_{r_gas} - volumes of gaseous fuel pressure reservoir

Chapter III

λ - wavelength of spectral lines

T_R - rotation temperature

T_R^* - rotation temperature of molecules in excited electron states

I_{lk} - intensity of a rotation structure spectral line

k_B - Boltzmann constant,

j - total molecular moment of momentum,

i - quantum mechanical coefficient of intensity

ν_{lk} - frequency of radiation quantum,

C – constant

B^* - rotation constant for upper state

B^o - rotation constant for the basic state

$I_{j'j''}$ - intensity of a rotary line for transition $j' \to j''$

j' - rotary quantum number of the top electronic state

j'' - rotary quantum number of the bottom electronic state

$\nu_{j'j''}$ - frequency of transition $j' \to j''$;

$S_{j'j''}$ - factor of intensity determining relative probability of transition $j' \to j''$

$F(j')$ - energy of a rotary term for the excited electronic state

h - Planck's constant

c - speed of light;

k - Boltzmann's constant

T - gas temperature

$F_1, F_2, F_3, f_1, f_2, f_3$ - the rotary terms concerning to components ${}^3\pi_0$; ${}^3\pi_1$ and ${}^3\pi_2$

A - constant of spin-orbital splitting

σ - value of broadening factor of spectral line

δ_1 - mistake of definition of gas temperature

v_X'' - vibration level of basic nitrogen electronic state

$v_C^{'}$ - vibration level of electronic $C^3\pi_u$ state of nitrogen

n_o - number of molecules in $X^1\Sigma_g^+$ state

$\langle \sigma v \rangle_{v_C^{'} v_X^{''}}$ - mean cross section of excitation of $v_C^{'}$ $C^3\pi_u$ levels

n_e - electron concentration

$A_{v_C^{'} v_B^{'}}$ - probability of radiation of the second positive nitrogen system

$v_B^{''}$ - vibration quantum numbers of $B^3\pi_g$ state

$n_{v_C^{'}}$ - stationary population of $C^3\pi_u$ vibration levels

$q_{v_C^{'} v_X^{''}}$ - Franc-Condon coefficients for the Tanaka system $C^3\pi_u \rightarrow X^1\Sigma_g^+$

$n_{v_C^{'}}$ - populations $v_X^{''}$ of the basic electron states as a solution of a set of equations

$I_{v_C^{'} v_B^{''}}$ - radiation intensity of a electron-vibration ban:

S_e - strength of electron transition

$q_{v_C^{'} v_B^{''}}$ - Franc-Condon factors

$\nu_{v_C^{'} v_B^{''}}$ - frequency of transition

C' - constant independent on the quantum numbers $v_C^{'}$ and $v_B^{''}$.

$C(n_e, T_e)$ - Stark constant

$\Delta\lambda$ - width of a hydrogen line H_β

$e=1{,}6\cdot10^{-19}$ C - charge of electron

S - capacitor plates section

d - distance between capacitor plates

U_o - potential difference between plates of the capacitor

v_{dr} - drift speed of electrons

μ_e - electron mobility

m_e - electron mass

ν_{en} - effective frequency of collisions of electrons with neutral particles

E - intensity of electric field

L - probe characteristic size

Chapter IV

L_e - spatial scale of inhomogeneity of electron concentration

D_a - coefficient of ambipolar diffusion

v – surface microwave discharge propagation velocity

T_e – electron temperature

T_i - ion temperature

b_i - mobility of ions

E_o - amplitude of electric field

ν_i= - ionization frequency

E_o/n_g – reduced electric field

E_b - breakdown electric field

ν_a - attachment frequency

n - density of air molecules

E_{eff} - effective value of electric field

ω - circular frequency of super-high frequency field

ν_{en1} - frequency of electron-neutral collisions at air pressure $p=1$ *torr*

σ - electronic conductivity

χ_e - coefficient of electronic heat conductivity

I_+ - ion density

S - area of a probe surface.

I_1 and I_2 - values of saturation of each of branches of double probe currents

$\left(\frac{\Delta U}{\Delta I}\right)_{I=0}$ - inclination of the voltage-current characteristic in a point where $I=0$

t_{del} - time delay of shadow picture registration regarding to beginning of a microwave pulse

W_{oc} - microwave power necessary for creation of a surface discharge on full body surface

Chapter V

E^D - dissociative energy limit of the $H_2(b^3\Sigma_u)$ term of hydrogen

$n_{ec} = \frac{m\omega^2}{4\pi e^2}$ - critical electron density

r - radius of the channel of microwave discharge

ν_{eff} - effective collision frequency between electrons and neutrals

I_{H_2} - intensity of lines of the top level $d^3\pi_u$ α-system

I_{H_α} - intensity of lines of Balmer's series of atomic hydrogen

n_{H_2} - concentration of molecules of hydrogen in the basic state

n_H - concentration of atoms of hydrogen in the basic state

$\left\langle \sigma_{H_2} \varepsilon_e \right\rangle$ - rate constant of excitation of a level $d^3\pi_u$ by electron impact

$\left\langle \sigma^{dis}_{H_\alpha} \varepsilon_e \right\rangle$ - rate constant of dissociative excitation of a line H_α by electron impact

$\left\langle \sigma_{H_\alpha} \varepsilon_e \right\rangle$ - rate constant of direct excitation of a line H_α by electron impact

$K_D = \dfrac{n_H}{2n^o_{H_2}}$ - dissociation degree of hydrogen molecules

$n^o_{H_2}$ - initial concentration of hydrogen molecules

EEDF - electron energy distribution function

Chapter VII

v_f - supersonic flow velocity

v_c - combustion front speed

s – cross section of the aerodynamic channel

U_d - voltage on the discharge gap

p_g^{st} - gas pressure corresponding of stoichiometry of a propane-butane-air mixture

p_o^{st} – air pressure corresponding of stoichiometry of a propane-butane-air mixture

m_g^{st} - mass consumption of gas corresponding of stoichiometry of a propane-butane-air mixture

m_{air}^{st} - mass consumption of air corresponding of stoichiometry of a propane-butane-air mixture

Chapter VIII

v_q - discharge propagation velocity

δ - wall boundary layer depth

z_q - position of ionization front

p_1 - pressure on an output of a nozzle

T_1 - temperature on an output of a nozzle

ρ_1 - density on an output of a nozzle

l_1 - typical size

p_o - pressure in open space

T_o - temperature in open space

$R_o = 8314{,}32\ J/(K \cdot kmol)$ -universal gas constant

$\mu = 28.964420\ kg/kmol$ - molecular weight of air

c_x - wave drag coefficient

Chapter IX

u and v - projections of a vector of speed to axes of orthogonal coordinates x and y

ρ - density

p – pressure

T – temperature

I – enthalpy

Q_v - the amount of heat brought in unit of time to the given point of gas from the outside

m - molecular weight of gas

R - universal gas constant

$<\rho' v'>$ - correlation of pulsations of density and normal component of flow speed

μ and μ_t – dynamic molecular and turbulent viscosity coefficients

c_p - specific thermal capacity of gas at constant pressure

Pr and Pr_t - Prandtl number and its turbulent analogue

T_w – near wall temperature

η - normal coordinate

$\delta(x)$ - normalizing function

Δx and $\Delta\eta$ steps of grid at numerical calculation

$\gamma=1,4$ - relation of specific thermal capacities

c_f - local coefficient of surface friction

τ_w - is friction stress

$\frac{\partial u}{\partial y}$ - transverse gradient of longitudinal flow velocity

Q_{int} - integral heat supplied to gas

δ^* - boundary layer displacement thickness

C_f - local friction surface coefficient

C_F - full friction coefficient

Chapter X

X_i - mole fractions of species i

R_u - universal gas constant

M - average molecular weight of the mixture

M_i - molecular weights of species i

h_i - molar enthalpy of species *i*

c_{pi} - molar heat of species *i*

$Q_i(T)$ - partition function per unit volume

h_i^0 - formation heat of species *i*

$V_m = R_u T / p$ - mole volume

ν_{ji}, ν'_{ji} - stochiometric coefficients

$[A_i]$ - symbol of chemical species *i*

k_j^f and k_j^r - forward and reverse rate constants

$\gamma_i = X_i / M$ - mass-mole fraction of *i*-th species

$\dot{\omega}_i$ - molar production rate of species *i* per unit volume due to all chemical reactions

$\vec{K}_{M,i}$ - molar diffusion fluxes

D_{ij} - binary diffusion coefficient

$\hat{\tau}_M = (\vec{\tau}_{M,x}, \vec{\tau}_{M,y})^\dagger$ - molecular stress tensor

$\hat{\varepsilon} = (\vec{\varepsilon}_x, \vec{\varepsilon}_y)^\dagger$ - tensor of deformation rates

$\hat{I}$ - unit tensor

μ_M - molecular viscosity

$\vec{q}_M$ - molecular heat flux

λ_M - molecular thermal conductivity

$Sc_i(T) = \mu_i / \rho_i \mathsf{D}_{ii}$ - Schmidt number of species *i*

D_{ii} - self-diffusion coefficient

μ_i - molecular viscosity of species *i*

$\bar{\Omega}_{ii}^{(1.1)}(T)$ - collision integrals of diffusion type

$\bar{\Omega}_{ii}^{(2.2)}(T)$ - collision integrals of viscous types

$\hat{\tau}_T$ - turbulent (Reynolds) stress tensor

$\vec{q}_T$ - turbulent heat flux

$\vec{K}_{T,i}$ - turbulent diffusion flux

k - turbulent energy rate

ω - specific dissipation rate

S - fixed control domain in a plane (x, y)

δS -a boundary of domain

$\vec{\mathbf{F}} = \vec{\mathbf{F}}^{inv} + \vec{\mathbf{F}}^{vis}$ - sum of the inviscid and viscous fluxes of **U** through the domain boundary

u, v - components of velocity vector $\vec{u}$

$e_0 = e + 0.5(\vec{u} \cdot \vec{u})$ - total energy per unit mass

$h_0 = e_0 + p / \rho$ - total enthalpy

b_h - heat source power

Re_θ - Reynolds number

ρ_∞ - free stream density

V_∞ - free stream velocity

T_w - wall temperature

p_w - wall pressure

Chapter XI

dT_g/dt - gas heating rate

γ_i - mole fraction of corresponding component i

N [mol/cm^{-3}] - total concentration

c_{pi} - molar heat capacity of species i at p=const

$C_{Pi}^{(a)}$ - coefficients in decomposition of c_{pi} for each component i

$h_{0i}[T_0]$ - molar enthalpy of formation of species i at $T_o = 298K$

M_1 - full number of components

$k_{+(-)q}$ - rate constants with participation of species i

M_2 - full number of such reactions

α_{iq}^{+} and α_{iq}^{-} - stochiometric coefficients

N_{in} - initial mole total concentration

T_{in} - initial gas temperature

T_{go} - initial gas temperature

T_e - electron temperature

INTRODUCTION

The intensive theoretical and experimental investigations of a boundary layers existing near the bodies streamlined by the flow of gas or fluid were fulfilled over a long years. The development of a modern aviation and especially the supersonic one requires effective means for the control of characteristics of flow near the aeroplane's surface, boundary layer heat and mass transfer in these regions, flow separation and boundary layer friction drag reduction. With the purpose of improvement of the aerodynamic characteristics of flight vehicles the set of the methods of an external influence on a boundary layer was offered. However existing methods of an application of energy to a boundary layer are ineffective or economically unprofitable.

The various type of the gas discharges were applied with the purpose of influence on the characteristics of a gas flow near a surface of the flying bodies. However there is a task of search of optimum ways of creation of non-equilibrium plasma in supersonic flow. One of such ways was offered in our laboratory. It is the new version of a surface microwave discharge, namely, a microwave discharge on an external surface into a boundary layer of a dielectric body, streamlined supersonic flow of air. We designed, experimentally created and investigated such type of the discharge within the framework of partner with EOARD ISTC Project #1866p [1].

The investigations were fulfilled within the framework of the ISTC Project #1866 have shown, that in conditions of a surface microwave discharge the neutral gas can be heated to high temperatures. Thus, a large amount of active particles are created because of large values of an electric field intensity and electron concentration in plasma of a surface microwave discharge. It can lead to high effectiveness of ignition of combustion mixtures at use of a surface microwave discharge for these purposes. Recently the heightened attention to possibility of using of external ignition of fuel in condition of supersonic flight was exhibited. Thus it is necessary to create the conditions for combustion of fuel on an external surface. The microwave discharge on an external surface of a dielectric body responds these requirements to the greatest degree.

The ISTC Partner Project #2248p consists of two tasks.

The task 1 is devoted to investigation of large-area plasma of surface discharge with the purpose of elucidating the interrelationship of electrodynamical, gasdynamical and kinetical properties of plasma of surface discharge. Such information is of paramount importance for practical application of gas surface discharge.

The task 2 is devoted to investigation of application of the surface and volumetric freely localized microwave discharges both for internal and for external ignition in supersonic flows of

combustion (air-propane) mixtures.

Problems which should be solved within the framework of the ISTC Project 2248 p.

Task 1.

1. Surface discharges on dielectric bodies with different geometry in subsonic and supersonic air flows should be created.
2. The spatial and temporal electrodynamical, gasdynamical and kinetical characteristics of the surface plasma created by different type discharges in subsonic and supersonic air flows should be determined.
3. The optimum conditions for creation of the surface discharges on bodies produced of different materials should be found out.
4. The methods of creation one and two zones of local heating of a metallic flat plate surface should be worked out with the help of surface microwave discharge in supersonic airflow.
5. The theory of the surface microwave discharge in a supersonic airflow should be developed.
6. Comparison of theoretical and experimental results should be fulfilled.
7. The recommendations for using of surface discharges for aerodynamics should be working out.
8. The final report for task 1 should be prepared.

Task 2.

1. The experimental installation should be modernized with the purpose of study of an opportunity of fuel ignition with the help of the surface microwave discharge.
2. The opportunity of ignition of a propane-air and hydrogen-air mixtures inside the aerodynamic channel with the help of the volumetric (freely localized) and surface microwave discharges should be studied.
3. The opportunity of fuel ignition on an external surface of the dielectrical antenna, streamlined by supersonic airflow should be investigated.
4. The parameters of plasma of a flame formed in a supersonic flow at fuel ignition with the help of the volumetric and surface microwave discharges should be measured.
5. The physical processes which are responsible for ignition and burning of supersonic flows of propane-air and hydrogen-air mixtures in conditions of the volumetric and surface microwave discharges should be determined.
6. The recommendations for using of microwave surface discharges for fuel ignition in supersonic aerodynamics should be worked out.
7. The final report for task 2 should be prepared.

The scientific and technical opportunities and specific development of the Physical Department of Moscow State University, which form a sufficient basis for performance of the program of works were used at performance of the Project.

⇒ Available experimental laboratory complex including:

- the aerodynamic wind tunnel ($M = 1\text{-}2$, flow duration - *2 sec*, flow diameter ≤ 3 *cm*);
- a *3* m^3 gas-vacuum chamber with pumping system and controlled gas injection at pressure range *0.1 - 760 torr*;
- a microwave power generator with mean power up to *300 W* on base of magnetron (wavelength *2.5 cm*, pulse duration *1 - 100* μs, pulse repetition rate *1 – 100 Hz*);
- a pulsed-periodic discharge (current pulse duration *1 - 500* μs, repetition frequency *1000 - 50 Hz*, discharge current *1 - 10 A*).

⇒ Experience of development of experimental techniques of measurement of parameters of the discharge:

- a set of electric probe equipment with digital registration of voltage-current characteristics;
- a set of spectroscopic equipment with photographic registration of spatial distributions of plasma radiation;
- an automated device of spectral diagnostics with high spectral, spatial and temporal resolution with digital registration of plasma spectra;
- a high speed camera for registration of discharge dynamics with a high temporary resolution;
- a Schlieren diagnostic set up for registration of plasma dynamics;

⇒ Experience of creation and investigation of various types of discharges;

⇒ Experience of mathematical modelling of complex plasma systems;

⇒ Experimental conditions:

- sort of gas: air, propane, hydrogen;
- flow Mach number: $M \leq 2$;
- type of discharge: surface and freely localized microwave discharges, surface transversal pulse-periodic discharge;
- pressure: *1 - 200 torr*.

At realization of the project the available experimental set up was modernized. Spectroscopic, probe and optic methods of measurement of spatial and temporary distributions of

parameters of charged and neutral components of non-equilibrium plasma of surface microwave discharge were used. Researches of physical processes in supersonic flows of non-equilibrium plasma of various types of the microwave discharges were carried out. In parallel with implementation of the experiments, the mathematical models were developed for the description of behaviour of the microwave surface discharge in a supersonic gas flow and ignition of gaseous fuels.

The purposes of the Project ″Surface microwave and surface transversal pulsed-periodic discharges in supersonic flow″ are completely executed:

- the basic properties of microwave discharges were investigated;
- the internal and external ignitions of a supersonic stream of a propane-air mixture were realized with the help of freely localized and surface microwave discharges;
- the stationary burning of supersonic propane-butane-air stream was realized with help of the electrode transversal surface discharge created in a stagnant zone;
- the influence of the discharge, created on a surface of a dielectric body being flown around by supersonic stream of air, on flow parameters was shown;
- the influence of non-equilibrium plasma of the gas discharge on reduction of an induction time and burning of hydrocarbon gaseous fuels was shown.

CHAPTER I
SUPERSONIC PLASMA AERODYNAMICS

1.1. Introduction

For gas discharge plasma application in a supersonic combustor it is necessary to give an answer on some important general questions. What kind of the gas discharge can produce the fast and complete mixing of supersonic streams of hydrocarbon fuels and air? Is it possible to realize a fast reliable ignition of supersonic combustible flow with help of gas discharge? Can we provide stable burning using the gas discharge? What kind of the gas discharge has got optimal parameters in order to realize completeness of fuel combustion at minimal electric energy deposition into supersonic flow?

There is another problem in aerodynamics. Recently it was offered to create plasma formations before flying vehicle and on its external surfaces for improvement of the aerodynamic characteristics of an aeroplane. The first laboratory experiments have shown an opportunity of a drag reduction at creation of the discharges of direct and alternative currents before a body, streamlined supersonic airflow. However electrode discharges in gas flow are unstable and spatially non-uniform. Such discharges result in strong erosion of electrodes and model surface (look *Fig. 1.1*) and reliably are not reproduced in various realizations. There was a task of search of optimum ways of creation of non-equilibrium plasma in supersonic flow.

In our laboratory for these purposes (ignition and drag reduction) the two types of the microwave discharges, namely, the freely localized microwave discharge and the surface microwave discharge were offered and used.

The freely localized microwave discharge emerging in the focus region of an electromagnetic energy beam (look *Fig. 1.2*) is a complex nonlinear phenomenon including a non-stationary breakdown of gas, propagation of ionization fronts interacting with microwave radiation, maintenance of non-equilibrium plasma formed in the beam focus region by an incident energy flux, and the excitation and heating of molecules accompanied by deformation of neutral gas density. It is known that under the effect of a strong focused beam of electromagnetic waves of the microwave range the gas breakdown occurs on the condition that the electric field strength in the focal region of the discharge chamber exceeds the threshold value. After this breakdown, the plasma formed in the beam focus starts to absorb intensively the energy delivered to the discharge. A study of the properties of a microwave discharge removed both

a *b*

Fig. 1.1. Appearance of models after one discharge realization

a - DC transversal discharge at $i=2,6$ *A*, pulse duration $\tau=5$ *s*, $M=2,3$.

b - AC longitudinal discharge at $i=1,5$ *A*, pulse duration $\tau=3$ *s*, $M=4,0$.

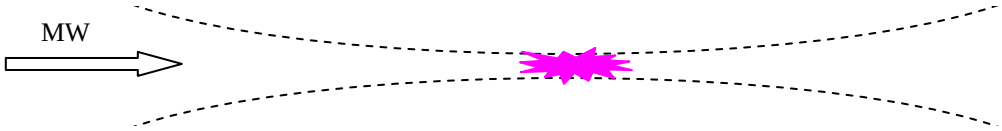

Fig. 1.2. **Scheme of freely localized microwave discharge creation.**

from the discharge chamber walls and from the radiation sources is topical from the point of view of both the solution of a number of fundamental problems of plasma physics and its practical application, for example, in plasma aerodynamics: i) combustion of fuel in supersonic engine; ii) creating plasma regions in front of flying vehicles for changing the conditions of gas flow near solid bodies and lowering the head resistance during their motion in the atmosphere with supersonic velocities; iii) for developing of jet propulsion using an energy source located outside of the flying vehicle being accelerated.

Another way of plasma creation under condition of gas flow, offered in our laboratory, is the new version of a surface microwave discharge, namely, a microwave discharge on an external surface of a dielectric body streamlined by supersonic flow of air. It is known that at creation of the microwave discharges inside dielectric tube, filled by gas at low pressure, the electromagnetic energy delivered to system is transformed to a surface wave (*Fig. 1.3 a*). Thus, there is a self-sustaining system when a plasma medium created by the surface wave is necessary for a surface wave existence, i.e. the presence of plasma is a necessary condition for spreading of a surface wave. The surface wave is travelled in space so long as its energy is sufficient for creation of plasma with electron density no less than a critical value. The project deals with a surface microwave discharge outside a dielectric body in a low-pressure chamber (*Fig. 1.3 b*). In this case plasma supported by a surface microwave is formed on an external surface of a dielectric antenna.

1.2. Reduction of boundary friction

The laminarization of airflow is one of the few possibilities of reducing of a surface friction and, consequently, improving the aerodynamic quality and efficiency of flight vehicles. For subsonic aircraft the frictional drag run up till 80-90 %, and for supersonic till 50-60 % from total drag. It is known, that the friction coefficient at laminar flow almost on the order is less than at turbulent one. From here, the importance of a problem of a laminarization of airflow is obvious for flight vehicles. In recent years, much attention has been given to the study of new possibilities for laminarization of flow, i.e. delay of transition to the turbulent flow mode in the boundary layer up to the highest possible Reynolds's numbers. One of the unconventional methods of controlling the laminar-turbulent transition [1] is the heating of a small area of the surface of a body being flown around.

It has been established in [1] that the heating of a part of a body surface in the vicinity of the leading edge helps to considerably increase the extent of the laminar portion of boundary

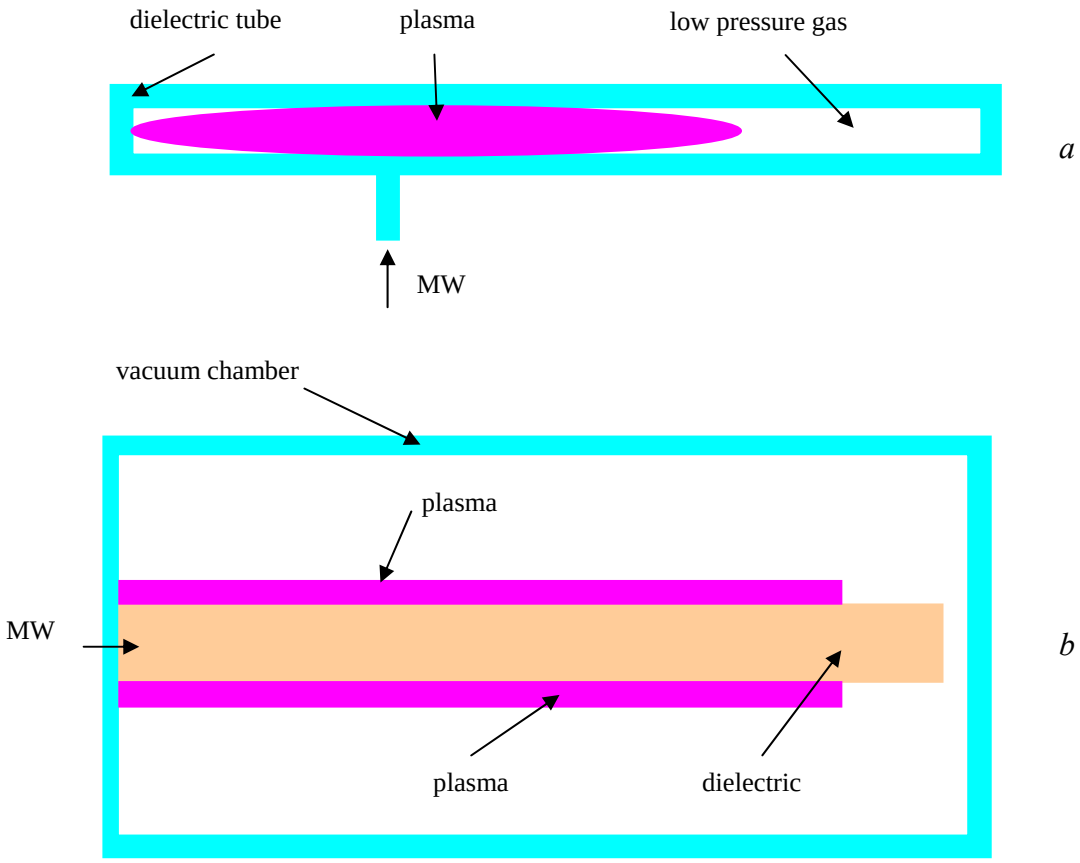

Fig. 1.3. Schemes of surface microwave discharge creation.

a –microwave discharge on an internal surface of a dielectric tube;

b - microwave discharge on an external surface of a dielectric antenna.

layer. In paper [1] was shown, that the heating of a small surface area in the vicinity of the leading edge to temperatures two to four times higher than the forward flow temperatures leads to delay of transition even if the body surface is heat-insulated downstream of a heating area. An example is provided of the surface temperature distribution, when the energy savings due to reduction of friction exceed the energy spent to heat the surface by a factor of three.

In [2] the results of experimental examination of an opportunity of a laminarization of a boundary layer by the method of suppression of Tollmien-Schlichting waves, existing in a boundary layer and responsible for transition, were represented. Thus, the artificial created waves of perturbation were inlet into a boundary layer in an antiphase to Tollmien-Schlichting waves. The opportunity of such laminarization was shown. The experiments were conducted on a direct wing in a low turbulent subsonic wind tunnel. The boundary layer, perceiving external fluctuations, quenches them in a broad band of frequencies except for the some narrow strip. Thus, it is possible to receive diminution of amplitude of the most dangerous vibration by introduction in a boundary layer the artificial created waves of perturbation. In such a way, a retardation of development of a dominant wave of instability takes place and, as result, the line of transition displaces downstream.

The problem of transition of a laminar boundary layer in a turbulent condition during several decades causes a big interest of the researchers. It is stipulated, at first, by necessity of the solution of practical problems, for example, the problem of control of a boundary layer with the purpose of a drag reduction of aircraft and calculation of its aerodynamic characteristics. Secondly, the study of process of appearance of turbulence is a part of more general fundamental problem of the turbulence description.

In the literature the conception of ″the transition″ is understood, as a rule, concept alone process of decay of a laminar mode and formation of a turbulent flow. A beginning of transition usually connects to occurrence of rough processes in the form of turbulent spots and low-frequency pulsations of large amplitude. However it became now absolutely understandable, that the long sequence of physical processes, resulting in a laminar flows destroying, takes the beginning much earlier, namely, in transformation of external perturbations of a different nature in an external flow in waves of a boundary layer or in their generation into the boundary layer happening on unevenness' of a streamline surface (ledges, roughness etc.).

The process of transition of a laminar boundary layer in a turbulent condition at small intensity of external perturbations consists of three conditionally parted stages: the generation of waves of a boundary layer, their amplification under the laws of the linear theory and non-linear destruction of a laminar mode of flow. Each stage of this sequence corresponds the typical area

in space in accordance with increase of distance from a leading edge of model. The described sequence of stages of transition is diagrammatically shown in *Fig.1.4* [3].

In [4] the opportunities of improvement of the aerodynamic characteristics of a plate are investigated at the expense of a combined laminarization including the optimization of pressure distribution and temperature of a surface. The class of the temperature distribution of a surface corresponding to a heating of a leading edge and cooling of a remaining part of a surface up to the recovery temperature of an incident flow was surveyed. It was shown, that thus it was possible: i) to increase a lift coefficient of a plate at invariable resistance and ii) to lower resistance and to increase a critical Mach number at invariable lift. In [4] was shown, that the energy expedient reduction of resistance can achieve by a heating of a part of a wing surface in a combination to other methods of flow laminarization.

The behaviour of a separated flow at a motion of flight vehicles is considered in [5]. The aerodynamic characteristics of flight vehicles are determined by features of their streamlining, that is relative motion of a surrounding medium. The flow separation is one of the fundamental phenomena of a mechanics of a fluid and gas. It consists that under certain conditions (for example, unfavourable gradient of pressure) the medium in vicinity of a streamlined body ceases to move along its surface and starts to moves away from it. In result the area of the separation flow will be formed. The flow separation renders influence on a manoeuvrability, controllability and aerodynamic efficiency of a vehicle. The behaviour of the separation flow differs for different aeroplane speeds, wing shapes and attack angles. At a separation of a stationary laminar stream the separated flow can again join a wing surface. Thus, the local separation zone arises. It has the small sizes as contrasted to the wing sizes. In this case separated area on a wing exists as a narrow strip elongate along its total wing-span. The position of a separated zone on a wing depends on an angle of attack. At its increasing the separation zone is shifted closer to a leading edge of a wing. One more separation of a non-stationary turbulent flow is appeared on back edge of a wing. At a turbulent separation there is no repeated connection of a separated flow to a wing surface and zone of a separation includes all area of flow from a line of a separation up to a back edge of a wing. A flow separation from a leading edge arises at further increase of an angle of attack and reaching it of critical value. It is called global or complete separation. The complete separation is accompanied by sharp decrease of lift of a wing, by magnification of its drag and gives in unfavourable consequences.

The method of a reduction of friction based on a heating of a part of a surface of a flat plate near to its leading edge was offered in [6]. In this case the diminution of a total resistance of friction on a plate was reached due to increase of stability of gas flow heated near to a leading

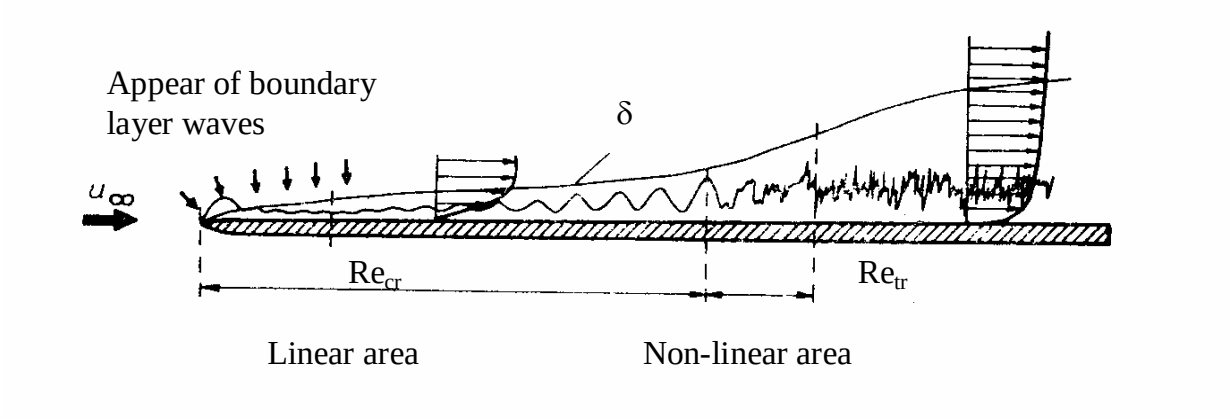

Fig. 1.4. The diagram of main stages of transition process in a boundary layer [3].

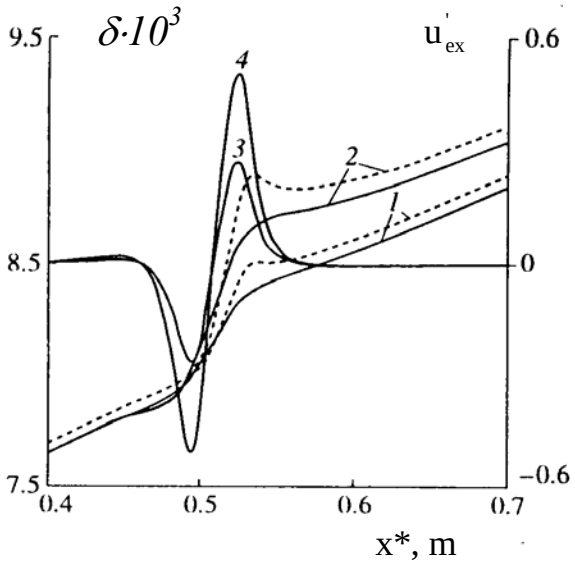

Fig. 1.5. The distribution of (1, 2) the displacement thickness of boundary layer and (3, 4) of the velocity gradient on its external boundary: (1, 3) $Q_w=10^{-4}$, (2, 4) $2\cdot10^{-4}$.

Dashed curves indicate δ in the case of ignoring the viscous-nonviscous interaction, and continuous curves indicate δ in the case of including the interaction [8].

edge and further travelling above more cold surface, that result in to essential magnification of length of a laminar part of boundary layer flow. However at large enough values of a typical Reynolds's number the extent of a turbulent part of a boundary layer considerably exceeds the length of a laminar part, owing to what in this case further diminution of a friction drag is possible only by a reduction of the turbulent friction. It is known that on an isothermal surface, which temperature is higher than the flow recovery temperature, the friction is less than that on an adiabatic surface. However uniform heating of all streamline surface is bound up to considerable technical difficulties and in this case the energy cost of a boundary layer heating considerably exceeds the profit received owing to a friction reduction.

In paper [7] the results of numerical investigations of influence of a heating of a local part of a surface of a flat plate on a flow in a developed turbulent boundary layer are submitted. The surface was assumed to be heat-insulated downstream of the heated portion. It is shown that at the beginning of the heating portion the friction is increased and then the friction coefficient decreases, and its minimum values are reached on the heat-insulated part of a surface following behind the heated portion. The reduction of coefficient of turbulent friction as contrasted to its value on an isothermal adiabatic surface is spread to considerable distance downstream from a heated portion. Due to ″long memory effect″ of a turbulent boundary layer the considerable friction reduction is reached at local heat input in comparison with the uniform heating of full streamline surface. At presence of several following one after another the heating portion this ″long memory effect″ intensifies and more essential diminution of value of the turbulent friction can be obtained. At identical total energy consumption the reduction of an integrated friction coefficient almost twice is more than in case of uniformly distributed on whole surface energy supplied to gas in a boundary layer.

In the article [8] the calculations are performed of a supersonic boundary layer on a flat plate with one and five zones of local heating of its surface. Within the concept of ″displacement body″, allowance is made for the interaction between the boundary layer and external nonviscous flow. It is shown that the inclusion of viscous-nonviscous interaction leads to significant variation in the distribution of the local friction coefficient.

It is known that the friction resistance decreases under conditions of heating of the surface being flown around [9, 10]. Based on the results of calculation of a compressible turbulent boundary layer using the algebraic model of turbulence, it was shown in [11] that the efficiency of the thermal method of reducing turbulent friction may be raised considerably owing to localization of the region of heat input to the boundary layer. In [12] the theoretical studies

were made into the effect of the thermal properties of the material of the surface being flown about on the reduction of turbulent friction under conditions of local heating of a flat plate.

The localization of regions of heat input to gas under conditions of fairly intense heating leads to the emergence of appreciable gradients of the displacement thickness of boundary layer. In this case, the interaction between external nonviscous flow and the boundary layer results, even under conditions of flow past a flat surface, in the emergence of a longitudinal pressure gradient. The presence of a pressure gradient obviously leads to a variation of the characteristics of the turbulent boundary layer. In view of this, it becomes necessary to include the viscous-nonviscous interaction and assess its effect on the parameters of the boundary layer in the presence of localized regions of heat input.

The authors of the article [8] treat the flow past a plate with the Mach number in the incident flow $M_\infty = 2$ and the velocity, density, temperature, and dynamic viscosity $u_\infty^*, p_\infty^*, T_\infty^*$ and μ_∞^*, respectively. The initial section is identified in the region of the developed boundary layer, which is characterized by the value of Reynolds number $Re_\theta = p_\infty^* u_\infty^* \theta_0^* / \mu_\infty^* = 4000$, calculated by the parameters of incident flow and momentum thickness in this section θ_0^*

Located at the distance L^* downstream of the above-identified section is the beginning of the heated portion of the plate surface, which has the length h^*. Two options will be treated below, namely, (*a*) a single heated portion, and (*b*) five series-arranged heated surface portions of the same length h^* with the constant distance H^* between the beginnings of two neighbouring portions. Outside of the heated portions, in which the heat flux distribution is preassigned, the plate surface is assumed to be adiabatic.

The simulation of the compressible turbulent boundary layer is performed using the two-parameter k-ε model of turbulence [13]. For numerical solution of the system of equations of the turbulent boundary layer in view of viscous-nonviscous interaction, in [8] dimensionless variables (without the superscript *) are introduced, defined by the following relations:

$$
\begin{aligned}
&x^* = l^* x, \qquad y^* = l^* \delta y, \qquad \delta^* = l^* \delta, \\
&u^* = u_\infty^* u_e u, \qquad v^* = u_\infty^* u_e \delta \left(V + \frac{yu}{\delta} \frac{d\delta}{dx} \right), \\
&k^* = \frac{u_\infty^{*2}}{Re^{1/2}} k, \qquad \varepsilon^* = \frac{u^{*3}}{l^*} \varepsilon, \qquad T^* = T_\infty^* T, \\
&\rho^* = \rho_\infty^* \rho, \qquad \mu^* = \mu_\infty^* \mu, \qquad Re = \frac{\rho_\infty^* u_\infty^* l^*}{\mu_\infty^*}.
\end{aligned}
\tag{1.1}
$$

Here, $\delta(x)-$ is the dimensionless displacement thickness of the boundary layer, $u_e(x)$ is the velocity on its external boundary, and k^* and ε^*, respectively, denote the kinetic energy of turbulence and its dissipation rate. Relations (1.1) further include the characteristic linear size l^* and characteristic Reynolds number *Re*, which may be preassigned arbitrarily, because the parameters of the developed boundary layer in the initial section are defined by the value of the Reynolds number.

The values of l^* and *Re*, preassigned in the calculations, define the value of the momentum thickness in the initial section according to the expression $\theta_0^* = l^* Re_\theta / Re$. In the calculations, the values of $l^* = 1m$, $Re=2\cdot10^6$ and, consequently, $\theta_0^* = 0.002m$ were preassigned.

In order to include the interaction between the turbulent boundary layer and external supersonic flow, in [8] the concept of ″displacement body″ is employed, according to which the effect of the boundary layer on external flow is equivalent to nonviscous flow past the effective surface formed by adding the displacement thickness of boundary layer to the real surface of the body.

In the calculations, constant values were preassigned for the distance from the initial section x_0 to the beginning of the first heated portion $L^* = 250\theta_0^* = 0.5$ m and for the length of each portion $h^* = 20\theta_0^* = 0.04$ m. The distribution of heat flux q_w in the heated portions was preassigned in the sine form. In the presence of one heated portion, the total amount of heat, equal to the integral of q_w over the portion length, was $Q_w = 10^{-4}$ (option 1) and 2×10^{-4} (option 2). When five heated portions were treated, the distance between the beginnings of two adjacent portions was $H^* = 100\theta_0^* = 0.2$ m, and the amount of heat supplied to every one of them was $Q_w = 10^{-4}$.

Fig. 1.5 gives the distribution of the displacement thickness of boundary layer and of the velocity gradient on its external boundary for a single heated portion for two above-identified values of total thermal power supplied to the boundary layer [8]. The dashed curves indicate, for comparison, the distribution of the displacement thickness ignoring the viscous-nonviscous interaction. Naturally, the displacement thickness in the heated portion and behind it increases with Q_w. The interaction between the boundary layer and external flow results, first, in a smaller

increase of the displacement thickness than in the case of ignoring the interaction and, second, in the upstream propagation of the effect of surface heating on the boundary layer thickness.

As a result of viscous-nonviscous interaction before the boundary layer, a fairly considerable gradient of velocity occurs on the external boundary of the boundary layer, whose absolute magnitude is the greater, the higher the power of heat input. A fairly intensive acceleration of external flow is observed in the greater part of the heated portion.

The longitudinal gradient of pressure, emerging upon inclusion of viscous-nonviscous interaction, affects considerably the local friction, as is shown in *Fig. 1.6* [8] which gives the distribution of the local friction coefficient for two values of Q_w defined by the expression

$$C_f = \frac{2}{p_e u_e \, Re \, \delta}\left(\mu \frac{\partial u}{\partial y}\right)_w . \qquad (1.3)$$

The dot-and-dash curve in *Fig. 1.6* indicates the distribution of the friction coefficient on a fully adiabatic surface, calculated for $u_e = 1$, and the dashed curves indicate the distribution of C_f on a heated surface ignoring the interaction.

The deceleration of external flow before the heated portion is accompanied by a considerable decrease of the friction coefficient. Due to acceleration of flow, the friction coefficient throughout almost the entire heated portion is higher than that on the adiabatic surface. This increase of C_f is the higher, the greater the heat input. The inverse dependence is observed when the interaction is ignored. As in the case of $u_e = 1$, the maximum reduction of local friction is attained behind the heated portion.

The interaction between the boundary layer and external flow has a marked effect both on the distribution of the local friction coefficient and on integral friction. The total reduction of friction due to local surface heating, attained at $x_m^* = 1.5$ m, is less than in the case of ignoring the interaction by approximately *3%* with $Q_w = 10^{-4}$ and by *10%* with $Q_w = 2 \times 10^{-4}$.

In the presence of several heated portions with one and the same value of Q_w the distribution of the velocity gradient on the external boundary of the boundary layer in the region of heat input is almost periodic, as is seen in *Fig. 1.7* [8]. A gradual downstream decrease is observed of the maximum (in absolute magnitude) values of u'_{ex}. The dashed curve in *Fig. 1.7* indicates the distribution of displacement thickness, calculated ignoring the interaction.

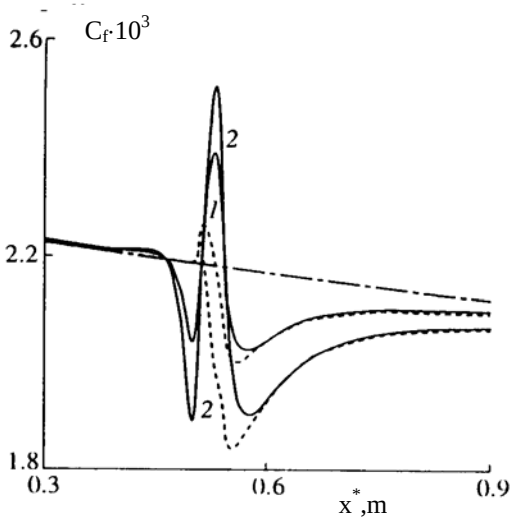

Fig. 1.6. The distribution of the local friction coefficient for a single heated portion: (1) $Q_w=10^{-4}$, (2) $Q_w=2\cdot10^{-4}$ [8].

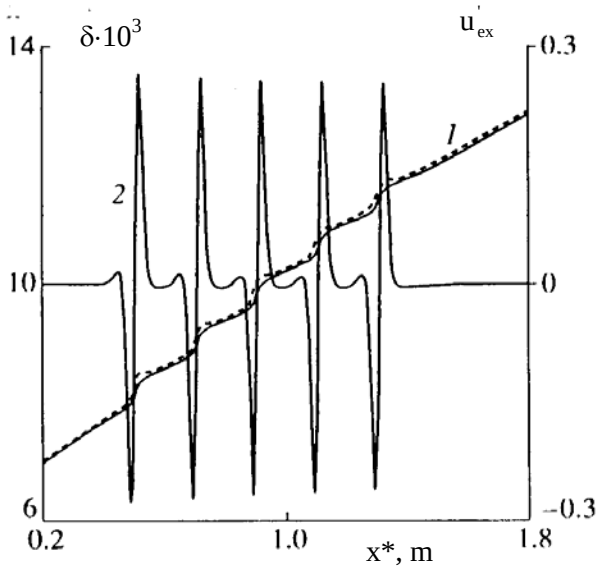

Fig. 1.7. The distribution of (1) the displacement thickness of boundary layer and (2) velocity gradient on its external boundary for five heated portion [8].

Fig. 1.8 reflects the effect of the boundary layer on external supersonic flow [8]. As a result of periodic deceleration-acceleration, the maximum value of velocity of nonviscous flow increases slowly downstream.

Fig. 1.9 gives the distribution of the local friction coefficient both ignoring (dashed curve) and including (continuous curve) the interaction for five heated portions [8]. The dot-and-dash curve indicates the distribution of the friction coefficient on the adiabatic surface. No qualitative changes are observed in the behaviour of C_f as compared with the case of a single heated portion.

From the obtained in [8] results one can make conclusions that the interaction between turbulent boundary layer and supersonic flow has a considerable effect on both local and integral friction. This effect increases with the power of heat input to the gas. In optimizing the thermal method of reducing turbulent friction, based on local heat input to the boundary layer, the viscous-nonviscous interaction must be included.

1.3. Surface microwave discharge in supersonic airflow

In Report [14] the first investigation of new type of surface microwave discharge on external surface of dielectric body was fulfilled. It was shown that the surface discharge represents uniformly luminous plasma coating whole surface of a dielectric body and supersonic airflow does not destroy the surface discharge. Number of the results was obtained at investigation of the main properties of the surface microwave discharge. The threshold characteristics of discharge formation, dynamics of its evolution, vibration and gas temperatures, heating rate of gas, the electrodynamic characteristics of a surface discharge (space distribution of an electric field strength, depth of penetration of a field in plasma, space distribution of electron concentration) were measured and calculated. It was obtained, that the power of used microwave generator is sufficient for formation of a surface microwave discharge at air pressure $p=10^{-3}$-10^{3} *torr*. The longitudinal size of a surface discharge at fixed pulse duration grows with increase of a microwave power. Thus on an initial stage of a surface discharge existence the longitudinal velocity reaches value $v=10^{7}$ *cm/s*. Gas temperature grows with increase of a microwave power and reaches value T_g~*2000 K*. The fast gas heating with rate $dT_g/dt>100$ *K/μs* is observed at initial stage of the surface microwave discharge existence.

These results confirmed to a feasibility of surface microwave discharges in aerodynamics, namely, for change of the characteristics of supersonic flow near a surface of

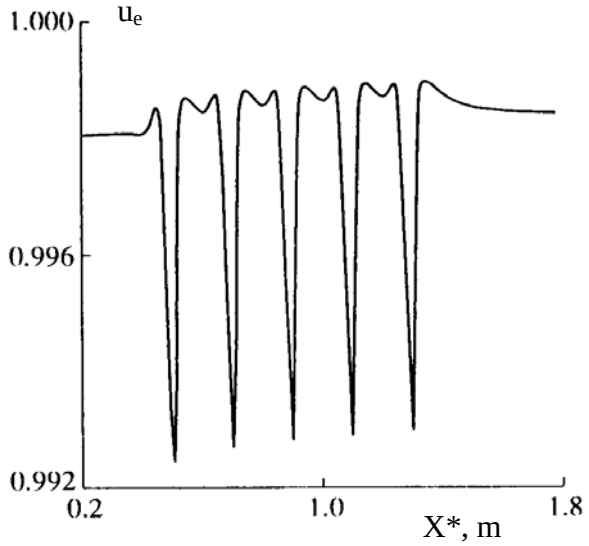

Fig. 1.8. The distribution of the velocity of external nonviscous flow [8].

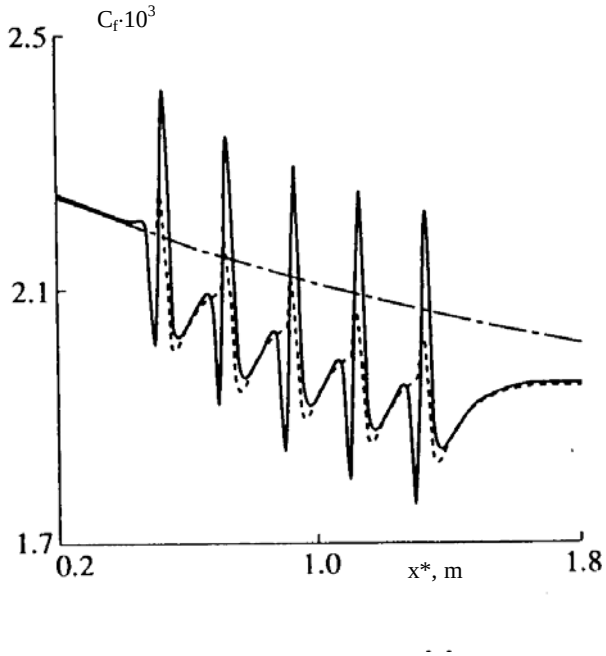

Fig. 1.9. The distribution of the local friction coefficient for five heated portion [8].

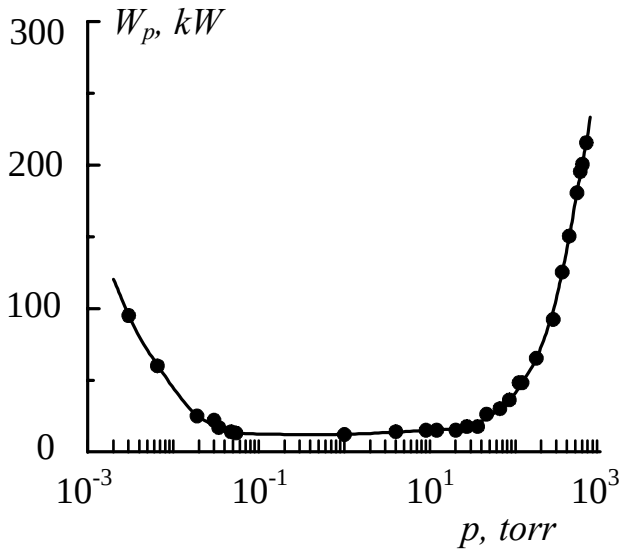

Fig. 1.10. Dependence of a minimum pulsed microwave power which is necessary for creation of a surface microwave discharge on air pressure at τ=1,5 μs and *f=40 Hz* [14].

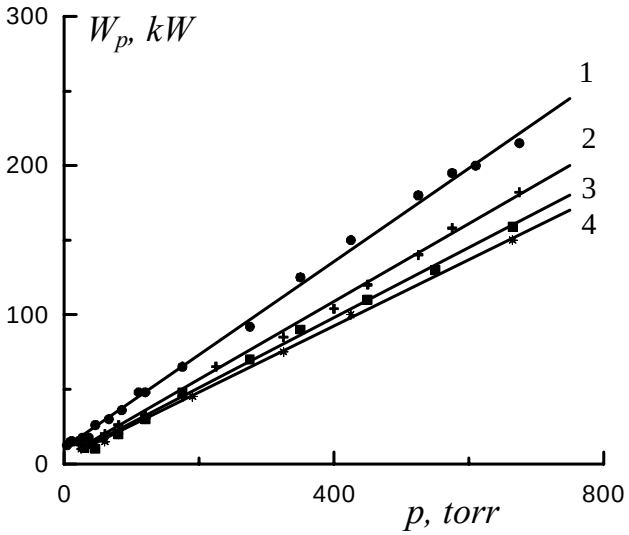

Fig. 1.11. The threshold characteristics of a surface microwave discharge created at different microwave pulses τ, μs: 1-1,5; 2-5; 3-10; 4-50-100 [14].

flying vehicles and by that improvements of their aerodynamic properties. Thus it is possible to improve a manoeuvrability of a flying vehicle, to radically lower the model resistance at its flight in atmosphere at the expense of destruction of a head shock wave and reduction of turbulent friction force.

Fig. 1.10 represents the dependence on air pressure of minimal microwave power which is necessary for a breakdown and beginning of formation of a surface microwave discharge on a dielectric body. One can see that the power of the used generator is sufficient for creation of the surface microwave discharge in a range of air pressures $p=10^{-3} \div 10^{3}$ *torr*. Thus, at increasing of air pressure the minimum power which is necessary for formation of a surface microwave discharge decreases at first and then grows. The obtained dependence is analogue of Pashen's curve. Such behaviour of power is explained by decrease of diffusional losses of electrons at increasing of air pressure and growth of inelastic losses at it. For compensation of the electrons losses it is needed a large ionization frequency. It is known that the ionization frequency is growing function of electron temperature $\nu_i=f(T_e)$, i.e. reduced electrical field E/n, or microwave power W. From here it is required to make a large power for creation of surface microwave discharge at small ($p<10^{-1}$ *torr*) and large ($p>10^{1}$ *torr*) pressure, as it is observed at experiment (*Fig. 1.10*).

In *Fig. 1.11* the threshold characteristics of a surface discharge created at different pulse durations are submitted. It is shown that at a fixed air pressure the power necessary for formation of a surface discharge sharply decreases with growth of a pulse duration from *1,5* up to *10* μs, whereas for $\tau \geq 50$ μs the threshold does not depend almost on pulse duration.

Let's admit that the external field is switched on quickly in comparison with characteristic time of creation of the charged particles and remains constant during time of development of a discharge. In this assumption $\nu_i(t), \nu_a(t)=const$ after the moment $t=0$ of an electric field power-up and the equation for full number of electrons in discharge area can be written down as

$$\frac{dn_e}{dt} = (\nu_i - \nu_a - \nu_D) n_e . \qquad (1.2)$$

At these assumptions the equation (1.2) has the exponential solution:

$$n_e = n_{eo} \exp\{(\nu_i - \nu_a - \nu_D) t\}, \qquad (1.3)$$

where n_{eo} is a number of backgrounded electrons, ν_i, ν_a, ν_D are the frequencies of ionization, attachment and diffusion.

From equation (1.3) it is possible to receive a frequency of ionization

$$\nu_i = \frac{1}{\tau} ln \frac{n_e}{n_{eo}} + \nu_a + \nu_D . \qquad (1.4)$$

In case of low gas pressure ($p<1$ *torr*) the diffusion coefficient is great ($D \sim 1/p$), and the losses of electrons due to diffusion are significant $\nu_D > \nu_a$. The large ionization rate is necessary for compensation of electrons losses that is a strong electric field is necessary. Thus, the threshold field is proportional to frequency of a microwave radiation and in inverse proportion to pressure of gas and sizes of discharge volume.

In case of high pressure the diffusional losses of electrons are insignificant and even not too large ionization rate provides gas breakdown. The losses of electrons for the account of attachment become main process. They also limit frequency of ionization. At pressure $p>10$ *torr* $\nu_a > \nu_D$ and the ionization frequency is defined by expression

$$\nu_i = \frac{1}{\tau} ln \frac{n_e}{n_{eo}} + \nu_a . \qquad (1.5)$$

Let's estimate a frequency of ionization for conditions of our experiment: $\tau = 50$ *μs*, $n_{eo} = 10^2$ *cm*$^{-3}$, $n_e = 10^{12}$ *cm*$^{-3}$. In this case first term in the right part of expression (1.5) approximately equals $4 \cdot 10^5$ *s*$^{-1}$, and second - $6 \cdot 10^5$ *s*$^{-1}$, i.e. the ionization frequency equals 10^6 *s*$^{-1}$. From here one can see that the ionization frequency at $p=10$ *torr* should be more than 10^6 *s*$^{-1}$. Thus at $\tau \leq 50$ *μs* for definition of a threshold of gas breakdown it is necessary to take into account duration of a microwave pulse. It is well co-ordinated with experimental data (*Fig. 1.5*).

During existence of the discharge a number of processes, such as a gas heating, an excitation of vibrational of freedom degrees of molecules, an accumulation of long living metastable molecules, an accumulation of charged particles (electrons, positive and negative ions), a change of chemical structure of gas and number of other processes proceed in plasma. All these processes can result to change of conditions of secondary breakdown of gas. For a surface microwave discharge in a supersonic flow of air the time of replacement of gas near a body equals $t=L/v$. This time is determined by the longitudinal size L of body and velocity v of supersonic airflow. Let's estimate this time for our case. The longitudinal size of antenna $L=15$ *cm*. The undisturbed flow velocity v under our conditions equals *500 m/s*. The flow velocity in boundary layer, existing near body, changes from *500 m/s* up to *0* on the surface of body. Let's the mean velocity of airflow in area of existence of surface microwave discharge equals *50 m/s*. Then the gas replacement time $t=3$ *ms*. A period of repetition of microwave pulses in experiment equals $T=25$-50 *ms*. From here all changes which have arisen during action of the previous microwave pulse will disappear to moment of switching-on of the following

pulse and the breakdown power should not depend on frequency of repetition of pulses, as it is observed in experiment.

Experiments [14] also shown that the supersonic flow of air at Mach number *M=2* does not influence on the microwave power which is necessary for creation of the surface microwave discharge. Thus the threshold of appearance of a surface microwave discharge does not depend on whether at first the discharge on a surface of a dielectric body is created and then the supersonic airflow is formed or, on the contrary, at first the supersonic airflow is included, and only then the surface microwave discharge is created.

In report [14] was shown that the surface microwave discharge represents uniformly luminous plasma coating all surface of a dielectric body and the supersonic flow of air at Mach number *M=2* does not influence on the common view of the surface discharge on the dielectric antenna of rectangular section, that is supersonic airflow does not destroy the surface discharge.

The longitudinal sizes of a surface discharge and its longitudinal velocities at *p=10 torr* as a function of a microwave pulse duration are submitted in *Fig. 1.12* and *Fig. 1.13*. The microwave power is parameter of these curves. It is shown that the longitudinal size of a surface discharge and its velocity at fixed pulse duration grow with an increasing of a microwave power. Thus, on initial stages of the surface discharge existence this velocity is much greater then sound speed and reaches $v=10^7$ *cm/s* at *W=175 kW*, whereas at late stages the velocity of the discharge propagation decreases up to $v=10^4$ *cm/s* at *W=25 kW*. From *Fig. 1.13* one can also see that all curves have the identical slope. The similar results were obtained in [14] also at other air pressures. The processing of the received data has shown, that the time dependence of longitudinal velocity of the surface microwave discharges can be described by the law:

$$v = A \cdot t^{-(0.875 \pm 0.035)}, \tag{1.6}$$

where *A* is a coefficient dependent on microwave power, *t* is a time of microwave discharge existence.

Experimentally received dependence of *A=f(W)* for various pressure of air is given in *Fig. 1.14*. One can see that at air pressure *p=10-100 torr* coefficient A is directly proportional to W/W_o, where W_o is a threshold power for the given gas pressure. Then, using dependence *A=f(W)* from the equation (1.6) it is possible to receive, that the longitudinal size of the surface microwave discharge is described by the law:

$$L = 17 \frac{W}{W_o} \cdot t^{(0.125 \pm 0.035)}, \tag{1.7}$$

here the length of surface microwave discharge *L* has a dimension [*cm*], and time *t* has a

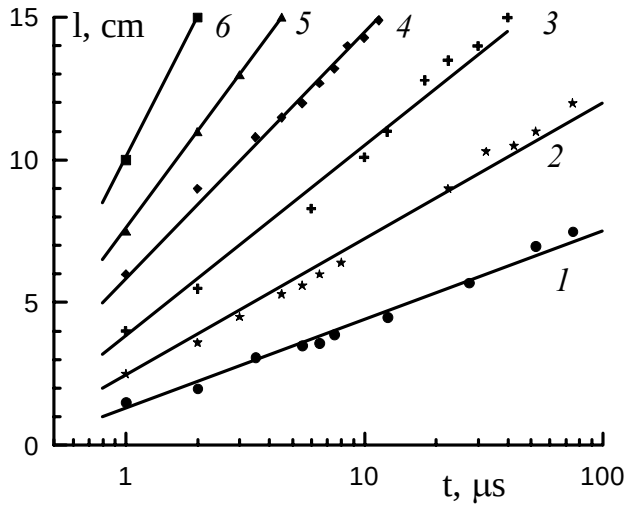

Fig. 1.12. Dependencies of the longitudinal sizes of a surface discharge on duration of a microwave pulse at *p=10 torr, f=20 Hz*, and pulsed microwave power W_p, *kW*: 1-25; 2-35; 3-55; 4-75; 5-100; 6-175 [14].

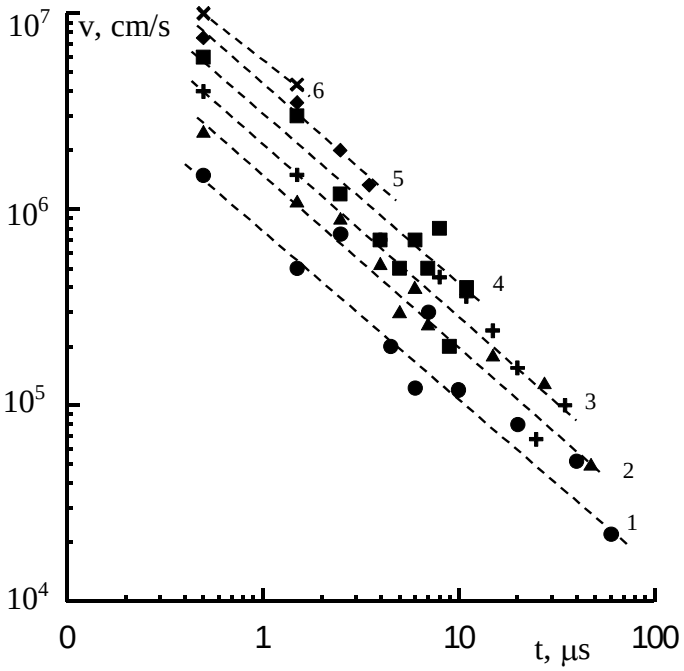

Fig. 1.13. Time evolution of longitudinal velocity of the surface microwave discharge at *p=10 torr, f=20 Hz*, and microwave power W_p, *kW*: 1-25; 2-35; 3-55; 4-75; 5-100; 6-175 [14].

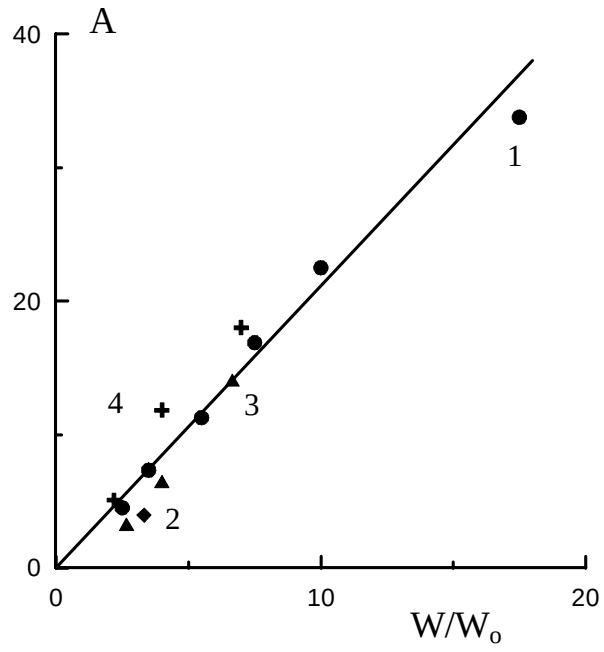

Fig. 1.14. Dependence of *A=f(W)* for various air pressure *p, torr*: 1-10; 2-40; 3-62; 4-100 [14].

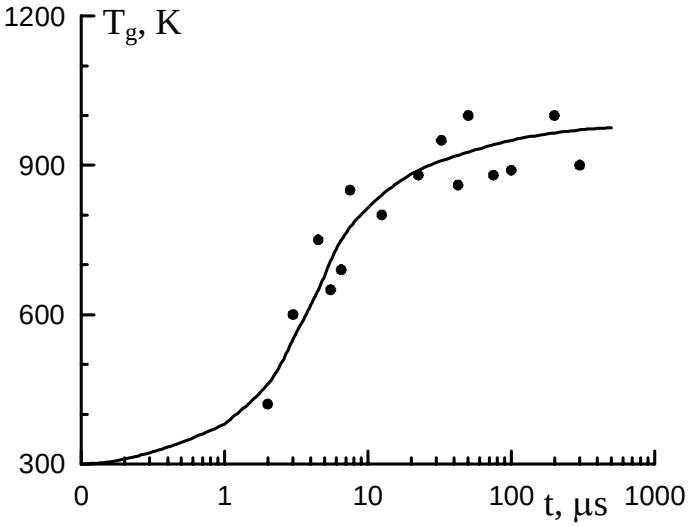

Fig. 1.15. Time evolution of gas temperature under conditions of surface microwave discharge at *p=10 torr, f=10 Hz* and W_p*=100 kW* [14].

dimension [*s*]. From here one can see that experimental installation allows receiving the surface microwave discharges with length up to *1 m*.

It was shown in [14] that the gas temperature grows with increase of a microwave power and reaches value $T_g \sim 2000\ K$, whereas vibrational temperature remains practically constant under these conditions, insignificantly decreasing with increase of microwave power. At this the maximal gas heating is observed in a place of excitation of a surface microwave discharge and gas temperature decreases by the end of the discharge.

The time evolution of gas temperature under conditions of surface microwave discharge is submitted in *Fig. 1.15*. At that, on initial stage of existence of the surface microwave discharge the fast gas heating with rate of $dT_g/dt > 50$ K/μs is observed. In [14] it was shown, that the mechanism connected with effective excitation of electron-exited states of nitrogen molecules at large values of the reduced electrical field $E/n \geq 100\ Td$ and their subsequent quenching is responsible for the gas fast heating.

The theoretical analysis of properties of the surface discharge was carried out with the help of the mathematical model of the discharge grounded on the joint solution of the balance equations of charged particles and Maxwell equations for an electromagnetic field [14]. The following results were obtained: i) the dispersion curves of a surface wave were calculated; ii) the field penetration depth in plasma was calculated; iii) the dependence of longitudinal length of the discharge supported by a surface wave from power transferred by a microwave was obtained; iiii) the spatial distributions of an induction of a magnetic field and electric field intensity are computed.

The calculated dependencies of plasma density on coordinate x along the antenna are given in *Fig. 1.16*. The dependence of inverse penetration depth x^{-1} of a surface wave in plasma as a function of electron density at $\nu/\omega=0$ is submitted in *Fig. 1.17*. From *Fig. 1.17* it is visible, that in case of a surface microwave discharge the microwave field is localized in a thin near-surface layer that promotes the effective contribution of energy to plasma and fast gas heating. The results of calculation of distribution of electrical and magnetic field in neighbourhood vicinity of the antenna are submitted in *Fig. 1.18* at electron densities in plasma $n_e/n_{ec}=5$.

1.4. Ignition of gaseous fuels under condition of supersonic flows

Airbreathing propulsion at supersonic velocities is subject to the stressing requirement that mixing, ignition, and combustion must take place on very rapid time scales [15]. In terms of

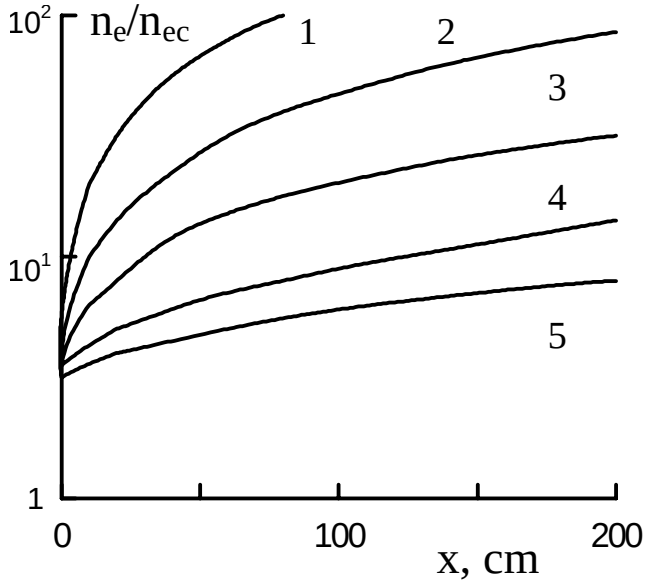

Fig. 1.16. Electrons density to electrons critical density ratio n_e/n_{ec} as a function of coordinate x at different collisions frequencies ν/ω: 1–0.01; 2-0.03; 3–0.1; 4–0.3; 5–1.0. Coordinate $x=0$ corresponds to the end of a discharge [14].

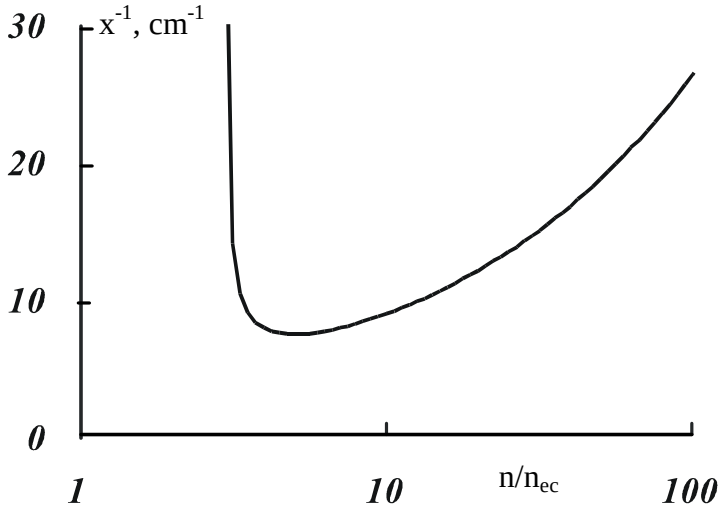

Fig. 1.17. Inverse penetration depth x^{-1} of a surface wave as a function of electron density at $\nu/\omega=0$ [14].

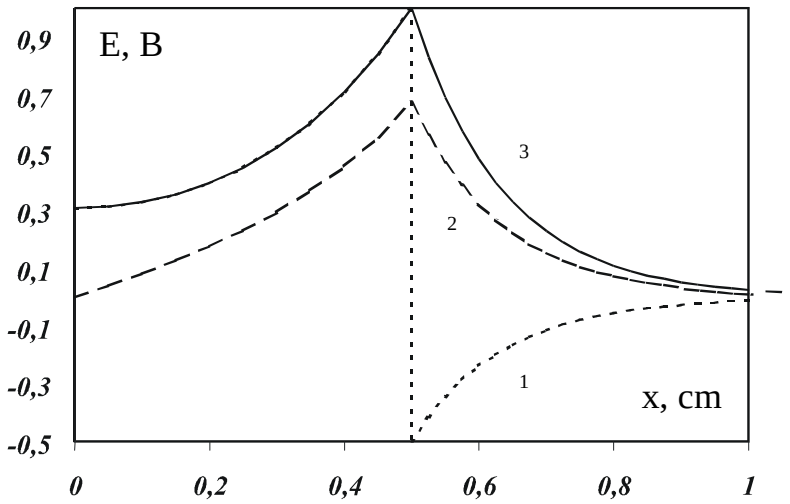

Fig. 1.18. A space distribution of electrical (E_y, - curve (1) and E_z – curve (2)) and magnetic (B_y – curve (3)) fields in a surface wave at $n_e/n_{ec}=5$ (greatest depth of penetration) [14].

combustion performance, the candidate fuel should have overall combustion times in the low-to-sub millisecond range at about *T=1000 K* and *p=0.5-2 atm*. Liquid hydrocarbons have been selected for use by the DoD as the fuels of choice due to their high energy density, excellent storage stability, good cooling capability, and compatibility with the existing fuels infrastructure. Unfortunately, liquid hydrocarbon fuels do not meet the necessary combustion time characteristics, thus placing emphasis on combustion enhancement techniques. A number of such methods have been suggested and explored to varying degrees. Hot gas piloting, photo irradiation, energy intensive ignition sources (e.g., laser, plasma), heterogeneous catalysts, and homogeneous catalysts are typical of the techniques that have been considered for combustion enhancement, particularly under conditions where ignition would not otherwise occur. However, a major hurdle for success of any of the above mentioned combustion enhancement techniques is the lack of combustion data and validated mechanisms at conditions relevant to scramjet operation. The paper [15] describes an experimental and computational program aimed at developing a better understanding of the important and relevant chemistry in these combustion environments.

Recent progress on efforts to develop a detailed kinetic mechanism for C_8H_m hydrocarbons and practical plasma igniters for plasma-assisted combustion were discussed in [15]. Shock tube validation experiments made in argon using a fixed stoichiometry (α=1.0), pressures of approximately 0.95 and 1.05 atm, and temperatures ranging from 850 to 1200 K (post reflected shock) were presented. The mechanism was being expanded to include electron kinetics and to allow for a degree of nonequilibrium modeled with separate electron and gas temperatures. Quantum calculations used to derive needed electron impact ionization/dissociation cross-sections for hydrocarbons were discussed. In addition, ignition of ethylene fuel in a Mach 2 supersonic flow with a total temperature of 590 K and pressure of 5.4 atm was demonstrated using a low frequency discharge with peak and average powers reaching 8 kW and 2.8 kW, respectively.

The problem of the uniform ignition of combustible mixtures is of crucial importance from both scientific and technological standpoints [16]. The reaction of fuel oxidization proceeds via a chain mechanism. It is well known that the chain reactions of fuel combustion are very fast and the combustion rate is limited by the rate at which active centers are produced, e.g. in the course of thermal dissociation. For this reason, the reaction rate is, in fact, higher with induced initiation of chain reactions. The easiest way to produce free radicals is to decompose the weakest bond of a molecule. The two mechanisms through which the discharge can affect a gas should be taken into account when using a discharge to initiate combustion. For discharges resulting in the formation of an equilibrium (or a nearly

equilibrium) plasma (e.g., sparks and arcs), the main factor that boosts up the chain combustion reaction is local gas heating and, accordingly, the increase in the thermal dissociation rate. In the case of a nonequilibrium plasma, the main mechanism responsible for the initiation of chain reactions is electron-impact dissociation of molecules. The question of the efficiency of using nonequilibrium plasmas still remains open. On the one hand, even relatively small amount of atoms and radicals (on the order of 10^{-5}-10^{-3} of the total number of the gas particles) can shift equilibrium in the system and initiate a chain reaction. Moreover, if such a concentration of active particles is produced uniformly over the entire gas volume, the combustion will certainly be nondetonation in character. On the other hand, the problem of igniting a spatially uniform discharge in a large gas volume with a relatively high initial density of neutral particles is rather complicated from the technical standpoint.

The spatial uniformity of the gas-mixture combustion initiated by a high voltage nanosecond volume discharge was investigated in [16] at gas pressures of *p=0.3-2.4 atm* and temperatures of *T=1000-2250 K*. The experiments were carried out behind a reflected shock wave propagating in a methane-air mixture diluted with argon. The self-ignition time and the time of discharge-induced ignition were determined. It was found that, at relatively low pressures (*~0.5 atm*), the discharge significantly (by *600 K*) decreases the ignition temperature. At higher pressures (*1.5-2 atm*), the ignition temperature decreases by only *100 K*. The discharge and the mixture combustion were monitored with a nanosecond ICCD camera under various experimental conditions. Comprehensive measurements of the deposited energy and the waveforms of the discharge voltage and current with a nanosecond time resolution made it possible to determine the efficiency of this type of discharge as a means for igniting combustible mixtures. In addition low-temperature experiments on different hydrocarbons oxidation in nanosecond discharge were represented.

In paper [17] the ignition of hydrogen-air and methane-air mixtures diluted with either argon or helium was studied. The mixtures were ignited by a spatially uniform nanosecond volume discharge. The experiments and calculations showed that, for certain gas parameters (the initial density and temperature), the discharge parameters can be optimized so that to significantly (in case of paper [17], by *600 K*) decrease the ignition temperature. An advantage of high-voltage nanosecond discharges is that they almost instantaneously (in experiments [17], over a time of a few nanoseconds) bridge the *20-cm*-long discharge gap and then produce atoms and radicals that are required to initiate spatially uniform combustion. The characteristic time during which energy is deposited in the gas can be increased to a few

hundred of nanoseconds and is limited by a transition of the discharge to an arc. It was also shown in [3] that the ignition delay time substantially depends on the discharge parameters and the gas density.

Flameholding, flame stabilization, and mixing enhancement, are fundamental aspects of supersonic combustion, and critical to the development of a hypersonic airbreathing propulsion engine [18]. In general, flameholding and flame stabilization can be achieved by the following techniques: 1) by organization of a recirculation area where the fuel and air can be mixed partially al low velocities. 2) by interaction of a shock wave with partially or fully mixed fuel and oxidizer, and 3) by formation of coherent structures containing unmixed fuel and air, where a diffusion flame occurs as they are convected downstream [4].

These three stabilization techniques can be applied in a supersonic combustor in different ways [18]. One of the simplest approaches is the transverse (normal) injection of fuel from a wall orifice. As the fuel jet interacts with the supersonic crossflow a bow shock is produced. As a result, the upstream wall boundary layer separates, providing a region where the boundary layer and jet fluids mix subsonically upstream of the jet exit. This region is important in transverse injection flowfields owing to its flame-holding capability in combusting situations. However, this injection configuration has stagnation pressure losses due to the strong *3-D* bow-shock formed by the normal jet penetration, particularly at high flight velocities.

Another way of achieving flame stabilization is by means of a step, followed by transverse injection [18]. The step creates a bigger recirculation area with the hot gases serving as a continuous ignition source. This approach can provide sustained combustion but, like the previously described method, has the disadvantage of stagnation pressure losses.

On the other hand, it is possible lo reduce the pressure losses associated with the injection process by performing angled injection (e.g., *60°* or *30°* rather than *90°*) where the resulting bow shock is weaker [18]. In this approach, jet axial momentum can also contribute to the net engine thrust. In [19], autoignition of a hydrogen jet transversely injected into high-total-enthalpy flow (simulating Mach *10-13* flight range) was observed in the upstream recirculation region of the jet. However, different experiments performed for similar geometry but at much lower total-enthalpy flow conditions showed that ignition occurred only far downstream of the jet. Based on those observations, angled injection is likely to reduce or eliminate these forms of autoignition and stabilization especially at flight speeds lower than

Mach *10*. Therefore, it is clear that a new technique will be required to obtain autoignition and downstream combustion stabilization.

In recent years, cavity flame holders, an integrated fuel injection/flameholding approach, have been proposed as a new concept for flame holding and stabilization in supersonic combustors. The experiments [20-22] showed that the use of a cavity after the ramp injector significantly improved the hydrocarbon combustion efficiency in a supersonic flow. Similar flame stabilization zones, investigated in [23], have been employed within a solid-fuel supersonic combustor, demonstrating self-ignition and sustained combustion of PMMA (Plexiglas) under supersonic flow conditions.

In paper [18], the known characteristics of cavities, in general, and the research efforts related particularly to cavities employed in low- and high-speed combustors were summarize. Before designing a cavity flameholder for a practical application in a supersonic combustion one should take advantage of the existing knowledge and examine the underlying physics of high-speed cavity flow dynamics.

The main mechanisms and peculiarities of operating process concerning combustor of high-speed hydrocarbon endothermic fueled dual-mode demonstrator scramjet were considered in [24]. Methods of experimental researches of methane combustion at large subsonic airflow velocities were suggested. Description of research combustor duct, results of calibration tests and methodology of model combustor operation initiation, equipped by methane/air igniters, step flame holders and fuel heater (T_{fuel}*=500-900 K*) were given. Air flow total parameters were P_t*=0.4-0.7 MPa* and T_t*=700-910 K*, main fuel was supplied through three jet injector sets placed along the combustor duct and fuel rate distributions between sets were different. Injector sets included wall and pylon injectors. Experimental data testifies about effective methane burning in high speed subsonic airflow (*M=0.5-0.6*) at fuel/air equivalence ratio ϕ*=0.3-0.8*.

In paper [25] experimental research of gaseous methane fueled combustor at fuel/air equivalence ratios equal to ϕ*=0-0.8* and fuel temperature T_f*=550-880 K* was conducted under connected pipe conditions. Intake total airflow parameters were varied within next ranges: P_t*=0.4-0.7 MPa*, T_f*=650-910 K*. Main fuel was supplied through the two injector sets along the duct arranged under different fuel rate distributions between sets. Injector sets included wall and pylon injectors. Additional fuel of 0-10% main fuel rate was injected into the base region behind the reverse steps for providing of combustion stabilization. Variations of fuel parameters and injection schemes

confirmed possibility of stable initiation and effective methane/air mixture combustion under $\phi=0.6\text{-}0.8$ and airflow velocities corresponding to $M=0.5\text{-}0.6$.

In paper [26], the oxidation of methane behind reflected shock waves has been studied in the temperature range of *1350-1900 K*. The mixture compositions studied ranged from *0.2* to *5.0* fraction stoichiometric, and the pressure range was from *1.5* to *4.0 atm*. Measurements were made of the pressure, chemiluminescent emissions of *OH*, *CH*, C_2 and *CO*, and the *306,7 nm* absorption of the *OH* radical during the induction period preceding rapid reaction. The induction times, based on the rapid increase in pressure and *OH* emission, were found to correlate with initial reactant concentrations of $(O_2)^{2,0}\ (CH)^{-0.4}$. To complement the experiments, an analytical study of methane oxidation was carried out, using a thirteen-step reaction mechanism. The time rate of change of concentrations and thermodynamic properties were calculated by numerically integrating the system of reaction kinetic and state equations. Induction times obtained from the calculations were in good agreement with the experimental results.

An experimental and modeling study of the preignition oxidation of methane and its sensitization by propane was reported in [27]. The ignition delay times were measured behind reflected shock waves at two different locations along the shock tube in *9.5% CH_4-19.O% O_2-Ar* mixtures with *0.19*, *0.475*, *0.95*, and *1.9% C_3H_8* added. The experiments were performed a nearly constant density of approximately $2\cdot10^{-5}\ mol/cm^3$ over a temperature range of *1300-1600 K*. A computer mode1, composed of *140* reactions and *34* species, was able to predict the experimental results. The model was subjected to a sensitivity analysis, which was performed using the saturated-design technique. The oxidation of methane during the induction period was found to proceed through three distinct phases: initiation, oxidation of CH_3 by O_2 and oxidation of CH_3 by HO_2. The sensitization by propane was found to be primarily determined by the decomposition of the propane molecule.

A number of kinetic schemes have been used to model premised, laminar, one-dimensional methane/air flames. In [28] seven such kinetic schemes, inducing two new models, were compared with one another and with experimental data. The two new models, one with *14* species and one with *20* species, both agree with the experimental data over a range of stoichiometries from lean to rich. All the models show good agreement for lean to slightly rich flames. This does not validate any of the models, even for this limited range. Rather, it was shown that the quantities measured arc fairly insensitive to much of the mechanism. Therefore, models with incorrect kinetics can agree with the experimental data. In particular, the contribution of the C_2 species to methane combustion is examined. While these species are important, the authors

conclude that there is insufficient information to determine quantitatively the effects of the C_2 chemistry reactions.

In paper [29], the analysis of an opportunity of a reduction of the kinetic scheme was carried out on the basis of numerical modelling at volumetric reaction of mixtures CH_4+O_2+Ar and CH_4+air. Comparison of calculated results with experimental data was fulfilled. It was shown, that for definition of an induction period it is possible to use simple enough kinetic scheme without taking into account reactions with nitrogen-containing components, however, this scheme is necessary to essentially expand at definition of time of burning and temperatures of products of reaction of CH_4+air mixture.

The significant number of papers (see for example [29]) is devoted to research of kinetic mechanisms of burning of methane in a mixture with O_2 or air. In these papers the basic attention has been given to the analysis of the processes determining of an induction time and revealing of mechanisms of formation of various hydrocarbonic compound. For CH_4+O_2+Ar mixes good enough conformity between the values of an induction period and also concentration of O, H atoms measured under shock waves facilities and the results received from numerical modelling has been achieved. That specifies that the kinetic mechanism of burning of CH_4+O_2 mixture is established well enough. Now it is considered, that the same mechanism can be used and for the description of burning of CH_4+air mixtures and N_2 acts only as a passive impurity.

However recently a lot of new problems which decision demands creation of detailed kinetic schemes and the analysis of mechanisms of formation $N0_x$ and others nitrogen-containing components were generated. It is connected to necessity enough exact definition of concentration of small impurity in products of combustion hydrocarbonic fuels and estimations of their influence on a condition of an atmosphere and an ozone layer of the Earth. Besides there are unresolved questions connected to a reduction of the kinetic scheme, used for definition of an induction period, time of burning and temperature of products of volumetric reaction of mixtures of CH_4+O_2 (air). For carrying out of researches in paper [29] the kinetic model including *433* convertible reactions with participation of *66* components has been developed. This model generalizes the kinetic circuits used earlier for the description of burning of mixes CH_4+O_2 and H_2+air. Time dependences of components densities at volumetric reaction in $CH_4+O_2+Ar=0.095:0.19:0.715$ mixture is given in *Fig. 1.19* at temperature $T_o=1613\ K$ and $\rho_o=2.2\cdot10^{-5}\ mol/cm^3$ [29].

With use of the expanded kinetic model in [30] the comparative analysis of features of oxidation kinetics of individual hydrocarbons C_3H_8 and C_4H_{10} in mixtures with air, and also

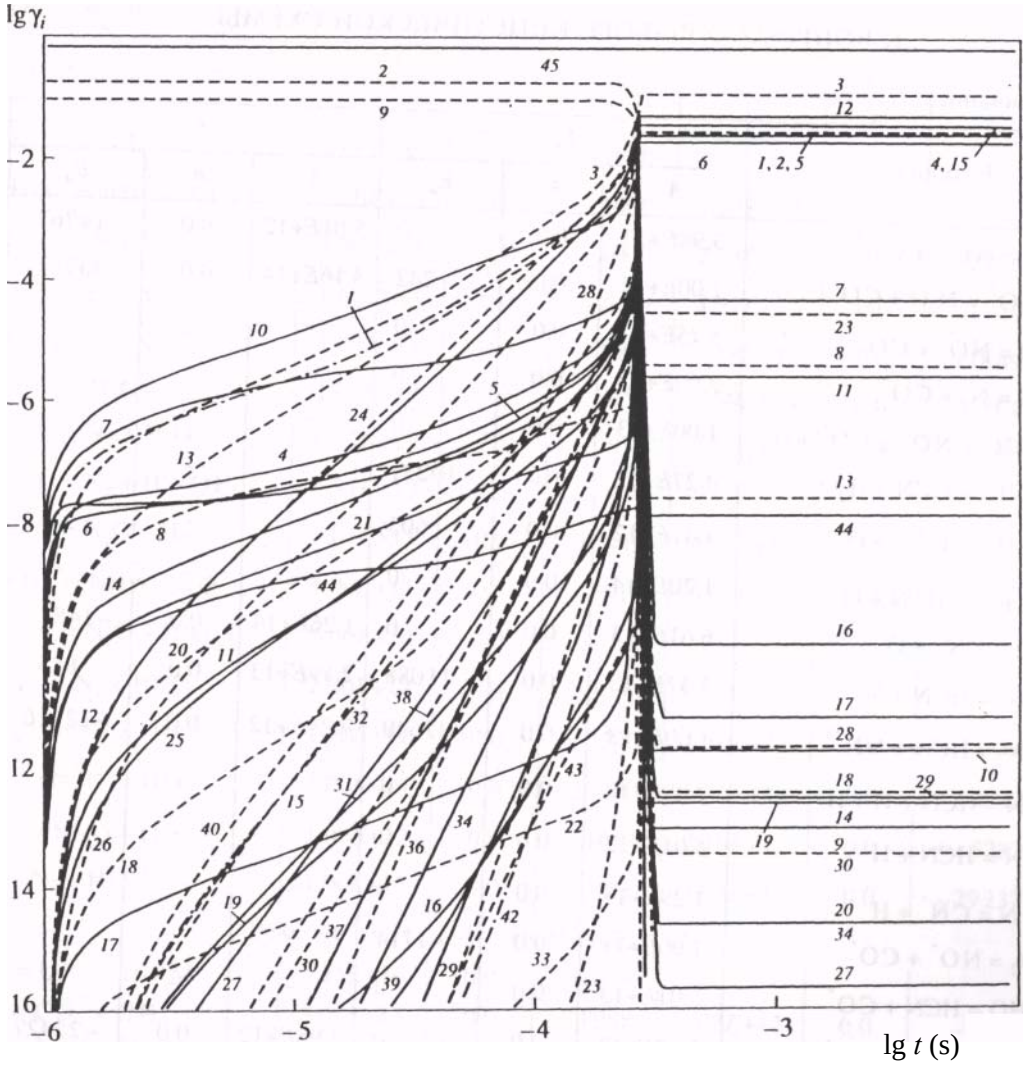

Fig. 1.19. Time dependences of components densities at volumetric reaction in mixture CH_4-O_2-Ar=0.095:0.19:0.715 at T_o=1613 K and $\rho_o=2.2\cdot10^{-5}$ mol/cm^3 [29].

1 - H_2, 2 - O_2, 3 - H_2O, 4 - OH, 5 - H, 6- O, 7 - HO_2, 8 - H_2O_2, 9 - CH_4, 10 - CH_3, 11 - HCO, 12 - CO, 13 - CH_2O, 14 - CH_3O, 15 - CO_2, 16 - C, 17 - CH, 18 - CH_2, 19 - CH_2OH, 20 - CH_3OH, 21 - $CH3O_2$, 22 - CH_3OOH, 23 - C_2, 24 - C_2H_6, 25 - C_2H_5, 26 - C_2H_4, 27 - C_2H_3, 28 - C_2H_2, 29 - C_2H, 30 - CH_2CO, 31 - CH_3CO, 32 -CH_3CHO, 33 - CH_3OOCH_2, 34 - C_2HO, 35 - C_3H_3, 36 - C_3H_4, 37 - C_3H_5, 38 - C_3H_6, 39 - C_3H_7, 40 - C_3H_8, 41 - C_4H_6, 42 -C_4H_8, 43 - C_4H_{10}, 44 - O_3, 45 - Ar.

products of their thermal decomposition is carried out. It is shown, that an induction period and time of burning of destruction products much less than corresponding parameters of burning of individual hydrocarbons. Dynamics of formation of nitric oxide and other ecologically harmful components is considered. It was shown, that time of achievement of equilibrium concentration of *N*- and *C*-containing components can essential (in 10^2 times) to differ from time of achievement of maximal values of *T* and practically equilibrium concentration of H_2O, CO_2, N_2.

CHAPTER II
EXPERIMENTAL INSTALLATIONS

2.1. General experimental set-up

The experimental set up is based on a stainless steel cylindrical gas/vacuum chamber three meters long with about a meter in diameter (*Fig. 2.1*). Supersonic airflow can be organized in it. Twenty six windows with different diameters (*10-50 cm*) are situated on its lateral surface that has allowed to visualize the discharge processes and to provide a vacuum-tight transport of electric current and electric signals. The gas/vacuum chamber consists of two sections that can form a vacuum-tight junction with help of a lever-operated gate. At installation and adjustment of diagnostic equipment and special purpose experimental tool inside the chamber its sections can be easily separated. A vacuum pump has allowed to achieve a pressure level of *1 torr* for *10-15* minutes of pumping.

The supersonic airflow was formed at filling the chamber with the atmospheric air through specially profiled converging-diverging nozzles with Mach number $M=2$. A detailed calculation of the nozzle shape has been carried out. The nozzle convergent part was made close to the ideal form providing a plane $M=1$ interface. The walls near the critical cross section had a sharp edge. The angle of the wall of the divergent part near the critical cross section was calculated from the theoretical formulae with use of the gas dynamic functions. The whole profile of the divergent part was calculated to obtain the output parallel supersonic airflow. This uniform $M=M_o$ airflow region in case of negligible pressure in the vacuum chamber is restricted by a surface with a shape of two Mach angle cones based on the nozzle exit circle; upstream $M<M_o$, downstream $M>M_o$. The nozzles were made of a dielectric (teflon or caprolactam). A cylindrical nozzle had an outlet diameter *3 cm* and a diameter *15,4 mm* of critical cross section. The characteristic period of time of regular nozzle operation was about 2 second.

The nozzles were screwed on a dielectric tube *5 cm* in diameter. On its opposite end a electric hydraulic valve with *∅5 cm* channel was fixed. All this construction was installed on a flange of a window of the chamber so that to position the supersonic airflow along the chamber's diameter. The nozzle end was situated on the level of big transparent windows on the lateral surface of the chamber. The electric hydraulic valve operated with a power supply unit which was synchronized with the discharge power supply units.

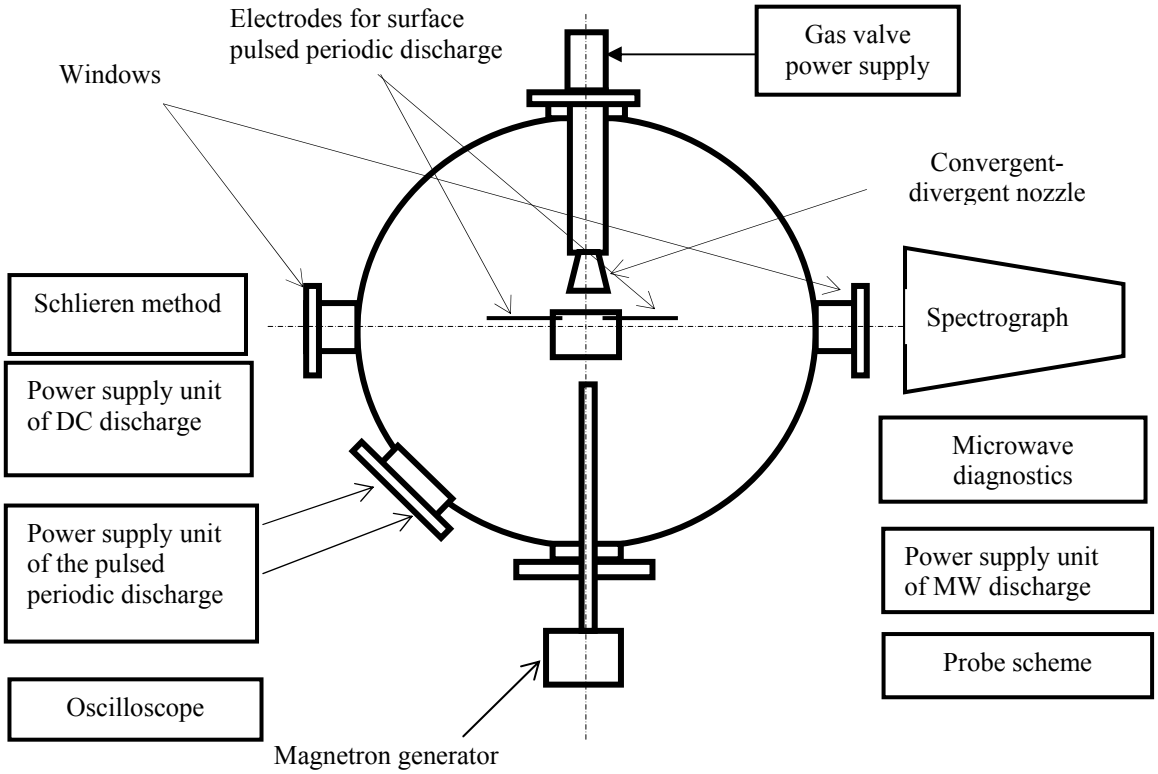

Fig. 2.1. General scheme of the experimental set up

The experimental set up was equipped with different types of diagnostics.

A Schlieren device was used for visualization of the free supersonic airflow and of the discharges in it. An electric incandescent lamp with radiating body area about *1 mm*^{2} was used as a light source for adjustment of the device. At registration of the airflow gas dynamical structure a pulsed (τ=10 μs) xenon lamp was applied.

Electron density in plasma of microwave discharge was measured by Stark broadening of spectral lines and by probe method.

A spectrograph *STE-1* and monochromators *MDR-3* end *DFS-12* were used for registration of plasma radiation spectra. The radiation detector (either a highly sensitive photo film, or *CCD* image sensor, or photomultiplier tube) was fixed in the focal plane of the spectral devices. For an experimental investigation of a surface microwave discharge in supersonic flow it is necessary to use contactless methods and the optical diagnostics of plasma fully satisfy this requirement. The vibrational temperature T_v was measured by the relative intensity of the nitrogen and *CN* bands. The gas temperature T_g was determined by the distribution of the intensity of rotational lines of molecular bands of a second positive system of nitrogen.

Double ray pulsed oscilloscopes with bandwidth *20 MHz* and sensitivity *1 mV/cm* were used for registration of the discharge voltage characteristics and the electric photomultiplier tube signals. For obtaining of the threshold characteristics of a surface microwave discharge the dependencies of the minimum input power at which the discharge on an external surface of a dielectric body starts to be formed were measured. The common view of a surface microwave discharge was registered on a film and a video camera in two projections (side view and top view).

For measurement of gas and vibration temperatures under condition of the surface microwave discharge in supersonic airflow, a diagnostic set up has been assembled. Radiation of the discharge that is formed in supersonic airflow is projected on input slots of two spectral devices through the windows of chamber, the mirrors, and the focusing quartz lenses. The lens diameter and its focal length were chosen so that to provide projection of the discharge image with reduction *k=10*, and use of all the light-gathering power of the devices. A spectrograph *STE-1* and monochromators *DFS-12* and *MDR-3* were used, their inverse linear dispersions being *0,35*, *0,5* and *1,3 nm/mm* accordingly for the spectral region of *300-600 nm*. The measuring system was calibrated by registration of standard iron arc spectrum (to get a wavelength scale) through a *9*-step light reducer (to reveal the linear region of radiation detectors) on the same radiation detector together with the tested spectrum. The photo films were analysed with use of a microphotometer *IFO-451*.

The electronic analyzer of optical spectra on base of a personal computer registers plasma radiation in visible, ultraviolet and infrared spectral ranges. The system is designed on base of an *IBM*-compatible personal computer. The sensor of plasma radiation on base of *CCD* image sensor forms a video signal directly proportional to the radiation intensity in the spectral band *300-900 nm*. The discharge spectra can be visualized on the monitor or printed out with use of program codes.

2.2. Experimental installations for creation of freely localized microwave discharge

The experimental set-up consists of metal vacuum chamber, magnetron generator, system for input of microwave energy into vacuum chamber, system for creation of supersonic airflow and diagnostic system. The microwave discharges are created in a metal vacuum chamber. The inside diameter of the vacuum chamber equals *1,05 m*, its length equals *3 m*. Pulse magnetron generator of centimeter wavelength range serves as a microwave energy source. The magnetron generator had the following characteristics: the wavelength $\lambda=2,4\ cm$; the pulse duration $\tau=1\text{-}200\ \mu s$; the pulse period-to-pulse duration ratio $Q=1000$; the pulsed microwave power $W_p<300\ kW$; the mean microwave power $W_m<300\ W$. The wave was linearly polarized in the vertical direction. A pulse modulator with the partial discharge of capacitor was used for a feeding of a magnetron. The work of the pulsed modulator is based on a principle of rather long accumulation of energy during a pause between pulses and short-term its feedback to microwave generator during a pulse. Microwave power is delivered to the discharge chamber by means of a waveguide, which includes all necessary elements for controlling and measuring of a microwave power. The vacuum system allowed investigating the microwave discharge at air pressure up to *1 atm*.

The microwave discharge in the focused beam was created both in motionless air and in supersonic airflow at Mach number $M=2$, both under condition of free space and before a body streamlined by supersonic airflow. Two schemes of creation of the microwave discharge in supersonic gas flow were used.

In the first case the dielectric lens was used for focusing of the energy delivered to the discharge chamber (*Fig. 2.2*). Diameter of the lens was *60 cm*. The microwave discharge was produced in the standing wave mode. For it the electromagnetic energy beam, focused by the lens, was directed to a spherical metallic mirror performing additional focusing of the beam. This mirror was positioned in the chamber opposite the microwave lens so that the discharge occurred in the plane of observation windows, approximately coinciding with the focal plane of the

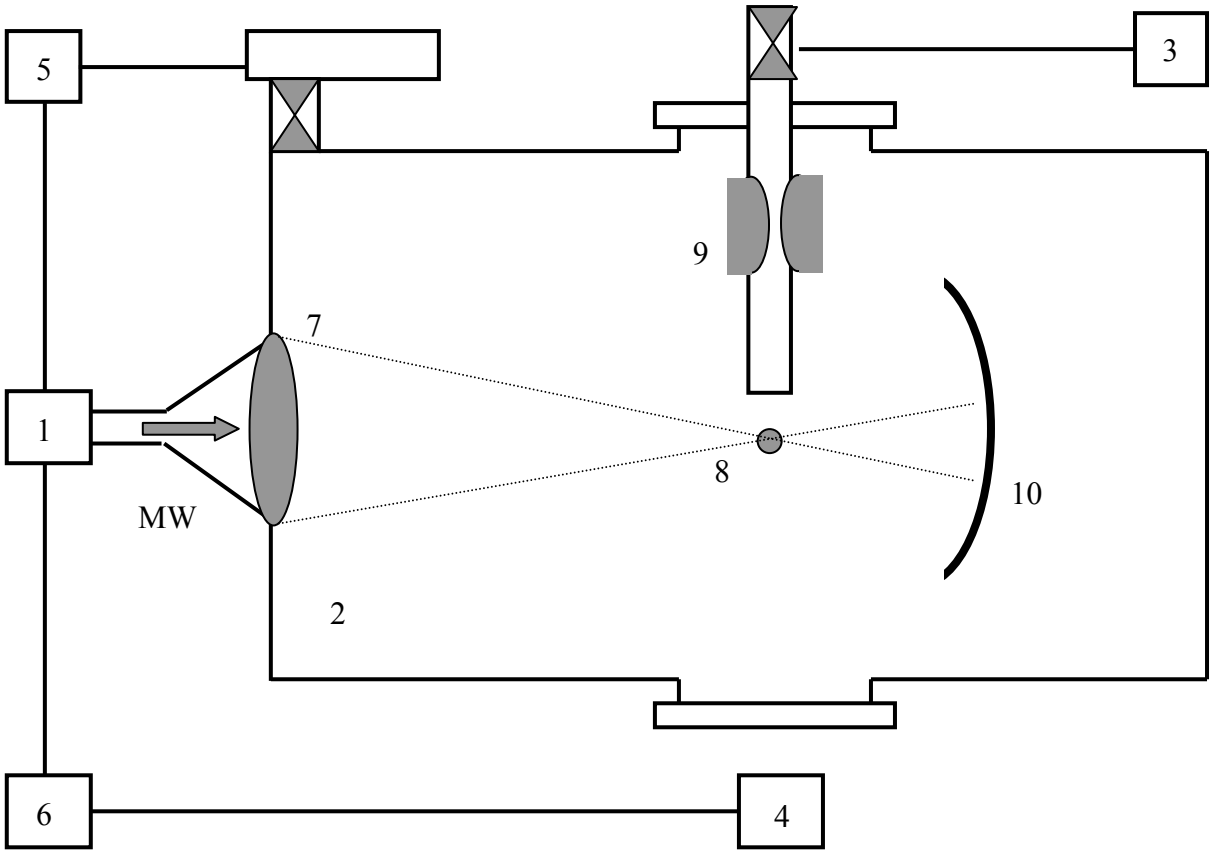

Fig. 2.2. The first scheme of experimental set-up for freely localized microwave discharge creation. 1 - magnetron generator; 2 - gas vacuum chamber; 3 - system for airflow creation; 4 - diagnostic equipment; 5 - pumping system; 6 - synchronization unit; 7 - microwave lens; 8 - microwave discharge; 9 - Laval nozzle; 10 - metallic mirror

mirror.

These experiments were performed under conditions when the chamber size is much greater than the wavelength of microwave radiation. The sharply convergent microwave beam was formed by a horn-type lens antenna. It turned out that the given type of the discharge is a reliable way of creation of plasma in supersonic flow of air.

However, in our opinion, for a fuel ignition in the real engine other type of a microwave discharge is more suitable and simple. We offer to use the second scheme consisting of a horn antenna microwave field applicator and a metal short-focus mirror (*Fig. 2.3*).

The microwave energy was introduced into the discharge chamber by a waveguide of a rectangular section $s=9,5x18\ мм^2$ through directional branching-off. The waveguide was hermetically soldered into a window of the discharge chamber. The end of a waveguide, entered into the discharge chamber, terminated in a rectangular horn. The horn formed a microwave energy flow falling on a spherical metal mirror. Focal length of a mirror was *16 cm*. The mirror settled down opposite to a radiating horn on distance of the order *30 cm* from it. A microwave discharge in supersonic flow was formed into the cylindrical channel made from a quartz glass. The aerodynamic channel was located between a horn and a mirror in a focal zone of a mirror. In the given series of experiments the smooth cylindrical aerodynamic channel by a diameter of 3 cm without a stagnant zone was used.

During realization of experiments the static air pressure in chamber changed from 1 up to *760 torr*. For avoidance of a microwave breakdown the waveguide was filled by SF_6 at pressure of *5* atmospheres. Therefore waveguide and discharge chamber have to be isolated. Teflon plate on horn played the role of a vacuum element.

The parameters of the microwave generator allowed creating the electrodeless microwave discharge in the focused beam at air pressure up to *100-200 torr*. If the pressure was more than *200 torr* it was necessary to use the initiators. However it is known, if the microwave discharge was initiated and gas breakdown has taken place, the plasma can be supported by under breakdown electrical fields for a long time. In the given series of experiments for this purpose we used the spark discharge. For it two thin (d<1 mm) electrode were entered into the aerodynamic channel. The high-voltage pulse ($\tau=1\ \mu s$, $U=20\ kV$) was applied to electrodes. The gas breakdown took place. The plasma, created at it, served as a source of primarily electrons, facilitating microwave breakdown of gas. A microwave pulse was applied after an initiating pulse with a time delay of $50\ \mu s$. The given design was a reliable way for initiation of the microwave discharge and enabled to create a microwave discharge up to atmospheric pressure.

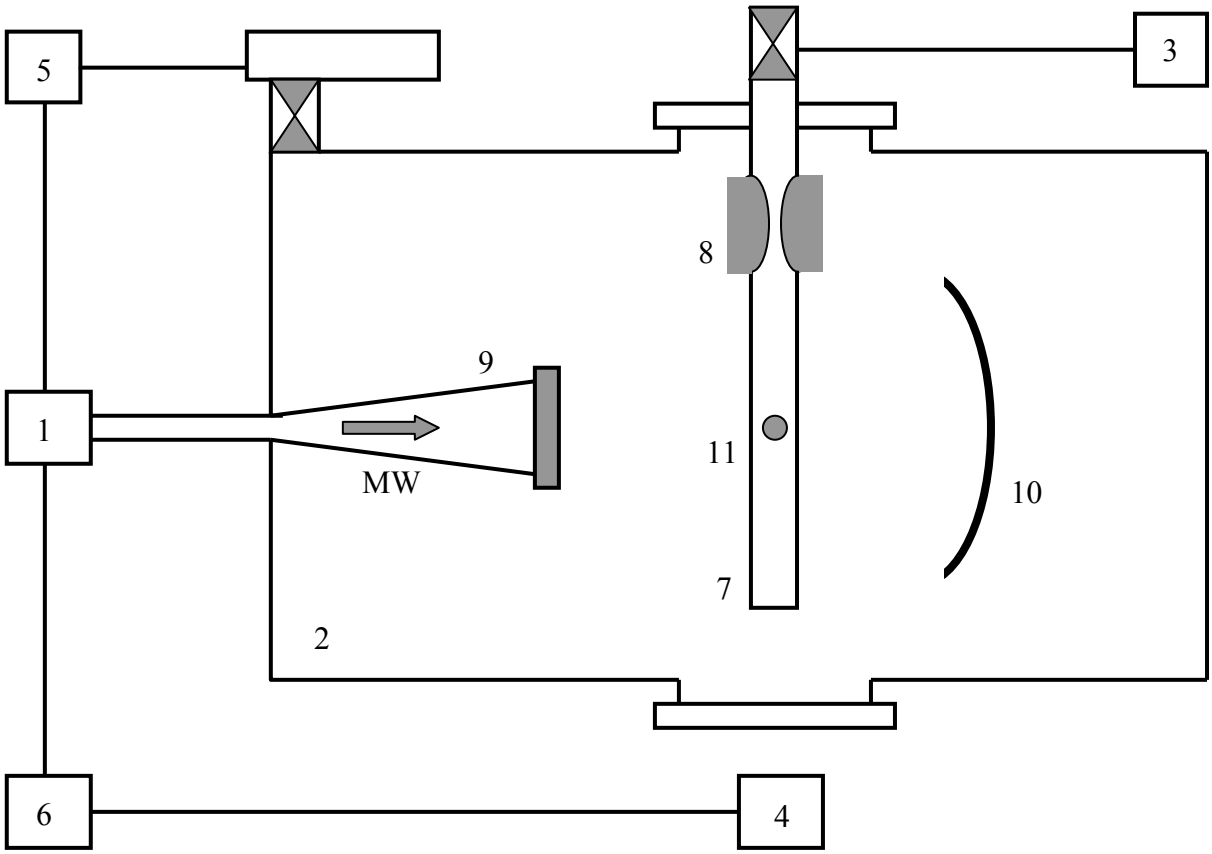

Fig. 2.3. The second scheme of experimental set-up for freely localized microwave discharge creation. 1 – magnetron generator; 2 – gas vacuum chamber; 3 – system for airflow creation; 4 – diagnostic equipment; 5 – pumping system; 6 – synchronization unit; 7 – aerodynamical channel; 8 – Laval nozzle; 9 – horn antenna; 10 – metallic mirror; 11 – microwave discharge.

The supersonic airflow with Mach number $M=2$ was formed at filling the chamber with the air through specially profiled converging-diverging nozzle. The nozzle was made of a dielectric material. The cylindrical nozzle had the outlet diameter $d_1=30$ *mm* and the diameter of critical cross section $d_2=15.4$ *mm*. The characteristic period of time of regular nozzle operation was about *2* second. The nozzle was screwed on a dielectric tube of 50 mm in diameter. On its opposite end an electric hydraulic valve with $d=50$ *mm* channel was fixed. All this construction was installed on a flange of the chamber window so that to position the supersonic airflow along the chamber diameter. The nozzle was situated on the level of big transparent windows on the lateral surface of the chamber. The electric hydraulic valve operated with a power supply unit which was synchronized with the discharge power supply units. The supersonic flow direction was perpendicular to the direction of a microwave radiation spreading.

2.3. Experimental installations for creation of surface microwave discharge

The system of creation of the surface microwave discharge in a boundary layer near to body streamlined by supersonic airflow was designed and manufactured. The modernization of the microwave generator used for creation of the surface microwave discharge inside a boundary layer, existing near bodies of different configuration streamlined supersonic airflow, is carried out. The block-scheme of experimental installation for surface microwave discharge creation is represented in *Fig. 2.4*. The experimental set-up is completed with the system of creation of supersonic airflow; the special system of input of a microwave energy into discharge chamber and transformations of the microwave energy into the energy of a surface wave; the system of recording of the parameters of microwave radiation and supersonic airflow, the diagnostic instrumentation for measuring of plasma parameters of the discharge and for recording of the photo and video information about common view of the surface microwave discharge in supersonic airflow.

The pulsed magnetron generator of a centimetric wave frequency was used as a source of microwave energy. The magnetron generator had the following characteristics: the wavelength $\lambda=2,4$ *cm*; the pulse duration $\tau=1\div200$ μs; the pulse period-to-pulse duration ratio $Q=1000$; the pulsed microwave power $W_p<300$ *kW*; the mean microwave power $W_m<300$ *W*.

A pulsed modulator with the partial discharge of capacity, developed in our laboratory, was used for a feeding of magnetron. The work of the pulse modulator is based on a principle of rather long accumulation of energy during a pause between pulses and short-term its feedback to microwave generator during a pulse. The microwave energy was introduced into the vacuum

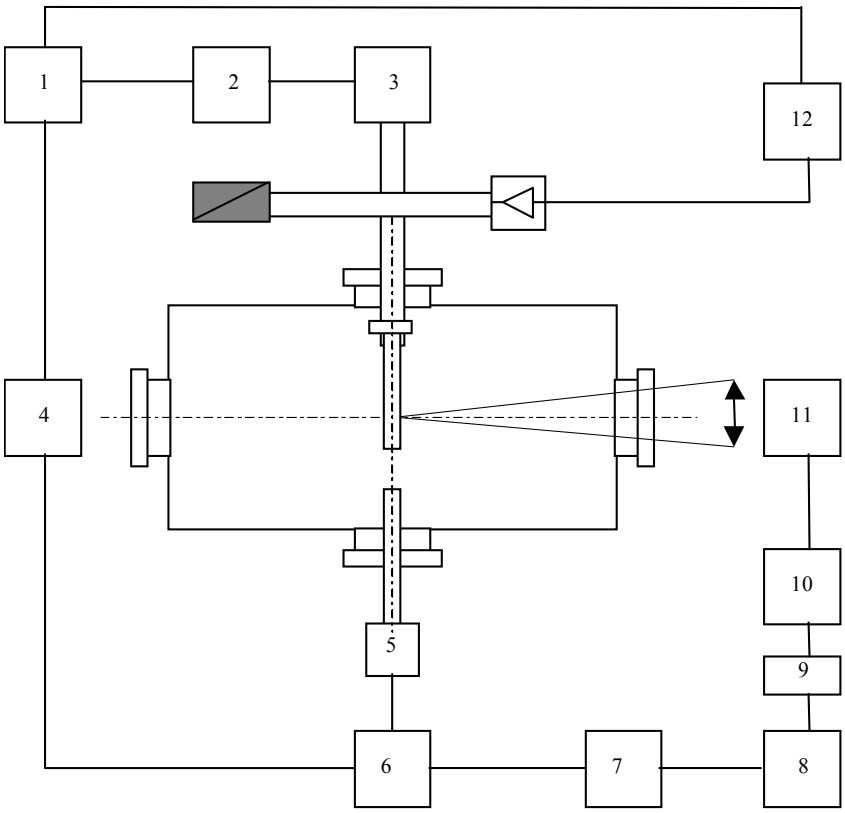

Fig. 2.4. Experimental installation. 1,6 – synchronisation units; 2 - modulator; 3 - magnetron; 4 – pulsed shadow graphics installation; 5 – system for creation of supersonic airflow; 7 – computer; 8 – supply system; 9 - *CCD* sensor; 10 - photomultiplier; 11 - monochromator; 12 – digital oscilloscope.

discharge chamber by the waveguide system of rectangular section *9,5x19 mm* through the directional coupler. All waveguide system was hermetic. It was filled by SF_6 at pressures up to 5 atmospheres for avoidance of an electrical breakdown. The discharge was formed in a cylindrical chamber. The vacuum system allowed to investigate the surface microwave discharge at air pressures *p=1,0-760 torr*. The waveguide entered into the discharge chamber ended the special antenna, on which the surface microwave discharge in supersonic airflow was created. The direction of supersonic flow was opposite to the direction of the surface microwave discharge spreading.

The output signal from the microwave detector was registered on an oscilloscope. The form of this signal was close to rectangular. The same signal acted on an input of the pulse digital voltmeter, under which indications the amplitude of a microwave pulse was determined. By meanings of this amplitude the microwave power supplied to the discharge chamber was measured. For it, the calibration of the voltmeter with the help of the power calorimeter was previously made. During calibration the power calorimeter was connected to an output of the basic shoulder of the directional branching-off.

The surface microwave discharges were formed on external surfaces of dielectric bodies of different geometry: on the flat plate; on the antenna of a rectangular section; on the antenna of a rectangular section with a wedge end part; on the cylindrical antenna with a spherical end part; on the cylindrical antenna with a conical end part; on the antenna of rectangular section with a smoothly transfer to the cylindrical antenna with a conical end part.

Additional experimental installation has been developed and assembled for measurement of parameters of a surface microwave discharge in motionless gas. The scheme of experimental installation is represented in *Fig. 2.5*.

The vacuum system works as follows. The forevacuum pump creates in all working volume preliminary pressure about 10^{-1} *torr*. Thus the valves V_1, V_3 and V_5 are open. At achievement of the preliminary pressure necessary for the beginning of work of the high-vacuum pump, the voltage from the power supply goes on this pump. When the high-vacuum pump achieves of operating conditions, valve V_3 is closed, and valve V_4 is open, and the working chamber is pumped out up to necessary high vacuum. The vacuum system allows to receive the pressure in working volume not less than 10^{-4} *torr*. After achievement of high vacuum, valve V_5 is closed, and the working chamber is filled by researched gas through leak V_6 and valve V_7 from high-pressure cylinder or by air through valve V_8 from a surrounding atmosphere. After the experiment completion all valves are closed, and the forevacuum pump is filled with an atmospheric air through valve V_2.

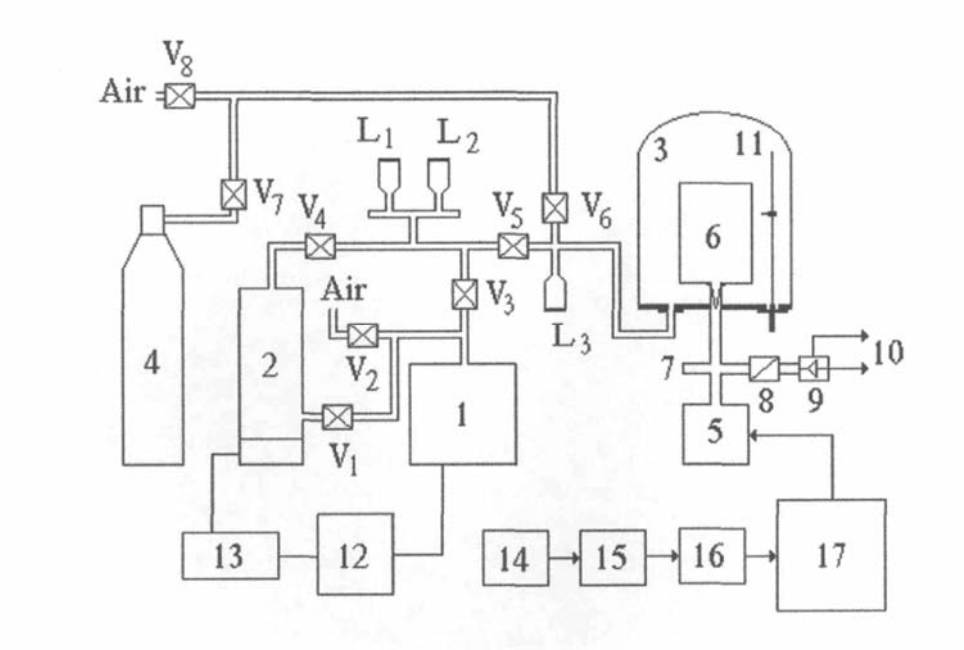

Fig. 2.5. The scheme of experimental installation.

1 - forevacuum pump, 2 - high-vacuum pump, 3 – discharge chamber, 4 - high-pressure cylinder with working gas, 5 - magnetron, 6 – dielectric antenna, 7 - directional coupler, 8 - attenuator, 9 - detector head, 10 - to oscillograph, 11 – fastening and moving probes system, 12 – control panel, 13 - high-vacuum pump power supply unit, 14 - driving oscillator, 15 – preamplifier, 16 – driver, 17 – modulator.

Preliminary pressure in system is checked by thermocouple lamps L_1 and L_3, and pressure of high vacuum - ionization lamp L_2. Pressure of researched gas is measured in the discharge chamber by means of lamp L_3.

The massive disk executed from steel of *40 cm* in diameter and *20 mm* in thickness is a basis of the discharge chamber. On a disk, located in horizontal plane, the glass chamber of *35 cm* in diameter and *40 cm* in height is placed through vacuum condensation. Inside a bell-glass there is a dielectric aerial. In a disk two vacuum sealing apertures are done: one for connection with pumping system, another - for a supply of the microwave power. Besides on a disk through vacuum condensation the special rack (11) is placed. On this rack the electric and magnetic probes are mounted. The design of this rack allowed moving probes in three spatial directions: in parallel and perpendicular directions with respect to surface of the dielectric antenna.

Control of vacuum pumps is carried out from the separate board (12) which allows to independently switching on the forevacuum pump and a power supply unit of the high-vacuum pump (13).

The microwave power is generated by powerful pulsed magnetron which radiation directs through waveguide into the discharge chamber. The part of the microwave power by means of directional coupler moves to registration system. The registration system consists from attenuator and the detector head. Attenuator allows changing a level of a signal on the detector. The form of a microwave pulse envelope was registered with the help of oscilloscope.

The operating mode of a microwave generator is adjusted by the specifying generator (14), which allows establishing both necessary pulse duration of the microwave energy, and its repetition rate. The signal from the specifying generator moves on a preamplifier (15) which amplifies an initial signal up to voltage about *600 V*. The gain signal acts on an driver input (16) which, in turn, strengthens a starting pulse up to voltage about *2 kV*. The pulse removed from an driver output, starts the modulator (17) in which the predetermined duration of the pulses with amplitude up to *30 kV* are formed, acting directly on magnetron (5).

For definition of value of microwave power input to the discharge the preliminary calibration was carried out. For this purpose instead of the antenna the microwave power meter was connected to a wave guide and the calibration curve of dependence of the power, generated by magnetron, on the voltage feed to magnetron was recorded. In experiment this voltage can reach value of *30 kV*. Therefore for calibration the voltage, displayed on a control panel from a voltage divider, was measured}, instead of voltage on magnetron. The received calibration curve is resulted on *Fig. 2.6*.

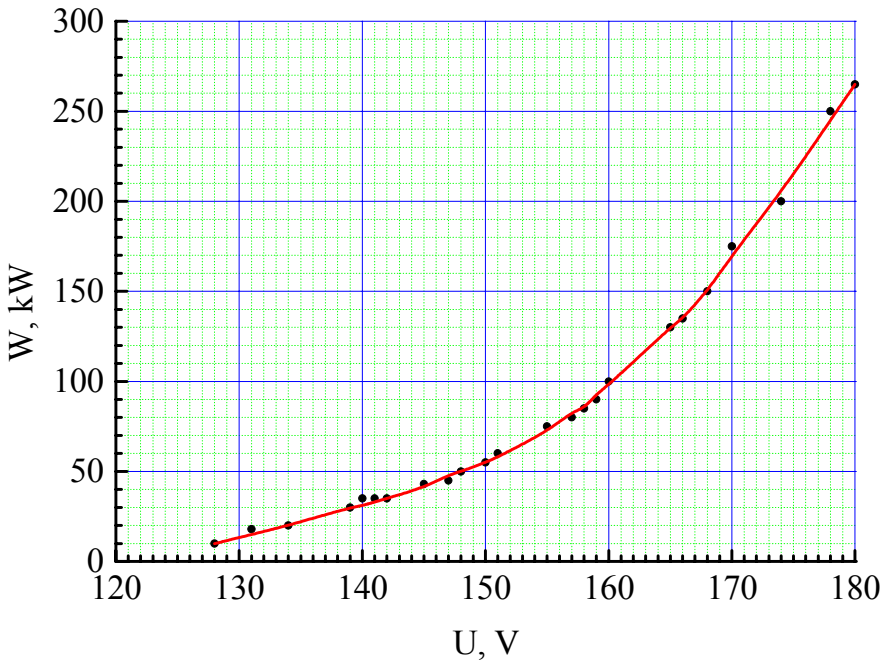

Fig. 2.6. The calibration curve of used microwave generator.

2.4. Set-up for creation of surface transversal pulsed-periodical electrode discharge

Experiments were carried out on the installation consisting of the vacuum chamber, the high pressure receiver of air, the high pressure receiver of propane-butane, the system for mixing propane-butane with air, the system for creation of a supersonic flow of a propane-butane-air mixture, the aerodynamic channel, the discharge section, the source of high-voltage pulses, the synchronization unit, and the diagnostic system. The block-scheme of experimental installation is represented in *Fig. 2.7*.

The base of the experimental installation is the evacuated chamber, which serves simultaneously for supersonic flow creation, and as a tank for the expiration of gases or combustion products. Internal diameter of the cylindrical vacuum chamber is *105 cm*, its length is *300 cm*. The windows, arranged on the lateral walls of the chamber, allow to conduct indispensable diagnostic of gas discharge and to execute hermetical input of an electrical feed of plasma generator and injection of different measuring signals. The vacuum system allowed to carry out researches in a wide range of air pressure *p=1,0-760 torr*.

The high-pressure air-supply system consists of gasholder by a volume of *0,2* m^3 with the high-pressure air compressor raising pressure up to maximum value of *p=12 atm*; the high pressure gauge; transducer of dynamic pressure; stop valve; and electromagnetic valve with opening time of *t~1ms*.

The system of storage and fuel supply consists of a standard reservoir by a volume of *0,04* m^3, which contains a liquid propane-butane. Through a stop valve and the reduction gearbox already a gas fuel goes into a receiver. The receiver represents a tank by a volume of *0,01* m^3. The fuel consumption during experiment was measured by value of a pressure fall in the pressure gauge of the reduction gearbox, or by sensor of dynamic pressure established directly behind an electromagnetic valve of the fuel supply system.

Air or air-propane-butane mixture originally goes into the mixing device, established in a subsonic part of a channel. The mixing takes place basically up to a throat of a supersonic nozzle. The passage diameter of the mixing device is *64 mm*. It was selected from a condition of arrangement and effective work of the mixer. Directly behind the mixer the supersonic nozzle is arranged.

The aerodynamic channel of rectangular section with a stagnation zone in the form of rectangular cavity in a broad wall of the channel was made for investigation of a possibility of ignition of supersonic propane-butane-air mixture with the help of a surface discharge. The Laval nozzle of rectangular section for creation in a rectangular aerodynamic channel of

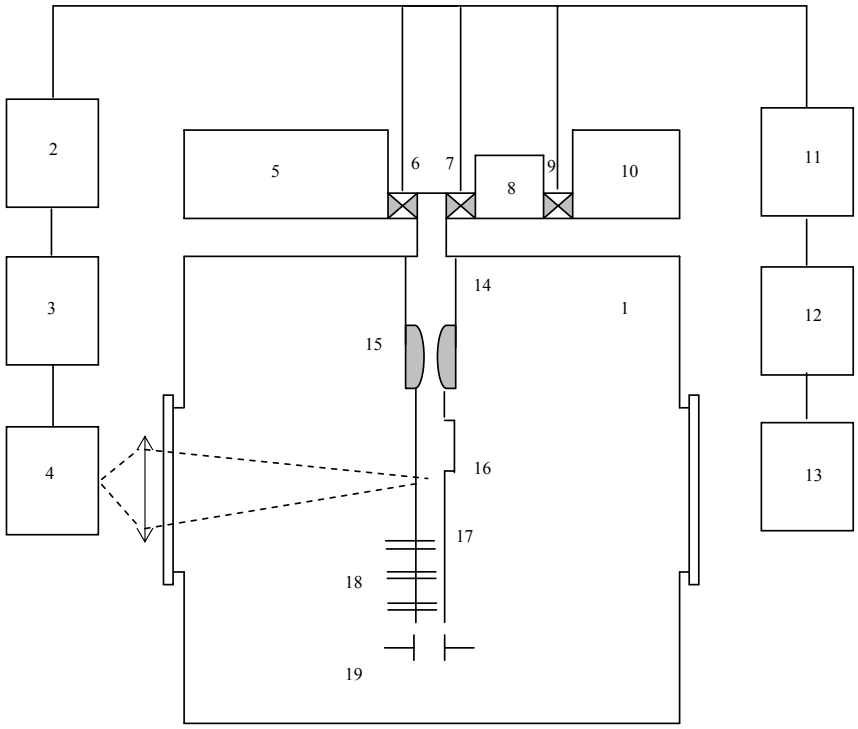

Fig. 2.7. Experimental set-up. 1 – vacuum chamber; 2 – synchronization unit; 3 - *CCD* sensor or photomultiplier tube; 4 – monochromator; 5 - air high pressure receiver; 6,7 - electric hydraulic valves; 8 – propane-butane high pressure receiver; 9 – valve; 10 - high-pressure cylinder with propane-butane, 11 – high-voltage power supply; 12 – digital oscilloscope; 13 - computer; 14 - mixer; 15 - Laval nozzle; 16 - dielectric insert; 17 - rectangular aerodynamic channel; 18 – double probes; 19 – capacitor.

supersonic flow of a combustible propane-butane-air mixture with flow Mach number $M=2$ was calculated and manufactured. The special system of attachment and precise spatial regulation of an aerodynamic channel position was designed and manufactured. The designed system has allowed hardly fixing the aerodynamic channel in a given place of a vacuum discharge chamber. The channel was hermetically fixed on the top flange of vacuum cylindrical chamber.

Two electromechanical valves connected with a high-pressure air receiver ($p_o=1\text{-}6$ *atm*) and a high-pressure propane-butane receiver ($p_g=5$ *atm*) are fastened on a flange from the external side of the chamber. At opening electromechanical valves the air and propane-butane got in the mixer and through the transitive chamber propane-butane-air mixture acted on an entrance of rectangular Laval nozzle where the supersonic stream of a propane-butane-air mixture with flow Mach number $M=2$ was formed. The nozzle exit section is equal to section of the rectangular aerodynamic channel.

In wide wall of the channel the dielectric insert was mounted. In experiments two inserts were used. The first formed a rectangular cavity $L=70$ *mm* in length, $b=18$ *mm* in width and adjustable depth $h=0\text{-}20$ *mm*. The second - *50 mm* in length, *23 mm* in width and adjustable depth $h=0\text{-}20$ *mm*. With the help of high-voltage cables the voltage was led to the electrodes fixed flush-mounted in a dielectric insert. The surface pulsed discharge in supersonic flow was formed on a dielectric flat plate placed on a bottom of a cavity of aerodynamic channel at air pressure in the vacuum chamber $p=150$ *torr*, air pressure in the receiver-chamber (the high-pressure system) $p_o=1{,}5\text{-}3{,}0$ *atm*, propane-butane pressure $p_g=3{,}0\text{-}5{,}0$ *atm*.

Two supply units for obtaining of the electrode discharge on a surface of a plate placed at supersonic airflow was designed and created.

1. The first source gave out voltage $U=5\text{-}30$ *kV*, pulse duration $\tau=1\text{-}1000$ *μs*, discharge current $i=1\text{-}20$ *A*.
2. The second source gave out voltage $U=2{,}5\text{-}4{,}5$ *kV*, duration of a pulse could change from *0,1* up to *2,0 s*, discharge current changes from 1 up to *30 A*.

The parameters of the first supply units allow creating the electrode surface discharge in supersonic airflow at two modes:

1. A mode of single pulsed discharge at pulse duration up to 1 ms, maximal pulsed power $W_p \leq 1$ *MW*.
2. A mode of pulsed-periodic discharge at pulse duration $\tau=10\text{-}300$ *μs*, pulse repetition frequency $f=10\text{-}100$ *Hz*, mean power consumption about $W_m \leq 1$ *kW*.

The parameters of the second supply units allow creating the electrode surface *DC* discharge in supersonic airflow at maximal input power *10 kW*.

The high-voltage pulses with the help of a high-voltage cable through the specially designed a vacuum cut-off point was lead to electrodes built-in flush into a dielectric plate. The special measures for avoidance of an electrical breakdown on the opposite surface of a dielectric plate outside of supersonic flow were undertaken. It was possible to adjust the cavity depth from *0* up to *20 mm* displacing a plate in direction perpendicular to supersonic flow one.

The synchronization system allows inputting air, propane-butane or air-propane-butane mixture into discharge chamber with fixed delays under the relation to each other. The developed synchronization system allows to create also the surface discharge in practical a constant mode (τ*=0,1-2,0 s*), or in a mode of a long single pulse (τ*<1000 μs*), or in a mode short periodical pulses (τ<100 μs), or in programmable regime. In the latter case the discharge is created in the mixed mode, that is the gas breakdown is fulfilled in a mode of short periodical pulses (τ*<10 μs*), and the basic energy pumping occurs during action of a long pulse. Thus it is possible to change in a wide range of the pulse duration, frequency of their following, a time delay between a pack of short pulses and a pumping pulse, number of pulses in a pack.

The aerodynamic channel of *40 cm* in length of rectangular section of *9x18 mm*^{2} with a stagnant zone as a cavity in a wide wall of the channel was used in the first experiments on ignition of a propane-air mixture. The surface pulse-periodic discharge in supersonic flow was created on the dielectric plate placed in a stagnant zone of the aerodynamic channel at air pressure in the chamber *p=150 torr*, pressure in air receiver *p=2 atm*, pressure in propane receiver p_g*=5 atm*, voltage on electrodes *U=20 kV*, discharge current *i=8-16 A*, pulse duration τ*≤1 ms*.

The structure of the discharge in a cavity differs from structure of the surface discharge. It is observed a stream turbulization, the wall boundary layer separation. The discharge is spread in two directions both upstream and downstream. The recirculation area with a vortex movement about a forward wall of a stagnant zone is formed.

A cavity has allowed us to use a direct current power supply unit with voltage *U=5 kV* for creation of the surface discharge. With the help of this source it is impossible to create the discharge in free stream or the surface discharge in the channel without a stagnant zone, as its voltage is not enough for maintenance of the free discharge in supersonic flow. However the source allows to support the surface discharge in a cavity during time *t=1-2 s*. The low-current

($i<10\ mA$) high-voltage pulsed source, generating high-voltage pulses ($U=20\ kV$) by duration of $\tau=10\text{-}50\ \mu s$ and repetition frequency of $100\ Hz$ was used for breakdown of a discharge gap.

A boundary layer renders the big influence on structure of a stream in the narrow aerodynamic channel ($s=9x18\ mm^2$). It is possible to lock-out of the channel under certain conditions. Therefore for reduction of this effect the further experiments were carried out in the second aerodynamic channel. The general view of the aerodynamic arrangement for investigation of ignition of supersonic flow of gaseous fuels is given in *Fig. 2.8*.

The arrangement was hermetically fixed on the top flange (1) of vacuum cylindrical chamber of *1 m* in diameter and of *3 m* in length. Two electromechanical valves connected with a high-pressure air receiver ($p_o=1\text{-}6\ atm$) and a high-pressure propane receiver ($p_g=5\ atm$) are fastened on a flange from the external side of the chamber. At opening electromechanical valves air and propane got in the mixer (2) and through the transitive chamber (3) propane-air mixture acted on an entrance of rectangular Laval nozzle (4) where the supersonic stream of a propane-air mixture with flow Mach number $M=2$ was formed. The nozzle exit section $s=12,5x23\ mm^2$ is equal to section of the rectangular aerodynamic channel (7). In a wide wall of the channel the dielectric insert (5) forming a rectangular cavity *50 mm* in length, *23 mm* in width and adjustable depth $h=0\text{-}25\ mm$ was mounted. With the help of high-voltage cables (6) the voltage was led to the electrodes fixed flush-mounted in a dielectric insert (5).

The general back, front and side views of the second aerodynamic channel one can see in *Fig. 2.9*.

Initially the fuel system calibration has been fulfilled for various geometry of supersonic nozzle. Calibration of the second mass consumption of air dm_{air}/dt and gaseous fuel (propane-butane mixture) dm_{gas}/dt has been get. With this purpose the initial and final pressures were measured in the discharge chamber and reservoirs of a high pressure of air and a propane-butane mixture. Knowing time of one start-up, a ratio of volumes of the discharge chamber ($V_c=3\ m^3$), reservoir of a high pressure of air ($V_{r\_air}=0,2\ m^3$) and reservoir of a high pressure of gaseous fuel ($V_{r\_gas}=0,01\ m^3$) it is possible to measure dependences of the second mass consumption of air and gaseous fuel as function of initial pressure of air and gas. Received in this way standard curves are submitted in *Fig. 2.10* and *Fig. 2.11*.

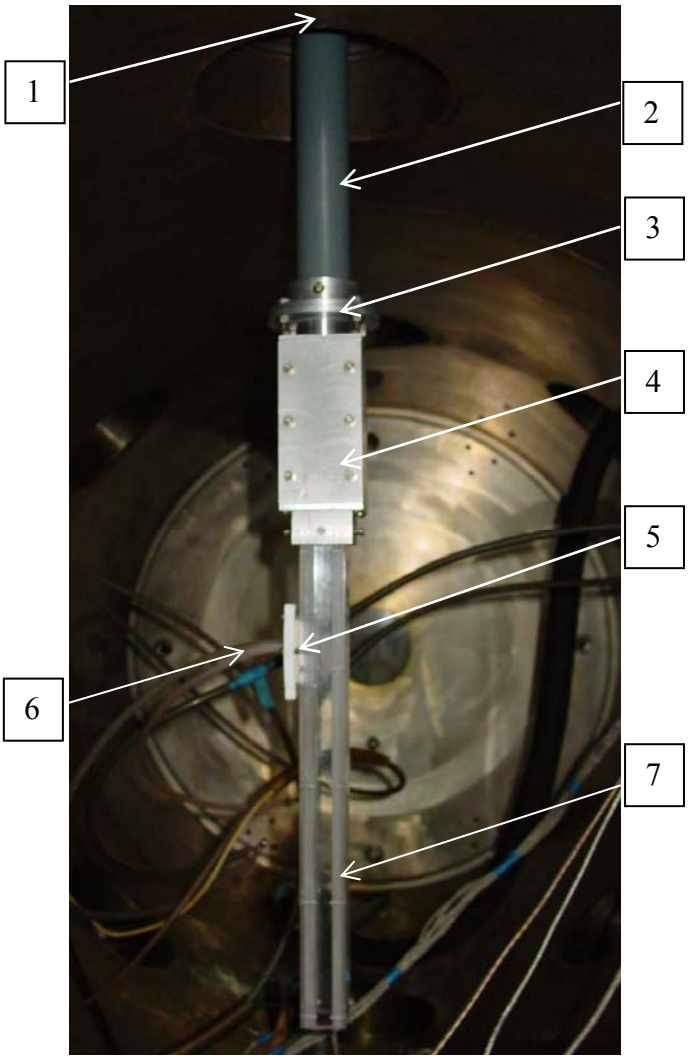

Fig. 2.8. Common view of the aerodynamic arrangement (side view). 1 - top flange of the vacuum cylindrical chamber; 2 - mixer; 3 - transitive chamber; 4 - Laval nozzle; 5 - dielectric insert; 6 - high-voltage cables 7 - rectangular aerodynamic channel.

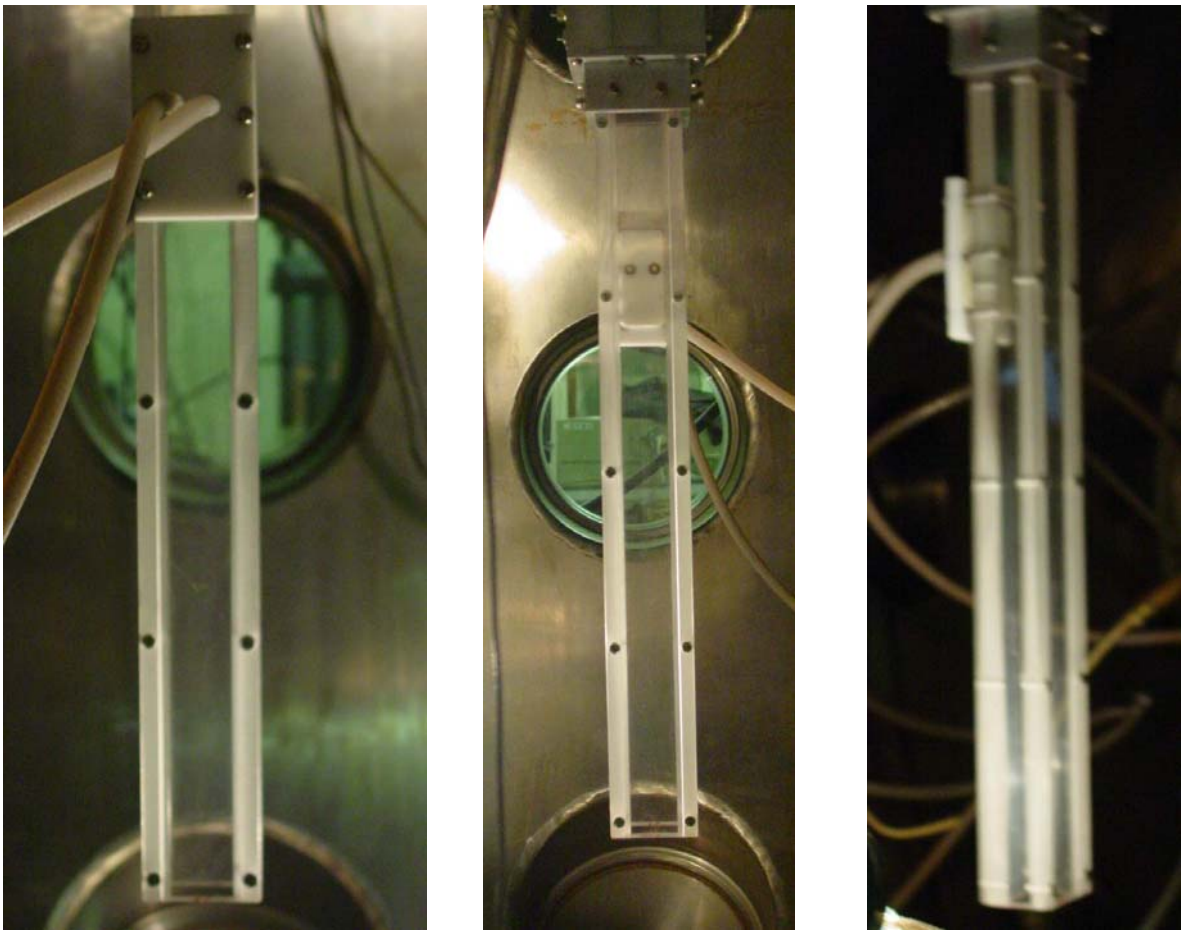

1 2 3

Fig. 2.9. The general view of the second aerodynamic channel
(1 – back view; 2 - front view; 3 - side view).

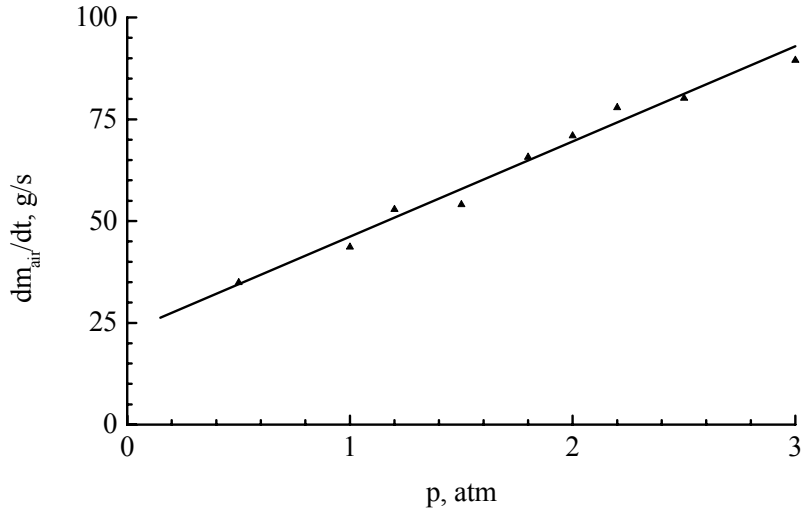

Fig. 2.10. Dependence of the second mass consumption of air on pressure into reservoirs of a high pressure of air.

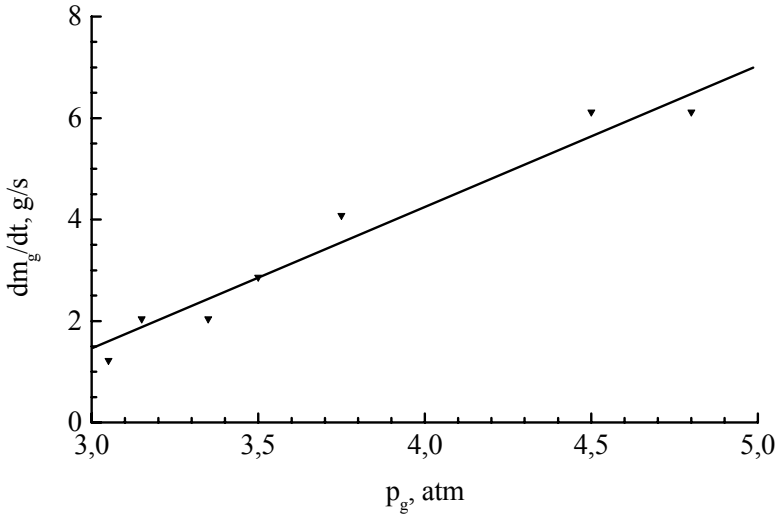

Fig. 2.11. Dependence of the second mass consumption of gas on pressure into reservoirs of a high pressure of propane-butane.

CHAPTER III
DIAGNOSTICS METHODS

3.1. Registration of the spectral characteristics of gas discharges

The monochromators *DFS-12* (return linear dispersion *0,5 nm/mm*), *MDR-3* (return linear dispersion *1,3 nm/mm*) and spectrograph *STE-1* (return linear dispersion changes in diapason *0,3-1 nm/mm*) were used at research of the spectral characteristics of gas discharges in supersonic flow of air, hydrogen and air-propane mixture. The block-scheme of optical measurements is shown in *Fig. 3.1*. The radiation of plasma from determined cross section of the gas discharge plasma or flame (2) through the system of lenses (4) and mirrors (5) was focused on an entrance slit of monochromator (6). The focal lengths of lenses were chosen so that to receive the reduced image of the channel on an entrance slit. Either the *CCD* image sensor (7) or the highly sensitive photoelectronic multiplier tube (10) were fixed in the focal plane of the monochromator or spectrograph. The *CCD* image sensor signal was in a direct proportion to the light intensity in the spectral region of *300-900 nm*. The electric signal from this sensor was coded by an analog-digital converter (8) and then stored in a personal computer (9) as an array of numeric data. Use of the photoelectronic multiplier allows us to determine a temporary behaviour of intensity of various elements radiation in the fixed places of the aerodynamic channel. Use of the multichannel *CCD* image sensor of a spectrum allows to fix or spectrum of radiation in the fixed place of the aerodynamic channel or spatial (longitudinal) distribution of radiation at fixed wavelength. Thus in the first case the multichannel *CCD* image sensor was established on the focal plane of the monochromator perpendicularly to the image of its entrance slit, and in a second case - parallel to it. Both the spectral calibration of the monochromator and spatial calibration of recording system was previously carried out. For measurement of spatial distributions of parameters of plasma the image of the discharge with the help of lenses was focused on an entrance slit of the monochromator parallel to it.

The electronic analyzer of optical spectra on base of a personal computer registers plasma radiation in visible, ultraviolet and infrared spectral ranges. The system is designed on base of personal computer. The sensor of plasma radiation on base of *CCD* image sensor forms a video signal directly proportional to the radiation intensity in the spectral band *300-900 nm*. The video signal is coded by an analog-to-digital converter situated on an interface card and is sent to the

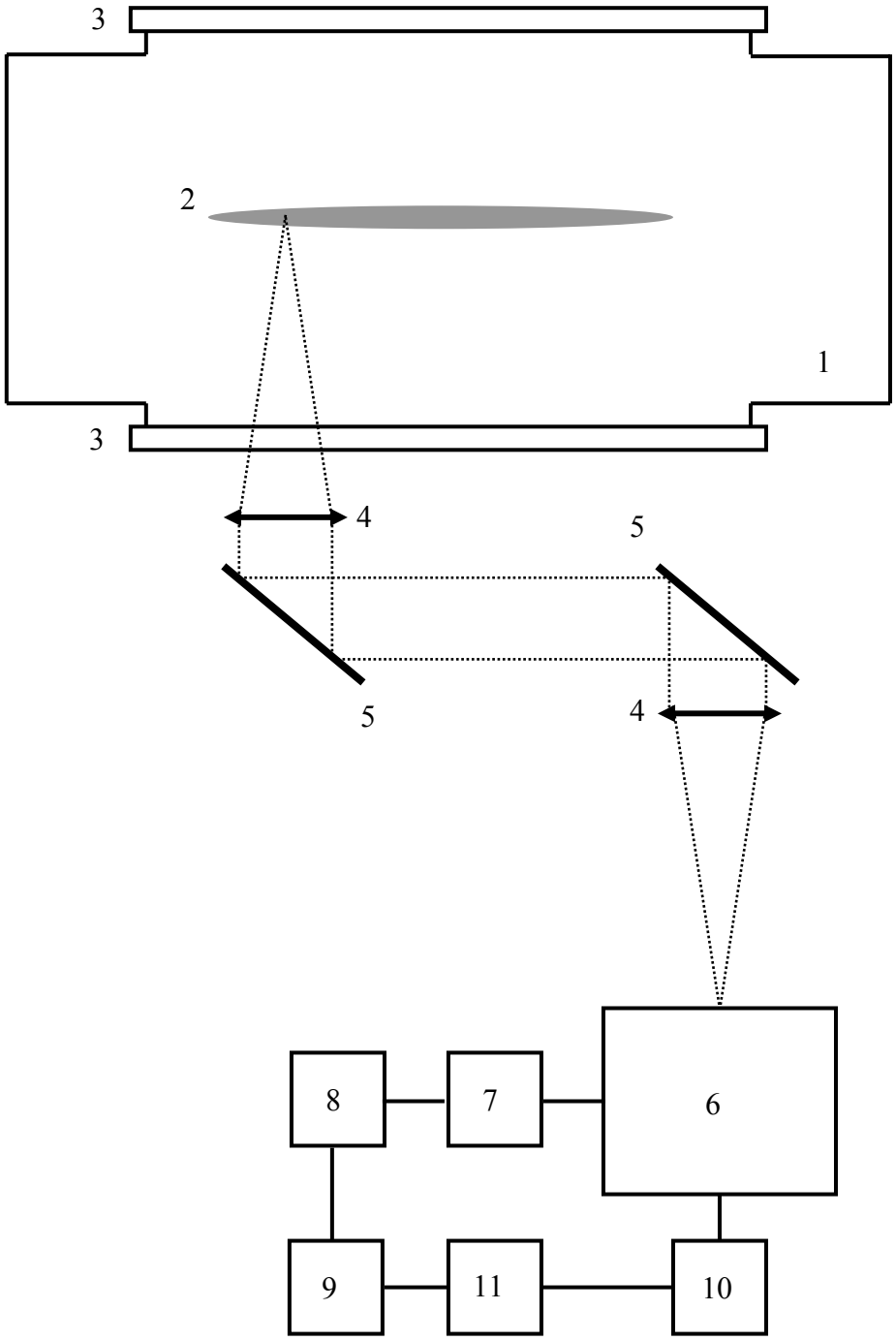

Fig. 3.1. The block diagram of optical measurements. 1 – vacuum chamber; 2 – discharge plasma or flame; 3 - side-viewing windows; 4 – lenses; 5 – mirrors; 6 – monochromator or spectrograph; 7 – *CCD*; 8 - interface card; 9 – personal computer; 10 - photomultiplier tube; 11 – oscillograph.

PC memory as an array of data. The discharge spectra can be visualized on the monitor or printed out with use of program codes. The system can operate in two regimes: synchronous and asynchronous. At synchronous operation the pulses of discharge are synchronized with the *CCD* cycles of exposition and pickup. This regime allows to research the properties of pulsed discharges or to integrate the information on pulse-periodical discharges. The asynchronous operation yields spectra that are averaged during all the time of exposition, it is useful for research of *DC* or *AC* discharges.

A schematic design of the device is shown on *Fig. 3.2*. *CCD* image sensor Toshiba *TCD 1300D* is used. The video signal formed by the *CCD* is passed to a broad-band differential amplifier for compensation of a constant component and amplification to the level sufficient for further coding by the analog-to-digital converter. Drivers of digital signals are necessary for formation of *CCD* controlling pulses.

The interface card (*Fig. 3.3*) contains a *12*-bit analog-to-digital converter, a quartz generator and a scheme of generation of synchronizing pulses for controlling of *CCD*, a universal parallel interface of control of executive devices (valves, pumps etc.) and an interface logic for fitting the card with the *ISA* bus.

As example an experimental spectrum of band (0;2) $\lambda=380,5\ nm$ of a second positive system of nitrogen, registered by the developed system, shows in *Fig. 3.4*. Registration time for one frame is *20 ms*. Integration of signals over several periods of *CCD* scanning and a digital low frequency filtration was applied for suppression of noises of the amplifier and of the thermal noise. The received after suppression of noises spectrum of the same band is shown in *Fig. 3.5*. The spectral data files were processed with use of program utilities of the shell *LabView* (*National Instruments*). During one experiment (duration *2 s*) several spectra were registered, that made it possible to measure the gas and vibration temperatures with temporary resolution about *20 ms*.

3.2. Spectral methods of measurement of gas temperature

Information about gas translation temperature T_g is important for study of plasma processes. The simplest possible case for molecular plasma corresponds to local thermodynamic equilibrium, then $T_g=T_V=T_R$, here T_V and T_R are vibration and rotation temperatures, respectively. T_V and T_R are parameters of fitting of population of vibration and rotation energy states of molecules to Boltzmann function, they characterise distribution function of molecules. Both T_V and T_R can be extracted from plasma radiation spectra.

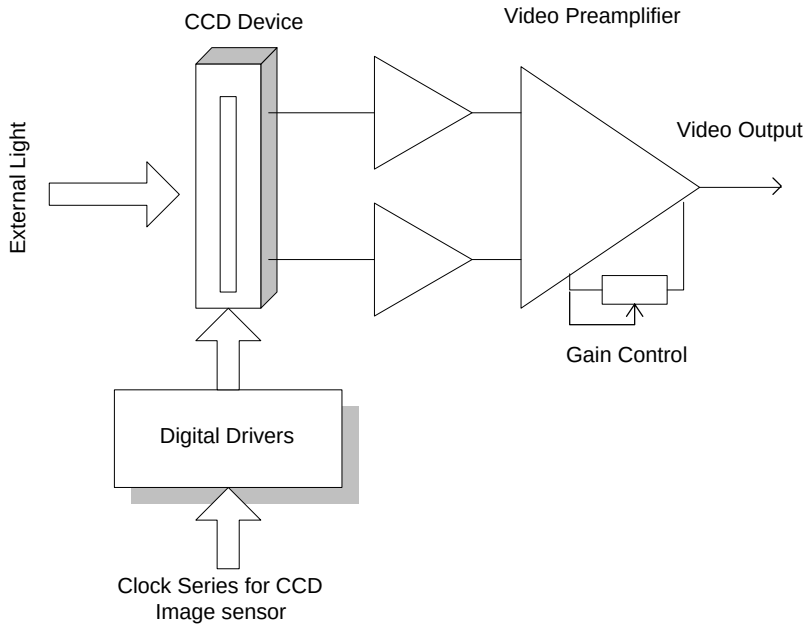

Fig. 3.2. Schematic design of the receiver of electronic analyzer of optical spectra.

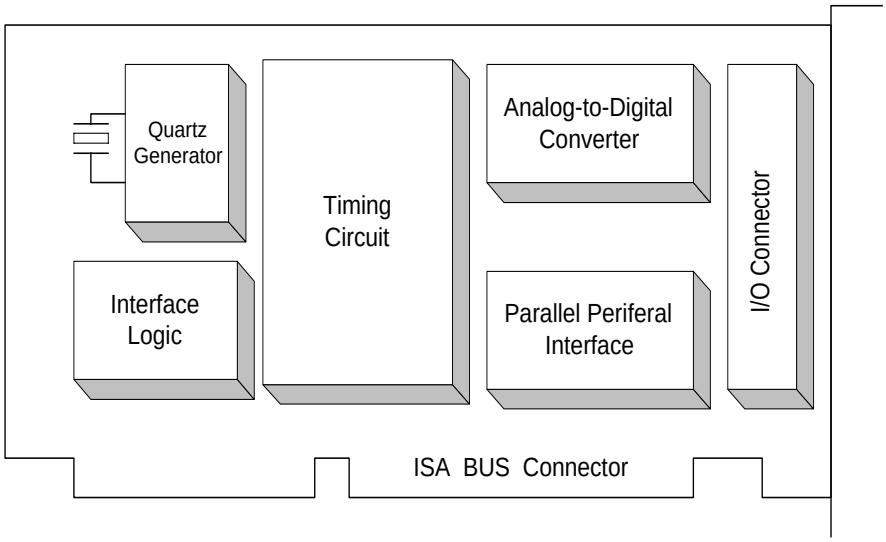

Fig. 3.3. Interface card.

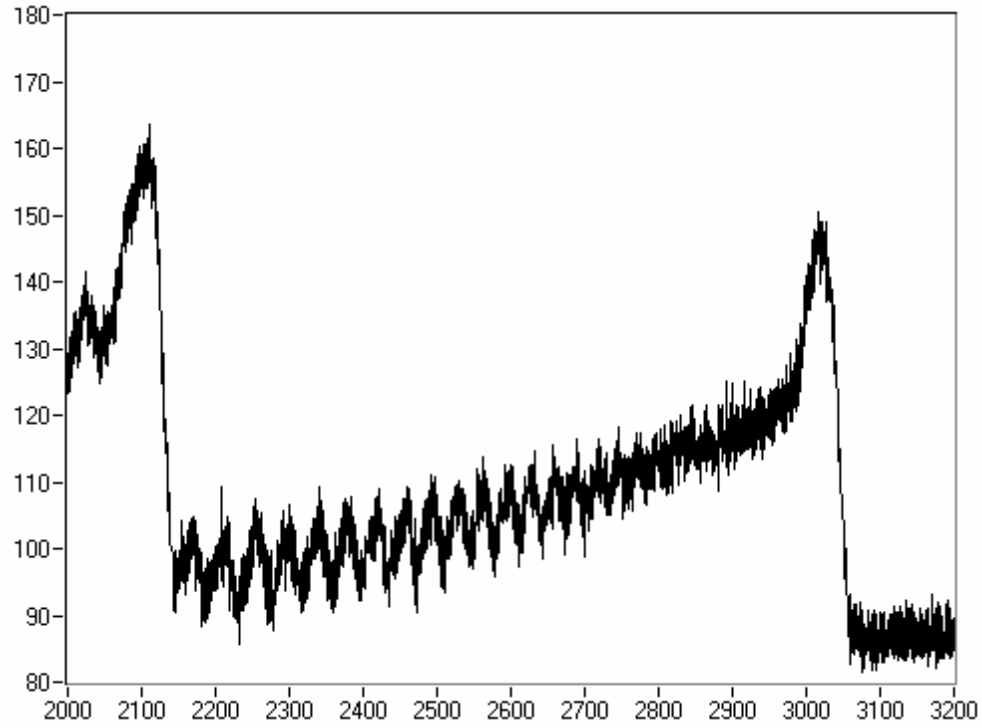

Fig. 3.4. Spectrum of the band (0;2) λ *=380,5 nm* of the second positive system of molecular nitrogen (no noise suppression).

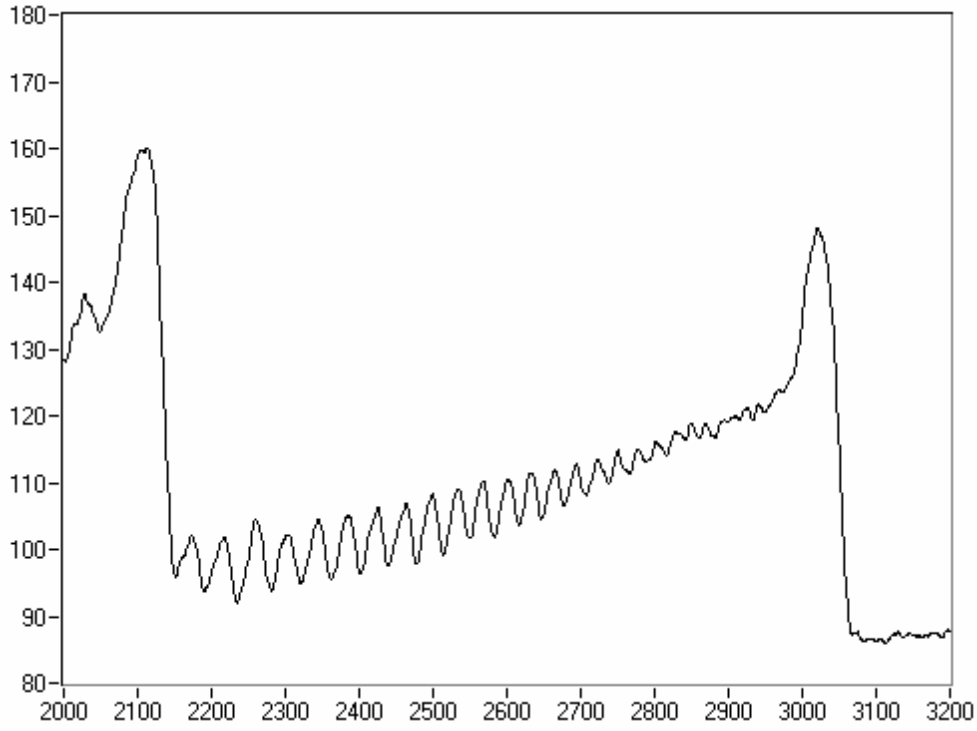

Fig. 3.5. The same spectrum as in *Fig. 3.4* after noise suppression.

In non-equilibrium plasmas T_g can be also determined on base of measurement of T_R. Spectra of plasma radiation provide information about rotation temperatures T_R^* of molecules in excited electron states. The dependence of T_R^* on intensity of a rotation structure spectral line I_{lk} that corresponds to a transition between *l-th* and *k-th* states is given by a formula

$$\frac{k_B}{B^*} ln \frac{I_{ik}}{i \nu_{ik}^4} = C - \frac{1}{T_R^*} j(j+1), \tag{3.1}$$

here k_B is Boltzmann constant, j is a total molecular moment of momentum, i is a quantum mechanical coefficient of intensity, ν_{lk} is the frequency of radiation quantum, C is a constant. One can extract T_R^* by plotting a function $(k_B/B^*)ln(I_{lk}/i\nu^4_{ik})$ over $j(j+1)$, and measuring its slope $tg\alpha$:

$$T_R^* = \frac{1}{tg\,\alpha}. \tag{3.2}$$

For a stable molecule a possibility of change its rotation energy at excitation is negligible, and rotation distribution functions for excited and basic molecular states are identical, $T_R = T_R^*$. Effective exchange of translation and rotation energies at collisions results in equality of T_g and T_R of molecules in basic electron state. But at realistic conditions there are some peculiarities that must be paid account to. If molecules take part in plasma chemical reactions, a part of their activation energy can transfer to rotation energy those results to distortion of initial rotation distribution function, and $T_R \neq T_R^*$. It is especially characteristic to chemically active radicals. Another source of errors is bound with the fact that spectra yield not T_R but B^*/T_R, here B^* is the rotation constant for upper state at radiation transition. At electron impact excitation of this state, rotation energy distribution can be conserved, but it corresponds to a temperature

$$T_R = T_g \frac{B^*}{B^o}, \tag{3.3}$$

here B^o is the rotation constant for the basic state.

Thus, stable molecules with $B^* \approx B^o$ should be chosen for measurement of T_g. The second positive band of nitrogen is widely used. Here one can take ν^4_{lk} to be a constant (the corresponding error $\approx 0.5\%$ is negligible), $B^* = 1{,}826$; the formula for T_R looks like

$$0{,}89\, lg \frac{I_{ik}}{i} = C - \frac{1}{T_R} j(j+1). \tag{3.4}$$

In number of work it is suggested to determine the gas temperature of nitrogen at high pressure on base of unresolved cyan bands with threshold wavelengths *388,3 nm* and *387,1nm*.

At the present experiments cyan is generated at model erosion. Three ways of temperature measurement are available. These methods are based on: 1) – ratio of integrals of radiation of the two bands; 2) – ratio of threshold intensities of these bands; 3) – distribution of rotation transition intensities of (0;0) band with threshold wavelength *388,3 nm*.

3.3. Method of measurement of gas temperature by the non-resolved rotary structure of molecular bands

For definition of gas temperature the method relative intensities of rotary lines of any vibronic band of a molecular spectrum can be used [1]. However under conditions of nonequilibrium low-temperature plasma this method requires the additional analysis. For its applicability it is necessary, that distribution of molecules on rotary levels of the electron-excited state was described by Boltzmann's function with the rotary temperature equal to gas temperature. At that the expression for intensity of a line in absence of reabsorption is well-known:

$$I_{j'j''} = const \cdot \nu^4_{j'j''} \; exp\left\{-\frac{hcF(j')}{kT}\right\} S_{j'j''}, \qquad (3.5)$$

where $I_{j'j''}$ is intensity of a rotary line for transition $j' \to j''$, j' and j'' are rotary quantum numbers of the top and bottom electronic states accordingly; $\nu_{j'j''}$ is frequency of transition $j' \to j''$; $S_{j'j''}$ is the factor of intensity determining relative probability of transition $j' \to j''$, $F(j')$ is energy of a rotary term for the excited electronic state; *h* is Planck's constant; *c* is speed of light; *k* is Boltzmann's constant; *T* is gas temperature. Temperature of gas usually determine from expression (3.1), having measured relative intensity of completely resolved rotary lines.

Gas temperature strongly influences on the flow parameters in the area of a boundary layer existing near body surface streamlined by supersonic airflow. However the measurement of the gas temperature by spectroscopic method (look previous section 3.2) under condition of a discharge in supersonic airflow, and also in a flame arising at ignition and burning of a mixture of combustible gases with air, is difficult task because of small intensity of a registered signal. In experiment it is necessary to use high aperture spectrographs. The discharge spectra are recorded with usage of a broad entrance slit. It results that the fine rotational structure of molecular bands is not separated and gas temperature measurement accuracy is insufficient. The problem has appeared to upgrade widely applicable method of gas temperature measurement. Thus the

upgraded method of measurement of gas temperature would need to be applied not only to experiment to discharge in supersonic airflow, but also in each concrete experiment, when it is impossible to get required for measurement of gas temperature the separated fine rotational structure of molecular bands.

Let's consider for example the second positive system of molecular nitrogen. In the top and bottom conditions of transition $C^3\pi_u \to B^3\pi_g$ the intermediate bound case is realized: for weak rotation the case *"a"*, at increase in rotation occurs fast transition to case *"b"* [1]. Let's enter the designations F_1, F_2, F_3, f_1, f_2, f_3 - the rotary terms concerning to components ${}^3\pi_0$; ${}^3\pi_1$ and ${}^3\pi_2$ conditions C and B (designations *"a"* bound are used). For rotary terms the following expressions are used:

$$F_1(j);\ f_1(j) = B_v[\,j(j+1) - \sqrt{z_1} + 2z_2\,] - D_v(j-0{,}5)^4,$$

$$F_2(j);\ f_2(j) = B_v[\,j(j+1) + 4z_2\,] - D_v(j+0{,}5)^4, \qquad (3.6)$$

$$F_3(j);\ f_3(j) = B_v[\,j(j+1) + \sqrt{z_1} - 2z_2\,] - D_v(j+1{,}5)^4,$$

where $z_1 = Y(Y-4) + \frac{4}{3} + 4j(j+1)$,

$$z_2 = \frac{1}{3z_1}\left[Y(Y-1) - \frac{4}{9} - 2j(j+1)\right],$$

$$Y = \frac{A}{B_v},$$

where A is constant of spin-orbital splitting. Each rotary term is doublet due to Λ-doubling. Components are designated as F_j, f_j and F_j', f_j'.

Values of molecular constants are presented in *Table 1*.

Table 1.

v	B_v	$D_v \cdot 10^6$	Y_v	A	$\Delta G(v)$	v	B_v	$D_v \cdot 10^6$	Y_v	A	$\Delta G(v)$
$C^3\pi$						$B^3\pi$					
0	1,8149	6,7	21,5	39,0	1994,34	4	1,55509	6,9	27,0	41,9	1589,25
1	1,7993	6,8	21,5	38,5	1940,72	5	1,53676	7,0	27,3	42,0	1560,26
2	1,7694	7,3	21,4	37,9	1873,95	6	1,51787	7,2	27,6	41,7	1530,95
3	1,7404	8,5	21,1	36,8	1781,21	7	1,49896	7,3			1501,72
4	1,6999	1,25	20,3	34,5		8	1,47940	7,5			1472,40
$B^3\pi$						9	1,46016				1442,69
0	1,62849	6,4	25,9	42,3	1705,55	10	1,44124				1412,91
1	1,61047	6,5	26,2	42,2	1676,32	11	1,42132				1383,08
2	1,59218	6,7	26,4	42,0	1647,36	12	1,40150		29,4	41,3	
3	1,57365	6,8	26,8	42,2	1618,34						

According to the selection rules the following of 16 main branches for $C^3\pi_u \to B^3\pi_g$ transition are possible.

For *P(j)* branch:

$$P_i(j) = F_i(j-1) - f_i(j)$$

$$P_i'(j) = F_i'(j-1) - f_i'(j) \qquad (3.7)$$

where *i=1, 2, 3*.

For *R(j)* branch:

$$R_i(j) = F_i(j+1) - f_i(j)$$

$$R_i'(j) = F_i'(j+1) - f_i'(j) \qquad (3.8)$$

where *i=1, 2, 3*.

For *Q(j)* branch:

$$Q_i(j) = F_i(j) - f_i(j)$$

$$Q_i'(j) = F_i'(j) - f_i'(j) \qquad (3.9)$$

where *i=1, 2*.

The diagram of levels explaining thin structure of transition $C^3\pi_u \to B^3\pi_g$ of nitrogen molecule is given in *Fig. 3.6.*

Formulas for calculation of the factors of intensity taking into account that in $C^3\pi_u$ and $B^3\pi_g$ states the intermediate type of bound is realized are given in [2]. For a limiting case - such as bound case *"b"* formulas for $^3\pi_u \to ^3\pi_g$ transition are presented in [3]. As lead in [2] Calculations under various formulas have shown that already for *j>8* factors of intensity practically coincide (difference makes less than *1 %*). In this area j factors of intensity for lines *R*- and *P*- branches can be submitted the next formulas [3]:

$$S_{j-1,j} = \frac{(J-2)J(2J-1)}{(J-1)(2J-1)} \qquad \text{for } P_1(j),$$

$$S_{j-1,j} = \frac{(J-1)^2(J+1)^2}{J^3} \qquad \text{for } P_2(j), \qquad (3.10)$$

$$S_{j-1,j} = \frac{(J+2)J(2J-1)}{(J+1)(2J+1)} \qquad \text{for } P_3(j),$$

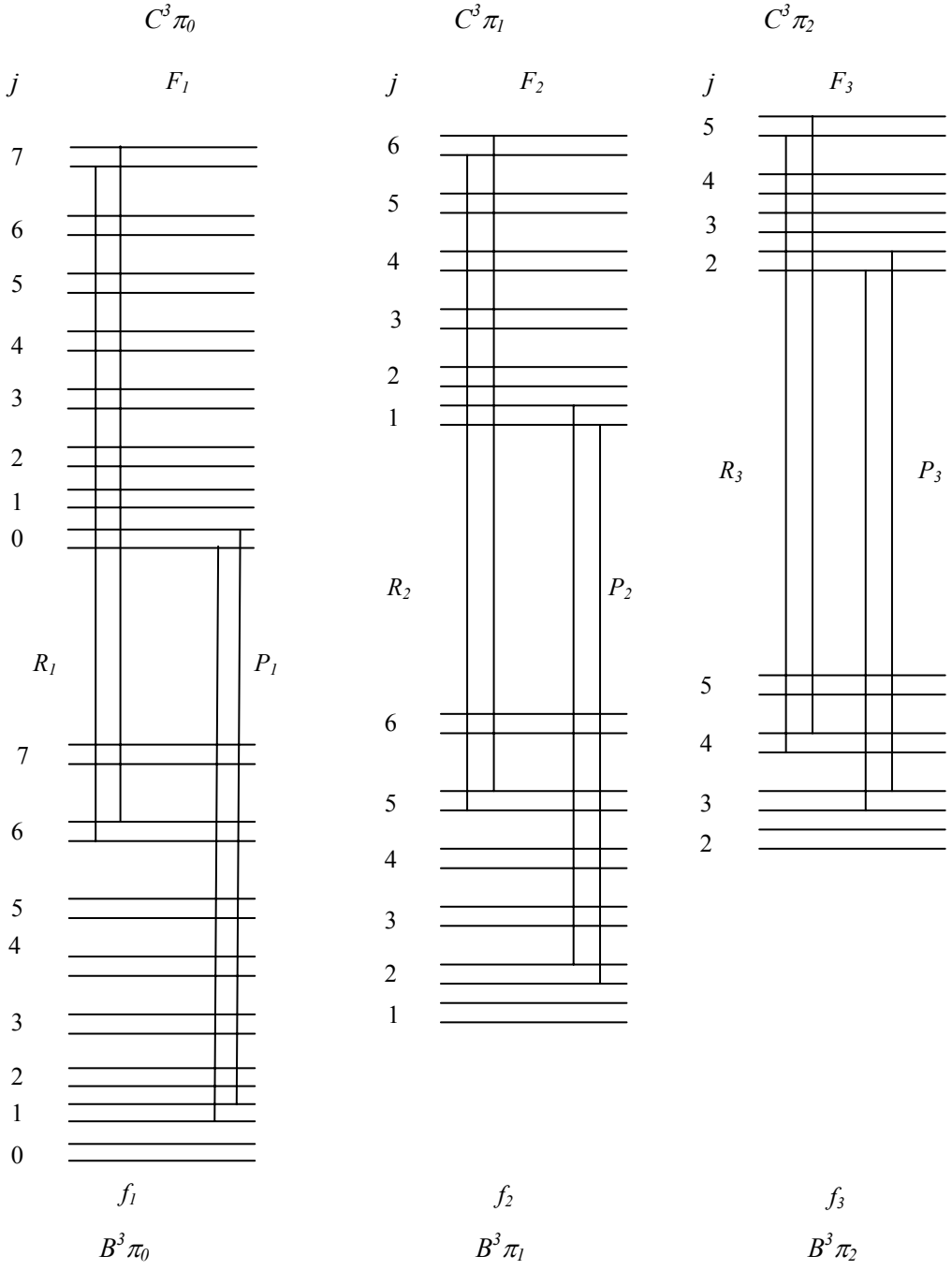

Fig. 3.6. Thin rotary structure of $C^3\pi_u \rightarrow B^3\pi_g$ transition for nitrogen molecule.

$$S_{j+1,j} = \frac{(J-1)(J+1)(2J+3)}{J(2J+1)} \quad \text{for } R_1(j),$$

$$S_{j+1,j} = \frac{(J+2)^2 J^2}{(J+1)^3} \quad \text{for } R_2(j), \qquad (3.11)$$

$$S_{j+1,j} = \frac{(J+1)(J+3)(2J+1)}{(J+2)(2J+3)} \quad \text{for } R_3(j).$$

Results of work [4] were used for spectra decoding. In [4] the frequencies of rotary lines are given.

The program of simulation of N_2, N_2^+, OH, C_2, CH, and CN spectra was designed. The synthesized spectra of molecular bands were calculated depending on gas temperature and for various values of the broadening factor in a source and instrumental broadening of the spectrograph.

At first the spectrum of radiation of the (0,0) band of the second positive system of nitrogen was calculated without taking into account any broadening factors at gas temperature T_g=*1000 K*. The result is given in Fig. 3.7. In the spectrogram one can see the triplet rotary structure and relative contribution of *P*- and *R*-branches in formation of the (0,0) band. Thus, at the given gas temperature a band head is basically defined by *P*-branch, whereas *R*-branch brings the main contribution in a band tail. However under experimental conditions it is impossible to receive completely resolved triplet structure of a spectrum at studying of the quickly proceeding processes in the pulsed discharge in supersonic airflow. It is connected to that fact, that, first, the spectral lines is strong broaden in plasma because of various mechanisms, and, second, under experimental condition it is necessary to register a spectrum with use of a wide entrance slit of the spectral device because of small intensity of a researched signal, that also results to some broadening of registered spectral lines

The calculated spectrograms of the (0,2) band of the second positive system of nitrogen at gas temperature T_g=*3000 K* and various values of broadening factor σ are submitted in *Fig. 3.8*. One can see that the value of the broadening factor strongly influences on spectrogram of the (0;2) band.

The temperature dependence of the general mistake of gas temperature definition on the non-resolved rotary structure at simultaneous registration of two rotary lines of the (0,2) band is submitted in *Fig. 3.9*. It is visible, that at low gas temperatures (T_g<*1000 K*) the mistake does not exceed *10 %*, whereas at high temperatures (T_g=*2000-3000 K*) it reaches about *20 %*.

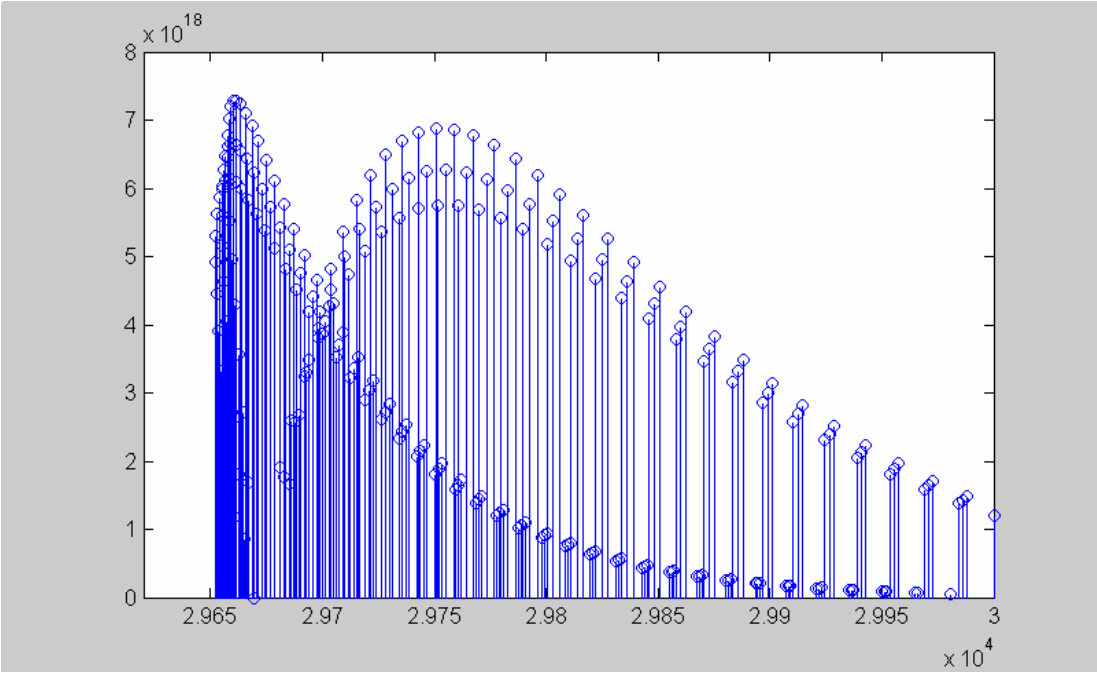

Fig. 3.7. The radiation spectrum of (0,0) band with wavelength λ=*337,1 nm* the second positive system of the nitrogen, calculated without taking into account any broadening factors at gas temperature T_g=*1000 K*.

1

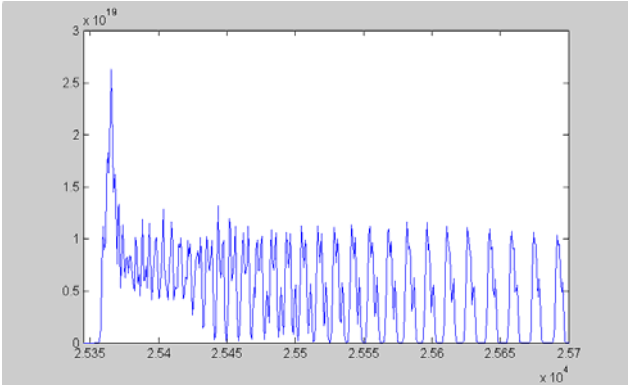

2

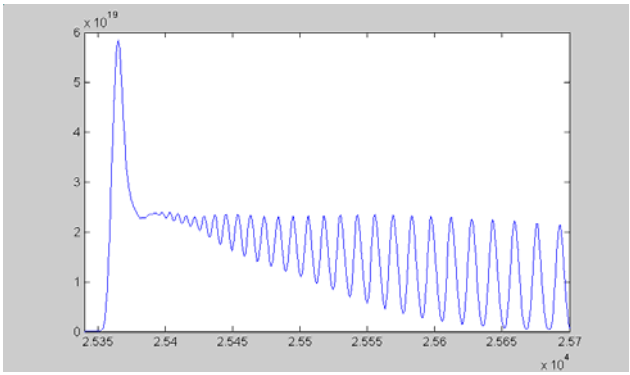

3

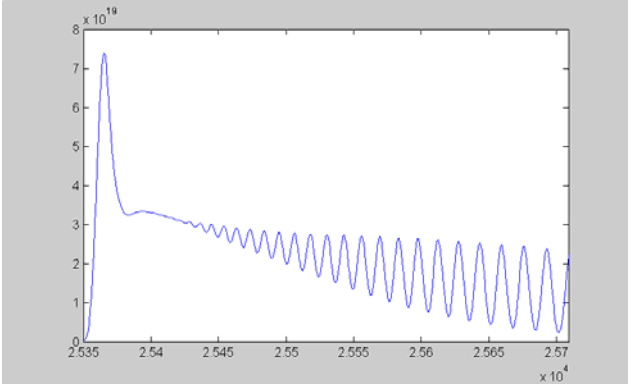

4

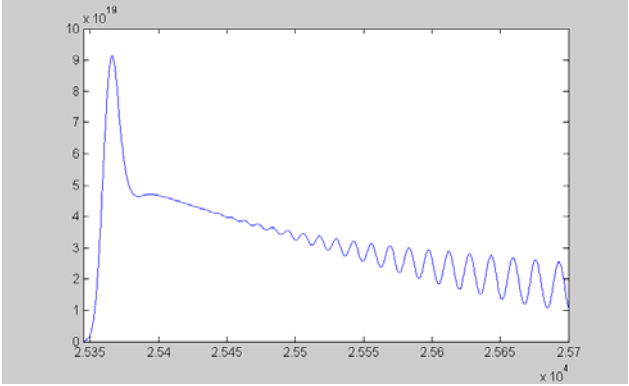

Fig. 3.8. Influence of the broadening factor on the calculated spectrograms of the (0,2) band with wavelength λ=*380,5 nm* of the second positive system of nitrogen at gas temperature T_g=*3000 K* and various values of broadening factor σ, cm^{-1}: 1–1; 2–10; 3–20; 4-40.

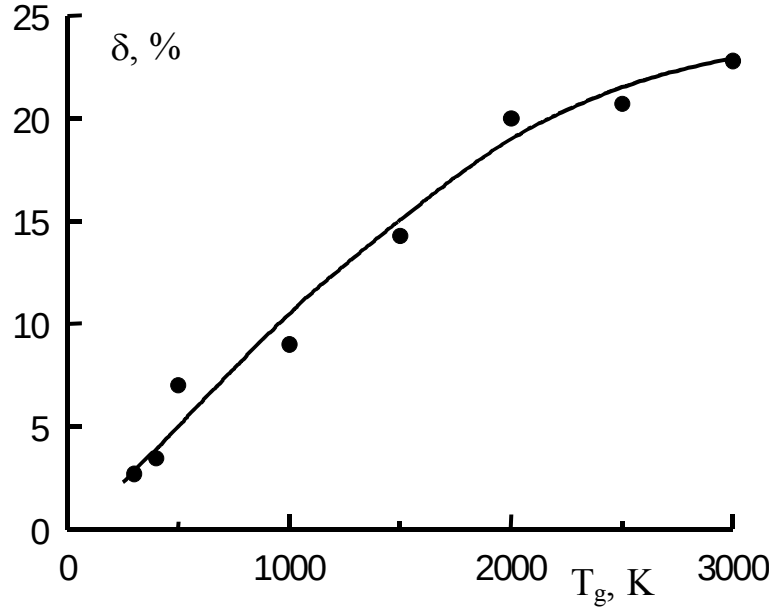

Fig. 3.9. The temperature dependence of the general mistake of gas temperature definition on the non-authorized rotary structure at simultaneous registration of two rotary lines of the (0,2) band of the second positive system of nitrogen (σ=*20 см*$^{-1}$).

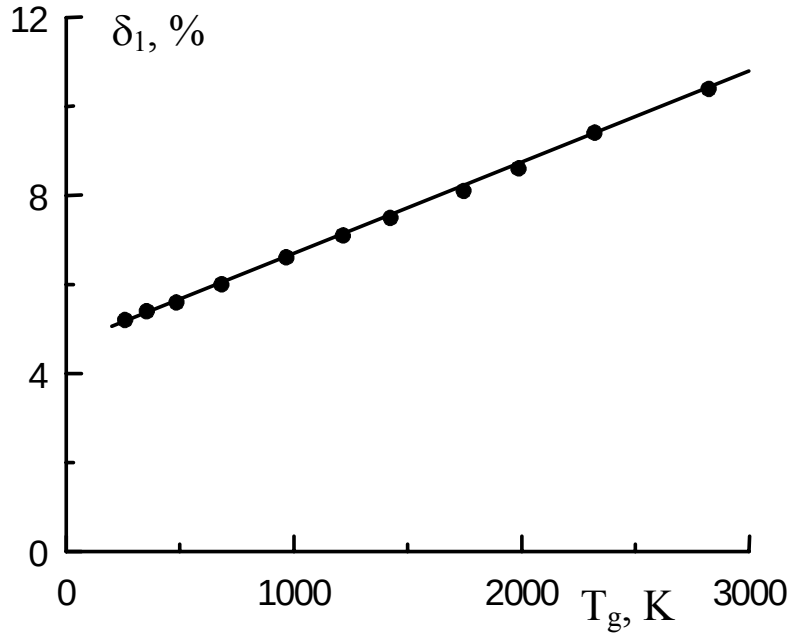

Fig. 3.10. Dependence of gas temperature determination mistake on the measured temperature at a mistake in monochromators adjustment Δj=*1*.

Let's estimate accuracy of gas temperature definition for a case of simultaneous registration only two lines of rotary structure of the (0,2) band the second positive system of nitrogen with use of two monochromators. We apply this method for registration of time dependences of gas temperature at use a photoelectronic multiplier as radiation receiver. Thus on an oscilloscope the time course of intensities of luminescence of two lines, for example, with rotary quantum numbers j_1 and j_2 are simultaneously registered. Let's assume, that monochromators are adjusted on registration, for example, spectral lines corresponding to rotary quantum numbers j_1+1 and j_2+1, but calculation is made for quantum numbers j_1 and j_2, that is each device is adjusted with mistake $\Delta j=1$. In this case the mistake of T_g definition linearly grows with increase in gas temperature from $\delta_1=5\ \%$ at $T_g=300\ K$ up to $\delta_1=10\ \%$ at $T_g=3000\ K$ (*Fig. 3.10*).

3.4. Spectral methods of measurement of vibration temperature

Vibration excitation in a molecular plasma as a rule affects ionization and gas heating. There is a method of determination of vibration levels population of nitrogen basic electron state $X^1\Sigma_g^+$. It is based on a measurement of radiation intensities in bands of the second positive nitrogen system. Conditions are pointed out, at which the electron state $C^3\pi_u$ is populated due to electron impact excitation of the basic $X^1\Sigma_g^+$ state. De-excitation of vibration levels of the state $C^3\pi_u$ is bound with radiation, because its characteristic time ($10^{-7}\ s$) is much less than that of vibration and rotation relaxation and of diffusion.

Let the vibration levels v''_X of the basic nitrogen electron state are distributed according to a function $f(v''_X)$, i.e.

$$n(v''_X) = n_o f(v''_X). \tag{3.12}$$

Then in case the conditions mentioned above are met, a stationary population of $C^3\pi_u$ vibration levels v'_C is given by

$$n_{v'_C} = \frac{n_e n_o}{A_{v'_C v'_B}} \sum_{v''_X} \left\langle \sigma v \right\rangle_{v'_C v''_X} f\left(v''_X\right), \tag{3.13}$$

here n_o is a number of molecules in $X^1\Sigma_g^+$ state with $v''_X = 0$; $\left\langle \sigma v \right\rangle_{v'_C v''_X}$ is a mean cross section of excitation of v'_C $C^3\pi_u$ levels, n_e is electron concentration, $A_{v'_C v'_B}$ is a probability of radiation of

the second positive nitrogen system, $v_B^{''}$ are vibration quantum numbers of $B^3\pi_g$ state.

As the process of excitation of the $C^3\pi_u$ vibration levels due to electron impact of the basic $X^1\Sigma_g^+$ state is fast in comparison with vibration period, these probabilities can be considered to be in a direct proportion to the Franc-Condon coefficients for the Tanaka system $C^3\pi_u \to X^1\Sigma_g^+$. Then the previous equation takes form

$$n_{v_C^{'}} = C\sum_{v_C^{'}} q_{v_C^{'}v_X^{''}} f\left(v_X^{''}\right), \tag{3.14}$$

here C is a constant independent on $v_X^{''}$.

At computation of the sum one can take only first 5 terms, because the population of the vibration levels is a steep falling function of v. Provided relative populations of the first 5 levels of the $C^3\pi_u$ state are known, one can calculate relative populations $v_X^{''}$ of the basic electron states as a solution of a set of equations

$$n_{v_C^{'}} = \alpha \sum_{v_X^{''}=0}^{4} q_{v_C^{'}v_X^{''}} n_{v_X^{''}}\ , \tag{3.15}$$

here α is a normalizing coefficient.

The relative populations of the $C^3\pi_u$ state levels can be determined experimentally with application of a usual method (on base of relative intensities of bands of the second positive nitrogen system $C^3\pi_u \to B^3\pi_g$).

Molecular spectroscopy gives the following formula for a radiation intensity of a electron-vibration band:

$$I_{v_C^{'}v_B^{''}} = C^{'} S_e n_{v_C^{'}} \nu^4_{v_C^{'}v_B^{''}} q_{v_C^{'}v_B^{''}}, \tag{3.16}$$

here S_e is a strength of electron transition, $q_{v_C^{'}v_B^{''}}$ are the Franc-Condon factors, $\nu_{v_C^{'}v_B^{''}}$ is a frequency of transition, C' is a constant independent on the quantum numbers $v_C^{'}$ and $v_B^{''}$. After taking logarithm, one can get

$$ln(n_{v_C^{'}}) = ln(C^{'}) + ln\frac{I_{v_C^{'}v_B^{''}}}{\nu^4_{v_C^{'}v_B^{''}} q_{v_C^{'}v_B^{''}}}. \tag{3.17}$$

Thus, one can get the relative populations $v_X^{''}$ and the vibration temperature of the nitrogen basic electron state on base of measurement of relative intensities of the electron-vibration bands $v_C^{'}$.

3.5. Spectral method of measurement of electron density

The Stark broadening effect in a stationary electrical field consists in splitting and displacement of spectral lines under action of an external electrical field. In the majority practically important cases an external field is not enough in comparison with an internal field of atom. In this case the influence of an internal field of atom can be considered as small indignation on atomic system. In plasma the radiating atom is under influence of high frequency fields of the charged particles. In the first approximation the electrical field of ions is possible to consider quasistationary, resulting to usual splitting of a line. The influence of electrons on atom, on the contrary, is possible to consider as sharp impact which is breaking off packet of fluctuations of radiating waves or, if the impact was weaker, changing a phase of fluctuations. As a result of electron impacts a line is broadened.

The statistical and shock theory are extreme approximations of the common theory of the Stark broadening of lines, in which at first the splitting a line is calculated because of quasistatistical action of ions, then the broadening of each components at the expense of shock interaction with electrons is taken into account. Structure of a spectral line receives by averaging on distribution of various ions fields. Thus, in the common theory the interaction both with ions and with electrons are taken into account. The central part of a line is well described in shock approximation, on wings prevails statistical ions broadening.

In [5] structures of a lines of hydrogen are theoretically designed for various temperatures and density of electrons, that allows reliably to measure n_e on width of a line, using a ratio

$$n_e = C(n_e,T_e)\ (\Delta\lambda)^{3/2}, \qquad (3.18)$$

where $C(n_e,\ T_e)$ is Stark constant, which is weak dependent on n_e and T_e. This ratio can be presented graphically as $ln(n_e)=f(ln\ \Delta\lambda)$. Most convenient for definition n_e is the H_β line. This is promoted by a number of the factors.

1. This line is located in spectral area, where the usual receivers of radiation have high sensitivity.
2. At concentration $n_e \geq 10^{13}\ cm^{-3}$ its broadening is great and its width it is possible to measure with the help of the usual spectral devices.
3. The accuracy of theoretical accounts of width of a line H_β is less than *5 %*, while accuracy of accounts for other lines of hydrogen of the order *10 %*.
4. The H_β line corresponds to transition between rather low laying levels. Therefore it is well radiated in plasma, even if the hydrogen is present as a small impurity, for example as

pollution of plasma.

In this work the concentration of electrons in the plasma of discharge in supersonic airflow was determined by spectral method from Stark broadening of a spectral line H_β with $\lambda=486,1\ nm$. Optical methods, which are widely used, require additional information on physical processes occurring in the plasma. When the electron density exceeds $10^{14}\ cm^{-3}$, Stark broadening of the hydrogen lines is much greater than broadening due to other effects.

Measurements were carried out at air pressure in the chamber *p=0,1-10 torr*. As a small impurity in the chamber the small amount of propane was added. Thus in a surface microwave discharge the effective decomposition of propane took place and hydrogen in amount sufficient for excitation of H_β line and registration of its profile was turned out.

The radiation from the discharge was projected by a system of lenses and mirrors (*Fig. 3.1*) to the entrance slit of the double monochromator *DFS-12* with a return linear dispersion of *0,5 nm/mm* and instrumental function of *0,015 nm* (*Fig. 3.11*). Dependence of apparatus function of the spectral device on width of an entrance split was determined at registration of width of a line *He-Ne* laser ($\lambda=632,8\ nm$). The output signal of the photomultiplier was entered either into a storing oscillograph or to a setup consisting of a time selector, two narrow-band amplifiers, a synchronous detector, a dc amplifier, and a strip chart recorder. The system enabled us to record the spectral line profile emitted by the pulsed-periodic surface microwave discharge.

3.6. Shadow graphics

It is known, that an input of energy in area of a boundary layer or the local heating of a plate surface in the field of a turbulent boundary layer result in noticeable reduction of a local coefficient of turbulent friction at the expense of decreasing of a transverse gradient of longitudinal flow velocity and increase of a displacement thickness. In the case of a surface microwave discharge the microwave field is localized in a thin near-surface layer that promotes the effective contribution of energy to plasma and fast gas heating, which should result in change of supersonic flow near a body surface.

For determination of a structure and Mach number of airflow the shadow installation was used. The optical scheme of set-up is given in *Fig. 3.12*. The incandescent lamp (power *30 W*) or flash lamp with a pulse duration $\tau=10\ \mu s$ were used as light sources for the shadow installation.

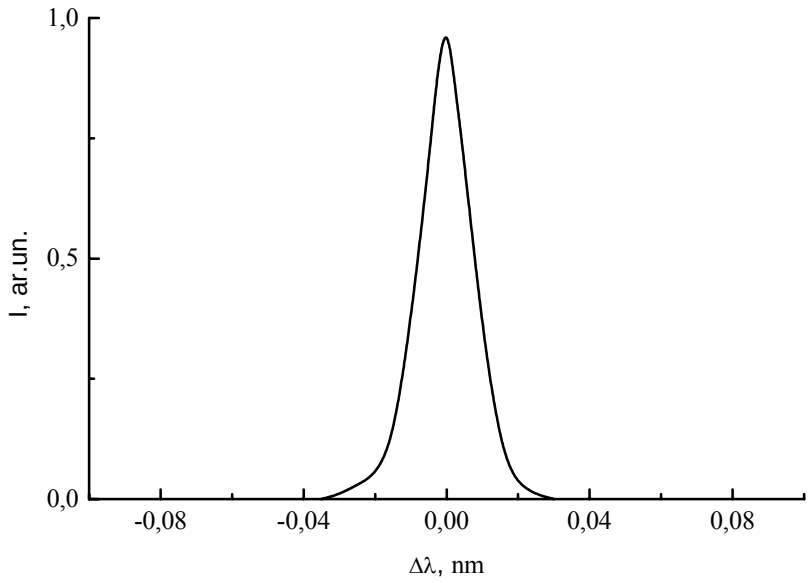

Fig. 3.11. Instrumental function of the double monochromator *DFS-12* (*Δλ=0,015 nm*). Width of an entrance slit of monochromator *δ=5 μ.*

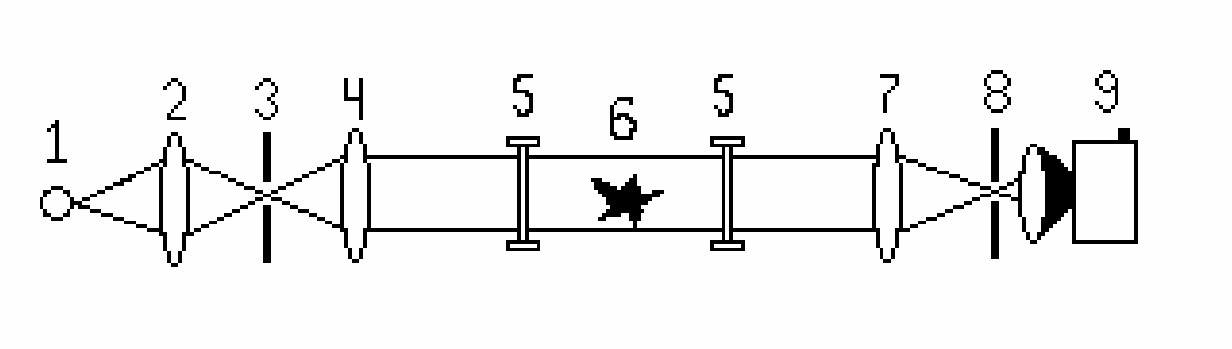

Fig. 3.12. The scheme of the shadow installation. 1 - flash lamp, 2 - converging lens, 3 - input diaphragm of the installation, 4 - long-focus objective, 5 - windows of vacuum chamber, 6 - inhomogeneous investigated object 7 - long-focus convergent lens, 8 - output diaphragm, 9 - camera.

The radiation of the lamp (1) through converging lens (2) was focalized on the input diaphragm (3) of the installation. The area of a round diaphragm equals *1 mm*^{2}. The converging lens (4) with focal length *150 cm* was placed on the other hand of the diaphragm (3) so that the diaphragm has appeared in its focal plan. Thus, on an output of this optical system the parallel beam of light by *15 cm* in diameter with homogeneous distribution of light intensity on beam section was formed. The parallel light beam, passing through the input window (5) of the chamber, the studied inhomogeneous area (6) and the output window (5) of the chamber, was directed to the output long-focus lens (7) of the installation. In a focal plan of the lens (7) there was the output diaphragm (8). The area of the round diaphragm (8) equals 1 mm^2. The shadow picture was recorded by the camera (9). Under the shadow picture we can determine the size and degree of the non-uniformity of investigated medium and study the process of burning of supersonic flow of combustible mixture.

With the help of the shadow graphic installation the interaction of supersonic airflow with the surface microwave discharge, created on an external surface (in a boundary layer) of the wedge dielectric body, was examined for check of the supposition that the surface microwave discharge in our conditions can render noticeable influencing on streamlining of model by supersonic airflow.

The pulsed microwave discharges with pulse duration no more than 100 μs were investigated. In this case it is obviously not possible to use the camera with time of exposure equals *30 ms* for registration without a time resolution, as the shadow photo of a body, streamlined by supersonic flow, strongly changes during time registration that result in impossibility of registration of effect. It is necessary to permit process in time. For this purpose the special pulse synchronization circuit, permitting to receive shadow graphics photos of investigated process with time resolution about *10 μs*, was designed.

Block-scheme of pulse synchronization circuit is given in *Fig. 3.13*. The crystal-controlled frequency divider (1) was basis of synchronization system. It developed periodic pulses with repetition rate from *0,5 Hz* up to *1 kHz* (epure 1 in *Fig. 3.14*). From an output of this device the periodic pulses came in on start of the synchronizing generator (6) (epure 2 in a *Fig. 3.14*) and on the coincidence circuit (2) (epure 4 in *Fig. 3.14*).

Signals from the generator (6) served, first, for start of a control oscillograph (12) and, second, with the certain delay (about 40-80 μs) for start of the entrance cascade of the generator of high-voltage pulses (7) (epure 3 in *Fig. 3.14*).

The amplified signal from the entrance cascade moved on the cathode amplifier (8), then

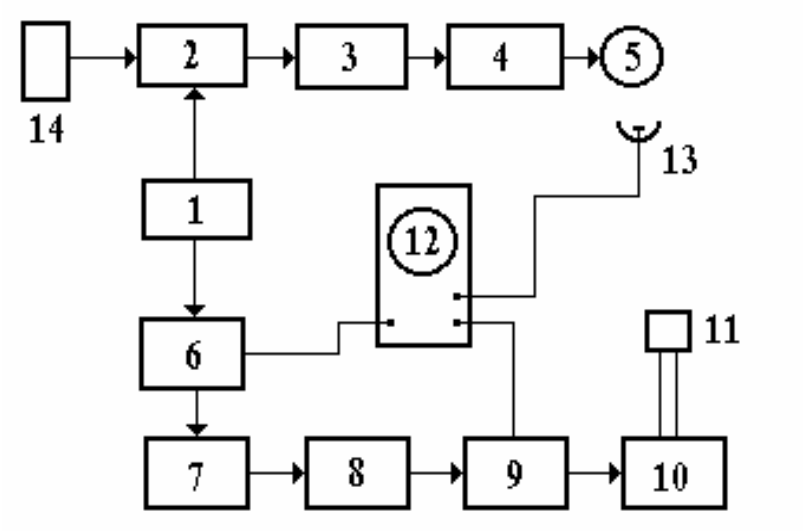

Fig. 3.13. Block-scheme of pulse synchronization circuit. 1 - crystal-controlled frequency divider, 2 - coincidence circuit, 3 - delayed-pulse generator, 4 - switch-mode power supply, 5 – flash lamp, 6 - synchronizing generator, 7 - high-voltage generator, 8 - cathode amplifier, 9 - driver, 10 - modulator, 11 - magnetron, 12 - oscillograph, 13 - photomultiplier tube, 14 - camera.

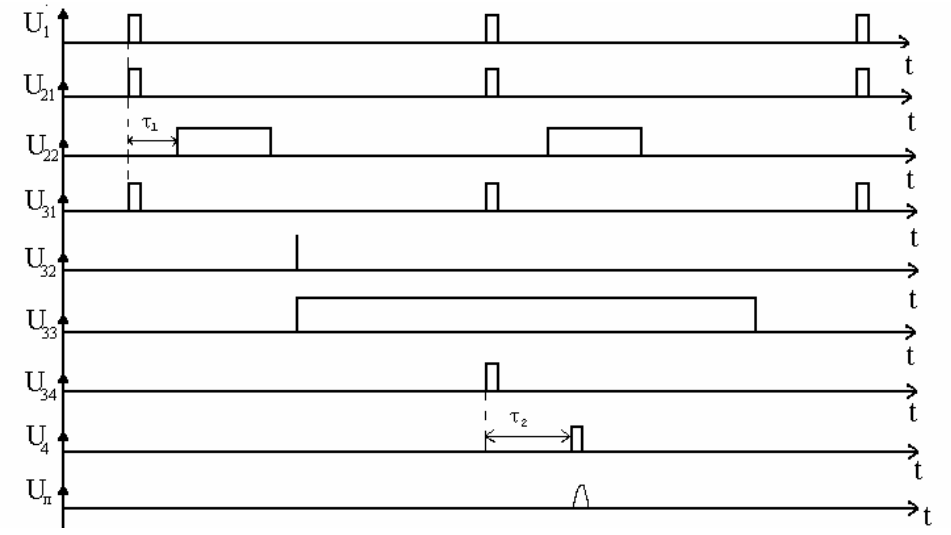

Fig. 3.14. Temporal voltage diagrams of synchronization system.

on driver (9), the signal with which started the modulator (10). The modulator developed pulses with a voltage *5-25 kV* which on a coaxial cable moved on magnetron (11). Duration of these pulses was established by generator (6), and could change in limits from *1 μs* up to *1 ms*, and pulse repetition frequency was defined by the driving generator (1). The signal from an output of the cathode amplifier was directed on an input of oscillograph (12) for the control over the form of a pulse envelope of the modulator. On the same oscillograph it was possible to submit a pulse-envelope from the microwave detector head.

Pulses from an exit of the crystal-controlled frequency divider (1) moved also on an input of the coincidence circuit (2) which has been collected on the basis of the serial block of the programmed counter of pulses. The input of the coincidence circuit has been closed in an initial condition.

By pressing of the camera starter button (14) the pulse driver moved on the coincidence circuit (epure 5 in *Fig. 3.14*). Thus the electronic key (trigger) closing up to it an input of the circuit, opened, and the coincidence circuit started to generate the pulse burst. The pack has consisted of the certain number of pulses which could be changed in limits from 1 up to 10^4 with step from 1 up to 100, accordingly. Last pulse in a pack overturned the trigger, the electronic key was closed, and the coincidence circuit came back in the initial closed condition (epure 6 in *Fig. 3.14*).

Under conditions of our experiment on an output of the coincidence circuit the single pulse was formed. It acted on start of the delayed-pulse generator (3) (epure 7 in *Fig. 3.14*). The generator (3) allowed to smoothly adjusting a time delay (from 0 up to 1000 μs) between a pulse of start of magnetron and a pulse of flash lamps (epure 8 in *Fig. 3.14* and *Fig. 3.15*) of shadow installation. Such delay allowed receiving shadow photos of investigated process with time sanction *~10 μs* during the active phase of the microwave discharge, and also in a stage of plasma deionization (*Fig. 3.15*).

The output signal of the delayed-pulse generator (3) moved on start of the switch-mode power supply (4) of flash lamp (5). The switch-mode power supply has been collected on the basis of the circuit with memory capacity and thyristor switch. In an initial condition thyristor is closed, and the condenser (*2 mF*) is charged up to *1,2 kV* from the power supply. At the moment of arrival of a starting pulse from the generator (3), thyristor opens, and the voltage pulse acted on a flash lamp. In this case pulse duration of a luminescence of a flash lamp is defined by capacity of the storage condenser and full resistance of circuit. In the given experiments duration of a luminescence (on a half-width of a pulse) was about *10 μs* that defined the time resolution of

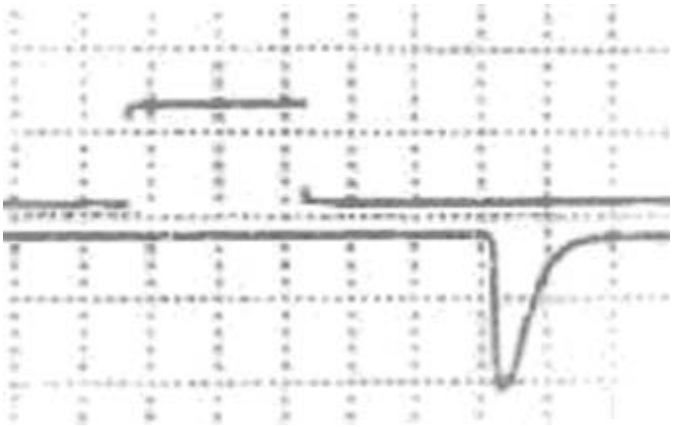

Fig. 3.15. Oscillograms of pulses of magnetron (1) and flash lamp (2) (time scanning 10 μs/div).

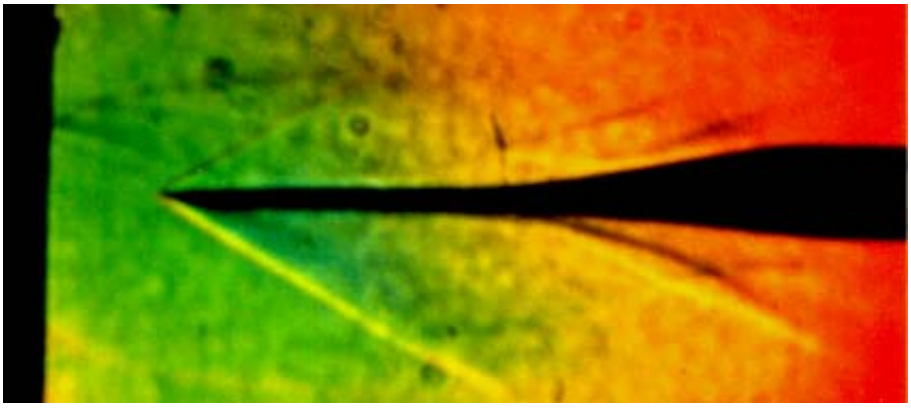

Fig. 3.16. Typical picture of the thin pointed plate being flown about.
(Flow Mach number *M=2*, initial pressure *p=40 torr*).

system. For definition of relative position in time of a microwave pulse and a pulse of a flash lamp the photomultiplier tube was used (epure 13 *Fig. 3.14*). At this, the signal from the detector head, or a pulse of start of the modulator of magnetron led to the first channel of a oscillograph. The signal of a photomultiplier tube led to the second channel of the same oscillograph (*Fig. 3.13*).

The typical shadow photo of a thin pointed plate streamlined by a supersonic flow of air, received on our experimental installation, is submitted on *Fig. 3.16*. Initial pressure of air in the discharge chamber *p=40 torr*, pressure of air in the high-pressure system *p=1 atm*. From the received photo one can see, that our system of creation of a supersonic flow of air works normally. The value of flow Mach number *M=2,0* received from *Fig. 3.16* coincides with calculated value for the experimental conditions. The supersonic flow does not change the characteristics during two seconds.

Registration of a shadow picture on a film with the help of the standard camera does not allow quickly (in real time) to receive the information about process of a flow of a researched body by supersonic stream or to fix the fact of ignition of supersonic flow of combustible gaseous mixtures. For improvement of the time sanction modernization of shadow installation has been made (*Fig. 3.17*). For this purpose the new system of synchronization has been collected. At this the standard camera was replaced by *CCD*. Minimal time of *CCD* exposition equals *2,9 μs*. As a illuminating lamp in shadow installation the pulsed flash lamp was used. The system of synchronization allowed combining a pulse driver of *CCD* with a maximum of a pulse of a luminescence of a flash lamp and the moment of time of researched process necessary for registration (*Fig. 3.18*).

3.7. Measurement of flame conductivity

It is known, that unexcited and unionized gases do not carry out an electric current whereas gases in a flame are good conductors of electricity. This circumstance has been used by us for registration of the fact of ignition of a supersonic stream of gaseous fuels and estimation of value of gas ionization degree at measurement of flame conductivity. For this purpose the flat capacitor was located on an exit of the aerodynamic channel (*Fig. 3.19*). Under experimental condition the time delay between a pulse of the discharge current, which is ignited a supersonic flow of propane-air mixture, and the moment of occurrence of an electric signal on the measuring resistance R, included in a circuit of the capacitor, was measured. It allowed determining the fact of ignition, the minimal pulse duration of the discharge current, necessary

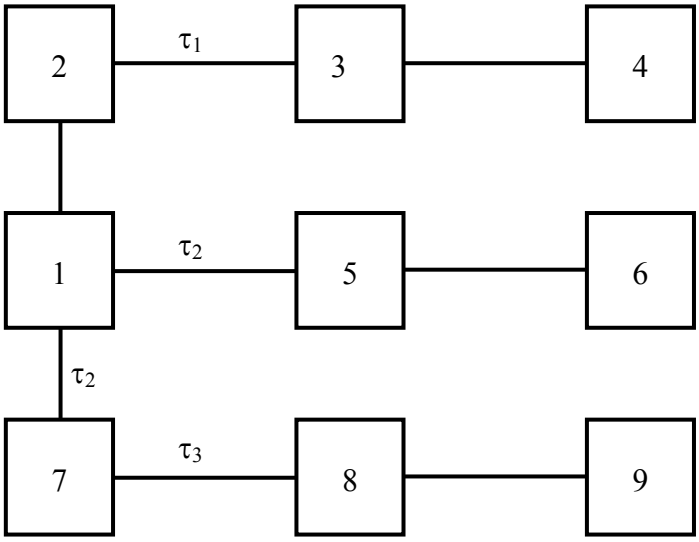

Fig. 3.17. Block-scheme of modernized system of synchronization. 1 - driving generator; 2, 7 - delayed-pulse generators; 3 – magnetron; 4 – microvave discharge; 5 - switch-mode power supply, 6 – flash lamp, 7 – *CCD* synchronization system; 9 – CCD.

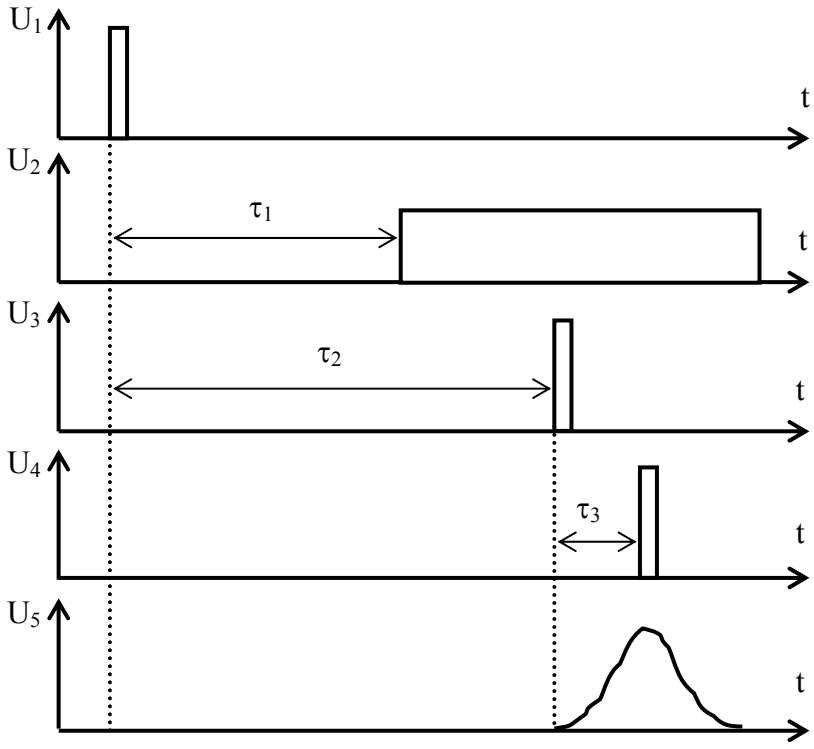

Fig. 3.18. Temporal voltage diagrams of modernized synchronization system.

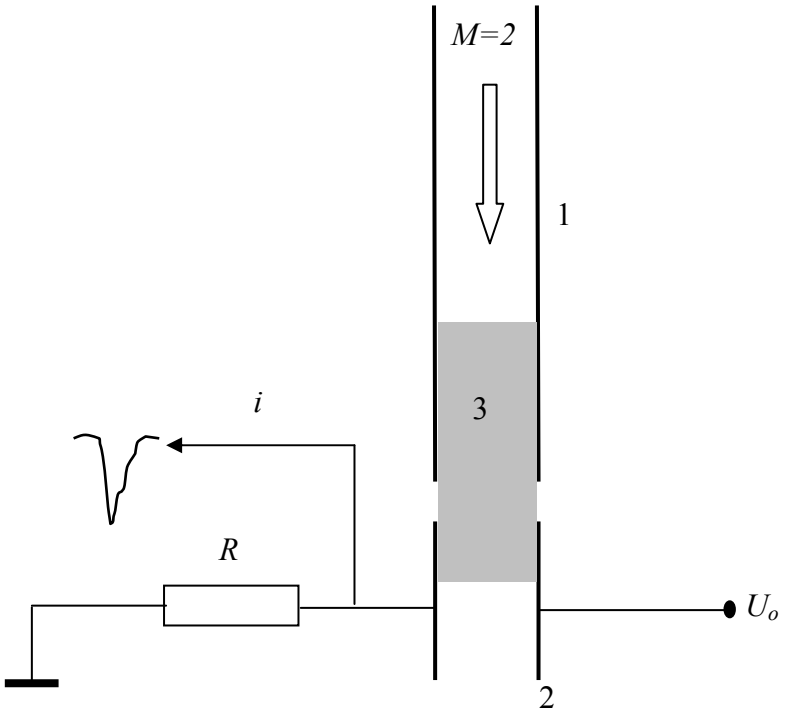

Fig. 3.19. The block-scheme of measurement of flame conductivity. 1 - the aerodynamic channel in whom the supersonic stream of gaseous fuel is ignited, 2 - the measuring capacitor, 3 - flame.

for ignition, and speed of flame distribution. The value of a current i between plates of the capacitor allowed to estimate a degree of gas ionization in a flame.

If the flat capacitor to place in a flame the current i in a circuit is determined by the following expression:

$$i = en_e v_{dr} S\,, \tag{3.19}$$

where $e=1,6\cdot10^{-19}\ C$ is a charge of electron, n_e is an electron density, S is the capacitor plates section, d is the distance between plates, U_o is a potential difference between plates of the capacitor, v_{dr} is drift speed of electrons

$$v_{dr} = \mu_e E\,, \tag{3.20}$$

where μ_e is electron mobility

$$\mu_e = \frac{e}{m_e \nu_{en}}\,, \tag{3.21}$$

where m_e is electron mass, ν_{en} is effective frequency of collisions of electrons with neutral particles of gaseous fuel.

As mean energy of electrons depends on intensity of electric field E the dependence v_{dr} from E is not strictly linear. In this case the mobility determined under the formula (3.21), depends on a field. However in our case with a sufficient degree of accuracy it is possible to use linear dependence (3.20) with $\mu_e=const$. This assumption does not influence on qualitative conclusions at registration of the fact of ignition and an estimation of value of electron density in a flame though for exact quantitative measurements of a degree of gas ionization it is necessary to take into account dependence v_{dr} from E. Another important circumstance is uncertainty of value of collision frequency of electrons with molecules of gas in the environment of products of burning of propane-air mixture. However in our case this uncertainty does not exceed *50 %* that affects accuracy of measurement of concentration of the charged particles in a flame, but does not influence at registration of the fact of ignition of a supersonic stream of gaseous fuel and definition of an induction time.

Under experimental conditions the capacitor has been the following parameters: $d=1\ cm$, $S=2\ cm^2$. Voltage $U_o=20\ V$ was put to plates of the capacitor. Thus the electron density can be defined under our conditions by the formula:

$$n_e[cm^{-3}] = 1,1\cdot10^{11} i[mA]\,. \tag{3.22}$$

Not looking at that accuracy of definition of electron density with the help of this method insufficiently good, it is reliable and simple way of research of process of ignition and burning of

supersonic streams of gaseous fuel.

3.8. Registration of common view and breakdown characteristics of microwave discharges

The common view of a surface microwave discharge was registered on a film and a video camera in two projections (side view and top view). It has allowed to fix the longitudinal size of a surface discharge and to measure longitudinal velocity of its distribution at different air pressures, pulse durations and microwave powers.

For example the common view of a dielectric wedge antenna without and with surface microwave discharge on its surface is given in *Fig. 3.20*. The common view of a surface microwave discharge on dielectric blunt-nosed antenna of rectangular section *1x2* cm^2 and length *15 cm* in a supersonic airflow at Mach number *M=2* is given in *Fig. 3.21*. One can see that the discharge represents uniformly luminous plasma coating all surface of a dielectric body and the supersonic flow of air at Mach number *M=2* does not influence on the common view of the surface discharge on the dielectric antenna of rectangular section, that is supersonic airflow does not destroy the surface discharge. The direction of propagation of supersonic airflow is opposite to a direction of a surface wave travelling, i.e. direction of propagation of the discharge.

For obtaining of the threshold characteristics of a surface microwave discharge the dependencies of the minimum input power, at which the discharge on an external surface of a dielectric body starts to be formed, on different values of air pressure in a vacuum chamber and on different durations of microwave pulses were measured. In experiments the moment of formation of the discharge was registered visually or on appearance of a signal on the screen of a double-beam oscilloscope from the collimated photoelectric multiplying tube (position (16) in *Fig. 3.22*), tuned on area of the antenna at an edge of a waveguide. Thus, on the second beam of an oscilloscope the signal from a microwave detector (position (12) in *Fig. 3.22*) was applied. For this purpose with the help of directional coupler (10) part of energy brought to the antenna was taken away through attenuator (11) to the microwave detector head (12). The amplitude of the microwave detector head signal was proportional to a pulsed microwave power

3.9. Probe method

The probe method allows carrying out the measurement of local parameters of plasma. At measurements in microwave plasma it is necessary to take into account that for a contact

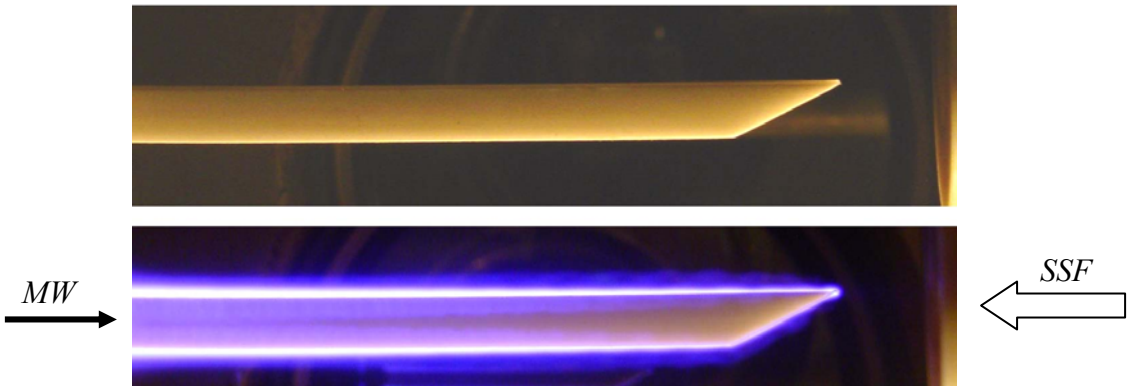

Fig. 3.20. The common view of a dielectric wedge antenna without and with surface microwave discharge on its surface at $M=2$, $p=40$ *torr*, $\tau=50$ μs and $f=100$ *Hz*.

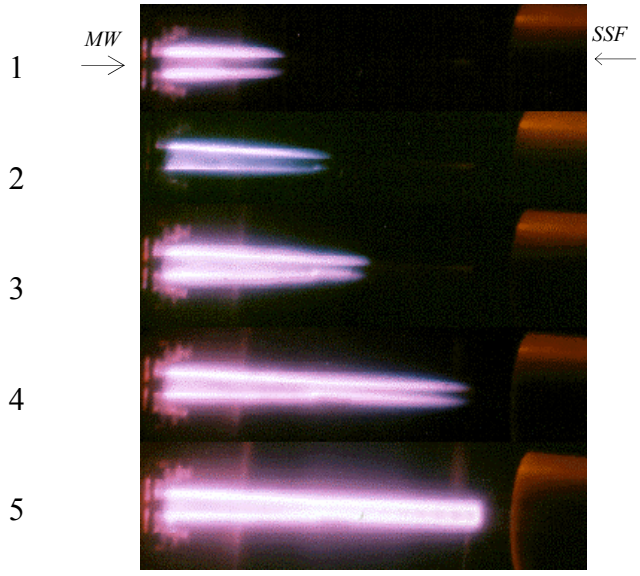

Fig. 3.21. The common view of a surface microwave discharge on an external surface of a dielectric antenna at $p=10$ *torr*, $W_p=50$ *kW*, $f=20$ *Hz* and at different microwave pulse duration τ, μs: 1-2; 2-5; 3-10; 4-25; 5-50.

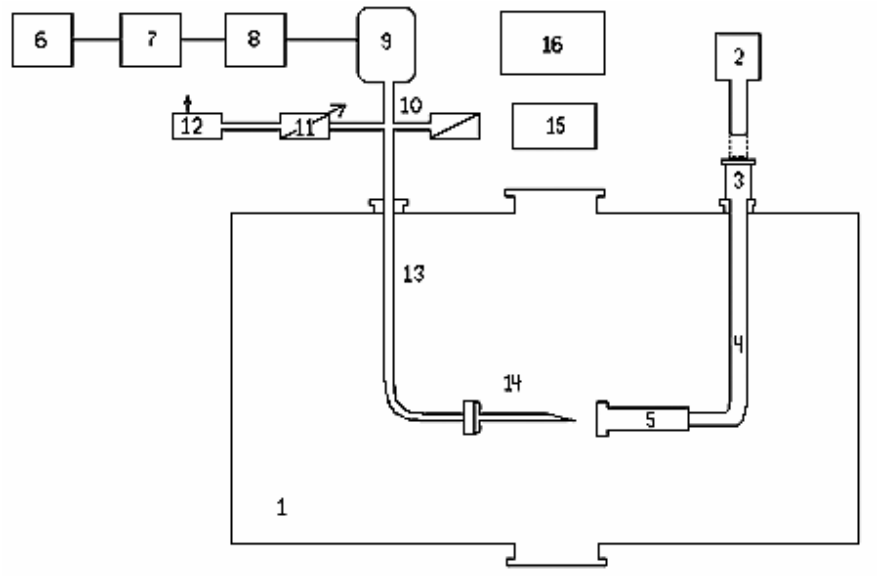

Fig. 3.22. Block-scheme of experimental installation for registration of common view and breakdown characteristics of microwave discharges. 1 - evacuated vessel, 2 - high-pressure compressor with receiver, 3 - electromechanical air-valve, 4- flexible rubberized-fabric hose, 5 - supersonic nozzle, 6 - driving generator, 7 - preamplifier, 8 - grid, 9 - magnetron, 10 - directional coupler, 11 - attenuator, 12 – microwave detector head, 13 - waveguide, 14 - dielectric antenna, 15 - imaging system, 16 - photomultiplier tube.

a

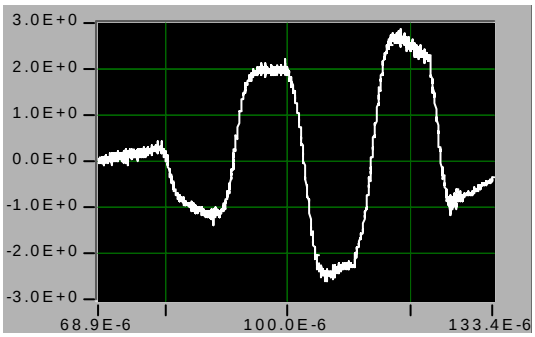

b

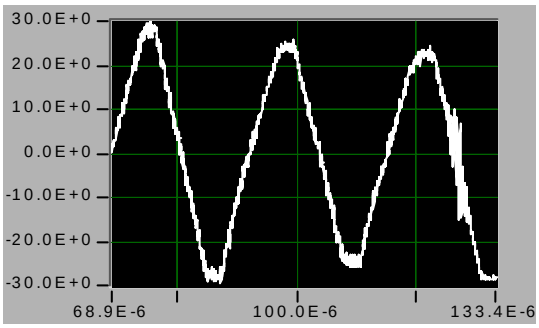

Fig. 3.23. Current (a) and voltage (b) oscillograms.

method, what is a probe method, the registration of action of a very high frequency field is principal moment. Especially it is important in a case of large pressure, as the very high frequency power which is necessary for creation of the surface microwave discharge grows with pressure.

The probe method allows carrying out the measurement of local parameters of plasma. At measurements in microwave plasma it is necessary to take into account that for a contact method, what is a probe method, the registration of action of a very high frequency field is principal moment. Especially it is important in a case of large pressure, as the very high frequency power which is necessary for creation of the surface microwave discharge grows with pressure.

For correct application of a probe method it is necessary to analyse the questions not only interpretations of received results, but also the probe measurement techniques (technical equipment), i.e. a choice of the electric scheme of probe circuits, the probe designs and sizes, an opportunity of its moving near a antenna surface, etc. At measurements in the microwave plasma it is necessary to take into account that the microwave field influence is a principle moment. Thus two major factors can be essential.

At first, it is the action of very high frequency electric fields on a probe as a metal conductor. At application of probes, connected with recorded instrumentation by the radio-frequency cables, the difficulties arise. They are bound up with the fact that the conductors, placed at strong alternating fields, are the passive electrical vibrators.

Basically it can result in to occurrence around them the secondary discharges and essential change of the distribution of parameters of explored plasma. This influence is most essential in a high frequency region. However in conditions of microwave powers, taking place in experiment, the elimination of this factor is advisable. Besides in conditions of microwave powers it is desirable to remove the recorded instrumentation on large enough distance.

The second factor is connected to action of very high frequency electric field on a probe layer. Due to effect of detection on a non-linearity of a probe layer of the variable electromotive force, existing between plasma and ground, a noticeable additional current, distorting a true current-voltage characteristic of a probe, appears in a probe circuit. Deforming influence of the microwave field of the discharge takes place only in the area of nonlinearity of a probe voltage-current characteristic. As a rule, nonlinearity is connected to an electronic branch of a voltage-current characteristic. The ionic part of the probe voltage-current characteristic, as a rule, is close to linear. Therefore use of this part of the characteristic allows to substantially diminishing a problem of the voltage-current characteristic distortion.

The theory of an ionic current on a single probe can be applied to a double probe provided that interference of probes minimally. In practice it is reached by removal of probes on distance about *10L* (where *L* is a probe characteristic size), i.e. on distance about several millimeters. In experiments the symmetric double cylindrical probes were used. The probes diameter can be changed from *0,1 mm* up to *1 mm*.

The electric circuit for measurement of the voltage-current characteristic of the double probe is developed and produced. The principle of measurement of the voltage-current characteristic is based on feeding of probes of a voltage scan sawtooth voltage. In the standard version a sawtooth voltage is linear. The range of a voltage variation lays in the range of *±28 V*. The minimal time of the voltage-current characteristic measurement is *10 μs*. In result a probe current *i(t)* flows in a circuit. Both the signal *U(t)* and the probe current *i(t)* transmit on an input of two-beam digital oscillograph *Tektronicx TDS 210*, and then they are transferred in memory of a computer.

With the help of specially developed program the necessary part on the oscillograms, corresponding to the required moment of time, is chosen. Then the desirable interval of averaging gets out and the average voltage-current characteristic of a double probe is plotted.

For carrying out of probe measurements the special device allowing mechanically with various speeds to move probes in two mutually perpendicular directions, parallel to a plane of the antenna, is designed and manufactured. The basic unit of the device is Wilson's two-level insulation with intermediate air pumping. It enables to carry out the turning of a pivot on any angle concerning a vertical axis and its movement along this axis on distances up to 300 mm without gas flow from the outside.

With the help of the special mechanism the rotary movement was transformed in a horizontal direction movement. Rotation of a pivot and its vertical moving are carried out by two reversible electric motors which can work as simultaneously, and in an independent mode. Thus in the first case the probe moves at once in two directions. In the second case the probe goes or in vertical direction, or in horizontal one. The engines management is carried out by remote with the help of the special board. The installation accuracy of a probe coordinates in both directions not less than *0,5 mm*. The probe was settled down perpendicularly planes of the antenna on distance of *2 cm* from its surface. Probes diameter was *0.3 mm*, its length – *10 mm*. As an example the oscillograms of a time course of a probe current and voltage are submitted in *Fig. 3.23.* The microwave pulse duration equals *100 μs*, mean power is *100 W*, air pressure is *0,5 torr*, registration time (duration of a voltage scan) is equal *10 μs*.

CHAPTER IV
SURFACE MICROWAVE DISCHARGE IN SUPERSONIC FLOW

In the Chapter IV the experimental data on study of properties of the surface microwave discharge on external surface of dielectric body being flown of supersonic stream of air are considered. The influence of supersonic airflow on properties of a surface microwave discharge was investigated too.

Recently it was offered to create plasma formations before flying vehicle and on its external surfaces for improvement of the aerodynamic characteristics of aeroplane. In our laboratory for this purpose the two types of the microwave discharges, namely, the freely localized microwave discharge [1-15] and the surface microwave discharge [16-40] are used. This investigation deals with the surface microwave discharge outside a dielectric body in a low pressure chamber. In this case plasma supported by a surface microwave is formed on an external surface of a dielectric antenna.

4.1. Common view of microwave discharges on external surfaces of dielectric bodies

In conditions of motionless air and supersonic airflow the surface microwave discharges were formed on external surfaces of dielectric bodies of different geometry:

- on flat plane;
- on antenna of a rectangular section;
- on antenna of a rectangular section with a wedge end part;
- on cylindrical antenna with a spherical end part;
- on cylindrical antenna with a conical end part;
- on antenna of rectangular section with a smoothly transfer to the cylindrical antenna with a conical end part.

The main plasma parameters and properties of such type of the microwave discharges were investigated.

In the project the pulse magnetron generator of a centimetre wavelength was used as a source of microwave energy. The magnetron generator had following characteristics: wavelength $\lambda=2,4\ cm$; mean microwave power $W_m<300\ W$; microwave pulse duration $\tau=1\text{-}200\ \mu s$; pulse repetition frequency $f=1–100\ Hz$, pulse period-to-pulse duration ratio $Q=1000$. The microwave energy was introduced into the vacuum discharge chamber by the waveguide system of the

rectangular section *9,5x19 mm*^{2} through the directional coupler. All waveguide system was hermetic. It was filled by SF_6 at pressures up to *5* atmospheres for avoidance of electrical breakdown. The discharge formed in a cylindrical chamber. The inside diameter of the chamber is *1 m*, its length is *3 m*. The vacuum system allowed to investigate the surface microwave discharge in diapason of air pressures *p=1-760 torr*. The waveguide, entered into the discharge chamber, ended the special antenna. The surface microwave discharge in supersonic airflow was created on the antenna external surface.

The different new ways of a microwave energy application to a dielectric wave-guide antenna were designed and tested. The dielectric and metal inserts were utilised. The optimum way of an application of energy for creation of a surface microwave discharge on an external surface of a dielectric body in supersonic airflow was determined.

The common view of a surface microwave discharge on an external surface of a dielectric blunt-nosed antenna of rectangular section *1x2 cm*^{2} and length *15 cm* at air pressure *p=40 torr* is given on *Fig. 4.1*. One can see that the discharge represents uniformly luminous plasma coating all surface of a dielectric body.

The common view of a surface microwave discharge on antenna of a rectangular section with a wedge end part is shown in *Fig. 4.2* at air pressure *p=40 torr*, microwave pulsed power W_p*=40 kW*, and microwave pulse duration τ*=100* μ*s*. It is visible, that microwave energy is put in thin near-surface layer in other words there is an opportunity to influence on parameters of a flow near a surface of a streamline body. This circumstance should result in reduction of force of surface friction of the body moving in dense layers of an atmosphere.

The experiments on creation of a surface microwave discharge on a flat plate were also carried out. For this purpose teflon plate by 1 cm thickness, 14 cm length and 20 cm width was used instead of the antenna. The common top view of the surface microwave discharge at air pressure *p=40 torr* is submitted in *Fig. 4.3*. One can see that in a place of plasma creation the microwave energy is transformed in a surface wave, which spreads in all directions, creating at air pressure *p>10 torr* thin uniformly luminous layer of plasma on a surface of a dielectric body. At fixed microwave pulse duration the part of a surface of a plate is coated by plasma increases when a microwave power growths. There is a reflection of a surface wave from edge of a plate when surface wave reaches to plate edge that leads to a mode of a standing wave.

The common front view of the surface microwave discharge on a flat plate is submitted in *Fig. 4.4* at the same condition that previous case (*Fig. 4.3*). It is visible, that plasma layer is really concentrated at a surface of a plate and its thickness does not exceed *~1 mm*. In this case the surface wave is propagated in the direction of the observer. It is distinctly possible to see,

1

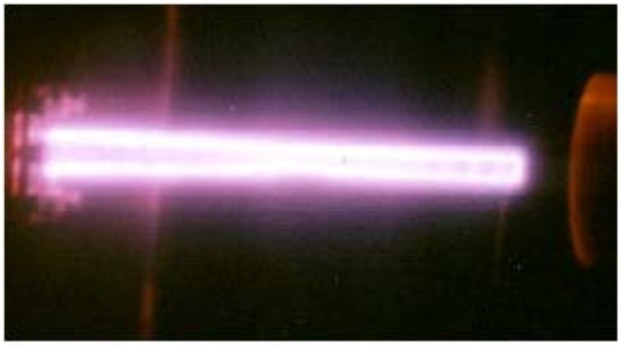

2

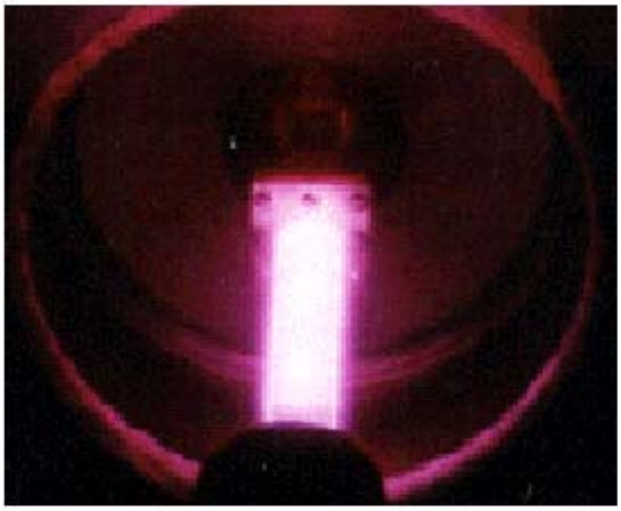

Fig. 4.1. The common view of a surface discharge on an external surface of a dielectric blunt-nosed antenna at $p=40$ *torr*, $\tau=50$ μs and $f=100$ *Hz*. 1 - side view, 2 - top view under 45^o to a vertical.

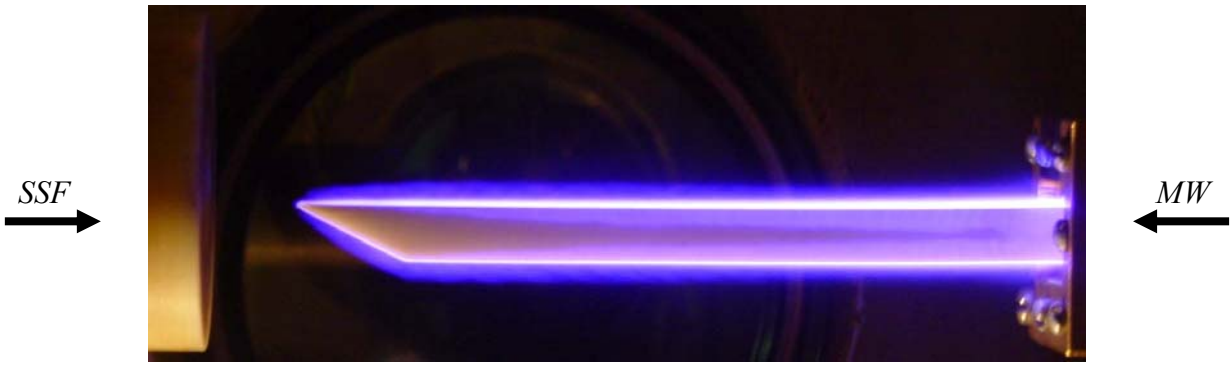

Fig. 4.2. Microwave discharge on external surface of wedge antenna at air pressure $p=40$ *torr*, microwave pulsed power $W_p=40$ *kW*, and microwave pulse duration $\tau=100$ μ*s*.

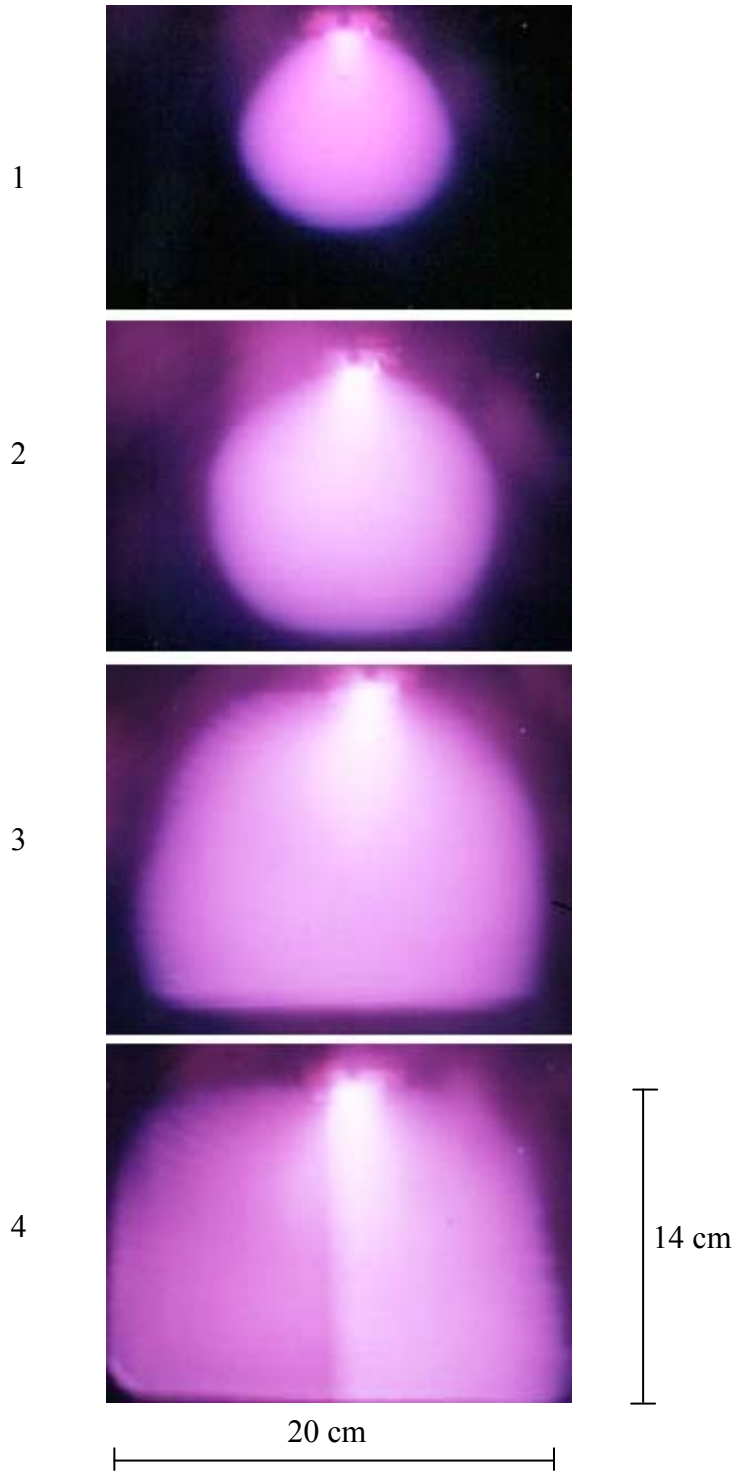

Fig. 4.3. The common view (top view) of a surface microwave discharge on a dielectric plate at $p=40$ *torr*, $\tau=50$ *μs*, $f=20$ *Hz*, and W_p, *kW*: 1-50; 2-100; 3-200; 4-250.

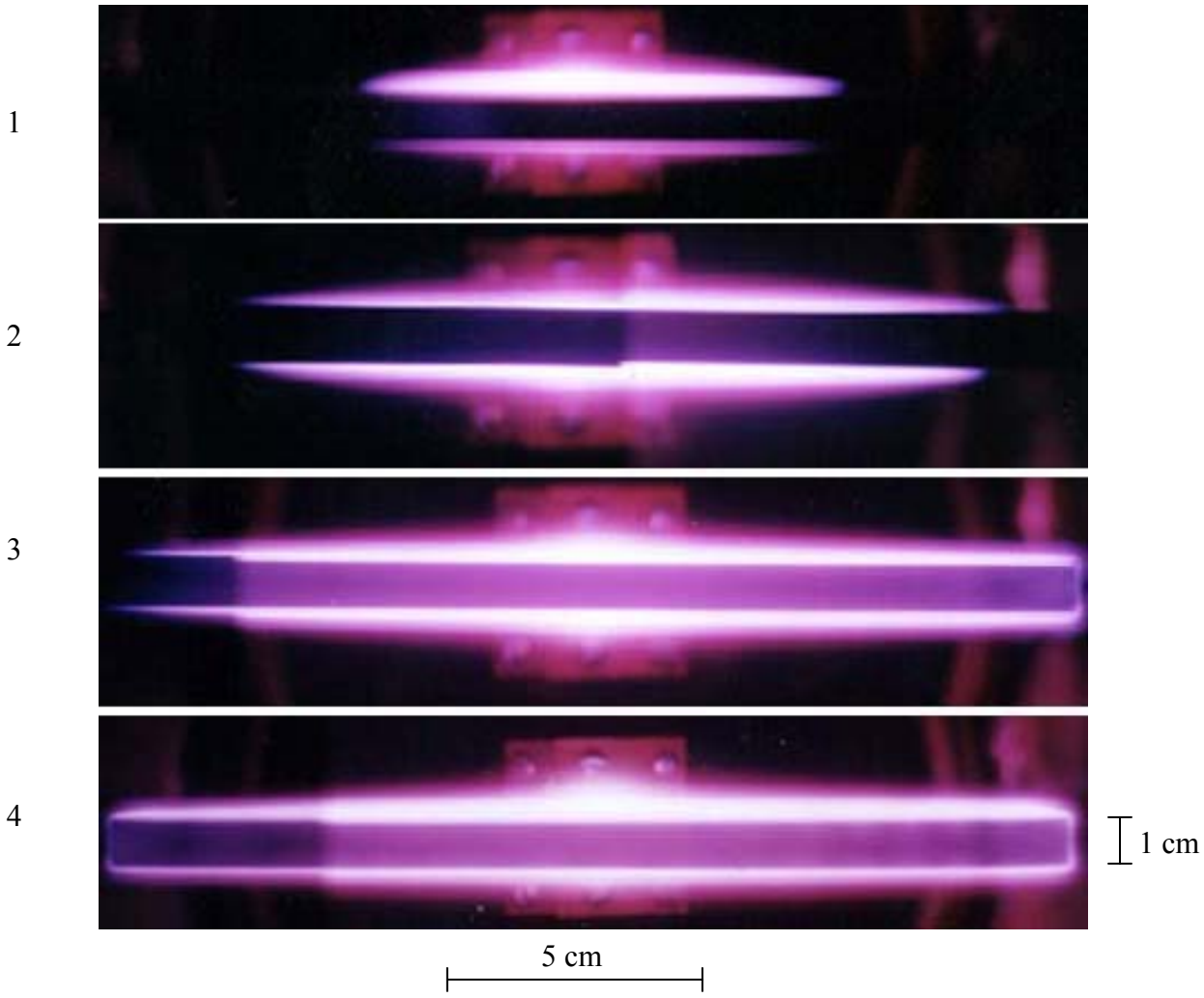

Fig. 4.4. The common view (front view) of a surface microwave discharge on a dielectric plate at $p=40$ *torr,* $\tau=50$ *μs,* $f=20$ *Hz,* and W_p, *kW*: 1-50; 2-100; 3-200; 4-250.

how at achievement by a surface wave of edges of a plate plasma starts to cover a front face and lateral surface of a plate. As the frequency mode of the discharge creation was used then the image of two discharges takes place in each picture at registration with the help of the camera having mechanical shutter

The velocity of the discharge propagation on a plate also depends on duration and power of the microwave pulse, as a velocity of the discharge propagation on the antenna. So the surface microwave discharge covers all plate with the area $S=14x20\ cm^2$ in time of $t=1\ \mu s$ at pulsed microwave power $W_p=350\ kW$.

With reduction of air pressure the radial sizes of the surface discharge are increased. The photographs of the common side and top views of the surface discharge on a plate at air pressure $p=7\cdot10^{-3}\ torr$ is given in *Fig. 4.5*. In this case the radial sizes of the discharge achieved a values $L_e\sim10\ cm$ for a pulse duration $\tau=100\ \mu s$. This is explained by that fact, that at reduction of pressure the role of diffusion of the charged particles is increased. Spatial scale of inhomogeneity of electron concentration L_e is possible to estimate from expression $L_e=\sqrt{D_a\tau}$, where D_a is a coefficient of ambipolar diffusion. Then for air pressure $p=10^{-3}\div10^{-2}\ torr$ value $L_e\sim10\ cm$, that well coordinate with experiment (*Fig. 4.5*).

The received results show, that on our experimental installation with use of the given way of discharge formation it is possible to cover with plasma not only a surface of the antenna with cross-section equal to section of the wave guide supplying electromagnetic energy to the dielectric body, but also big enough surfaces.

The special design antennas are developed and made for creation the complex form of local gas-heating zones with the help of one microwave generator.

The first type of antenna represents a plate of *1 cm* in thickness, *4 cm* in width and *15 cm* in length, cut on a narrow wall (the length of a cut part of antenna is equal *12 cm*). The aerial is made of a teflon. The teflon is a soft material. In experiment, bending definitely parts of the aerial, it was possible to receive a surface microwave discharge of a complex configuration. In particular, the ring surface microwave discharge on an internal and external surface of the antenna of the cylindrical form which is planned to use for ignition of a propane-air mixture in the cylindrical aerodynamic channel has been created.

The second type of antenna represents the trident, which has been cut out from a plate of *1 cm* in thickness, *5 cm* in width and *15 cm* in length. Under supply of electromagnetic energy to such antenna on its surface the microwave discharge was created. Thus the length of the discharge on each trident was approximately identical.

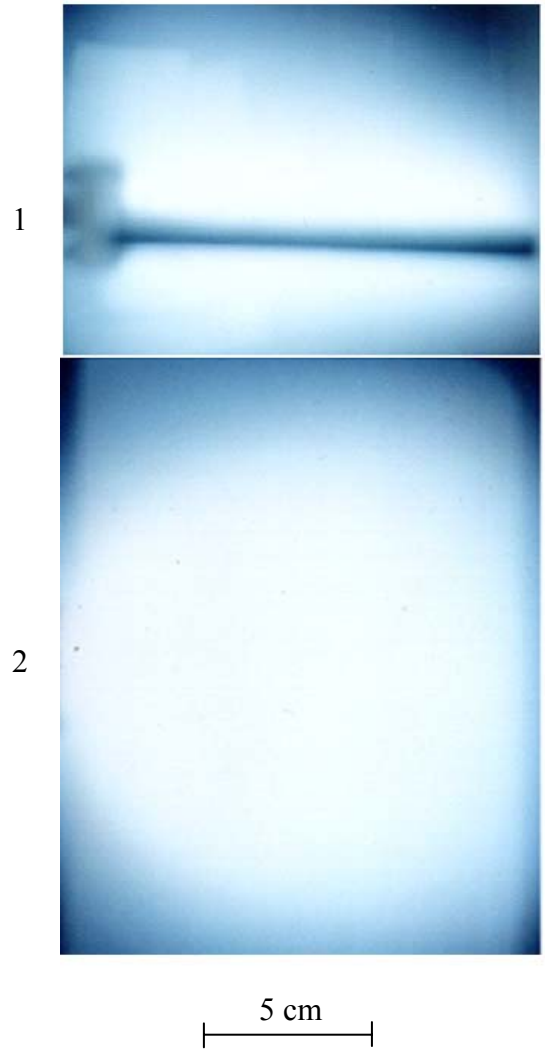

Fig. 4.5. The common view of a surface microwave discharge (1 - side view, 2 - top view) on a dielectric plate at $p=7\cdot10^{-3}$ *torr,* $\tau=50$ *μs,* $f=20$ *Hz*, and $W_p=100$ *kW*.

For research of influence of metal details on properties of the surface microwave discharge the special device has been made. It represents a wave-guide at which one wide wall is cut off. Inside of a wave-guide the dielectric antenna was located precisely on the size. In this case the discharge was created on one wide wall of the aerial. Thus the common view of the discharge and its main parameters are identical with parameters of the surface microwave discharge on the free antenna.

The new type of a microwave discharge was created by us on the antenna of a rectangular section with a wedge end part (*Fig. 4.6*). The discharge represents a combination of a surface discharge created in the area of a boundary layer on an external surface of a dielectric body, and a volumetric microwave discharge which is generated on a leading edge of a dielectric wedge body. The volumetric microwave discharge arises on a forepart of the antenna only at the power and microwave pulse duration more, than the power and duration which is necessary for creation of a surface microwave discharge on all surface of the dielectric wave-guide antenna. Thus, the size of spherical plasma formation is increased at growth of microwave power and pulse duration.

4.2. Mechanisms of propagation of surface microwave discharge

Dynamics of a surface microwave discharge created in a boundary layer near to a body streamlined by supersonic airflow was researched. It was shown that the longitudinal size of a surface discharge and its velocity at fixed pulse duration grow with an increasing of a microwave power. Thus, on initial stages of the surface discharge existence this velocity is large and reaches of value $v=10^7$ *cm/s*, whereas at late stages the discharge propagation velocity decreases up to $v=10^4$ *cm/s* to the end of the microwave pulse with duration $\tau=100$ μ*s*.

Experimental data show, that speed of propagation of the discharge along a surface of the dielectric antenna on some orders is less than speed of spreading of an electromagnetic wave in vacuum. It is possible to explain such speed of propagation of the discharge if to compare it with ionization rate of molecules of gas, i.e. with creation of critical concentration of electrons. Dependences of velocity of the discharge spreading along the dielectric antenna from longitudinal coordinate (z) are submitted in *Fig. 4.7*. One can see that on all curves the characteristic break is observed. This fact specifies that various mechanisms answer for spreading at an initial and final stage of the discharge existent. The following mechanisms can provide movement of front of the discharge: breakdown wave, ambipolar diffusion, photoionization, heat conductivity (a mode of slow burning), electronic heat conductivity, etc.

1

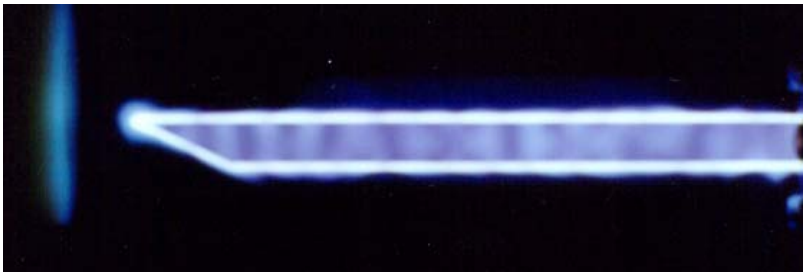

2

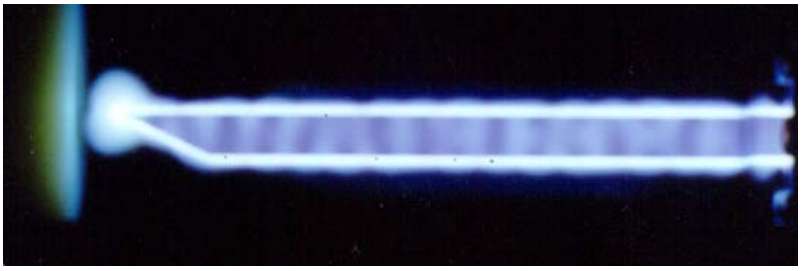

Fig. 4.6. Common view of the combined microwave discharge on a wedge dielectric body in supersonic airflow at τ=*60 μs* and *p=30 torr* (1 – W_p=*150 kW*, 2 – W_p=*200 kW*).

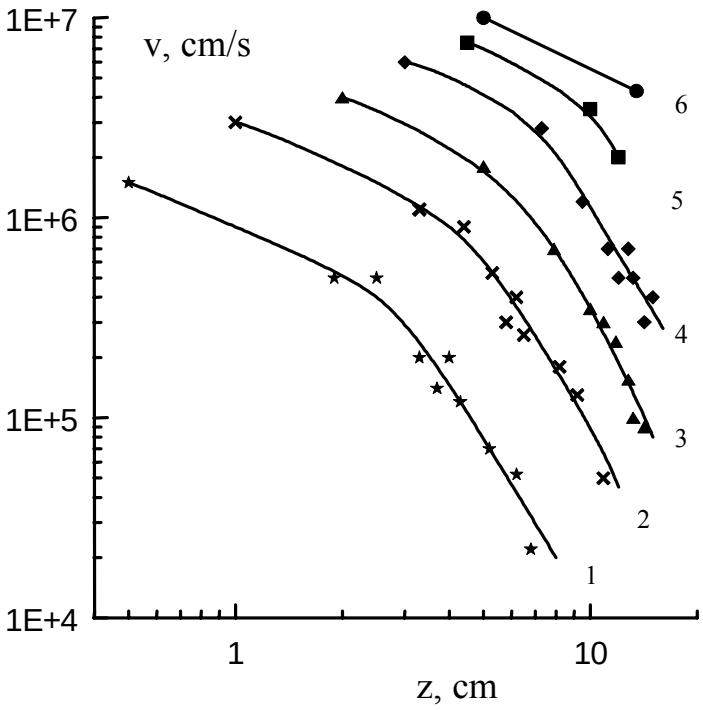

Fig. 4.7. Dependences of the discharge distribution velocity on longitudinal coordinate at *p=10 torr* and pulsed microwave power W_p, *kW*: 1-25, 2-35, 3-55, 4-75, 5-100, 6-175.

The breakdown wave defines movement of plasma at initial moment (t=*1-3 μs*) of the surface microwave discharge existence in the area of an energy supply to the antenna. Movement of a surface microwave discharge due to the mechanism of slow burning is possible only at late stages of the discharge existence (t>*100 μs*). At a stage of the discharge development ambipolar diffusion can be the most probable mechanism of discharge propagation at low pressure of gas, while photoionization and electronic heat conductivity can be responsible for distributions of the discharge at high pressure. To find out, what from these mechanisms is determining, it is necessary to carry out comparison of experimentally received results with the calculated data.

Let's assume, that the mechanism of movement of the surface discharge is defined by ambipolar diffusions. It is known, that the electron temperature in the investigated plasma practically does not vary during discharge existence, therefore within the limits of errors of experiment its change can be neglected. We shall put, that on forward front of discharge T_e=*2 eV*, T_i=T_g=*300 K*. If ambipolar diffusion is the dominating mechanism of loses of the charged particles in plasma then dependence of propagation speed v of the surface discharge from ionization frequency ν_i is determined by the formula:

$$v = 2\left(D_a \nu_i\right)^{1/2}, \tag{4.1}$$

where D_a - coefficient of ambipolar diffusion, equals

$$D_a = \frac{b_i k T_e}{e}, \tag{4.2}$$

where k – Boltzmann's constant, b_i - mobility of ions which is determined for air as [41]:

$$b_i p = \frac{2{,}7\sqrt{1 + M_g / M_i}}{\sqrt{(\alpha / a_o^3)29 \cdot 10^{-3}}}, \tag{4.3}$$

here p - pressure of gas in *[torr]*, $\alpha / a_o^3 = 11{,}54$.

To receive value of amplitude E_o of an electric field from experimental data, it is necessary to use dependence ν_i=$f(E_o/n_g)$, resulted in work [42].

$$\frac{\nu_i}{\nu_a} = 0{,}94\left(\frac{E_o}{E_b}\right)^2 exp\left\{-6\left(\frac{E_b}{E_o} - 1\right)\right\}\left[1 + 1{,}3\, exp\left\{-\frac{3E_b}{E_o}\right\}\right], \tag{4.4}$$

where E_o is amplitude of electric field, E_b is breakdown electric field, $\nu_a \approx 4 \cdot 10^{-12} n$ is attachment frequency, n is density of air molecules.

From here one can find a critical field of breakdown:

$$E_o = E_b = 28\left(\frac{n}{2{,}69\cdot 10^{19}}\right)\left(1+\frac{\omega^2}{\nu_{en}^2}\right)^{1/2}, \tag{4.5}$$

where $\nu_{en} = 1{,}7\cdot 10^{-7}\, n$.

For the further calculations we apply Mayhan's formula [43]:

$$\frac{\nu_i}{p} = 8{,}35\cdot 10^{-4}\left(\frac{E_{eff}}{p}\right)^{5{,}24}. \tag{4.7}$$

From this it follows that:

$$\frac{E_{eff}}{p} = \left(\frac{\nu_i}{8{,}35\cdot 10^{-4}\, p}\right)^{0{,}191}, \tag{4.8}$$

Peak value of intensity of an electric field is connected to effective value the formula:

$$E_o = \sqrt{2}\,\frac{E_{eff}}{p}\left(p^2+\frac{\omega^2}{\nu_{en1}^2}\right)^{1/2}, \tag{4.9}$$

where ω is circular frequency of super-high frequency field, ν_{en1} is frequency of electron-neutral collisions at air pressure *p=1 torr*. Under our conditions $\nu_{en1} = 5{,}3\cdot 10^9$.

In result at air pressure *p=10 torr* we receive the formula:

$$E_o = 45{,}3\cdot v^{0{,}382}, \tag{4.10}$$

here dimension of intensity of electric field is [*V/cm*], and dimension of velocity is [*m/s*].

Similar calculations have been carried out for air pressure *p=40 torr* $E_o = 109{,}3\cdot v^{0{,}382}$, *p=62 torr* $E_o = 163{,}0\cdot v^{0{,}382}$ and *p=100 torr* $E_o = 258{,}7\cdot v^{0{,}382}$.

Dependence of amplitude of an electric field on the longitudinal size of the discharge at pressure of *10 torr* is submitted in *Fig. 4.8* in logarithmic scale. Parameter of curves is the microwave power input to the antenna. It was shown (*Fig. 4.8*), that the amplitude of an electric field in the surface microwave discharge plasma changes from *E=5500 V/cm* on an initial stage of the discharge at microwave power W_p*=175 kW* up to *250 V/cm* at final stage at W_p*=25 kW*.

Using the formula:

$$E_o = 28\sqrt{S}, \tag{4.11}$$

where *S* is power flux density, dimension of *S* is [W/cm^2], dimension of amplitude E_o of electric field is [*V/cm*], and knowing section of our waveguide, we can define an electric field in waveguide. For example, at input microwave pulsed power W_p*=175 kW* the amplitude of electric field in waveguide $E_o \approx$*8 kV/cm* and at W_p*=25 kW* the electric field in waveguide $E_o \approx$*3 kV/cm*.

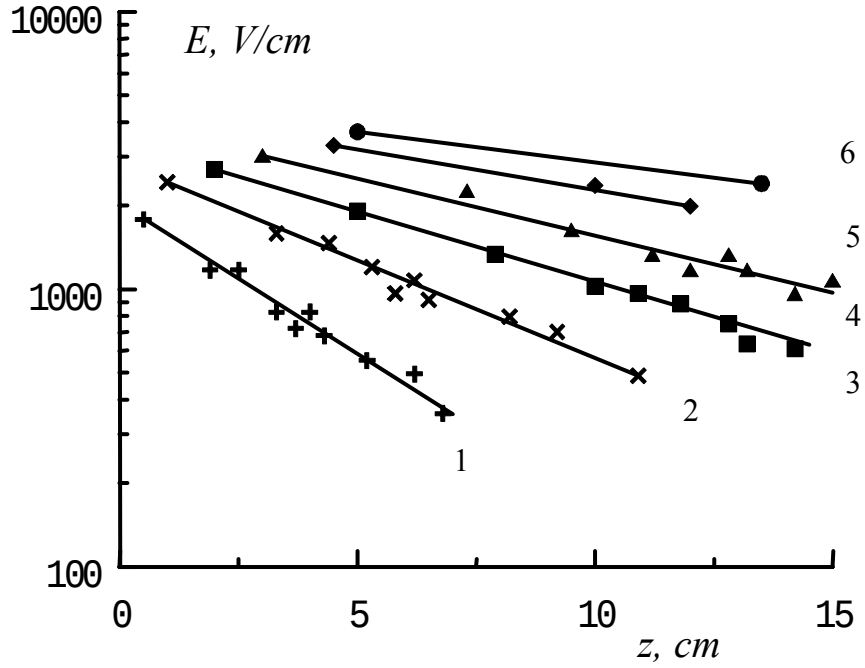

Fig. 4.8. Electric field strength as a function of a longitudinal coordinate *z* at air pressure *p=10 torr* and at different values of input pulsed microwave power W_p, *kW: 1-25; 2-35; 3-55; 4-75; 5-100; 6-175*.

As it is possible to notice, at air pressure *p=10 torr* the experimental results (look *Fig. 4.8*) not only do not contradict, but also well coincide with the value of amplitude of electric field in waveguide. For more high pressures the results obviously contradicting to the calculated data have been received. So, for example, for pressure of *100 torr* the amplitude of intensity of an electric field in the surface discharge, calculated in approximation of propagation of the discharge the account of ambipolar diffusions, reaches *15 kV/cm*, that contradicts experimental conditions.

Let's consider propagation of the discharge due to the mechanism of electronic heat conductivity. In this case dependence of intensity of an electric field on velocity of the discharge propagation looks like:

$$v = \frac{\sqrt{\chi_e \sigma T_e}}{\frac{3}{2} k T_e n_e} E_o , \tag{4.12}$$

where σ is electronic conductivity and

$$\chi_e = 2{,}56 \cdot 10^{-2} \frac{T_e^{5/2}}{\ln \Lambda} \tag{4.13}$$

is coefficient of electronic heat conductivity, dimension of χ_e is [*W/(cm·K*], T_e is electron temperature [*eV*].

For air

$$\chi_e = 1{,}93 \ W/m \cdot K, \tag{4.14}$$

$$\frac{\sigma p}{n_e} = 7{,}2 \cdot 10^{-18} \ [\text{torr} \cdot \text{m}^2/\text{Ohm}]. \tag{4.15}$$

Finally we receive

$$E_o = 1{,}46 \cdot 10^{-5} \sqrt{p}\, v , \tag{4.16}$$

where dimension of velocity *v* is [*m/s*], dimension of pressure *p* is [*torr*], and dimension of amplitude of electric field is [*V/cm*].

At pressure *p=100 torr* and velocity of the discharge propagation $v=10^5$ *m/s* the maximal amplitude of the electric field received in the assumption, that propagation of the surface discharge is provided due to electronic heat conductivity, is equal *14,6 V/cm*. Thus, the received values of an electric field contradict conditions of experiment and, accordingly, the mechanism of electronic heat conductivity does not provide propagation of the surface discharge for all range of the investigated pressure.

4.3. Kinetics of gas heating under condition of surface microwave discharge

As it has been shown in the previous paragraph, electric field amplitude reaches several kilovolts per centimeter in plasma of a surface microwave discharge. At such fields there is an effective ionization and dissociation of molecules of air, and also a lot of electron-excited molecules are created. All this should conduct to effective fast heating of gas, and gas heating rate should grow with increase in input microwave power.

On the basis of a method developed within the framework of the given project (see paragraph 3.3, Chapter III), the measurement of a temporary evolution of gas temperature in plasma of surface microwave discharge in air was fulfilled.

The gas temperature was determined at simultaneous registration only two lines of rotary structure of the (0,2) band of the second positive system of nitrogen with use of two monochromators. We apply this method for registration of time dependences of gas temperature at use a photoelectronic multiplier as radiation receiver. Thus on an oscilloscope the time dependence of intensities of luminescence of two lines, for example, with rotary quantum numbers j_1 and j_2 are simultaneously registered. The examples of oscillograms of two lines ($I_{j=19}$ and $I_{j=25}$) of rotary structure of the (0,2) band of the second positive system of nitrogen under condition of the surface microwave discharge are submitted in *Fig. 4.9-4.11* at different values of microwave power. In these cases one can get gas temperature vs time during one discharge realization.

Plasma radiation was registered from area of a surface microwave discharge, located on distance *z~2 cm* from waveguide end, where microwave energy leads to dielectric body. It is visible, that at the big powers the luminescence arises practically without a delay whereas at small input energies there is a time delay of occurrence of a luminescence that is defined by dynamics of development of the surface microwave discharge. So at a pulsed microwave power of *15 kW* the surface microwave discharge reaches area from which the spectrum of radiation is registered only through 60 μs after the pulse beginning. However already at microwave power of *55 kW* the delay is practically equal to zero as in these conditions longitudinal speed of the discharge propagation exceeds value of 10^6 cm/s.

Measurements of gas temperature were carried out on installation which block-diagram is represented on *Fig. 2.5* of Chapter II. Time dependences of gas temperature in plasma of surface microwave discharge at air pressure *p=10 torr*, pulse duration $\tau=100\ \mu s$ and different values of microwave power are given in *Fig. 4.12*. It is visible, that at any powers the fast gas heating is observed on forward front of the discharge. At this after passage of a front of ionization wave the

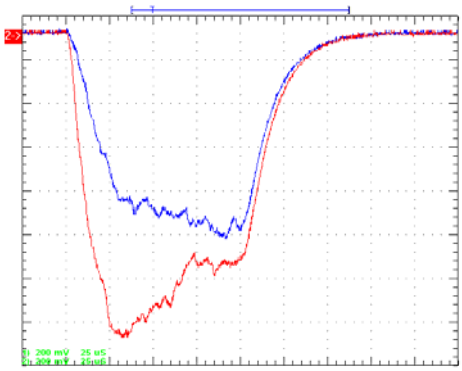

Fig. 4.9. The example of oscillograms of two lines ($I_{j=19}$ (red) and $I_{j=25}$ (blue)) of rotary structure of the (0,2) band of the second positive system of nitrogen. Surface microwave discharge at $p=10$ *torr,* $\tau=100$ *μs,* $W_p=55$ *kW.*

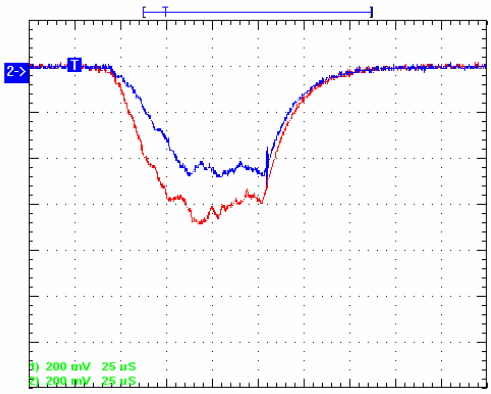

Fig. 4.10. The same oscillograms as in *Fig. 4.9,* $W_p=25$ *kW.*

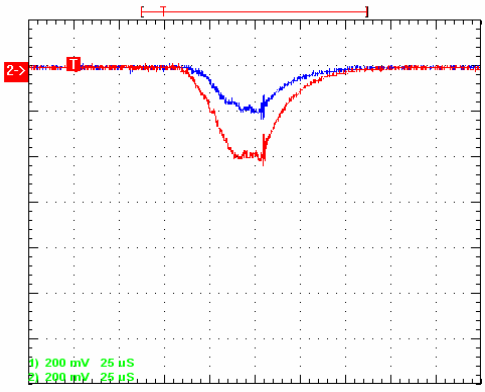

Fig. 4.11. The same oscillograms as in *Fig. 4.9,* $W_p=15$ *kW.*

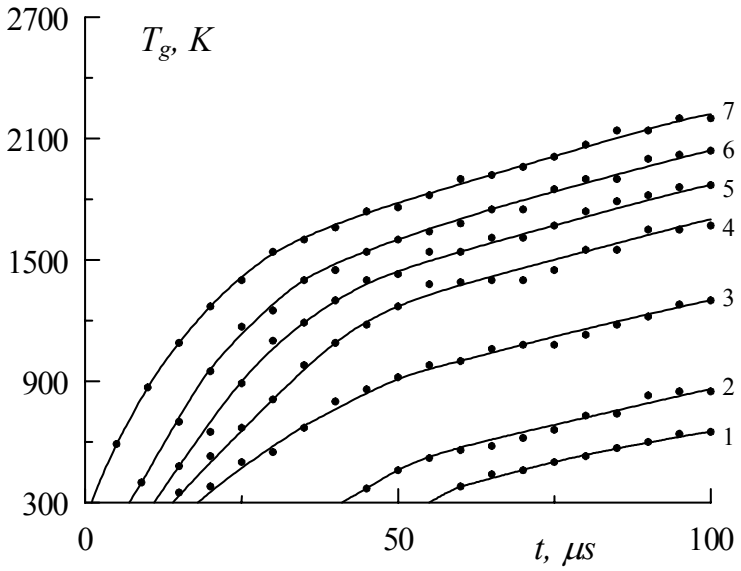

Fig. 4.12. Gas temperature in plasma of surface microwave discharge at air pressure *p=10 torr, τ=100 μs, f=10 Hz* and different values of microwave power W/W_o: *1-1.0; 2-1.07; 3-1.2; 4-1.33; 5-1.4; 6-2.33; 7-4.* W_o is a minimum pulsed microwave power, which is necessary for creation of a surface discharge under these conditions.

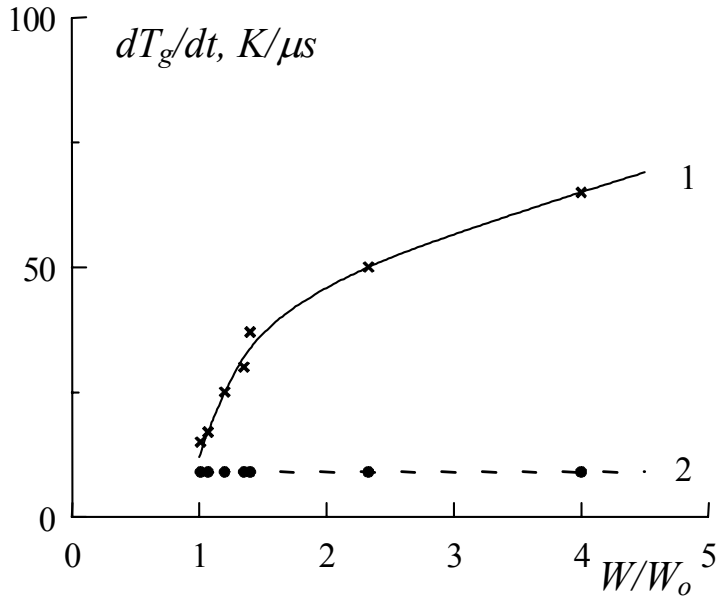

Fig. 4.13. Gas heating rate as a function of a microwave power. Initial phase (1) and stationary phase (2) of the discharge.

gas heating rate in the given area of space decreases not up to zero, and up to finite quantity, identical to all powers at which measurements were carried out. It specifies that in any area of space heating occurs during all times of the microwave pulse. From here follows, that using long enough pulses it is possible to gradually heat gas up to necessary temperature without formation of shock waves.

Dependences of gas heating rate at initial and stationary phases of the surface microwave discharge existence on a microwave power are given in *Fig. 4.13*. One can see that at stage of discharge formation the gas heating rate grows with increase of power and reaches value *~70 K/μs* at W_p*=200 kW*, whereas on a stationary phase of the discharge gas heating rate is constant and does not depend on power.

Various mechanisms are known which might lead to the heating of molecular gas [1, 11, 12, 14].

In the case of elastic interaction the part of the electron energy is transferred to the translational freedom degrees of molecules. However, because of the big difference between the mass of interacting particles and the small degree of plasma ionization (in our conditions $n_e/n=10^{-6}$-10^{-5}) the gas heating rate due to elastic interactions does not exceed *~0,01 K/μs* which is several orders less than the measured value.

For moderate values of reduced electric field *E/n=50 Td* the main part (up to *80%*) of electron energy is spent for vibration excitation of molecules. Due to vibration-translational relaxation part of the energy may be transferred to the gas heating. However in the case of nitrogen and air because of the big value of vibrational quantum the probability of *VT*-relaxation at low temperatures is small and the *VT*-relaxation time is hundreds of milliseconds [1], while the experimental time of gas heating is *~20 μs*.

Under the experimental conditions, the gas could be heated owing to the process associated with the quenching of vibration-excited *NO* molecules formed in a microwave discharge in the air because the probability of *VT*-relaxation of *NO* molecules is much greater than that of vibration-excited nitrogen molecules. However, the results of experiments in the pulse-periodic mode of microwave discharge in air [1] have demonstrated that the gas starts being heated even in the first pulse after the switching-on of the microwave energy, while a significant concentration of *NO* molecules is produced in the plasma only after several tens of pulses. Moreover, the gas is heated also effectively in pure nitrogen at the absence of *NO*.

The vibrational quantum exchange plays an important role in forming of the distribution of molecules over the vibrational levels. This process, with due regard for the anharmonicity of

vibrations, is accompanied by conversion of only a small part of vibrational energy to translational. Therefore, its rate is high even at low temperatures. It is able, in principle, to provide a fairly high rate of gas heating. However, as demonstrated by our experimental results [1, 11, 12], the fast heating of gas in a fixed region of space stops after a time on the order of *10-20 μs,* which is associated with the discharge movement and field screening, although, if *VV*-exchange was responsible for the gas heating, the fast heating would have been observed even after the switching-off of the microwave field. However, as demonstrated by our calculation [14], the relatively slow heating of gas at the rate of *0,1 K/μs*, which is observed after the switching-off of the electric field in the stage of deionization, is supported by this process quite well.

As the value of reduced electric field *E/n* increases the fraction of energy transferred to vibrational excitation of molecules decreases, and the fraction of energy for excitation of the electron states of molecules increases. It is known that vibration-translational relaxation in the air is slow but the processes of quenching of electron-excited molecules, which occur in various channels and involve the transfer of a part of energy of electron-excited molecules to translational degrees of freedom, are rather fast and may, in principle, support the observed fast gas heating.

In [1, 11, 12, 14] it was shown, that the mechanism connected with effective excitation of electron-exited states of nitrogen molecules at large values of the reduced electrical field *E/n≥100 Td* and their subsequent quenching is responsible for the gas fast heating. At this the part of excitation energy of these states is transferred in the heat of air. As our estimations show, only the quenching of electron-exited long-living states of the nitrogen molecules, which are effectively created in conditions of a surface microwave discharge in air, provides the observed gas heating rate.

In various sections of a surface microwave discharge the dependencies of gas and vibrational temperatures on a pulsed microwave power were measured too. It was shown, that the gas temperature increases up to *~2000 K* at growth of microwave power, whereas the vibrational temperature remains practically constant under these conditions, insignificantly decreasing with increase of microwave power. At this the maximal gas heating is observed in a place of excitation of a surface microwave discharge and gas temperature decreases by the end of the discharge

4.4. Electron density in plasma of surface microwave discharge in air

With the help of probe method the electron density and temperature were measured in plasma of a surface microwave discharge in air. The electron density and temperature were determined from the voltage-current characteristic of the double probes.

For measurements of spatial distribution of concentration of ions constant voltage *36 V* switches on between probes. Measuring resistance *23 Ohm* was series switched with a source. The signal from the measuring resistance, proportional a probe current, was transmitted on an entrance of digital oscilloscope *TDS-210.* A feed of an oscilloscope was carried out from an uninterruptible power supply *UPS* disconnected from a power circuit for the period of measurements. Start of an oscilloscope has been synchronized with a pulse of the microwave discharge, therefore measurements were carried out not only with spatial, but also with the time resolution. The typical picture of a received signal is shown on *Fig. 4.14.*

For measurement of voltage-current characteristics of the double probe in conditions of the pulsed-periodic discharge the sawtooth-voltage generator was included instead of course of constant voltage. The amplitude of sawtooth generator *±30 V* has been chosen from achievement of saturation of an ionic current. The signal from measuring resistance on the shielded cable with the earthed screen acted on vacuum sealing electric lock and further on one of channels of oscilloscope *TDS-210*. Similarly on a double probe the bias from the generator of a saw was feed.

The example of the voltage-current characteristic of the double probe, average for *10 μs* at the moment of time *50-60 μs* from the beginning of a microwave pulse, is given in *Fig. 4.15.* It is visible, that measured voltage-current characteristic is typical for a double probe. Feature is well expressed saturation of ionic parts of voltage-current characteristic: the ionic current practically does not depend on a voltage in a range from *10* up to *30 V*. Already this fact testifies to rather high concentration of the charged particles in researched plasma.

Value of ion density can be found from an ionic current of saturation I_+ under the formula [45]:

$$I_+ \cong 0.4en_0\sqrt{\frac{2kT_e}{M}}S, \qquad (4.17)$$

where for conditions of experiment S is the area of a probe surface.

For a finding-out of electron temperature the formula [46] applied generally when the voltage-current characteristic is asymmetrical was used:

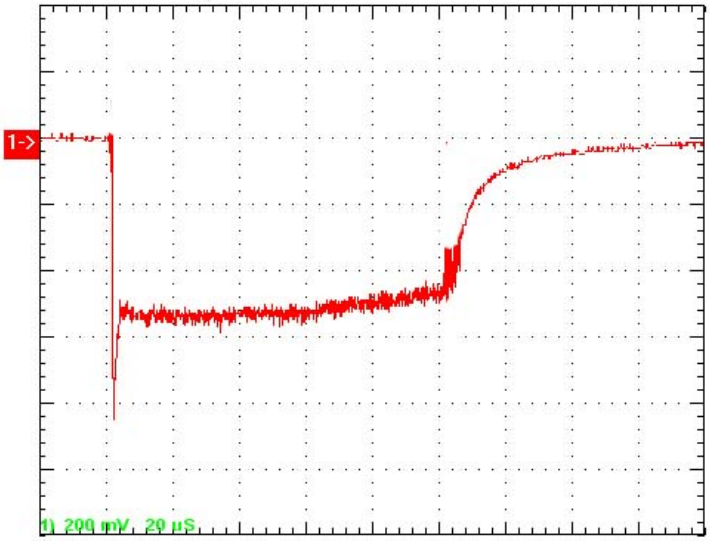

Fig. 4.14. The typical oscillogram of a double probe current.

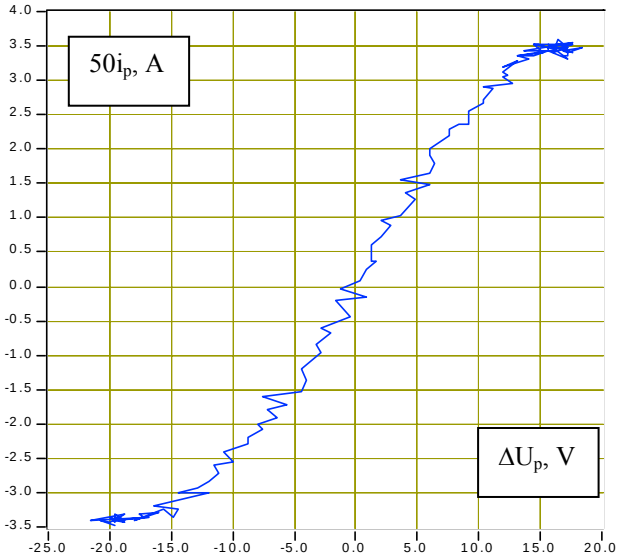

Fig. 4.15. Instantaneous voltage-current characteristic of the double probe in plasma of a surface microwave discharge at $p=10^{-3}$ *torr*, $W_p=50$ *kW*, $\tau=100$ *µs*, $y=2$ *cm*. Probe diametr is *1 mm*, time of registration of voltage-current characteristic is *10 µs*.

$$T_e \cong \frac{e}{k}\left(\frac{\Delta U}{\Delta I}\right)_{I=0} \frac{I_1 I_2}{I_1 + I_2}, \qquad (4.18)$$

where I_1 and I_2 are values of saturation currents of each of branches, and $\left(\frac{\Delta U}{\Delta I}\right)_{I=0}$ is the inclination of the voltage-current characteristic in a point where the current is equal to zero.

In this conditions the electron density equals $2 \cdot 10^{13}$ cm^{-3}. Experimentally found values of electron temperature lay within the limits of *2-4 eV*. Such values correspond to the values of T_e, received in the direct current discharge in air, that indirectly testifies to a correctness of the used measurement technique.

The cross-section distribution of electron density in plasma of a surface microwave discharge in air is submitted in *Fig. 4.16* at pulse microwave power *W=20 kW*. It is visible, that electron density during a pulse does not almost change and on distance of *y=6 cm* from a surface of the antenna, exceeds value of 10^{12} cm^3. At air pressure $p=10^{-3}$ *torr* electron density grows with increase of power and on distance *y=1 cm* from antenna exceeds 10^{13} cm^{-3} at *W=100 kW* (see *Fig. 4.17*) whereas on distance *y=5-10 cm* electron density is equal $n_e=(3\text{-}6)\cdot 10^{12}$ cm^{-3}.

It is necessary to pay attention to that fact, that at approach of a probe to the aerial on distance less than *1 cm* the measured electron density starts to decrease. It is connected to that fact, that at approach to a dielectric surface the rate of the charged particles loses increases. At the same time amplitude of an electric field exponentially decreases in process of removal from a surface of the aerial, that confirms as the data of mathematical modelling, and experimentally. The distortion of probe signal appears only at distance less than 1 mm.

The time dependence of probe current at various positions of a double probe concerning a plane of the antenna at air pressure $p=10^{-1}$ *torr* is resulted on *Fig. 4.18*. It is visible, that near antenna the probe current is constant during the microwave pulse whereas in process of removal from a surface there is the time delay growing with increase of distance from the body.

Longitudinal distribution of electron density in plasma of a surface microwave discharge in air is submitted in *Fig. 4.19* at pressure $p=10^{-1}$ *torr*. One can see, that electron density on distance *z=5-10 cm* from the surface lays within the limits of 10^{11}-10^{12} cm^{-3}.

The concentration of electrons in plasma of surface microwave discharge was also determined by the Stark broadening of the H_β (λ*=486,1 nm*) line of hydrogen. The radiation from the discharge was projected by a system of lenses and mirrors onto the entrance slit of the double monochromator *DFS-12* (look *Fig. 3.1*, Chapter III) with a return linear dispersion of *0,5 nm/mm* and instrumental function of *0,015 nm* (look *Fig. 3.11*, Chapter III). The output

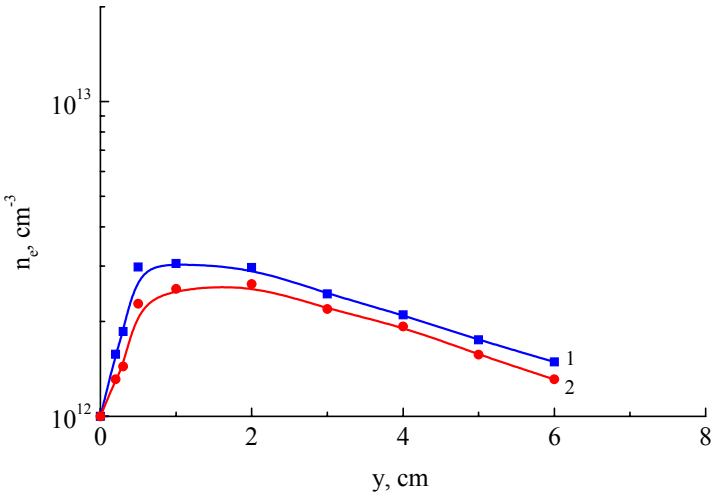

Fig. 4.16. Cross-section distribution of electron density in section with longitudinal coordinate *z=2 cm* in plasma of a surface microwave discharge in air at pressure $p=10^{-3}$ *torr*, pulse duration $\tau=200$ *μs*, pulsed microwave power $W_p=20$ *kW*, at the moment of time *t, μs*; 1-50, 2-150.

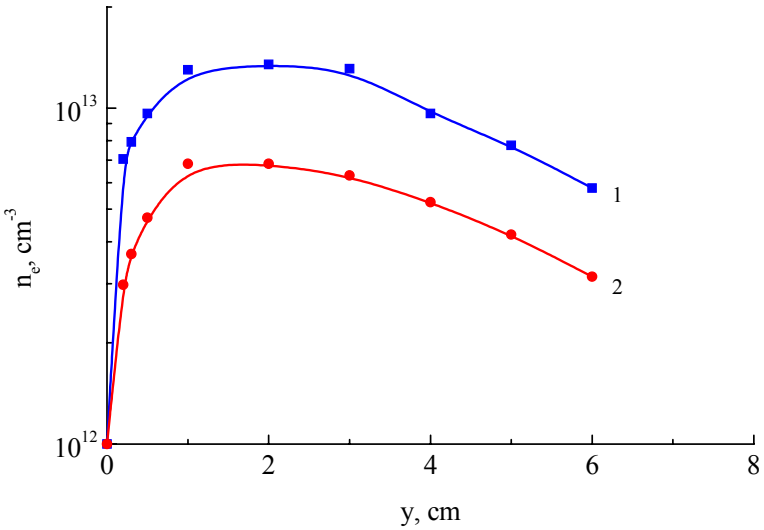

Fig. 4.17. Cross-section distribution of electron density in section with longitudinal coordinate *z=2 cm* in plasma of a surface microwave discharge in air at pressure $p=10^{-3}$ *torr*, pulse duration $\tau=200$ *μs*, pulsed microwave power $W_p=100$ *kW*, at the moment of time *t, μs*; 1-50, 2-150.

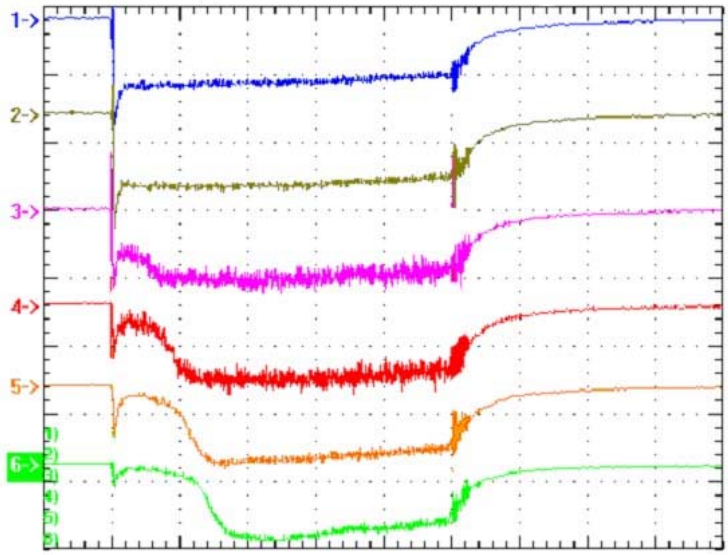

Fig. 4.18. Time dependence of probe current at *z=1,5 cm*, air pressure $p=10^{-1}$ *torr* and various positions of a double probe concerning a plane of the antenna *y, cm*: 1-1, 2-2, 3-3, 4-4, 5-5, 6-6.

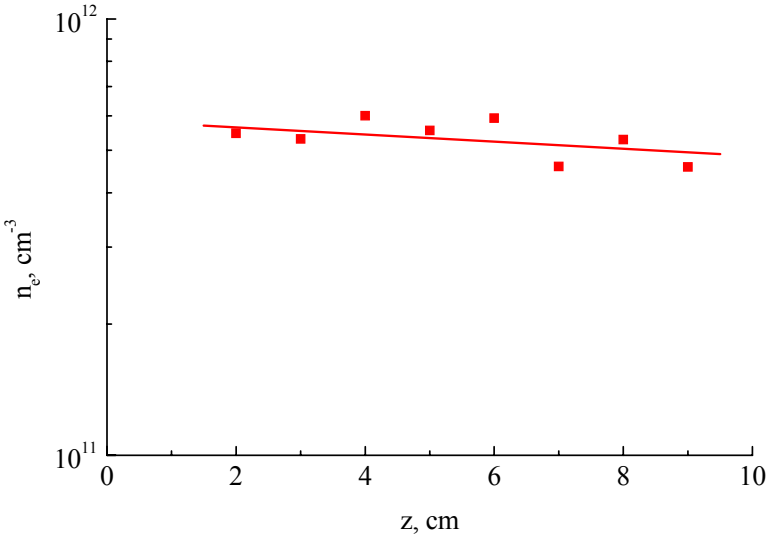

Fig. 4.19. Longitudinal distribution of electron density in plasma of a surface microwave discharge on distance *y=5,5 cm* from the surface at $p=10^{-1}$ *torr*, $\tau=100$ *μs*, *W=20 kW*, and at the moment of time *t=30 μs*.

signal of the photomultiplier was entered either into a storing oscillograph or to a setup consisting of a time selector, two narrow-band amplifiers, a synchronous detector, a dc amplifier, and a strip chart recorder. The system enabled us to record the spectral line profile emitted by the pulsed-periodic discharge.

Measurements were carried out at air pressure in the chamber $p=0,1\text{-}10$ *torr*. As a small impurity in the chamber the small amount of propane was added. Thus in a surface microwave discharge the effective decomposition of propane took place and hydrogen in amount sufficient for excitation of H_β line and registration of its profile was turned out. The profile of hydrogen H_β line ($\lambda=486,1$ *nm*) at air pressure $p=10$ *torr*, microwave power $W_p=100$ *kW* and pulse duration $\tau=50$ μs is shown in *Fig. 4.20*. The electron density was deduced from the H_β profile with taking into account broadening factors such as the instrumental function (*0,015 nm*), the Doppler effect (about *0,01 nm*), the external microwave Stark effect (about *0,01 nm*), and finite width of the monochromator entrance slit.

It has been received, that within the limits of an experimental mistake the electron concentration near to antenna surface reaches the value $(5\text{-}10)\cdot 10^{13}$ cm^{-3}, that well coordinates with electron density $2\cdot 10^{13}$ cm^{-3}, measured by probe method on distance of $y=2$ *cm* from an antenna surface.

4.5. Shock wave generation by surface microwave discharge

The previous measurements have revealed that there is a big intensity of electric field in plasma of a surface microwave discharge. The electric field is concentrated in narrow near-surface layer. It conducts to the effective contribution of energy to gas and fast rise in gas temperature with a rate of some tens degrees for microsecond. It should result in thermal explosion on a surface of the antenna.

Investigation with the help of a shadow method of process of formation of the microwave discharge on an external surface of a dielectric body has revealed that generation of a flat single shock wave takes place at the initial stage of pulse inclusion of energy on a surface of the aerial. Shadow photos were fixed at various time delays of a flash lamp concerning forward front of a microwave pulse. The exposition time of each frame is $2,9$ μs.

Evolution of shock wave generated by surface microwave discharge is shown in *Fig. 4.21* at various time delay of picture registration regarding to beginning of a microwave pulse. It is possible to see, how at breakdown and appearance of a surface microwave discharge in the field

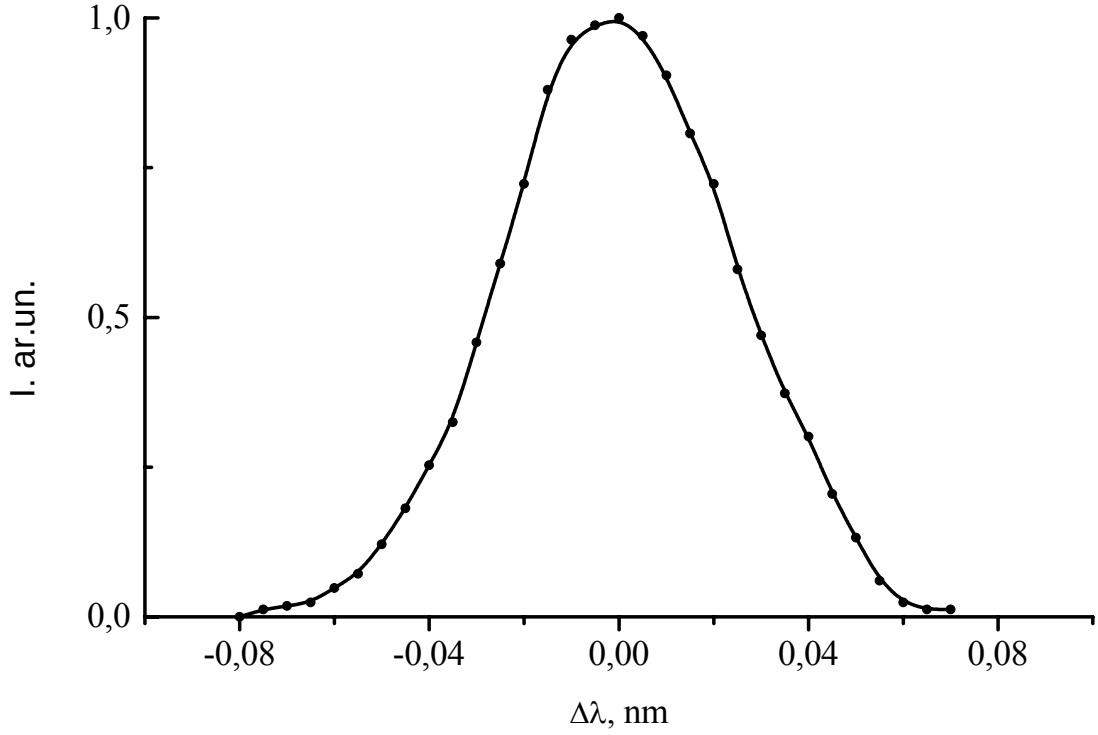

Fig. 4.20. H_β profile of hydrogen line *(λ=486,1 nm*) at air pressure *p=10 torr*, microwave power W_p*=100 kW* and pulse duration τ*=50* μ*s*.

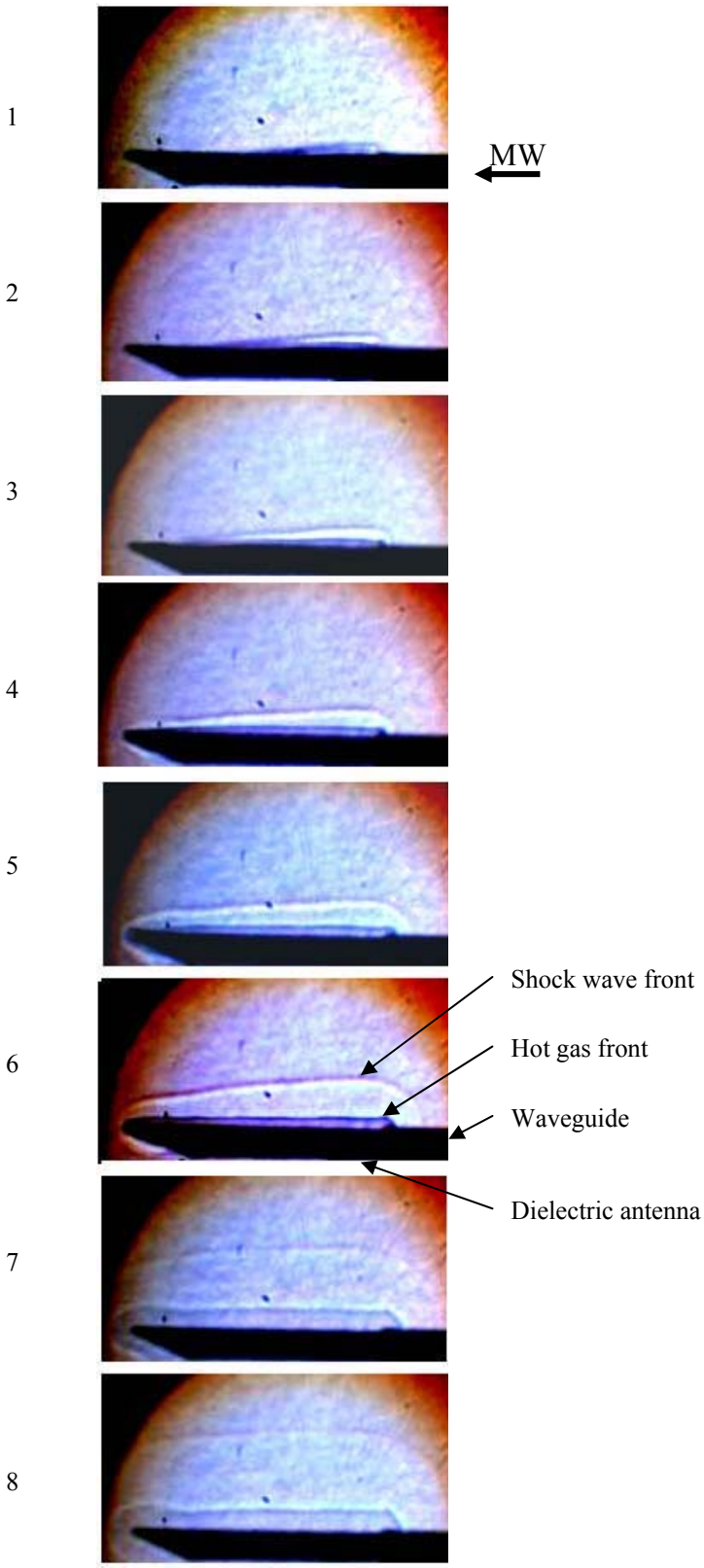

Fig. 4.21. Evolution of shock wave generated by surface microwave discharge. Time delay of picture registration regarding to beginning of a microwave pulse t_{del}, μs: 1-9,5; 2-11, 3-13,5; 4-18,5; 5-28,5; 6-38,5; 7-58,5; 8-78,5.

of energy supply there is a generation of a shock wave. In process of propagation of the discharge along the antenna, generation of a shock wave occurs in the next areas. It is visible also (see *Fig. 4.21*, fragment 2-8), that after some time interval the front of shock wave leaves the area of heated gas.

Time dependence of a shock wave front position (transverse coordinate y) concerning of the antenna surface is submitted in *Fig. 4.22* for various longitudinal coordinates *z*. Time dependence of a shock wave front velocity is shown in *Fig. 4.23*. From this figure follows, that cross-section concerning the aerial velocity of a shock wave can reach of *1100 m/s* at the initial stage of discharge formation whereas at late stages this velocity decreases up to *370 m/s*.

Preliminary experiments on research of influence of the surface discharge created before a step, on position of front of the shock wave arising on an obstacle streamlined by supersonic airflow have been carried out also. The received shadow photos are submitted in *Fig. 4.24.* It is visible, that plasma of the surface microwave discharge duration only *20 μs* renders essential influence on a shock wave arising on a step. Through *30-40 μs* after switching-on of the surface microwave discharge the shock wave vanishes and again arises after that only through *~200 μs*. It is possible to draw preliminary conclusion that with the help of the surface microwave discharge is possible to operate characteristics of a supersonic stream near a body moving with supersonic velocity in dense layers of an atmosphere.

4.6. Interaction of supersonic airflow with the surface microwave discharge, created on an external surface of the dielectric body

In *Fig. 4.25* the general view of the combined microwave discharge created in motionless air on a surface of a wedge dielectric body at various microwave pulse duration is submitted. It is visible, that at the fixed microwave power plasma covers the increasing part of the antenna when pulse duration grows. The volumetric microwave discharge arises on a fore-part of the antenna only at the values of a microwave pulse duration more, than duration necessary for creation of a microwave discharge on all surface of the dielectric antenna. At microwave pulse duration *τ=50 μs* on a forward edge of the antenna volumetric plasma formation starts to be formed. Thus, with growth of pulse duration the size of spherical plasma derivation is increased.

The shadow photos of a surface microwave discharge created in motionless air on the antenna of rectangular section with a wedge forward part are represented in *Fig. 4.26* at microwave pulse duration *τ=100 μs.* The shadow photos at all values of the microwave power

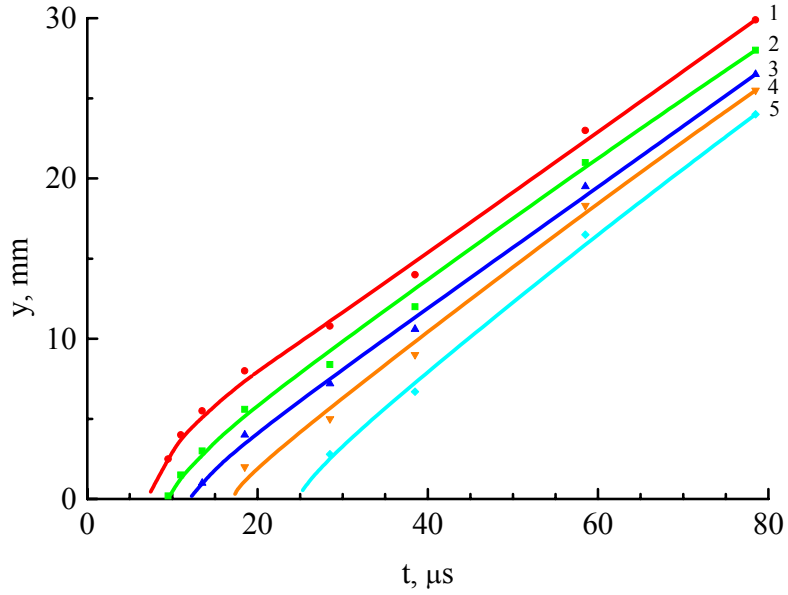

Fig. 4.22. Time dependence of a shock wave front position (transverse coordinate y) concerning of the antenna surface at various longitudinal coordinates *z, cm*: 1-1; 2-3; 3-5; 4-6; 5-7.

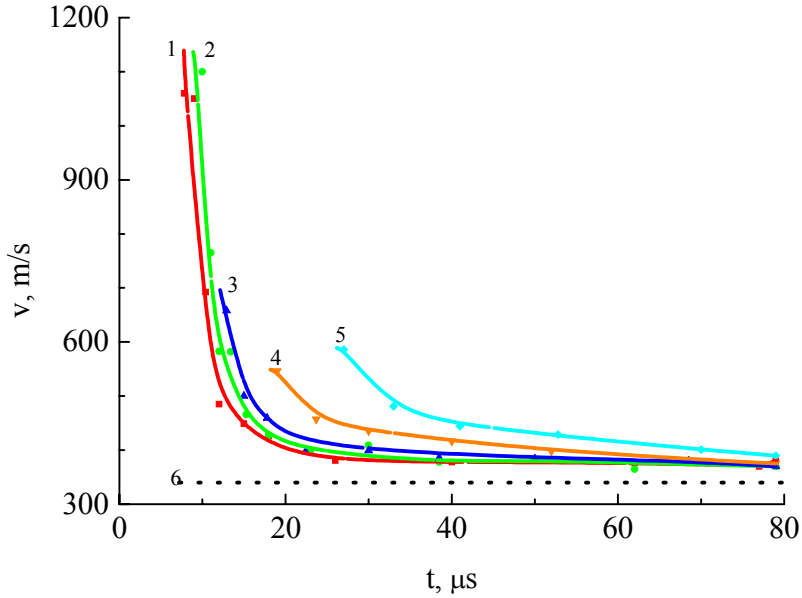

Fig. 4.23. Time dependence of a shock wave front velocity at various longitudinal coordinates *z, cm:* 1-1; 2-3; 3-5; 4-6; 5-7. (Dot line (6) – sound velocity)

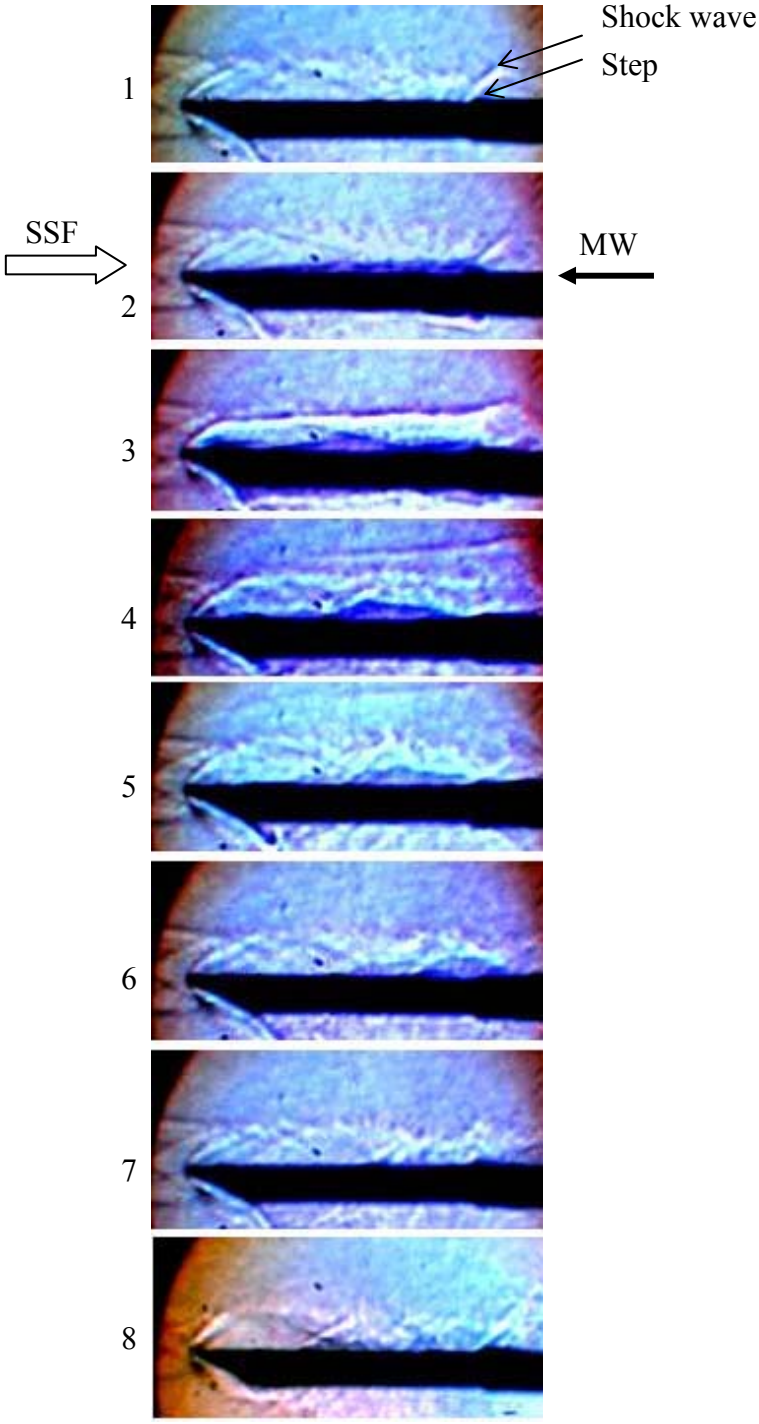

Fig. 4.24. Influence of the surface microwave discharge created before a step, on position of front of the shock wave arising on an obstacle streamlined by supersonic airflow at $M=2$, air pressure $p=40$ *torr,* pulsed microwave power $W_p=55$ *kW,* microwave pulse duration $\tau=20$ μs. Time delay of picture registration regarding to beginning of microwave pulse t_{del}, μs: 1-0; 2-17; 3-37; 4-57; 5-77; 6-119; 7-159; 8-259.

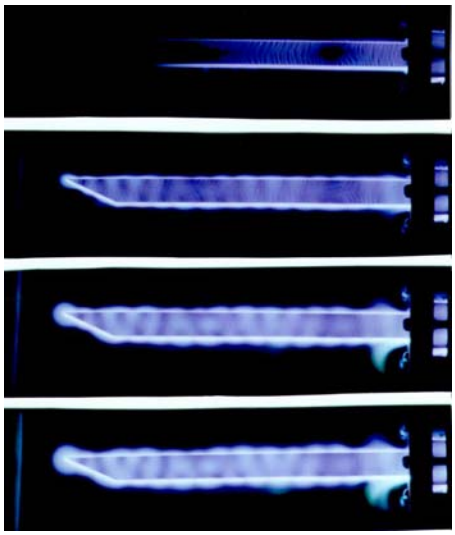

Fig. 4.25. Common view of the combined microwave discharge on a wedge dielectric body in motionless air at pressure *p=40 torr*, microwave power *W=130 kW*, and at various pulse duration *τ, μs*: 1 – 5; 2 – 50; 3 – 75; 4 – 100.

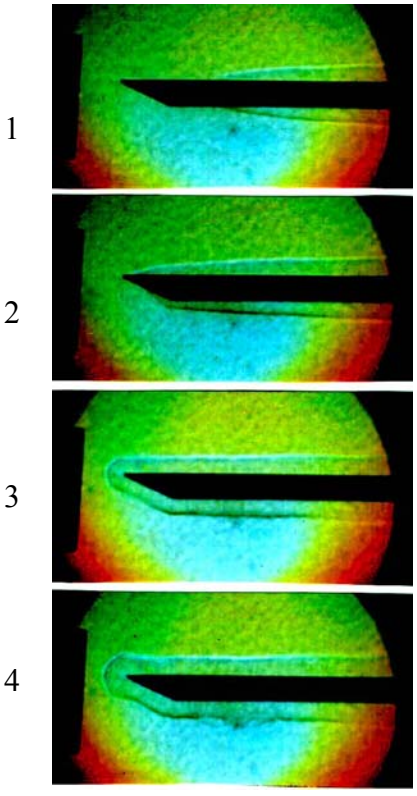

Fig. 4.26. Shadow graphics photos of the antenna with a surface microwave discharge at *p=40 torr; τ=100 μs*; time delay of picture registration regarding to beginning of a microwave pulse t_{del}*=100 μs; W, kW*: 1 – 75; 2 – 95; 3 – 130; 4 – 170.

were registered at the end of the microwave pulse. At this the pulse of a flash lamp of shadow installation was delayed *on* $t_{del}=100\ \mu s$ concerning forward front of the microwave pulse.

It is visible, that at threshold values of the microwave power when the discharge has not time to cover whole antenna surface during a microwave pulse, the gas density deformation is observed only about a part of the antenna surface. When the microwave power increases the discharge covers full antenna to the end of a pulse duration $\tau=100\ \mu s$, and the gas density deformation is observed around all body. Thus because of the discharge movement the gas is heated during greater time in the zone of the microwave energy input to the antenna in comparison with average parts of the body, and, especially, on a forward edge of the antenna. Therefore the thickness of the disturbed gas density area decreases on body length. At great values of the microwave power the discharge achieves a forward edge of the aerial during several microseconds; therefore gas temperature, and accordingly the thickness of the disturbed gas density area, vary insignificantly on length of the antenna.

It is known, that an input of energy in area of a boundary layer or the local heating of a plate surface in the field of a turbulent boundary layer result in noticeable reduction of a local coefficient of turbulent friction at the expense of decreasing of a transverse gradient of longitudinal flow velocity and increase of a displacement thickness. In the case of a surface microwave discharge the microwave field is localized in a thin near-surface layer that promotes the effective contribution of energy to plasma and fast gas heating, which should result in change of supersonic flow near a body surface.

With the help of the shadow graphic installation the interaction of supersonic airflow with the surface microwave discharge, created on an external surface (in a boundary layer) of the wedge dielectric body, was examined for check of the supposition that the surface microwave discharge in our conditions can render noticeable influencing on streamlining of model by supersonic airflow The process of streamlining of a short dielectric wedge-shaped antenna ($l=5\ cm$) by supersonic airflow is submitted in *Fig. 4.27*. One can see the surface microwave discharge influence on the change of a head shock wave (the shock wave inclination angle is increased) and both attenuation and disappearance of the jumps on area of a separated flow on the upper plane of the antenna, and also degradation of the jumps on the lower plane of the antenna in the field of turning-point of supersonic airflow.

Streamline by supersonic airflow of a wedge dielectric body without microwave discharge and with a combined microwave discharge, created on wedge antenna at air pressure $p=40\ Top$, microwave pulse duration $\tau=100\ \mu s$, and microwave pulsed power $W_p=200\ kW$ is

Fig. 4.27. Streamlining of a short dielectric wedge-shaped antenna by supersonic airflow (on top - without surface microwave discharge; below - with surface microwave discharge).

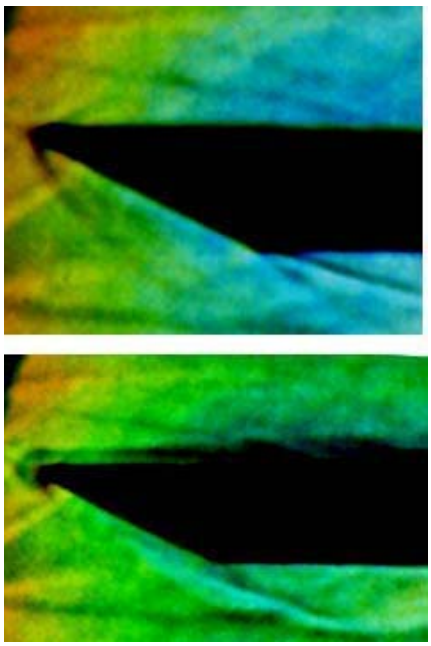

Fig. 4.28. Streamlining of a short dielectric wedge-shaped antenna by supersonic airflow (on top - without combined microwave discharge; below - with combined microwave discharge).

shown in *Fig. 4.28*. It is visible, that the head shock wave completely disappears at creation of the combined microwave discharge. It confirms our assumption that the microwave discharges can render essential influence on movement of a body in dense layers of an atmosphere.

The general view of a surface microwave discharge on an external surface of a wedge dielectric body, streamline by supersonic airflow at Much number $M=2$ is submitted in *Fig. 4.29* at various microwave pulse durations. One can see that supersonic flow does not destroyed the microwave discharge from the body surface whereas in experimental conditions the volumetric plasma formation is not created on a forward edge of a wedge.

The shadow photos of a surface microwave discharge created in supersonic airflow on the antenna of rectangular section with a wedge forward part are represented in *Fig. 4.30* at microwave pulse duration $\tau=100\ \mu s$. The shadow photos at all values of the microwave power were registered at the end of the microwave pulse. At this the pulse of a flash lamp of shadow installation was delayed on $t_{del}=100\ \mu s$ concerning forward front of the microwave pulse.

It is visible, that the boundary layer thickness and the shock wave inclination angle increase at increasing of microwave power that should result in reduction of boundary friction force and wave resistance. Thus at the large power the formation of vortex flow near a surface of the aerial is distinctly visible, that well coordinates with the calculation data (see Chapter VIII).

The shadow graphics pictures of the wedge antenna at the different microwave discharge existence instants ($t=0\text{-}100\ \mu s$) and in plasma deionization stage ($t=100\text{-}180\ \mu s$) are submitted on *Fig. 4.31*. One can see that in process of discharge evolution the boundary layer thickness starts to increase. It should result to decrease of a turbulent friction coefficient, as it is inversely proportional to a displacement thickness and directly proportional to a transverse gradient of longitudinal flow velocity. It is experimentally reveal also, that the inclination angle of a shock wave which is generated in supersonic airflow on a leading edge of the antenna is increased at creation of a surface microwave discharge.

It was experimentally shown, that in process of discharge evolution the boundary layer thickness starts to increase. It should result to decrease of a turbulent friction coefficient. The time evolution of the inclination angle of a head shock wave arising on a wedge dielectric body in supersonic airflow is submitted in *Fig. 4.32.* One can see that in process of the surface discharge evolution the inclination angle of the head shock wave is increased. To the end of a microwave pulse $\tau=70\ \mu s$, when the plasma layer covers the whole antenna, the variation δ of the inclination angle reaches *~20 %*, that corresponds to reduction of flow Mach number in this area of the antenna. Thus, if the microwave pulse should was the greater duration, the effect would

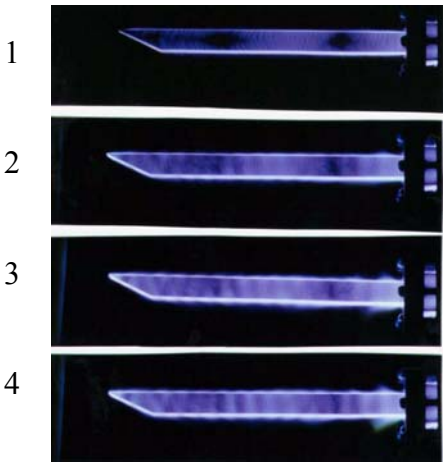

Fig. 4.29. Common view of the surface discharge on a wedge antenna in supersonic flow at *M=2, p=40 torr,* W_p*=130 kW*, and various pulse durations τ, μs: 1–20; 2–50; 3–75; 4–100.

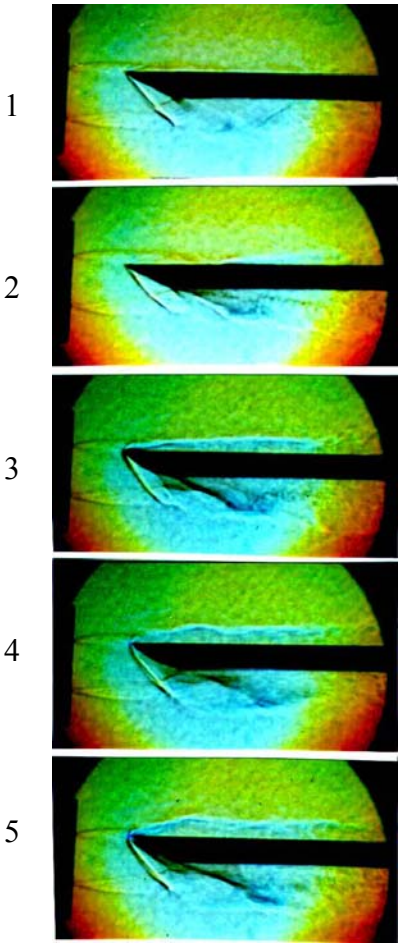

Fig. 4.30. Streamlining of a dielectric wedge-shaped antenna by supersonic airflow at *M=2; p=40 torr;* τ*=100* μs*;* t_{del}*=100* μs, and *W, kW*: 1–60; 2–75; 3–95; 4–130; 5–170.

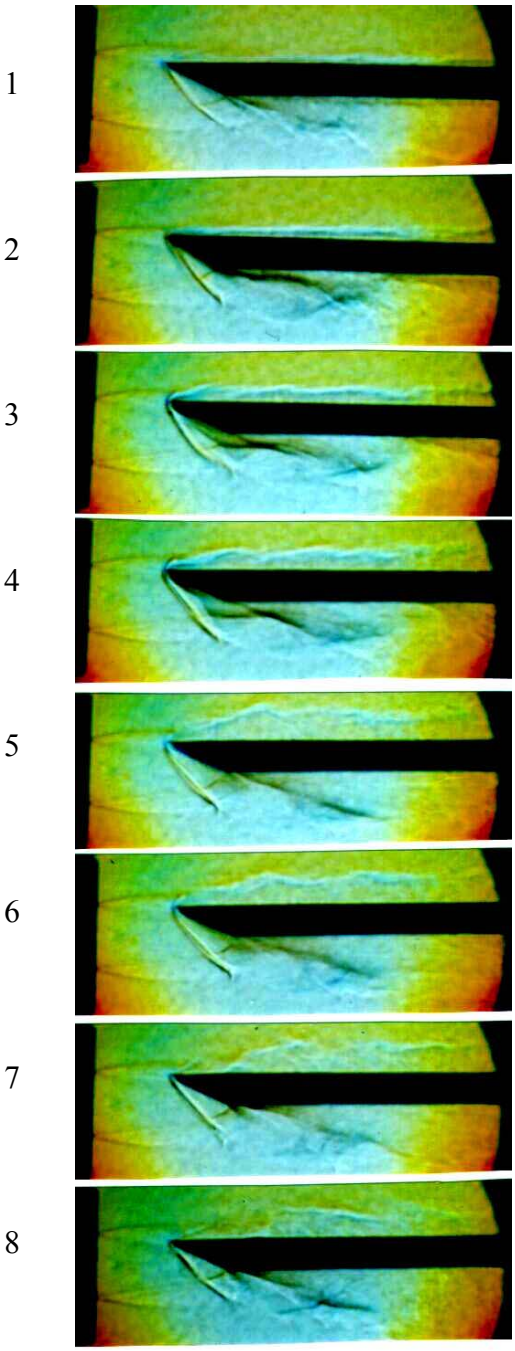

Fig. 4.31. Shadow graphics photos of process of streamlining by supersonic airflow of the antenna with a surface microwave discharge at *p=40 torr; τ=100 μs; W=130 kW; M=2*; time delay of picture registration regarding to beginning of a microwave pulse *t, μs*: 1-20; 2-45; 3-60; 4-80; 5-100; 6-125; 7 – 160; 8 – 180.

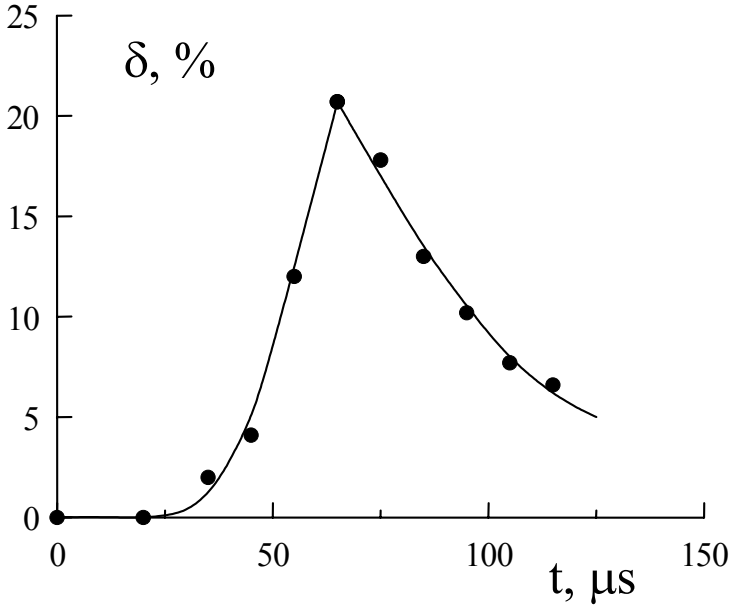

Fig. 4.32. The surface microwave discharge influence on the inclination angle of a head shock wave, arising on a leading edge of the wedge antenna at τ*=70 μs, p=40 torr, M=2,* and microwave power $W/W_{ow}=2$. W_{ow} is microwave power necessary for creation of a surface microwave discharge on all surface of the wedge dielectric body.

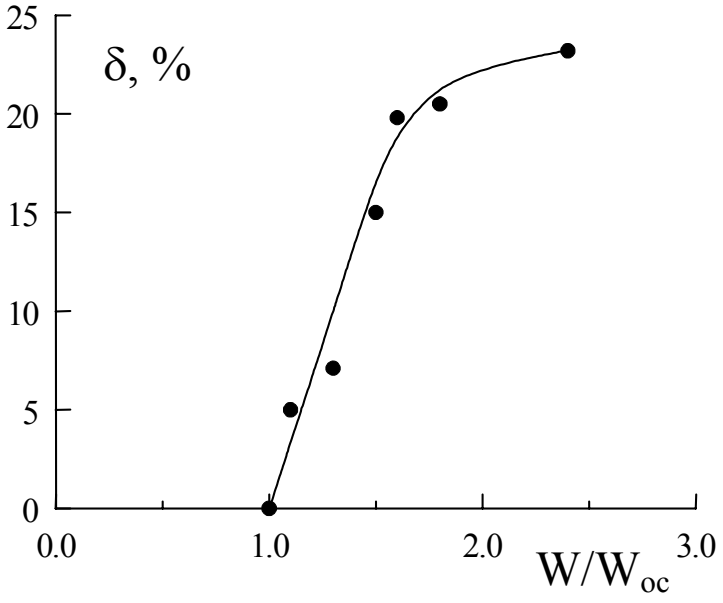

Fig. 4.33. The variation of a shock wave inclination angle at creation surface microwave discharge vs the input power. W_{oc} is microwave power necessary for creation of a surface microwave discharge on all surface of the cylindrical antenna with cone tip. Air pressure *p=25 torr,* τ*=100 μs*.

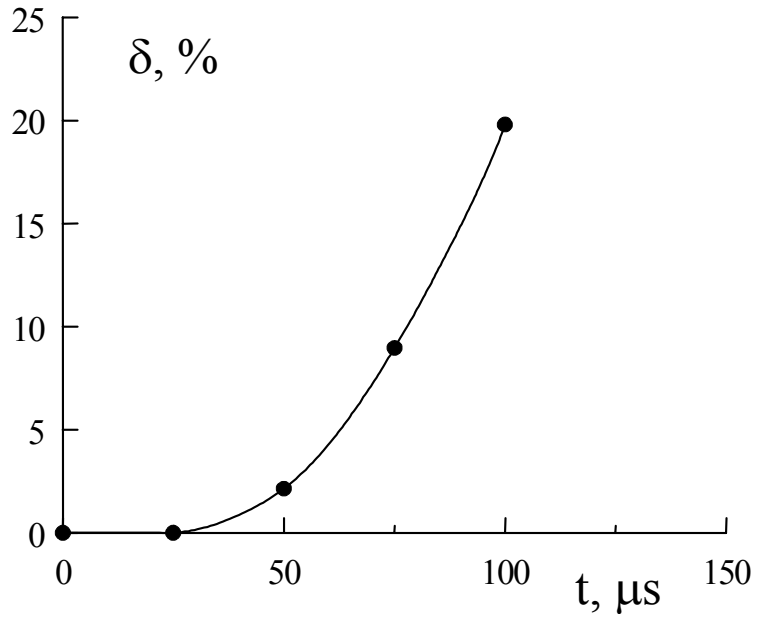

Fig. 4.34. The time evolution of a shock wave inclination angle at creation surface microwave discharge on the cylindrical antenna with cone tip. $W/W_{oc}=1.8$. Air pressure $p=25$ *torr*.

prolong to be increased, as transition to a saturation does not take place in *Fig. 4.32*. After switch off of a microwave energy, the effect exists *~100μs* continuously decreases in process of the heated gas drift by supersonic airflow.

It is experimentally shown, that the inclination angle of a shock wave, arising on a leading edge of the cylindrical antenna with conical tip, also increases at presence of a surface microwave discharge, accordingly, the Mach number of airflow decreases. The microwave power influence on parameters of supersonic airflow near to a cylindrical antenna with a conical end part is given in *Fig. 4.33*. One can see, that the surface microwave discharge starts to influence on flow parameters when microwave power increases up to value necessary for creation of a surface microwave discharge on all surface of the cylindrical antenna with cone tip, and at *W/Woc=2* Mach number of a airflow decreases about *25 %* (*Fig. 4.33*).

The time evolution of a shock wave inclination angle at creation surface microwave discharge on the cylindrical antenna with cone tip at microwave power $W/W_{oc}=1.8$ is represented in *Fig. 4.34*.

CHAPTER V
IGNITION OF SUPERSONIC PROPANE-BUTANE-AIR FLOW WITH USE OF FREELY LOCALIZED MICROWAVE DISCHARGE

5.1. Introduction

In the Chapter V the experimental data on study of properties of a freely localized microwave discharge created in motionless gas and in supersonic flow of air and air-propane mixture with Mach number $M=2$ are discussed. The influence of supersonic airflow on properties of a freely localised microwave discharge was investigated too. The ignition of propane-air mixture in supersonic flow with Mach number $M=2$ was studied.

The intensive researches in the field of physics of non-equilibrium plasma of a various type of the microwave discharges are stimulated by their wide application in various areas of modern plasma technologies.

In the last time advances in the development of microwave electronics have led to the possibility of creating of a new form of gas discharge, namely, the electrodeless microwave discharge in free space [1]. A study of the properties of a microwave discharge removed both from the discharge chamber walls and from the radiation sources is topical from the point of view of both the solution of a number of fundamental problems of plasma physics and its practical application in fields such as: i) combustion of fuel in supersonic engine; ii) creating plasma regions in front of flying vehicles for changing the conditions of gas flow about solid surfaces and lowering the head resistance during their motion in the atmosphere with supersonic velocities; iii) the transfer of the energy of powerful electromagnetic radiation through the Earth's atmosphere along the space-Earth route; iiii) the creation of radio-reflecting regions of artificial ionization in the upper layers of the atmosphere; iiiii) the solution of environmental problems (for example, cleaning the Earth's atmosphere of harmful impurities); iiiiii) for developing of jet propulsion using an energy source located outside of the flying vehicle being accelerated.

A study of the free-localized discharge in air is one of the fundamental problems of plasma physics, related to the investigation of physical processes occurring in a microwave discharge induced by a powerful focused beam of electromagnetic energy in a predetermined place in space under conditions in which electromagnetic and gas-dynamic phenomena affect

significantly plasma kinetics, and kinetic and gas-dynamic processes influence the space-time evolution of the discharge.

A microwave discharge emerging in the focus region of an electromagnetic energy beam is a complex nonlinear phenomenon including a non-stationary breakdown of gas, propagation of ionization fronts interacting with microwave radiation, maintenance of non-equilibrium plasma formed in the beam focus region by an incident energy flux, and the excitation and heating of molecules accompanied by deformation of neutral gas density. It is known that under the effect of a strong focused beam of electromagnetic waves of the microwave range the gas breakdown occurs on the condition that the electric field strength in the focal region of the discharge chamber exceeds the threshold value. After this breakdown, the plasma formed in the beam focus starts to absorb intensively the energy delivered to the discharge, and the microwave discharge in the beam with a small angle of convergence has the tendency to shift toward the radiation source due to certain mechanisms (breakdown wave, resonance radiation diffusion, diffusion of charged particles, the mode of heat-conductive slow combustion, and a number of other processes).

In the experiments the properties of freely localized microwave discharge were investigated. With this purpose the scheme of realisation of a microwave discharge in supersonic airflow with Much number *M=2* was developed (look Chapter 2, *Fig. 2.2*).

The basic characteristics of used facilities:

- magnetron generator: $\lambda=2,4$ *cm,* $W_p<500$ *kW,* $\tau=1\text{-}200$ *μs, Q=1000*;
- experimental conditions: freely localized microwave discharge in air, hydrogen and air-propane mixture;
- waveguide system: $S=9,5x19$ mm^2, SF_6, *p=5 atm*;
- discharge chamber: *D=1 m* and *H=3 m*;
- vacuum system $p=10^{-1}\text{-}10^3$ *torr*;
- microwave lens: *D=60 cm*;
- cylindrical aerodynamic channel: quartz tube *d=3 cm* and *L=50 cm*;
- converging-diverging nozzle (Laval nozzle): supersonic flow *M=2, t=2 s, d=3 cm*.

The parameters of the microwave generator allow receiving an electrodeless microwave discharge in the focused beam at air pressure up to *100 torr*. For formation of microwave discharge at large pressure it is necessary to use the initiators. However it is known, if the microwave discharge was initiated and gas breakdown has taken place, the plasma can be supported by under breakdown electrical fields for a long time. In the given series of experiments for this purpose the special initiator was used. The initiator was located in focal area

of the focused beam. With the help of the initiator it is possible to receive a microwave discharge in a wide range of air pressure and microwave power flux density.

5.2. Parameters of freely localized microwave discharge

Understanding of the physics of non-equilibrium plasmachemical systems, to which one can also assign the freely localized microwave discharge in air, is impossible without full information on the kinetics of processes occurring in plasma. The translational gas temperature is one of the basic parameters of plasma, governing the rate and direction of many processes. The heating of gas in the discharge, created in a supersonic air flow, results in essential change of the characteristics of flow. The plasma ionization degree influences on rate of formation of radicals and active particles that can essentially influence on ignition of combustible gaseous mixtures.

The common view of a microwave discharge in the focused beam under condition of motionless air is submitted in *Fig. 5.1*. One can see that the microwave discharge has got complex periodic structure. It consists from several plasmoids. The sizes of these plasmoids and distance between them do not exceed centimeter.

The common view of freely localized microwave discharge in supersonic airflow at Mach number $M=2$ is submitted in *Fig. 5.2.* It was obtained too that the sizes of a microwave discharge decrease with growth of air pressure.

Fig. 5.3 represents the common view of a microwave discharge in supersonic airflow at $M=2$, $p=350$ torr, $\tau=300$ μs, $f=10$ Hz. The common view of a microwave discharge, created before a body streamlined supersonic airflow is submitted in *Fig. 5.4.* The received results point out that there is an opportunity of creation of a microwave discharge before a body moving with supersonic velocity in an atmosphere.

In all photos the supersonic stream is directed from top to down, is perpendicular to a direction of distribution of the microwave energy from left to right.

In a case of the electrodeless microwave discharge the electric field is located in space in focal area of the focused beam. This localization does not depend that electromagnetic energy is focused either in motionless gas or in supersonic stream of gas. From here supersonic stream does not blow off the microwave discharge from the area of space fixed by a beam as opposite of the electrode discharges. Plasma exists in the fixed area of space during all duration of the microwave pulse.

The experiments have shown that supersonic airflow does almost not influence on a level of a microwave power required for maintenance of the discharge, and on a common view of the

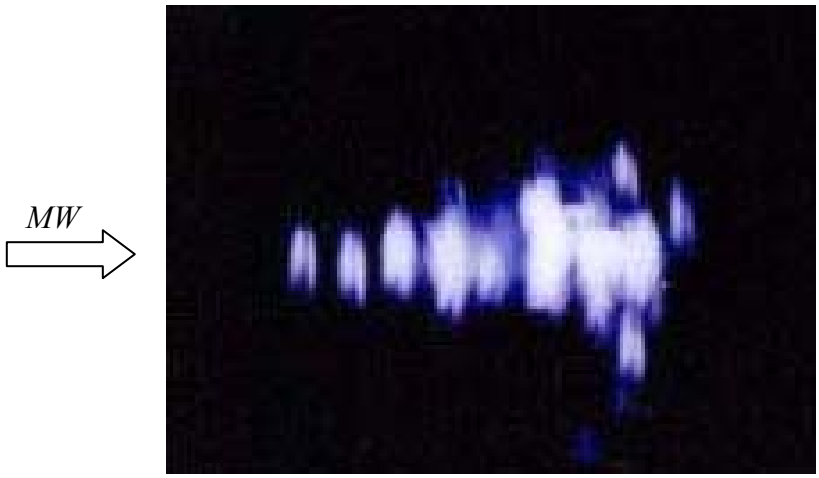

Fig. 5.1. The common view of freely localized microwave discharge under condition of motionless air at pressure *p=40 torr*, pulse duration τ*=200 μs*; pulse repetition frequency *f=10 Hz*. → *MW* – microwave direction.

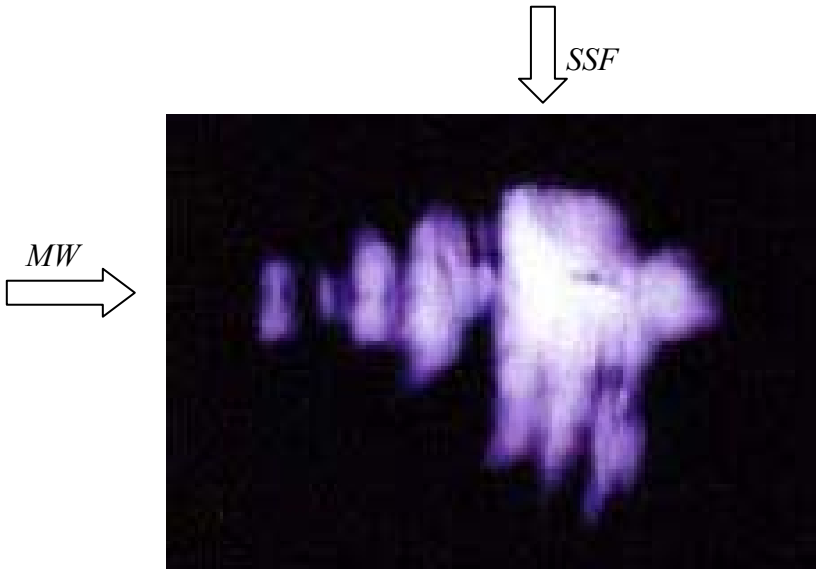

Fig. 5.2. The common view of freely localized microwave discharge in supersonic flow at Mach number *M=2*, air pressure *p=40 torr*, pulse duration τ*=200 μs*; pulse repetition frequency *f=10 Hz*. ↓ *SSF* – supersonic flow direction. → *MW* – microwave direction.

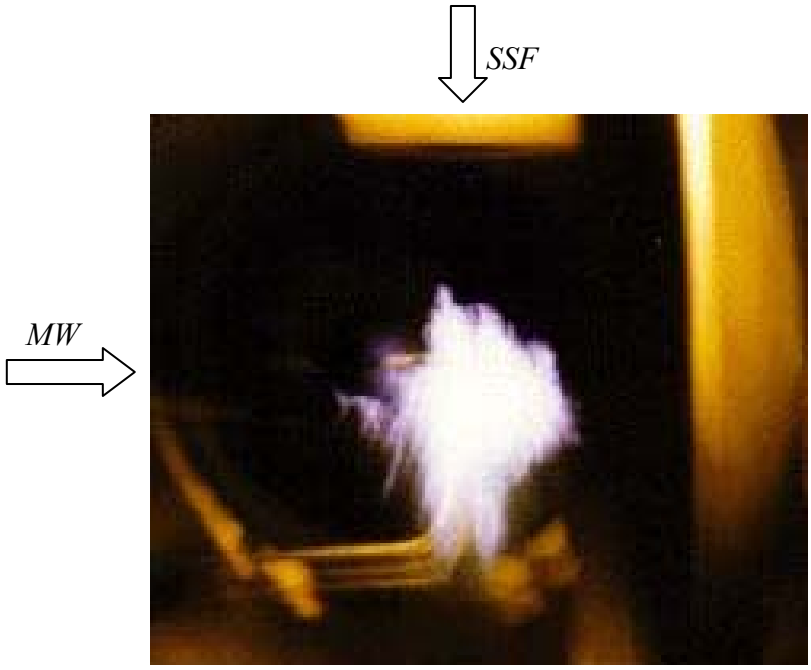

Fig. 5.3. The general view of freely localized microwave discharge in free supersonic stream of air at *M=2, p=350 torr, τ=300 μs, f=10 Hz*.

↓ *SSF* – supersonic flow direction. → *MW* – microwave direction.

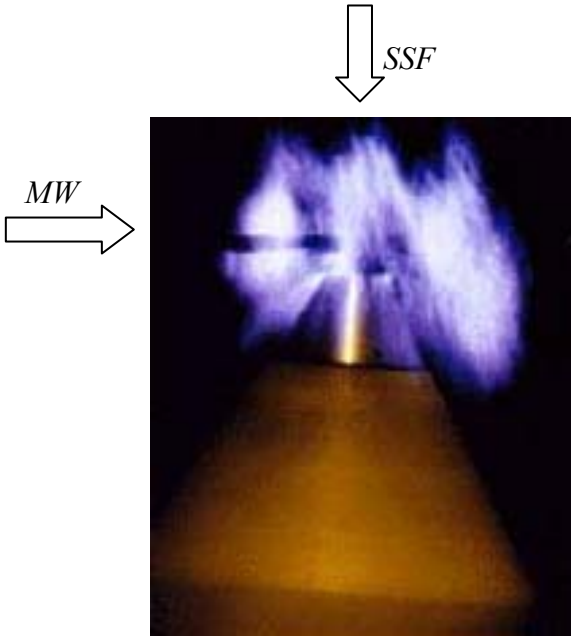

Fig. 5.4. The common view of a microwave discharge created before a body streamlined by supersonic airflow at *τ=30 μs; f=100 Hz; p=40 torr*.

↓ *SSF* – supersonic flow direction. → *MW* – microwave direction.

microwave discharge. There is no appreciable difference between cases when at first a pulse microwave discharge in air is created, and then the supersonic airflow is formed and in opposite case when at first supersonic flow of air is formed and then the microwave discharge in the focused beam is created.

The dependence of the gas temperature in the microwave discharge at the threshold value of input energy on the air pressure is shown in *Fig. 5.5.* One can see that the gas temperature monotonously increases from *500 K* up to *2000 K* with the air pressure growth from *10 torr* up to *100 torr*. In the same conditions the dependence of vibrational temperature on air pressure has obviously non-monotonous kind with a minimum at air pressure *p~30 torr* (*Fig. 5.6*). This pressure corresponds to a minimum of Pashen's curve for used wavelength of a microwave radiation, i.e. at this pressure the minimal threshold power for creation of the freely located microwave discharge in air is required.

The dependencies of gas and vibrational temperatures from a microwave power at air pressure *p=60 torr* are submitted on *Fig. 5.7* and *Fig. 5.8* accordingly (W_b is breakdown power at air pressure *p=60 torr*). One can see that the temperature of gas at first increases, and then passing through a maximum decreases with increase of a microwave power. At this, vibrational temperature of molecules with growth of power monotonously decreases. The carried out experiments have shown also, that the supersonic flow of air does not influence on gas heating. The gas temperature under condition of microwave discharge in motionless air and in supersonic flow coincides with each other within the limits of accuracy of measurements.

Under conditions of self-sustained microwave discharge in the focused beam at threshold values of microwave energy the electron density in plasma is within limits of critical concentration, the field freely penetrates into plasma, the velocity of spreading of the discharge is small. In this case effective excitation of electronic states of molecules takes place, and the gas is heating in fixed place during of a microwave pulse. The gas temperature is increased (look *Fig. 5.7*). The further increase of microwave power results to increase of velocity of a movement of the discharge and growth of electron concentration in plasma, that conducts to reduction of value of a electric field in plasma due to skin-effect and accordingly to decrease of gas heating rate.

Gas temperature under condition of microwave discharge in hydrogen have been determined with the temporary resolution (*~1 μs*) with the help of optical method based on registration of distribution of rotary structure lines of the Fulcher α-spectrum bands of a hydrogen [2].

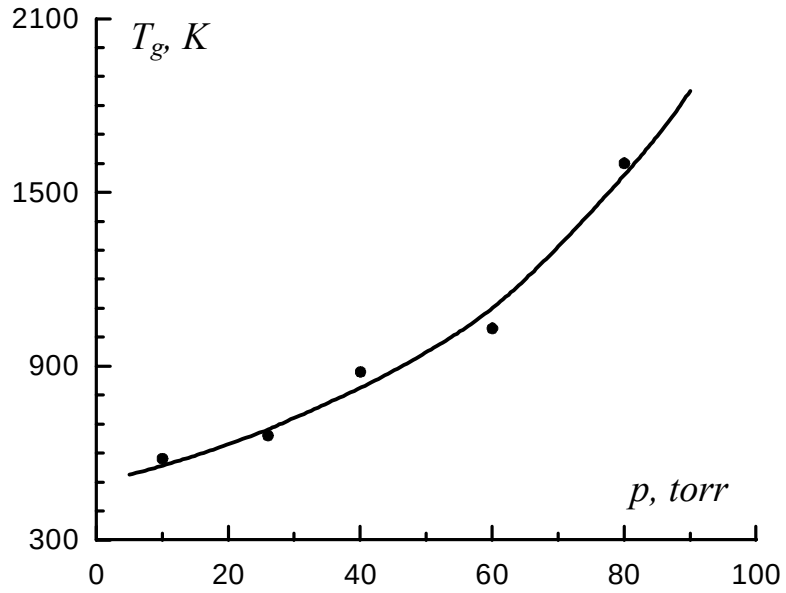

Fig. 5.5. The dependence of the gas temperature on the air pressure at the threshold values of input microwave energy.

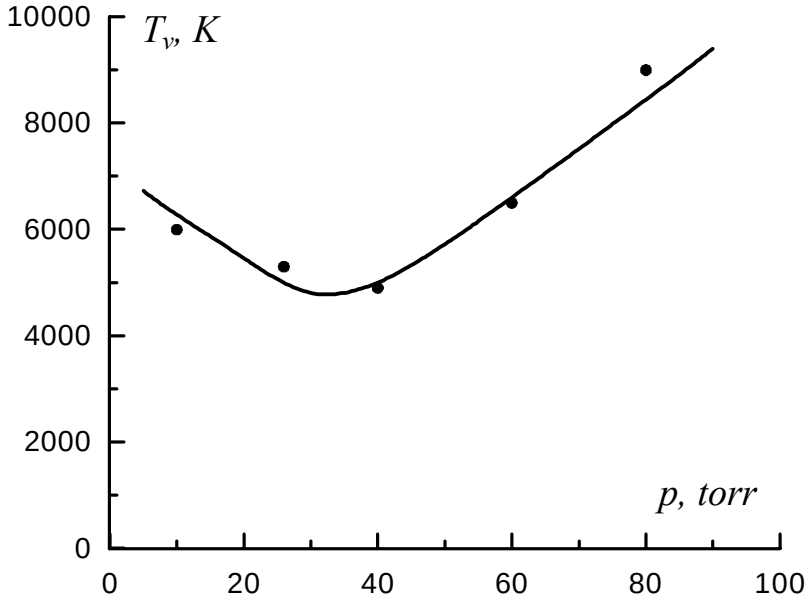

Fig. 5.6. Vibrational temperature as a function of air pressure at the threshold values of input microwave energy

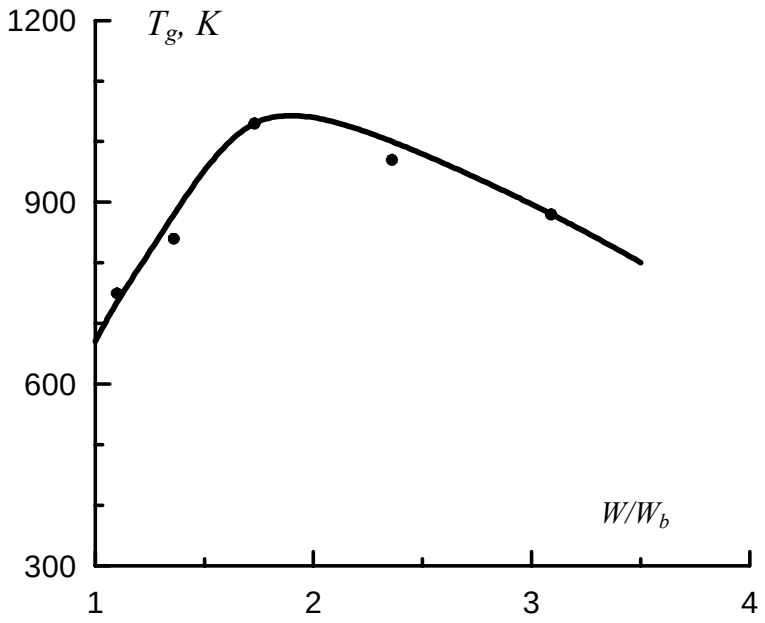

Fig. 5.7. Gas temperature as a function of a microwave power.
Air pressure *p=60 torr.* W_b is breakdown power at air pressure *p=60 torr*.

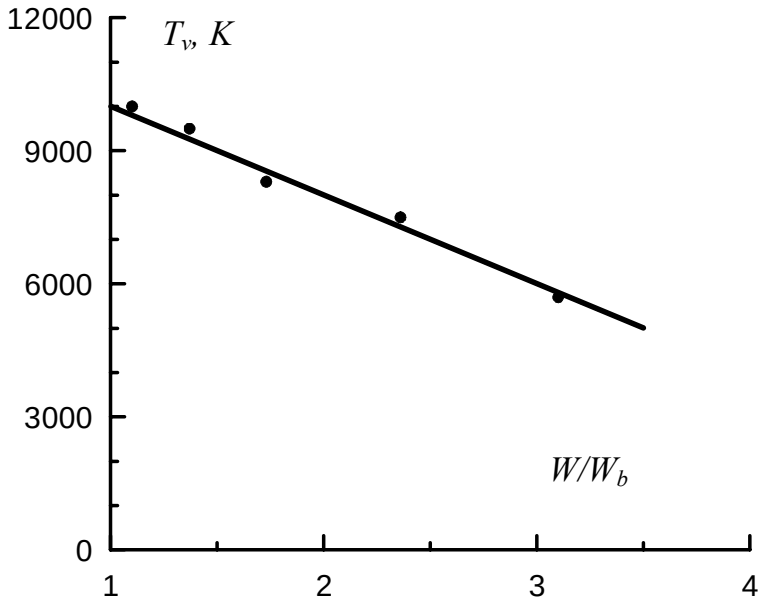

Fig. 5.8. Vibrational temperature as a function of a microwave power.
Air pressure *p=60 torr.* W_b is breakdown power at air pressure *p=60 torr*.

Temporary dependence of gas temperature for a microwave discharge in hydrogen is presented in *Fig. 5.9.* It is important that at initial stage of the discharge the gas heating rate exceeds *300 K/μs*. It is much higher than in pure air plasma at microwave discharge at the same conditions. The estimations show, that so fast gas heating is not provided elastic heating, neither *VT*-relaxation, nor non-resonance *VV*-exchange. The similar temporary evolution of gas temperature was experimentally observed by us at research of kinetics of gas heating in a various type of the discharge in air, hydrogen, nitrogen and mixture of nitrogen with oxygen [1, 3-6]. It was shown, that the fast gas heating is provided at quenching of the electronically-exited states of molecules, which are very effectively populated by electron impact at large values of the reduced electric field in plasma *E/n>50 Td*.

In conditions of our experiment in hydrogen the fast gas heating can be provided at the expense of the mechanism offered in [7]. This mechanism is connected with excitation unstable $b^3\Sigma_u$ state by electron impact in process:

$$H_2(X^1\Sigma_g) + e \rightarrow H_2(b^3\Sigma_u) + e \rightarrow H + H + e\,. \qquad (5.1)$$

The $b^3\Sigma_u$ state breaks up to two hydrogen atoms for times compared to a typical period of molecular fluctuations (*~10^{-14} s*). At this a part of excitation energy of the $b^3\Sigma_u$ state equalled $E\text{-}E^D$ (where E^D is the dissociative energy limit of the $H_2(b^3\Sigma_u)$ term) immediately transforms into the kinetic energy of gas. In [7] the accounts of gas heating kinetics in conditions of the pulse powerful discharge in hydrogen (concentration of heavy particles *n=3.10^{16} cm^{-3}*, discharge current *i=300 A*, diameter discharge tube *D=0,4 cm*, electron density *n_e=3.10^{15} см$^{-3}$*) are carried out. The gas heating rate received in [7] is equal to *~10^6 K/μs* in stage of formation of the discharge. If this gas heating counts on conditions of our experiment, the gas heating rate turns out *~10^2 K/μs* that well coordinates with our data (look *Fig. 5.9*).

The concentration of electrons in a channel of a microwave discharge in nitrogen was determined as a function of the gas pressure by the Stark broadening of the H_β (*λ=486,1 nm*) line of hydrogen. It is known that the microwave discharge is inhomogeneous at gas pressures above *100 torr*. The plasma formation consists of a large number of thin filaments (*0,1-0,3 mm* in diameter) spreading along the direction of the electric field in the incident microwave wave.

Optical methods, which are widely used, require additional information on physical processes occurring in the plasma. When the electron density exceeds *10^{14} cm^{-3}*, Stark broadening of the hydrogen lines is much greater than broadening due to other effects.

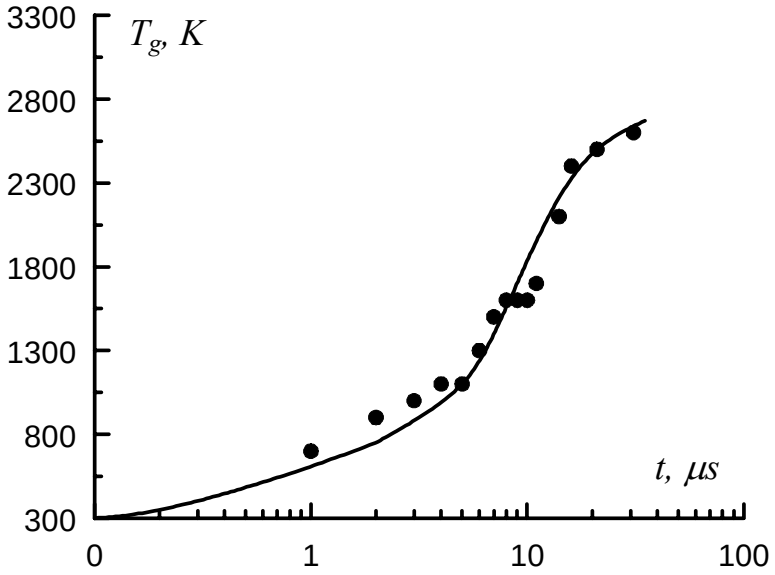

Fig. 5.9. Temporary dependence of gas temperature for a microwave discharge in hydrogen.

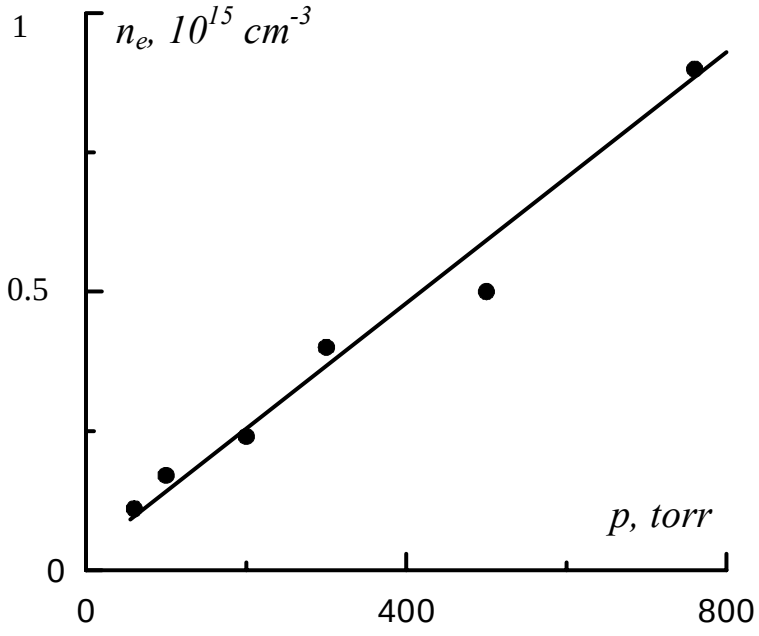

Fig. 5.10. The electron density as a function of pressure in channel of microwave discharge.

We use the following setup to produce a microwave discharge in the form of a single channel. Two metal wires pointing at one another were fused into a glass tube, *5 cm* in diameter and *15 cm* long, provided with flat windows. The distance between the ends of the wires was fixed at about *10 mm*. The tube was placed in the vicinity of the horn of a microwave source. A microwave generator (λ*=2,4 cm*) produced *25* μ*s* pulses at a repetition frequency of *20 Hz*. The output power could be varied from *50* to *200 kW*. The vacuum system was capable of evacuating the discharge chamber down to a pressure of about 10^{-2} *torr* and to let in either pure hydrogen or a mixture of hydrogen with nitrogen. The radiation from the discharge was projected by a system of lenses and mirrors onto the entrance slit of the monochromator. The output signal of the photomultiplier was entered either into a storing oscillograph or to a setup consisting of a time selector, two narrow-band amplifiers, a synchronous detector, a dc amplifier, and a strip chart recorder. The system enabled us to record the spectral line profile emitted by the pulsed-periodic discharge. The H_β profile was recorded for gas pressures between *30* and *760 torr*. At low pressures (*30-70 torr*), the microwave discharge was a plasma formation occupying the entire discharge chamber *5 cm* in diameter. At pressures of *100-200 torr*, the discharge took the form of a channel, about *1 mm* in diameter, and it was a channel with a size of the order of *0,1 mm* at pressures more than *200 torr*. It was obtained that as the pressure increases the H_β line becomes broader: the line half-width is *0,07 nm* at *p=100 torr* and it is *0,26 nm* at *p=760 torr*. The electron density was deduced from the H_β profiles with taking into account broadening factors such as the instrumental function (about *0,01 nm*), the Doppler effect (about *0,01 nm*), the external microwave Stark effect (about *0,01 nm*), and finite width of the monochromator slit. The electron density as a function of pressure is shown in *Fig. 5.10.* One can see that, to within of experimental error (about *40 %* for *p≤100 torr* and about 20% for *p=760 torr*), the electron density rises from about 10^{14} cm^{-3} at *50 torr* to 10^{15} cm^{-3} at atmospheric pressure *760 torr*. At this the electron density remains constant throughout the microwave pulse duration.

The estimation of the parameters in the microwave discharge channel was reported in [8]:

$$n_e < \frac{2cn_{ec}\nu_{eff}}{\omega^2 r}, \qquad (5.2)$$

where $n_{ec} = \frac{m\omega^2}{4\pi e^2}$ - critical electron density, r is the radius of the channel, and ν_{eff} is the effective collision frequency between electrons and neutrals. Hence, if we assume that at atmospheric pressure *760 torr* *r~0,1 mm,* $n_{ec}=2\cdot10^{12}$ cm^{-3}, and $\nu_{eff}=10^{12}$ s^{-1}, we find that $n_e<2,5\cdot10^{15}$ cm^{-3}, which is close to the measured result.

The dissociation degree of hydrogen molecules was determined on the method [9] based on registration of the ration of H_α-line intensity of atomic hydrogen and of integrated intensities of lines $\alpha(d^3\pi_u \rightarrow a^3\Sigma_g)$-system of molecular hydrogen. It is known [10, 11], that in low-temperature hydrogen plasma at large values of the reduced electric field $E/n>50$ *Td* the dissociation of molecules occurs mainly by electron impact. The process proceeds as a result of excitation of unbound vibration levels of electronic terms of the H_2 molecules. The formation of hydrogen atoms is possible also in processes of dissociative ionization and dissociative attachment. The analysis of experimental data on cross-sections of various processes resulting to dissociation of hydrogen molecules by electron impact shows that the hydrogen atoms can be formed in the discharge in this case mainly as a result of process (5.1). Providing that population of the top level $d^3\pi_u$ α-system occurs at the expense of transition from the basic state $H_2(X^1\Sigma_g)$ by electron impact, the intensity of lines of this system can be presented as

$$I_{H_2} = const\, n_e n_{H_2} \left\langle \sigma_{H_2} \varepsilon_e \right\rangle, \tag{5.3}$$

If the lines of Balmer's series of atomic hydrogen are excited because of in mainly dissociative and direct excitation by electron impact then intensity of a line H_α is possible to present as:

$$I_{H_\alpha} = const\left(n_e n_{H_2} \left\langle \sigma^{dis}_{H_\alpha} \varepsilon_e \right\rangle + n_e n_H \left\langle \sigma_{H_\alpha} \varepsilon_e \right\rangle\right), \tag{5.4}$$

where n_e, n_{H_2} and n_H - concentration of electrons, molecules and atoms of hydrogen in the basic state; $\left\langle \sigma_{H_2} \varepsilon_e \right\rangle$, $\left\langle \sigma^{dis}_{H_\alpha} \varepsilon_e \right\rangle$ and $\left\langle \sigma_{H_\alpha} \varepsilon_e \right\rangle$ - rate constant of excitation of a level $d^3\pi_u$, dissociative and direct excitation of a line H_α by electron impact accordingly.

Thus, if the equation (5.4) is divided on (5.3), the formula for determination of a dissociation degree of hydrogen will be received

$$\frac{I_{H_\alpha}}{I_{H_2}} = \frac{\left\langle \sigma^{dis}_{H_\alpha} \varepsilon_e \right\rangle}{\left\langle \sigma_{H_2} \varepsilon_e \right\rangle} + \frac{2K_D}{1-K_D} \frac{\left\langle \sigma_{H_\alpha} \varepsilon_e \right\rangle}{\left\langle \sigma_{H_2} \varepsilon_e \right\rangle}, \tag{5.5}$$

here $K_D = \dfrac{n_H}{2n^o_{H_2}}$ - dissociation degree, $n^o_{H_2}$ - initial concentration of hydrogen molecules.

The electron energy distribution function (*EEDF*), temperature and density of electrons were determined by a Langmuir probe method. The probe characteristic was measured in the various moments of time of a discharge current pulse: at the beginning - through *5 μs*, at the end

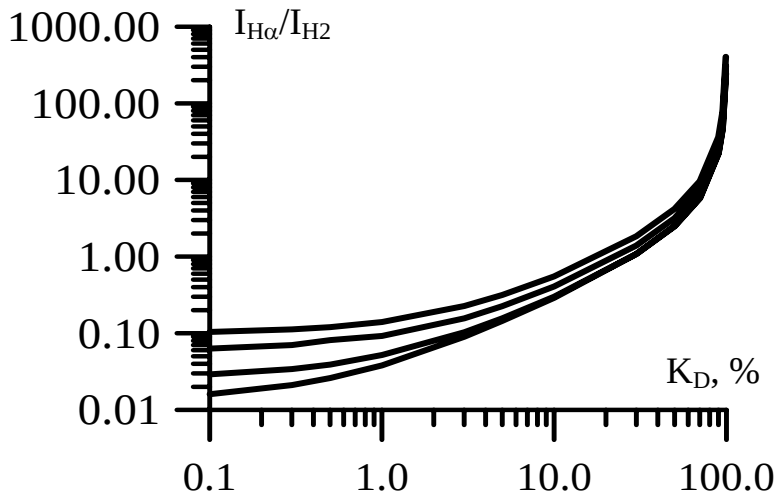

Fig. 5.11. Calibration curves in the assumption of maxwellian electron energy distribution function for various values of electron temperature T_e, *eV:*
1 (lower curve) - 2, 2 - 3, 3 - 5, 4 (upper curve) - 7.

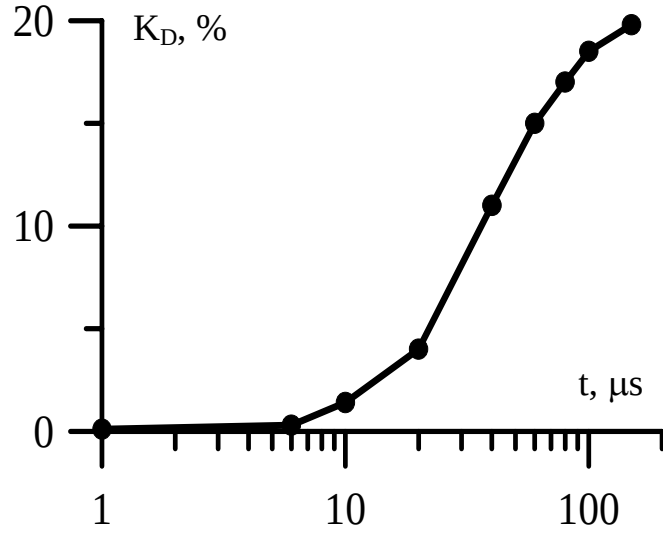

Fig. 5.12. The temporary dependence of a hydrogen dissociation degree.

of a pulse - through 10 μs. Dependence the ratio of intensity of a line H_α to whole intensity of diagonal $\alpha(d^3\pi_u,v' \rightarrow a^3\Sigma_g,v''; v'=v''=0,1,2,3)$-system on a dissociation degree K_D designed on the formula (5.5) is submitted in *Fig. 5.11* in the assumption of maxwellian electron energy distribution function for various values of electron temperature T_e, *eV*: 1-2, 2-3, 3-5, 4-7. These diagrams were used by us for definition of a hydrogen dissociation degree. It is possible to see, that at large dissociation degrees ($K_D>1\%$) this method can be used with a good accuracy for a finding of atomic hydrogen density without measurement of electron energy distribution function, whereas at $K_D<1\%$ the additional data about *EEDF* are necessary. The temporary dependence of a hydrogen dissociation degree received by this method is given on *Fig. 5.12.* One can see that the dissociation degree of hydrogen molecules reaches *20%* in conditions of our experiment to the end of a pulse by duration *200 μs.*

5.3. Ignition of supersonic flow of a propane-air mixture with use of freely localized microwave discharge

The photograph of a general view of a microwave discharge in the aerodynamic channel in motionless gas is submitted in *Fig. 5.13* at pulsed microwave power $W_p=100$ *kW*. One can see that the discharge exists inside the aerodynamic channel near the initiator and its size increases with increasing of microwave power (look *Fig. 5.14*). The gas temperature reaches *~2000 K* in this type of the discharge.

The common views of the microwave discharge inside the aerodynamic channel in supersonic (*M=2*) flow of air (without propane) are submitted in *Fig. 5.15* and *Fig. 5.16*. Thus two types of the microwave discharge have been realized: running and localized microwave discharge.

In case of running microwave discharge the discharge is distributed in the direction of a source of microwave radiation. The more the input microwave flow density, the more speed of distribution of the microwave discharge. The gas temperature in this case does not exceed *1500-2000 K*.

Under certain conditions the speed of distribution of the discharge sharply decreases, the microwave discharge is located in the fixed area of space. Thus during time of microwave field action the energy is put in the given area of space and gas temperature can amount to *4000 K-5000 K* in localized microwave discharge. In this case the intensity of plasma radiation increases

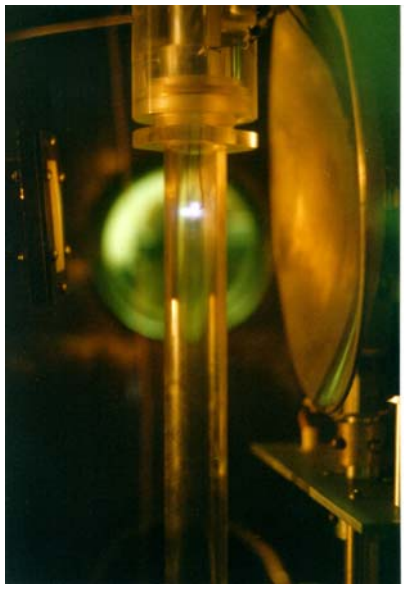

Fig. 5.13. The common view of freely localized microwave discharge inside the aerodynamic channel in motionless air at $p=300$ *torr*, $\tau=150$ *μs*, $f=10$ *Hz*, $W_p=100$ *kW*.

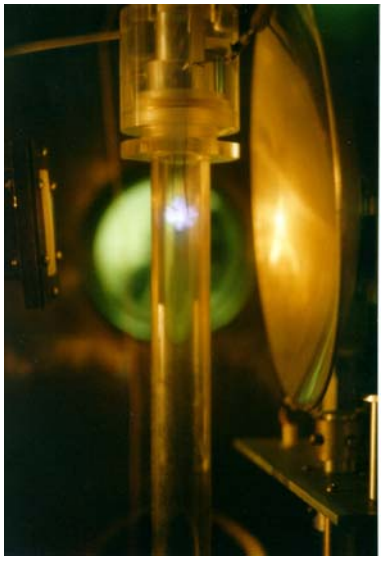

Fig. 5.14. The common view of freely localized microwave discharge inside the aerodynamic channel in motionless air at $p=300$ *torr*, $\tau=150$ *μs*, $f=10$ *Hz*, $W_p=200$ *kW*.

Fig. 5.15. The common view of the running microwave discharge inside the aerodynamic channel in supersonic (*M=2*) flow of air (without a propane).
Microwave pulse duration $\tau=100\ \mu s$.

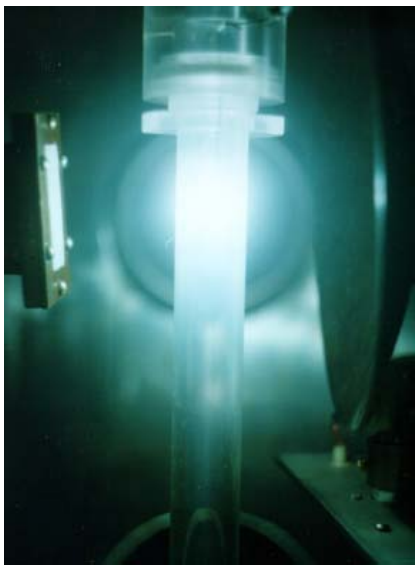

Fig. 5.16. The common view of the localized microwave discharge inside the aerodynamic channel in supersonic (*M=2*) flow of air (without propane).
Microwave pulse duration $\tau=100\ \mu s$.

with comparison of the radiation of the running microwave discharge (compare *Fig. 5.15* with *Fig. 5.16*).

The photo of a common view of freely localized microwave discharge inside the aerodynamic channel in supersonic flow of propane-air mixture is submitted in *Fig. 5.17.* It turned out that with help of a microwave discharge one can easy ignite a combustible propane-air mixture in supersonic flow even at pulse duration $\tau=25\ \mu s$.

At ignition of propane-air mixture in spectrum of plasma radiation one can see intensive molecular bands of C_2, *OH, CH, CN,* N_2 and atomic lines of *O, N, H* and some other weak lines. The oscillogram of a plasma radiation (band of *CH*) from the area of the aerodynamical channel at distance of z=7 cm downstream from focal region of the electromagnetic energy beam under condition of microwave discharge in supersonic (*M=2*) airflow (without a propane) is submitted in *Fig. 5.18*. As indicated in the picture the luminescence of the discharge sharply stops after ending of a microwave pulse. The oscillogram of a plasma radiation (band of *CH*) from the same area of the aerodynamical channel under condition of microwave discharge in supersonic (*M=2*) flow of propane-air mixture is given in *Fig. 5.19*. One can see the radiation of products of propane-air fuel burning may be observed after microwave pulse at distance of *7 cm* downstream from focal region of electromagnetic energy beam.

It is necessary to note that if the electrode pulse-periodic discharge results in ignition of a combustible propane-air mixture only at a pulse duration more than *150 μs*, then the microwave discharge results in reliable ignition already at duration of a microwave pulse of the order *20 μs*.

It is connected to that fact that in the microwave discharge is turned out more active particles in comparison with the electrode pulse-periodic discharge. Besides under conditions of the freely located microwave discharge the fast gas heating takes place that also promotes fast ignition of supersonic stream of gaseous fuel.

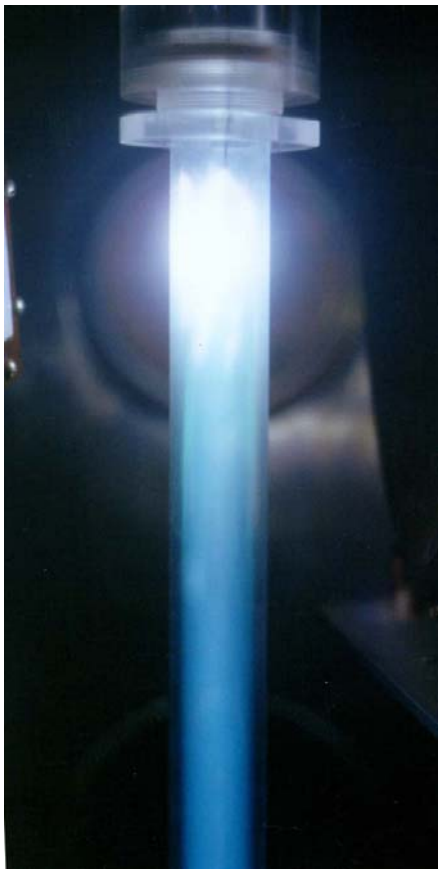

Fig. 5.17. Ignition of a propane-air mixture inside aerodynamic channel with the help of a microwave discharge in supersonic flow with Mach number *M=2* at *p=300 torr,* W_p*=200 kW, f=10 Hz,* τ*=100* μ*s*.

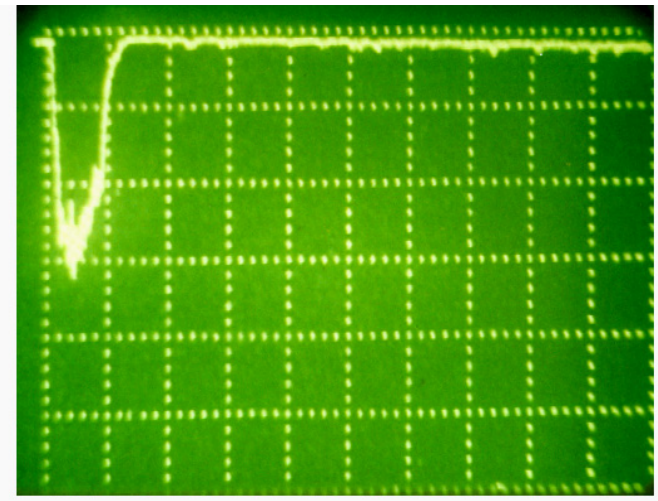

Fig. 5.18. The oscillogram of radiation (*CH* band) from the area of the aerodynamical channel at distance of *z=7 cm* downstream from focal region of the electromagnetic energy beam under condition of microwave discharge in supersonic (*M=2*) air flow (without propane). Microwave pulse duration $\tau=200\ \mu s$.

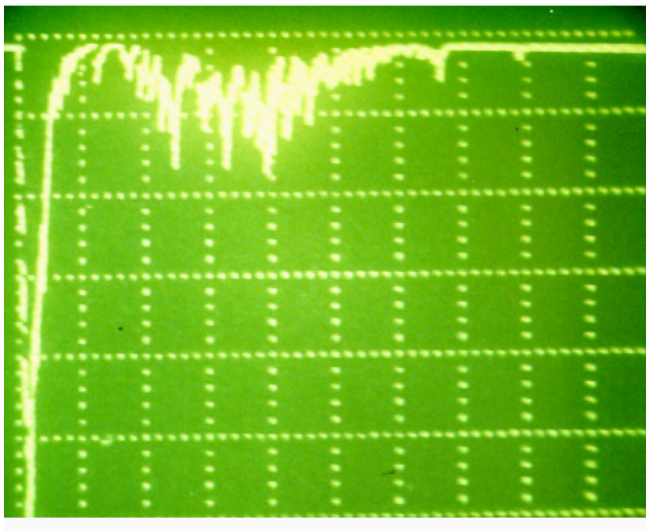

Fig. 5.18. The oscillogram of a plasma radiation (*CH* band) of a microwave discharge in supersonic (*M=2*) flow of propane-air mixture. Microwave pulse duration $\tau=100\ \mu s$.

CHAPTER VI
IGNITION OF SUPERSONIC PROPANE-BUTANE-AIR FLOW WITH USE OF SURFACE MICROWAVE DISCHARGE

6.1. Introduction

As have shown the results of researches of a surface microwave discharge (look Chapter IV), with its help it is possible to easily put high energy into thin boundary layer and to create in this area plasma with a high degree of gas ionization (electron density reaches of 10^{14} cm^3), high concentration of the excited atoms and molecules, the large dissociation degree of molecular components of plasma, the fast heating rate of neutral gas. These properties of a surface microwave discharge are extremely favorable from the point of view of its application for fast and reliable internal and external ignition under conditions of flight with supersonic and hypersonic speeds.

Therefore Chapter VI is devoted to research of an opportunity of application of a surface microwave discharge for ignition of a supersonic stream of hydrocarbon fuel. As an example process of ignition of a propane-butane-air supersonic mixture with flow Mach $M=2$ with the help of a surface microwave discharge created on the antenna of rectangular section with a wedge forward part is considered.

6.2. Dynamics of a surface microwave discharge

At first the researches of dynamics of development of the surface microwave discharge in motionless air have been carried out for studying opportunities of use of this type discharge for ignition of a supersonic stream of a propane-butane-air mixture. Measurements were carried out at two pulsed microwave power $W_p=40$ *kW* and *60 kW*, identical pressure in the discharge chamber $p=40$ *torr* and at variation of the microwave pulse duration from *3* up to *200* μs.

The common views of the surface microwave discharge at two microwave power and different microwave pulse duration in motionless air at pressure $p=40$ *torr* are resulted in *Fig. 6.1* and *Fig. 6.2.* From figures it is visible, that the longitudinal size of the discharge increases with growth of duration of microwave action. Thus at $W_p=40$ *kW* the discharge covers whole surface of the aerial only by the end of a pulse with duration of $\tau=200$ μs whereas at $W_p=60$ *kW* full surface of the antenna becomes covered by plasma already at microwave pulse

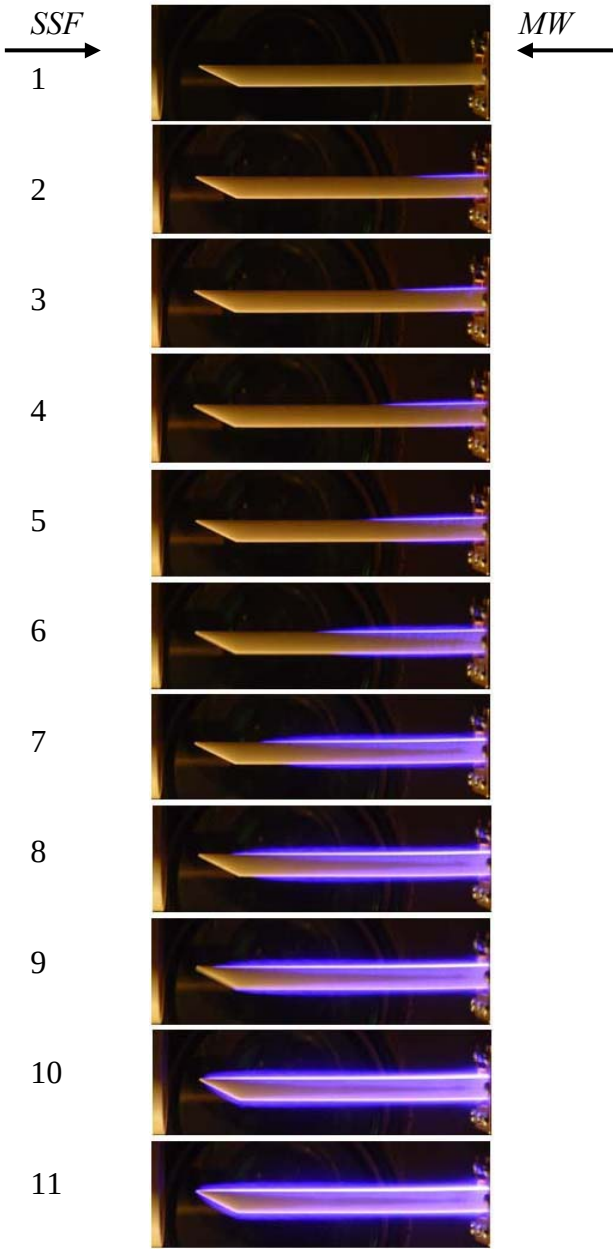

Fig. 6.1. Dynamics of the surface microwave discharge on a wedge dielectric body at air pressure *p=40 torr*, pulsed microwave power W_p*=40 kW*, and microwave pulse duration τ, μs: 1-0; 2-2; 3-5; 4-7; 5-10; 6-25; 7-50; 8-75; 9-100; 10-150; 11-200.

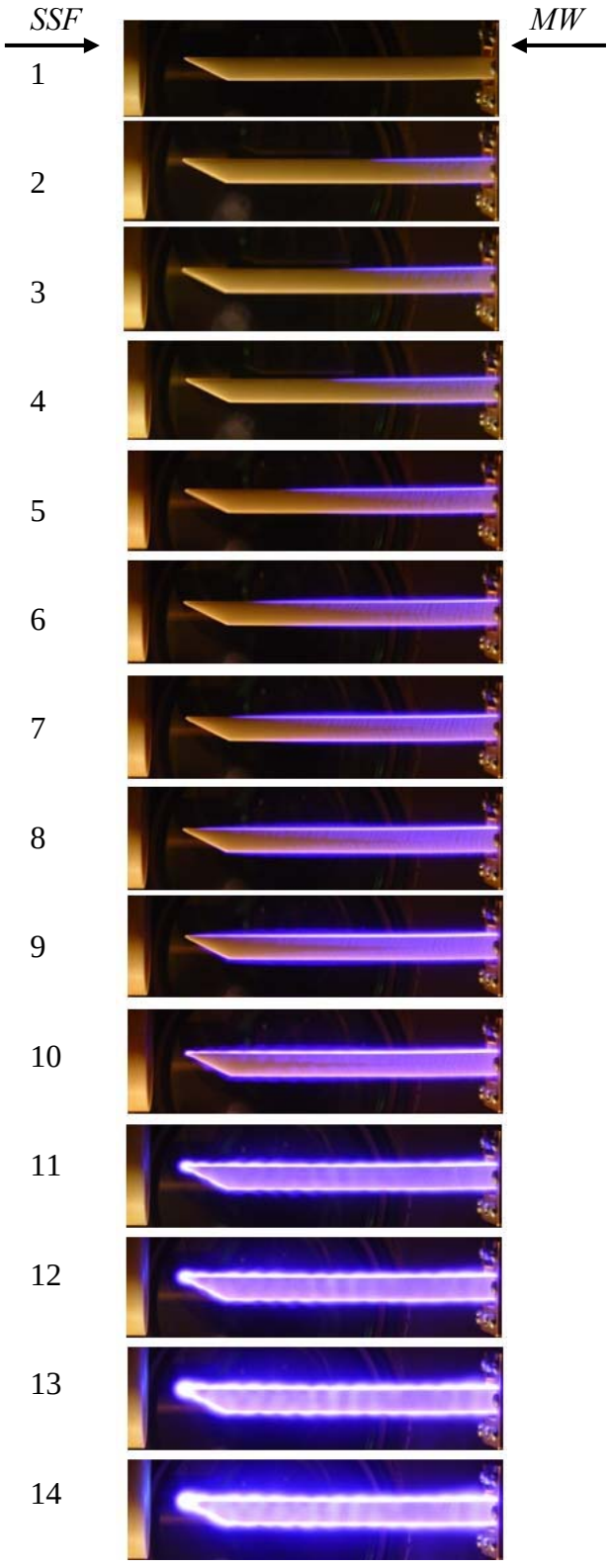

Fig. 6.2. Dynamics of the surface microwave discharge on a wedge dielectric body at air pressure *p=40 torr*, pulsed microwave power W_p*=60 kW*, and microwave pulse duration τ, μs: 1-0; 2-2; 3-5; 4-7; 5-10; 6-15; 7-20; 8-30; 9-40; 10-50; 11-75; 12-100; 13-150; 14-200.

duration $\tau=50\ \mu s$. It is visible too, that the size of the discharge at the fixed pulse duration grows when the microwave power increases.

When pulse duration exceeds the value necessary for formation of the surface microwave discharge on whole antenna surface the volumetric microwave discharge starts to be formed on a forward part of the wedge antenna. Its sizes increase with growth of microwave power and pulse duration. As in a volumetric part of the combined discharge the microwave energy is also input this circumstance can promote the most effective ignition of gaseous fuel.

Dependences of the longitudinal sizes of plasma formation on antenna surface from pulse duration at two values of microwave power are represented in *Fig. 6.3* and *Fig. 6.4*. The mistake of definition of longitudinal sizes of the microwave discharges was basically defined by accuracy of scaling and contrast forward luminous border of plasma and change of input power from a pulse to a pulse during measurement under condition of pulse-periodic discharge. In our case the error can be estimated about *30 %.*

The longitudinal velocity of surface microwave discharge as a function of a time is given in *Fig. 6.5* at microwave power $W_p=40\ kW$ and is shown in *Fig. 6.6* at microwave power $W_p=60\ kW$. One can see that at the beginning of microwave pulse the longitudinal velocity exceeds the value of $v=10^6\ cm/s$, whereas at late stages of existence of the surface microwave discharge the velocity of discharge distribution decreases up to $v=10^4\ cm/s$. At $W_p=60\ kW$ the discharge is distributed slightly faster.

The discharge moving speed can be approximated by power-mode function

$$v = At^{-\alpha}, \qquad (6.1)$$

where v has got dimension [*cm/s*], A has got dimension [*cm/s*], and α is dimensionless quantity. Time is substituted in the formula (6.1) in seconds.

To find unknown sizes A and α, let's construct the received dependences $v=f(t)$ in double logarithmic scale. The results are shown in *Fig. 6.7* and *Fig. 6.8*. From these diagrams the values $A=4\ cm/s$ and $\alpha=0,94$ for microwave power of $40\ kW$ and $A=5\ cm/s$ and $\alpha=0,96$ at $W_p=60\ kW$ have been received.

These results are very well coordinated to the data received earlier with use of antennas from different materials and various configurations. It also specifies good repeatability of results and reliability of creation of the surface discharge in the given way, its high stability and as a result of this for supersonic plasma aerodynamics this method holds much promise.

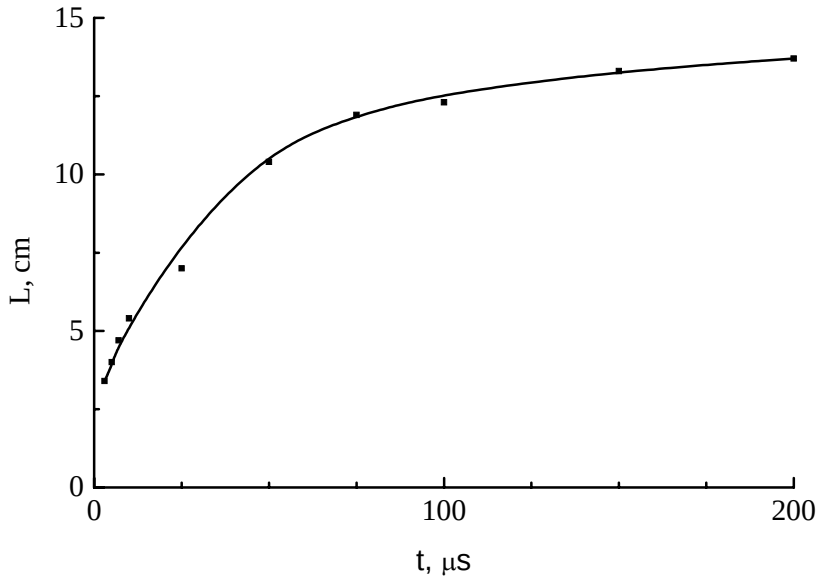

Fig. 6.3. The longitudinal size of surface microwave discharge vs time at pulsed microwave power W_p=*40 kW*.

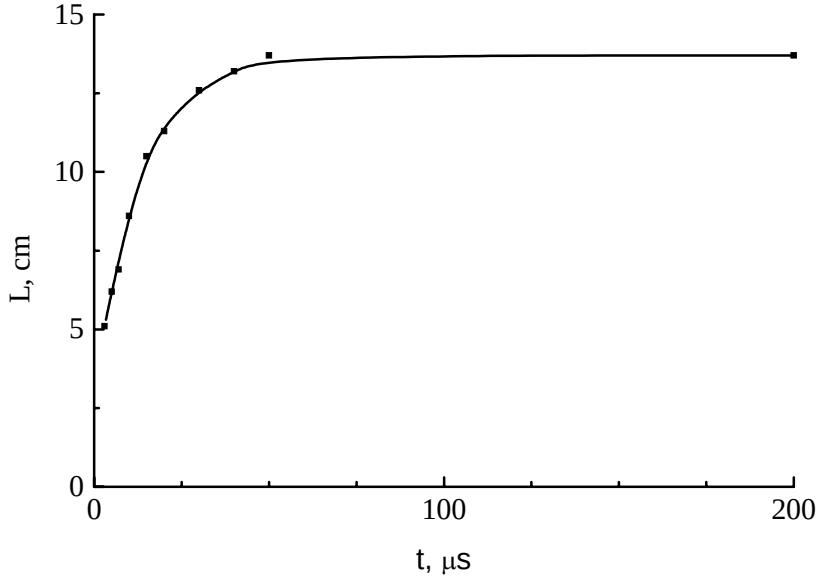

Fig. 6.4. Dependence on pulse duration of the longitudinal size of plasma formation on antenna surface at pulsed microwave power W_p=*60 kW*.

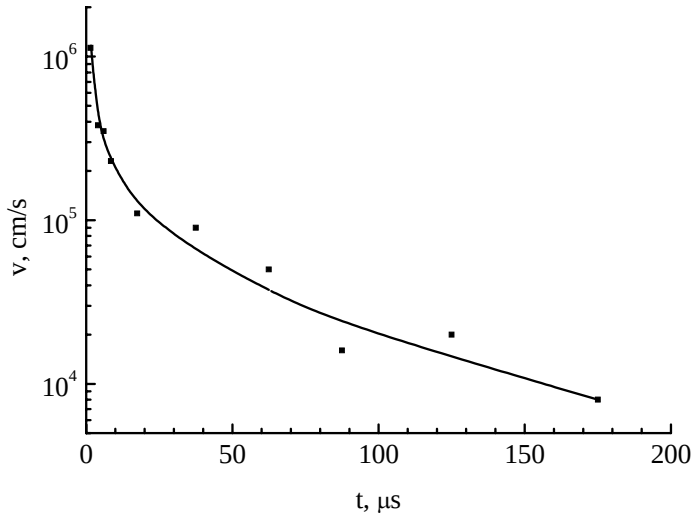

Fig. 6.5. The longitudinal velocity of surface microwave discharge vs time at pulsed microwave power W_p=*40 kW*.

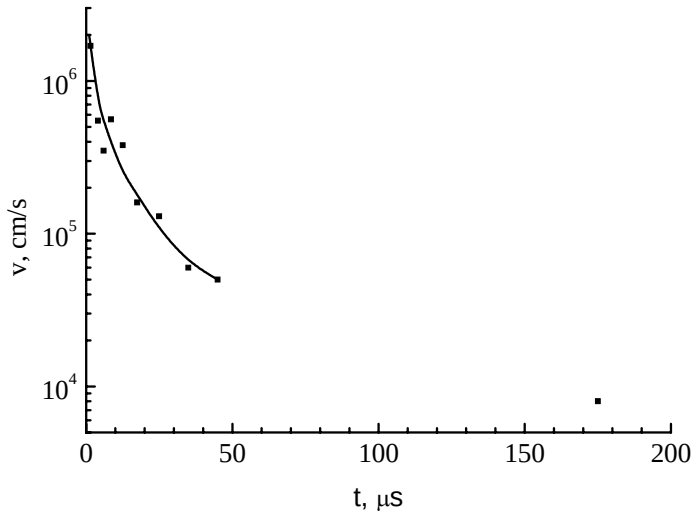

Fig. 6.6. The longitudinal velocity of surface microwave discharge vs time at pulsed microwave power W_p=*60 kW*.

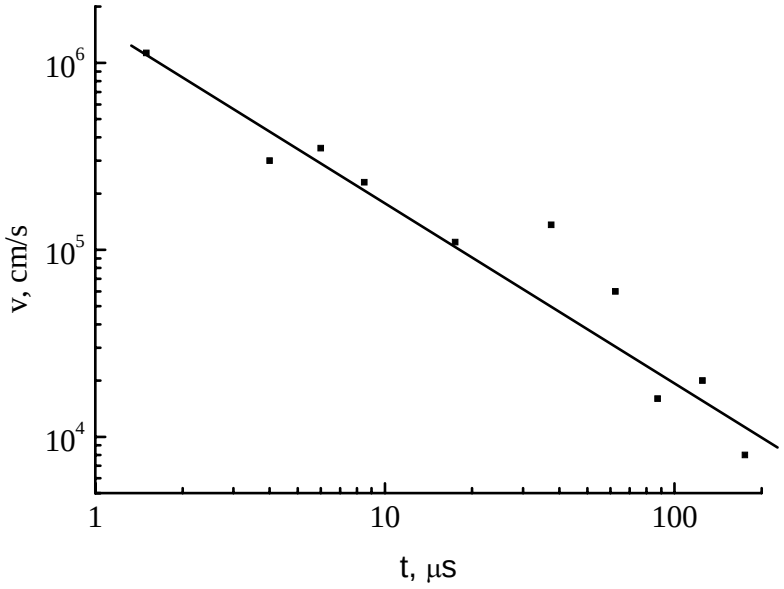

Fig. 6.7. The longitudinal velocity of surface microwave discharge vs time at pulsed microwave power W_p=*40 kW*.

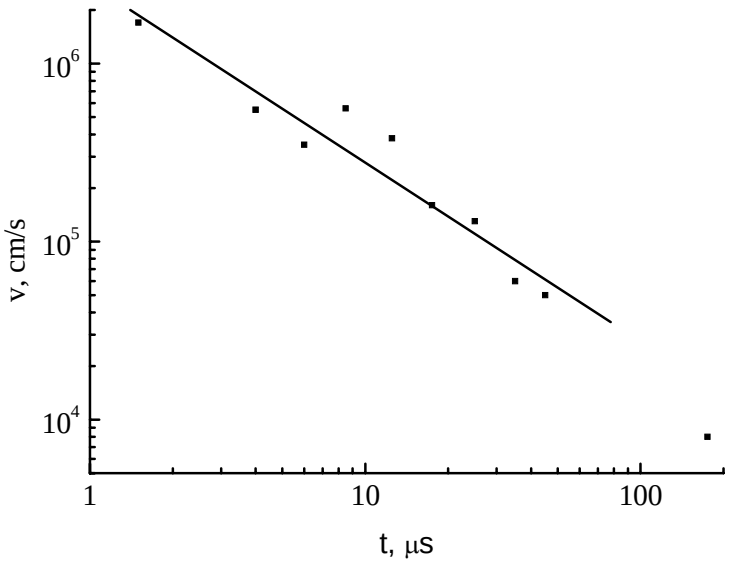

Fig. 6.8. Dependence on pulse duration of the longitudinal size of plasma formation on antenna surface at pulsed microwave power W_p=*60 kW*.

6.3. External ignition of supersonic propane-butane-air flow

For studying an opportunity of realization of external ignition of supersonic propane-butane-air stream with flow Mach number *M=2* the antenna was located in area of a stream coaxially supersonic nozzle. Thus the direction of surface microwave discharge distribution was opposite to a direction of supersonic stream. The recording equipment have added: camera, shadow installation, monochromator, *CCD*, photomultiplier tube and digital oscilloscope Textronix TDS-210, the information with which was transferred to the personal computer. The discharge was created both in a stream of pure air, and in a propane-butane-air mixture.

Not only a general view of a surface microwave discharge, but also intensity of radiation of excited radical *CH** were registered. Thus with the help of monochromator the area of a spectrum of radiation from plasma of the microwave discharge, corresponding to a band *431,5 nm* of radical *CH*, was chosen. As the receiver of radiation the photo multiplier was used. The signal from the photo multiplier acted on an input of digital oscillograph. On distinction of values of signals for the discharge in air and in propane-butane-air mixture could judge presence of burning (intensities of bands of *CH* were compared). As well as at research of the discharge in motionless air the experiments were carried out at two values of the pulsed microwave power of *40 kW* and *60 kW*.

The typical integrated photos of the surface microwave discharge in supersonic flow of propane-butane-air mixture (1) and air (2) are resulted in *Fig. 6.9* at flow Mach number *M=2*, static air pressure into discharge chamber *p=40 torr*, pulsed microwave pulsed power W_p*=40 kW* (at this microwave mean power W_m*=40 W*), pulse duration τ*=100* μ*s*, air pressure into high pressure receiver p_o*=1 atm*, and propane-butane pressure into high pressure receiver p_g*=4,5 atm*. From these photos it is visible, as air and propane-butane-air streams influence on a surface microwave discharge created at various powers. Namely, at low power W_p*=40 kW* in both cases (air and propane-butane-air flows) a drift the discharge in direction of a stream takes place in comparison with the discharge in motionless air. The discharge drift occurs on slightly greater distance in propane-butane-air mixture, than in air.

This circumstance is connected to that fact that during existence of a supersonic stream the static pressure in the discharge chamber raises a little. Thus it is known, that the power, necessary for creation of the surface microwave discharge, grows with increase of pressure. From here the microwave power necessary for creation of the of the surface microwave discharge of the fixed length at the end of the supersonic stream initiation should be a little bit

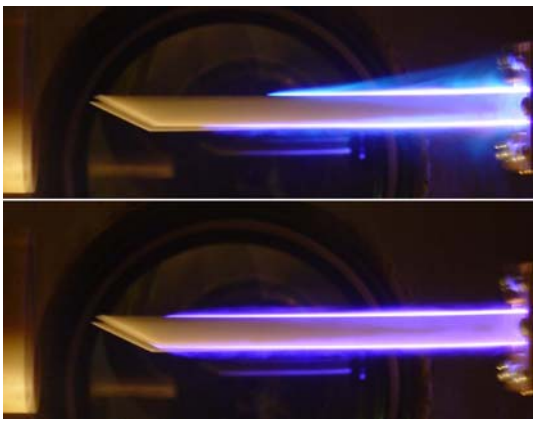

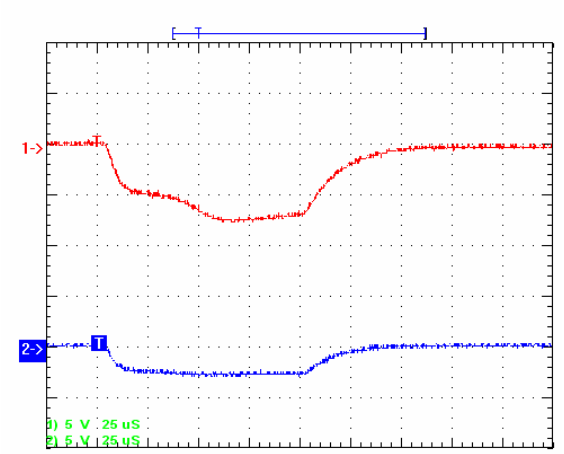

Fig. 6.9

Fig. 6.10

Fig. 6.9. General views of the surface microwave discharge in supersonic flow of propane-butane-air mixture (1) and air (2) at pulsed microwave power W_p=*40 kW*.

Fig. 6.10. Temporal behaviour of *CH** emission under condition of the surface microwave discharge in supersonic flow of propane-butane-air mixture (1) and air (2) at pulsed microwave power W_p=*40 kW*.

Fig. 6.11. External ignition of supersonic flow a propane-butane-air mixture with help of the surface microwave discharge at *M=2, p=40 torr,* W_p*=40 kW,* τ*=100 μs,* p_o*=1 atm,* and p_g*=4,5 atm*.

more in comparison with the microwave power necessary for creation of the discharge of the same length in the beginning of the test-firing. In these experiments of pulsed microwave power was supported by a constant both in motionless gas, and in a supersonic stream and was equaled *40 kW*. This value of power was threshold for creation of the microwave discharge on all surface of the antenna in motionless gas. It is natural, that in a stream of gas when pressure in the chamber during experiment grew, this power was insufficiently for covering plasma of all surface of the antenna.

It is confirmed also with the experiments executed at the greater powers. In this case the discharge was created on all surface of the aerial both in motionless gas, and in a supersonic stream (look, for example, *Fig. 6.14*).

Temporal behaviour of CH* emission under condition of the surface microwave discharge in supersonic flow of propane-butane-air mixture (1) and air (2) are given in *Fig. 6.10* at pulsed microwave power W_p*=40 kW*. It is visible, that later of *30-40 μs* after the beginning of a pulse the intensity of a luminescence of *431,5 nm CH* band starts to grow that testifies about ignition of supersonic stream of propane-butane-air mixtures. Thus in an integrated photo of the surface microwave discharge the characteristic luminescence of a flame in a supersonic stream (look *Fig. 6.9*) is observed.

In more details process of supersonic burning on an external surface of a plate can be seen in *Fig. 6.11*. In this case the localization place of the greatest burning occurs in a zone of the beginning of the antenna at a supply waveguide where intensity of electric field is maximal. It is necessary to note that process of burning stops with the ending of the microwave pulse duration.

Simultaneously with it the spectrum of radiation in the diapason of wavelengths *λ=350-425 nm* was recorded with the help of spectroscope. Spectroscope was adjusted on the area of the antenna located on distance *z=2,5 cm* from the supply waveguide. The multichannel recorder of a spectrum on base *CCD* was used as a receiver of radiation. The spectrum of radiation received in that way is resulted in *Fig. 6.12*. It is visible, that in this spectrum area the intensive bands of the second positive system of nitrogen and bands of sequence *Δv=0* of cyanogen are observed. In this case the gas temperature measured by various molecular bands is equal *800-1000 K*.

The general view of a spectrum in this area of wavelengths essentially varies (look *Fig. 6.13*), namely, intensity of a luminescence of *CN* bands sharply grows, whereas intensity of a luminescence of bands of the second positive system decreases at ignition of supersonic stream of propane-butane-air mixtures. The gas temperature measured in this case by *CN* bands,

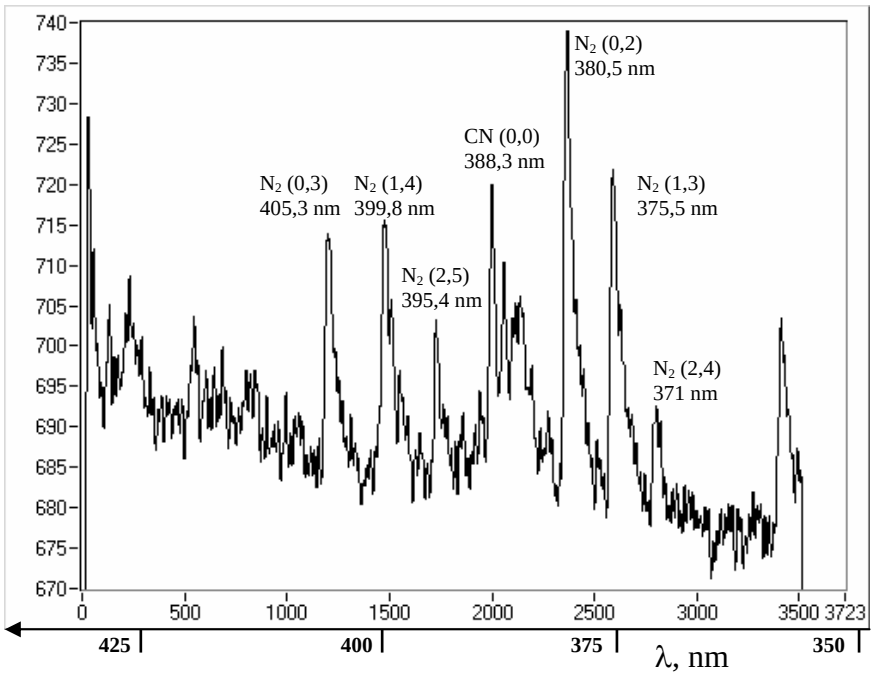

Fig. 6.12. Spectrum of radiation of the surface microwave discharge in supersonic airflow *M=2* in the diapason of the wavelengths *λ=350-425 nm* at *z=2,5 cm, p=40 torr, τ=100 μs*, and pulsed microwave power W_p*=40 kW*.

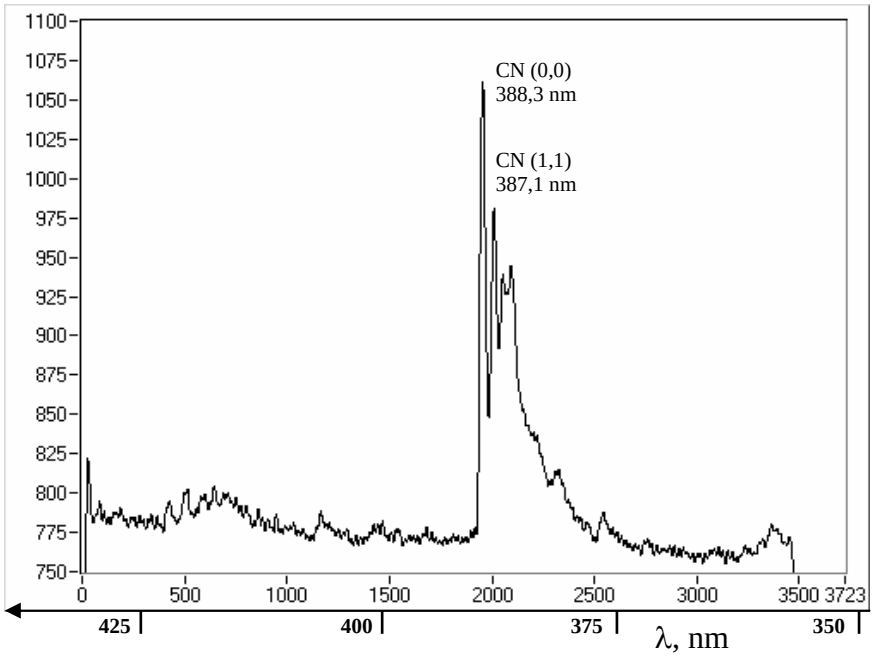

Fig. 6.13. Spectrum of radiation of the surface microwave discharge in supersonic propane-butane-air flow M=2 in the diapason of the wavelength *λ=350-425 nm* at *z=2,5 cm, p=40 torr, τ=100 μs*, and pulsed microwave power W_p*=40 kW*.

effectively formed at burning of propane-butane-air mixtures, sharply grows. In this case the gas temperature is equal *2750 K*, that also testifies to ignition of supersonic stream of gaseous fuel on an external surface of a plate with the help of a surface microwave discharge.

At greater power W_p*=60 kW*, also in both cases (air and propane-butane-air flows), the discharge covers all surface of the aerial, only plasma spherical formation at the forward end of the aerial (look *Fig. 6.2*) practically disappears in a stream (look *Fig. 6.14*).

Oscillograms of intensity of a luminescence of band λ*=431,5 nm* of *CH* radical are resulted in *Fig. 6.15*. From oscillograms it is visible, that in supersonic propane-butane-air mixture flow the intensity of *CH* luminescence in some times exceeds intensity of a luminescence in air. Thus the luminescence starts to sharply grow already during the first moments of action of a microwave energy. It shows, that at a pulse microwave power W_p*=60 kW* ignition of a propane-butane-air mixture occurs faster, than at W_p*=40 kW*. It also confirms that fact that an electric field in the area of existence of a surface microwave discharge grows with increase in microwave power. Thus effective ionization, dissociation and formation of the active excited particles and radicals takes place in microwave plasma that promotes sharp reduction of induction time. From oscillograms of a plasma luminescence (look *Fig. 6.10* and *Fig. 6.15*) it is visible how ignition occurs at full and incomplete covering of the antenna by the surface microwave discharge. At an incomplete covering of the aerial the intensity of a luminescence is appreciable less than at a full covering. It is necessary to note, that in accordance with *Fig. 6.15* intensity of a luminescence of the given band falls approximately during *50-80* μ*s* after pulse of the microwave power.

In more details process of supersonic burning on an external surface of a plate can be seen in *Fig. 6.16*. At that the process of burning occupies the bigger area of an antenna surface at the greater power W_p*=60 kW*.

6.4. Research of external ignition with the help of a shadow method

The process of external ignition of a propane-butane-air mixture by means of a surface microwave discharge is registered in a shadow photo as well. It is necessary to remind, that the shadow method allows registering any areas in which the gradient of refraction index of environment is perpendicular to a direction of a light beam distribution. In our case such areas can be or fronts of the shock waves arising in a supersonic stream on a forward edge of an antenna, or on fronts of distribution of thermal streams of gas, i.e. on fronts of burning.

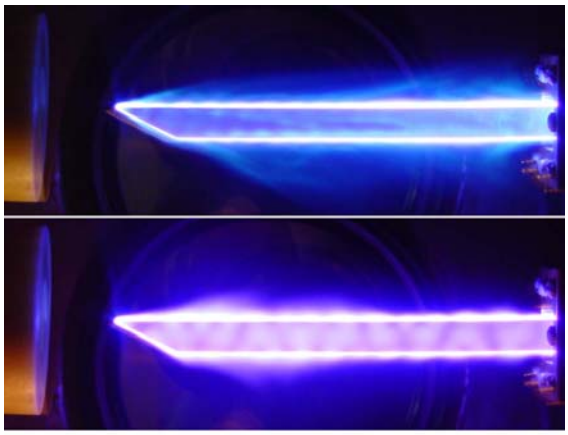

Fig. 6.14

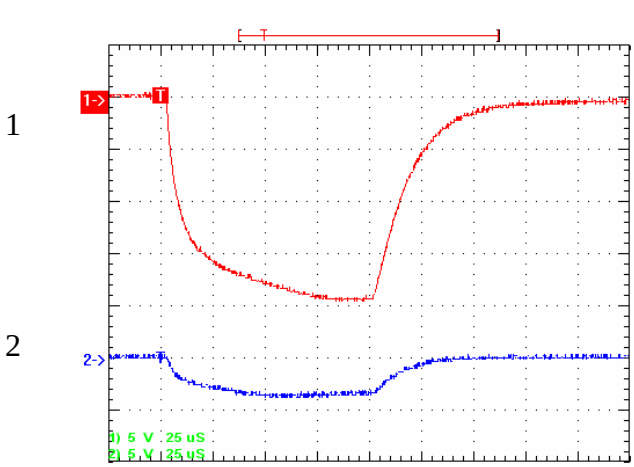

Fig. 6.15

Fig. 6.14. General views of the surface microwave discharge in supersonic flow of propane-butane-air mixture (1) and air (2) at pulsed microwave power W_p=*60 kW*.

Fig. 6.15. Temporal behaviour of *CH** emission under condition of the surface microwave discharge in supersonic flow of propane-butane-air mixture (1) and air (2) at pulsed microwave power W_p=*60 kW*.

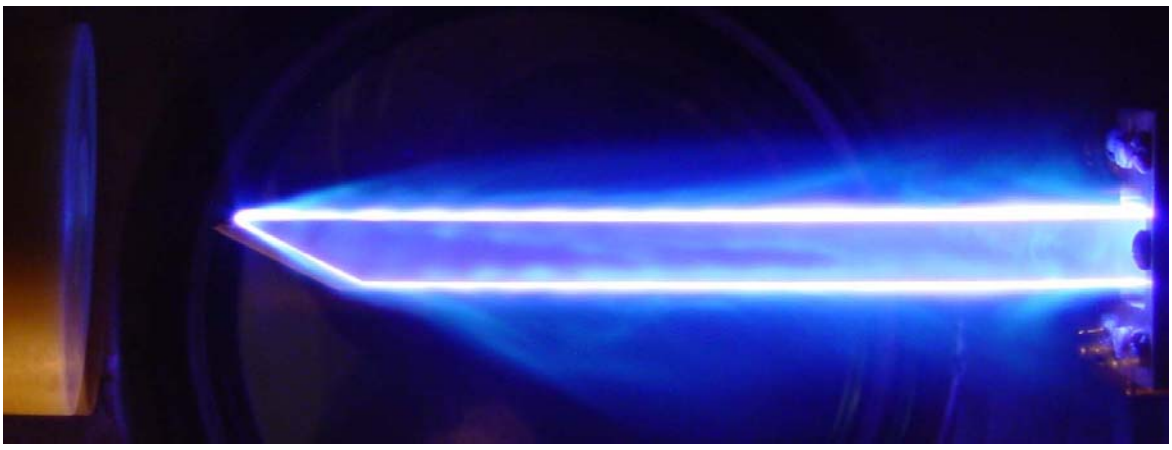

Fig. 6.16. External ignition of supersonic flow a propane-butane-air mixture with help of the surface microwave discharge at *M=2, p=40 torr,* W_p*=60 kW,* τ*=100* μ*s,* p_o*=1 atm,* and p_g*=4,5 atm*.

Unfortunately, in these experiments flash pulse duration was *~25 μs*, that, in turn, has not allowed to receive good enough time and spatial resolution, therefore shadow photos have turned out low-contrast.

The typical shadow photo of process of external ignition of a propane-butane-air mixture with help of the surface microwave discharge is shown in *Fig. 6.17*. In the photo the front of the shock wave which has arisen on a sharp forward edge of the antenna is distinctly seen. It once again confirms that a stream is supersonic one. Furthermore, in a photo the extending front of burning of a supersonic propane-butane-air mixture which practically coincides with front of burning in an integral photo (see *Fig. 6.11*) is seen. Thus this result confirms presence of ignition and burning by means of a surface microwave discharge.

Time evolution of shadow picture of ignition of supersonic flow a propane-butane-air mixture with the help of surface microwave discharge at flow Mach number *M=2*, static air pressure into discharge chamber *p=40 torr*, air pressure into high pressure receiver p_o*=1 atm*, propane-butane pressure into high pressure receiver p_g*=4,5 atm*, pulsed microwave pulsed power W_p*=60 kW* (at this microwave mean power W_m*=60 W*), pulse duration τ*=100 μs* and different time delay of a flash lamp concerning forward front of the microwave pulse is shown in *Fig. 6.18.*

It is visible, that ignition occurs already in the beginning of a microwave pulse. The form of the head attached shock wave varies at beginnings of burning on all surface of the aerial. After the ending of a microwave pulse during some time the residual burning, which gradually blows off a supersonic stream downstream, is observed.

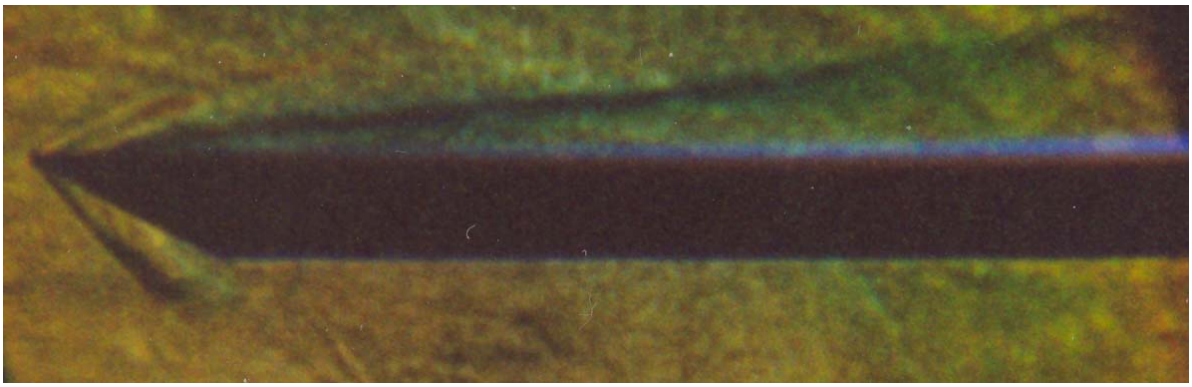

Fig. 6.17. Shadow picture of external ignition of supersonic flow a propane-butane-air mixture with the help of surface microwave discharge at $M=2$, $p=40$ *torr*, $p_o=1$ *atm*, $W_p=60$ *kW*, $\tau=100$ μs and gas (propane-butane) pressure $p_g=4,5$ *atm*.

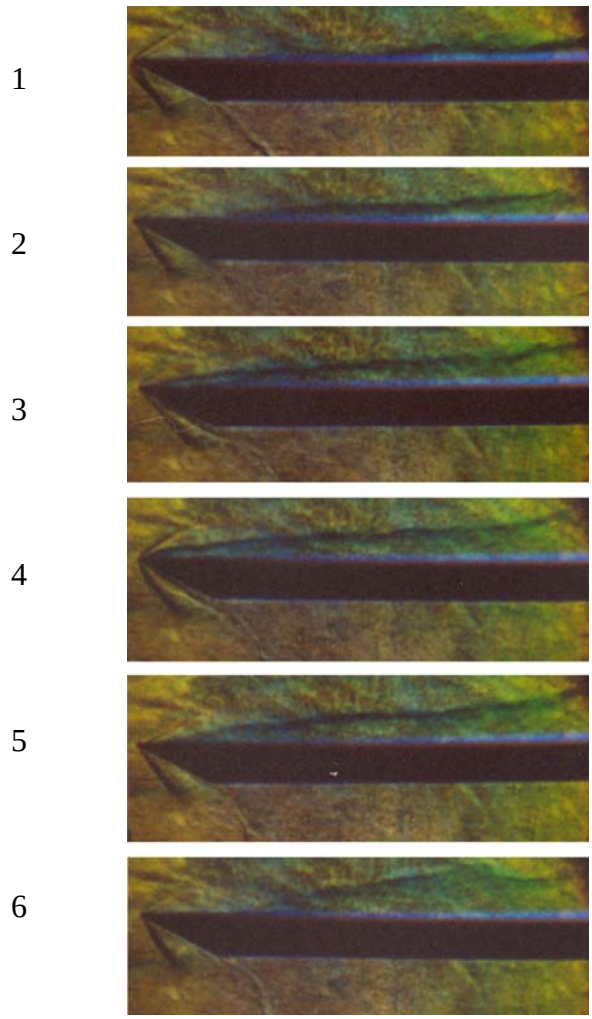

Fig. 6.18. Time evolution of shadow picture of ignition of supersonic flow a propane-butane-air mixture with the help of surface microwave discharge at $M=2$, $p=40$ torr, $p_o=1$ atm, $p_g=4{,}5$ atm, $W=60$ kW, $\tau=100$ μs and time delay of a flash lamp concerning forward front of the microwave pulse t_{del}, μs: 1-20; 2-40; 3-60; 4-80; 5-100; 6-140.

CHAPTER VII

PROPANE-BUTANE-AIR MIXTURE IGNITION AND COMBUSTION IN THE AERODYNAMIC CHANNEL WITH THE STAGNANT ZONE

7.1. Introduction

In the Chapter VII the ignition of supersonic propane-butane-air mixture with the help of the electrode transversal surface discharge and stabilizing action of a stagnant zone in the aerodynamic channel of rectangular section on process of propane-butane-air mixture burning were examined. In experiment stable burning supersonic (*M=2*) mixtures of propane-butane with air during *t=2 s* (maximal time of supersonic flow for our installation) has been received at use of a stagnant zone by depth of *h=17 mm*.

During some years cavities have gained the attention of scientists and engineers as a promising flame holding and flame stabilization device for a supersonic combustor in scramjets. However till now there are the many unresolved problems connected to use of a cavity for improvement of a combustor work.

The various types of the discharges were studied by us from the point of view of their application for a supersonic propane-air mixture ignition. In experiments a direct current discharge, a surface pulse-periodic transversal discharge, volumetric pulse-periodic transversal and longitudinal discharges in supersonic gas flow were studied. It has been received that a propane-air mixture ignition can be achieved with the help of any kind of the discharges at the corresponding energy contribution to supersonic flow. At this the ignition time differs for various types of the discharges. However, after ignition the organization of the long time stable combustion in free space is impossible.

We have fulfilled the preliminary experiments in which the pulsed-periodical discharge and *DC* discharge, created under condition of a stagnant zone located on a wide wall of the aerodynamic channel of rectangular section, were investigated. The ignition beforehand mixed supersonic propane-butane-air stream with flow Mach number *M=2* was obtained. The stabilizing actions of a stagnant zone in the aerodynamic channel on process of burning of a fuel were considered.

Experiments were carried out on the installation consisting of the vacuum chamber, the high pressure receiver of air, the high pressure receiver of propane-butane, the system for mixing

propane-butane with air, the system for creation of a supersonic flow of a propane-butane-air mixture, the aerodynamic channel, the discharge section, the source of high-voltage pulses, the synchronization unit, and the diagnostic system. The block-scheme of experimental installation is represented in *Fig. 2.7* (Chapter II).

7.2. Electrode pulsed-periodical transversal surface discharge in supersonic flow

At first the electrode surface pulsed-periodic discharge in supersonic free jet with flow Mach number of $M=2$ was created on a dielectric plate placed at the angle of approximately twenty degrees to the direction of supersonic airflow at air pressure into discharge chamber $p=40$ *torr*, initial voltage on the discharge gap $U=15$ *kV*, discharge current $i=10$ *A*, and different values of gas pressure p_g into the receiver-chamber. The common view of the discharge in supersonic airflow on an external surface of a dielectric body is given in *Fig. 7.1.*

This discharge does not differ from the common view of the volumetric discharge in supersonic airflow. Without supersonic airflow the discharge represents the plasma channel existing on a surface of a dielectric body between two electrodes, fixed in a dielectric flush with a surface. The supersonic flow leads to blowing of plasma jets from each of electrodes, which are overlapped among them downstream. The length of each jet depends on pulse duration, gas pressure, velocity of supersonic flow, and energy supplied into the discharge

Dynamics of development of the surface pulsed-periodical discharge in supersonic stream of air in the aerodynamic channel has been investigated depending on discharge current, a stagnant zone depth, distances from the beginning of a stagnant zone to electrodes.

In *Fig. 7.2-7.5* the common view of the pulse-periodic transversal surface discharge in the aerodynamic channel are represented at various depth of a stagnant zone.

One can see that the transversal surface discharge represents two smooth plasma jets extended along a stream in the aerodynamic channel without a stagnant zone (*Fig. 7.2*). In wind tunnels the volumetric transversal discharge has the same structure. It testifies to uniformity of a supersonic stream in our channel without a stagnant zone.

The discharge structure starts to vary sharply at its creation in a cavity. It is observed a stream turbulization, the wall boundary layer separation (*Fig. 7.3-7.5*). At depth of a stagnant zone $h=3$ *mm* there are the opposites separated currents and the discharge is gone in two directions both upstream, and downstream. The recirculation area with a vortex movement about a forward wall of a stagnant zone is formed. At use of a stagnant zone by depth of $h=5$ *mm* the

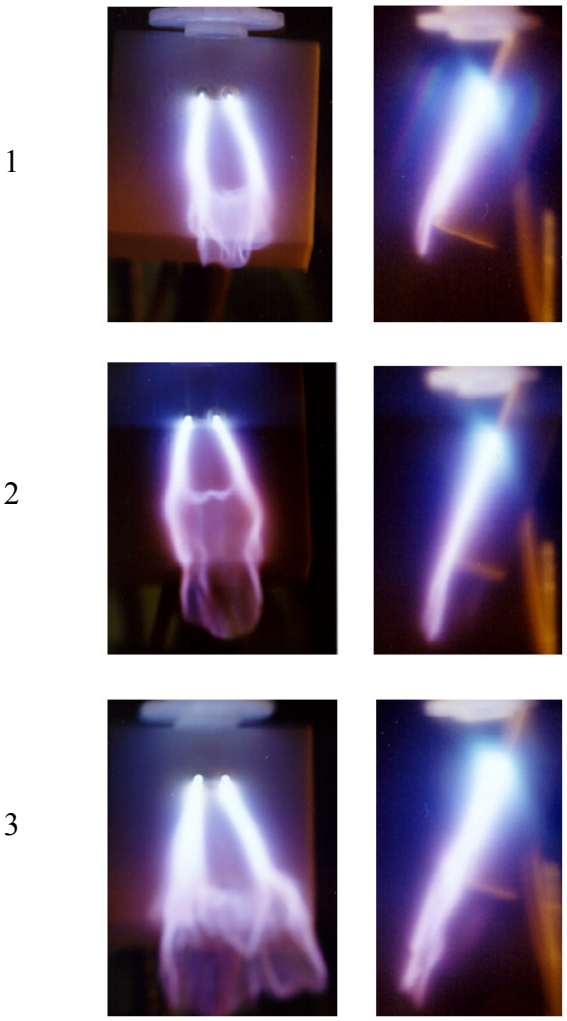

Fig. 7.1. The common view (*a* - front view, *b* -side view) of the pulse-periodic discharge in supersonic airflow on a surface of a flat plate at different values of air pressure in the high-pressure system p_o, *atm*: 1 - 1; 2 - 3; 3 - 6. The supersonic airflow is directed from top to down.

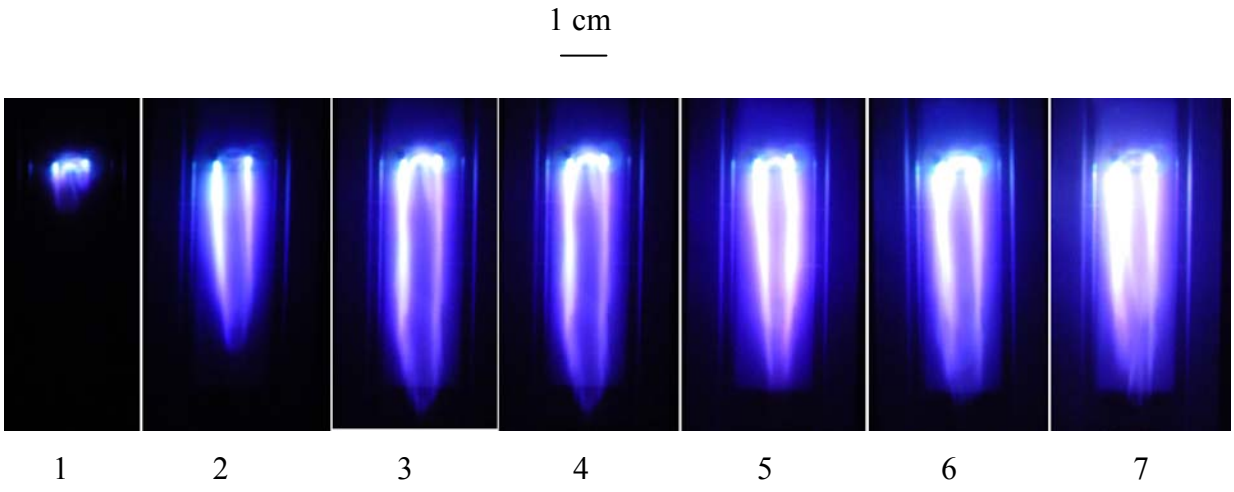

Fig. 7.2. The pulse-periodic transversal surface discharge in supersonic airflow with *M=2* in the aerodynamic channel of rectangular section *10x18 mm*^{2} without stagnation zone (*h=0 mm*). Front view. The supersonic airflow is directed from top to down. *p=150 torr, p_o=2 atm, i=8 A*.

Pulse duration *τ, μs*: 1 - 100; 2 – 200; 3 – 300; 4 – 400; 5 – 600; 6 – 800; 7 – 1000.

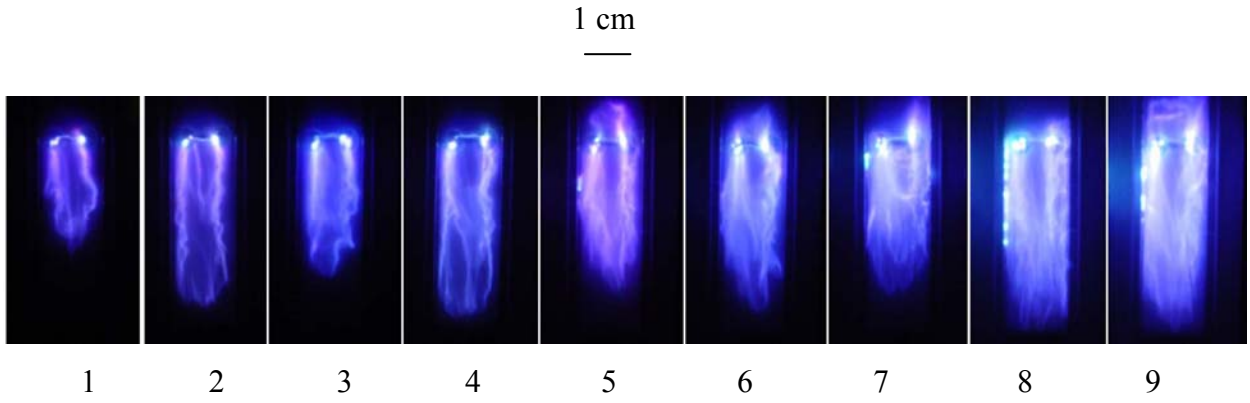

Fig. 7.3. The same, that *Fig. 7.2, h=2 mm*.

Pulse duration *τ, μs*: 1-150; 2-200; 3-250; 4-300; 5-400; 6-500; 7-600; 8-800; 9-1000.

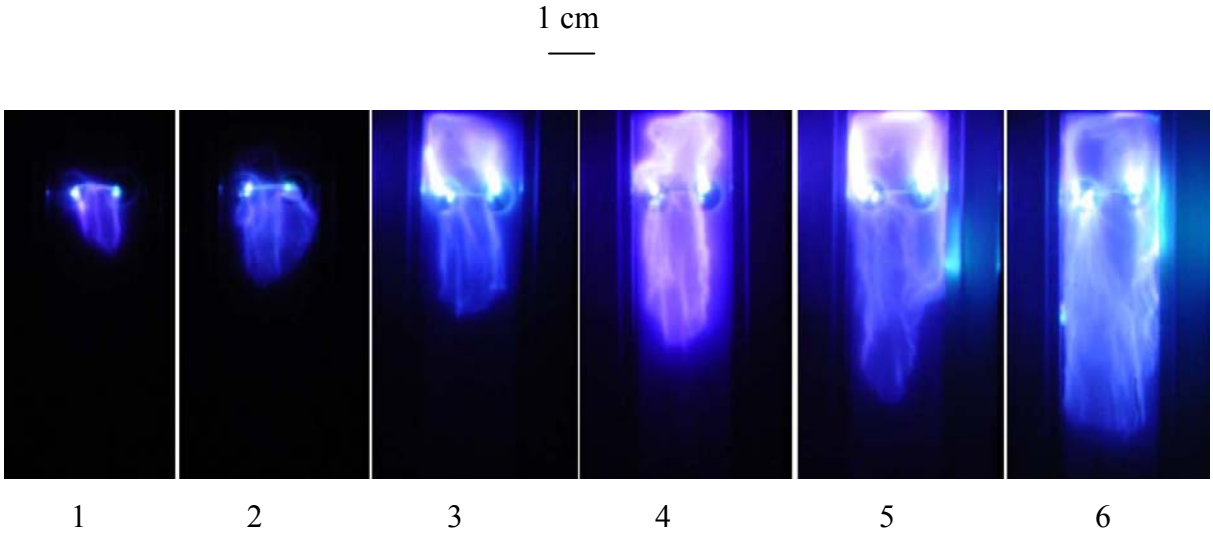

Fig. 7.4. The same, that *Fig. 7.2, h=3 mm*.

Pulse duration τ, μs: 1 – 75; 2 – 150; 3 – 300; 4 – 600; 5 – 800; 6 – 1000.

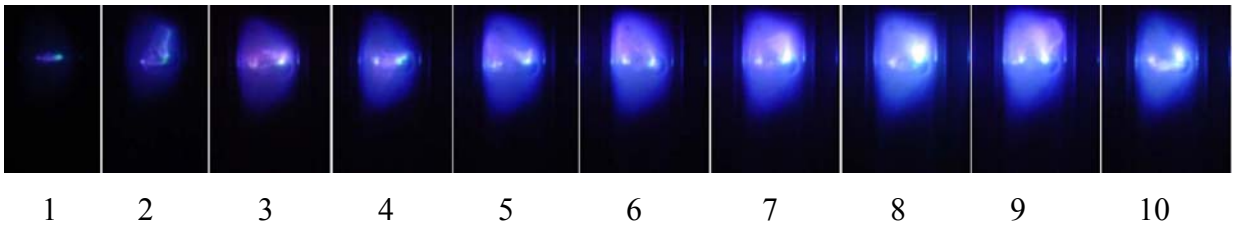

Fig. 7.5. The same, that *Fig. 7.2, h=5 mm*.

Pulse duration τ, μs: 1-100; 2-200; 3-300; 4-400; 5-500; 6-600; 7-700; 8-800; 9-900; 10-1000.

discharge exists only about a forward wall of a cavity and is not spread downstream.

These circumstances are promising from the point of view of use of a cavity as a source of the active particles, promoting of ignition and stable burning of a supersonic stream of a gas mixture.

7.3. Ignition of supersonic flow of gaseous fuel (propane-butane-air mixtures) with help of electrode pulsed-periodical surface discharge inside the aerodynamic channel

The aerodynamic channel of rectangular section *10x18 мм*^{2} was produced for investigation of a possibility of ignition of supersonic propane-air mixture with the help of a surface pulsed-periodical transversal discharge. For creation in aerodynamic channel of supersonic flow of a combustible propane-butane-air mixture with Mach number $M=2$ the Laval's nozzle of rectangular section was manufactured.

The discharge on an internal surface of the aerodynamic channel (without a cavity) could be created only at use of a high-voltage source. The output voltage of a source could be changed from *10* up to *30 kV*, discharge current $i=8\text{-}16$ *A*, pulse duration $\tau=50\text{-}1000$ μs.

The surface pulsed-periodical transversal discharge in supersonic flow was formed on a dielectric wall of aerodynamic channel The high-voltage pulses with the help of a high-voltage cable through the specially designed a vacuum cut-off point are lead to electrodes built-in flush into a dielectric plate. For avoidance of an electrical breakdown on the opposite surface of a dielectric plate outside of supersonic flow the special measures are undertaken.

The experiments were carried out at initial air pressure in the vacuum chamber $p=150$ *torr*, air pressure in the receiver-chamber (the high-pressure system) $p_o=2$ *atm*, propane-butane pressure in the high-pressure system $p_g=5$ *atm*.

The use of the pulsed surface discharge results in an ignition of a propane-butane-air mixture in the aerodynamic channel without a stagnant zone. The common back views of the aerodynamic channel with the discharge in supersonic flow of air (*a*) and propane-butane-air mixture (*b*) are shown in *Fig. 7.6*. One can see that the use of the pulsed surface discharge results in an ignition of a propane-air mixture in the aerodynamic channel.

The flame jet, leaving the discharge, extends in a direction (*x*), perpendicular to a supersonic flow direction (*z*). Knowing a supersonic flow velocity v_f it is possible to estimate the combustion front speed $v_c=v_f tg\alpha$, where $tg\alpha=x/z$. In experimental conditions the combustion front speed $v_c=40$ *m/s*.

Under the condition of a propane-butane-air mixture ignition the intensive radiation of

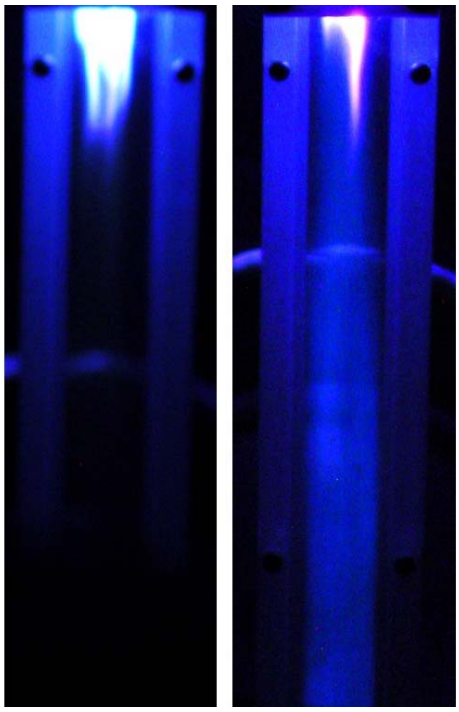

a *b*

Fig. 7.6. The common back view of the aerodynamic channel with the discharge in supersonic flow of air (*a*) and propane-butane-air mixture (*b*). *p=150 torr, p_o=2 atm, p_g=5 atm, M=2, i=16 A, τ=500 μs.*

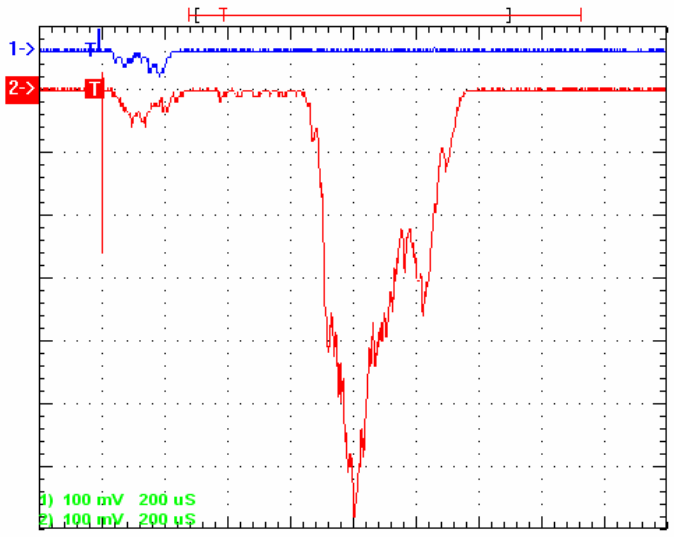

Fig. 7.7. Typical temporal behaviour of CH^* emission (the transition *A-X*, the band (0,0), the wavelength *λ=431,5 nm*). 1 (blue) – discharge in supersonic flow of air; 2 (red) – discharge in supersonic flow of propane-butane-air mixture. *p=150 torr, p_o=2 atm, p_g=5 atm, M=2, τ=200 μs, i=16 A, z=30 cm.*

CH band is registered from the area of the aerodynamic channel located on the distance *z=30 cm* downstream from electrodes through the time of *t~600 μs* after the switch on of a discharge current. Typical temporal behaviour of CH^* emission (the transition *A-X*, the band (0,0), the wavelength *λ=431,5 nm*) is given in *Fig. 7.7* at $p=150$ *torr*, $p_o=2$ *atm*, $p_g=5$ *atm*, $M=2$, $\tau=200$ *μs*, $i=16$ *A*. 1 – discharge in supersonic flow of air; 2 – discharge in supersonic flow of propane-butane-air mixture. The area of the aerodynamic channel, from which the CH^* emission was registered, located on the distance *z=30 cm* downstream from electrodes.

It is necessary to note, that in the discharge area the intensive emission not only *CH* bands, but also bands of *CN*, C_2, *OH*, atomic lines of hydrogen *H* and oxygen *O* is observed. Thus the intensity of *CN* emission from the discharge in propane-butane-air mixture is approximately in 3-5 times more, than the one from the discharge in air. However already on distance some centimeters from the discharge in propane-butane-air mixture the luminescence of *CN* band is not observed, then as the luminescence of *CH* bands does not decrease downstream. Therefore we identify a luminescence of *CH* band as the indicator of burning of a propane-butane-air mixture.

Alongside with an optical method the probe method was also used for diagnostic of process of ignition and combustion of a propane-air mixture. Probe current and typical temporal behaviour of CH^* emission (the transition *A-X*, the band (0,0), the wavelength *λ=431,5 nm*) are given in *Fig. 7.8*. Probe located on the distance of *z=32 cm* downstream from electrodes. The area of the aerodynamic channel, from which the CH^* emission was registered, located on the distance *z=30 cm* downstream from electrodes. One can see that the probe method as well as an optical method is a reliable way of diagnostic of process of combustion of a propane-butane-air mixture.

Under condition of *Fig. 7.7* the flame luminescence time is *350 μs* whereas discharge pulse duration is equal *200 μs*. Knowing the geometrical sizes of the channel and the supersonic flow velocity it is possible to estimate the combustion front speed v_c. In our conditions $v_c=45$ *m/s*, that well coincides with the combustion front speed $v_c=40$ *m/s*, that we have received earlier.

It is necessary to note, that the stagnant zone results in stabilization of burning of a supersonic propane-butane-air mixture. For example (*Fig. 7.9*), even a stagnant zone by depth of *h=2 mm* results in sharp increase of a burning time up to *1000 μs* at duration of discharge pulse $\tau=200$ *μs*.

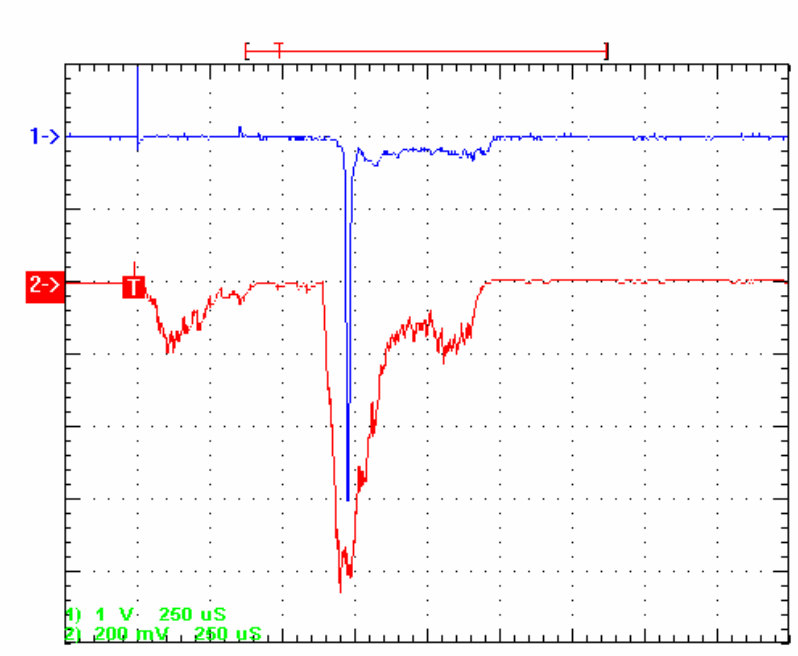

Fig. 7.8. Ignition of the supersonic propane-butane-air mixture at $p=150$ *torr*, $p_o=2$ *atm*, $p_g=5$ *atm*, $i=16$ *A*, $\tau=350$ *μs*. 1 (blue) - probe current at $z=32$ *cm*, 2 (red) - typical temporal behaviour of CH^* emission at $z=30$ *cm*.

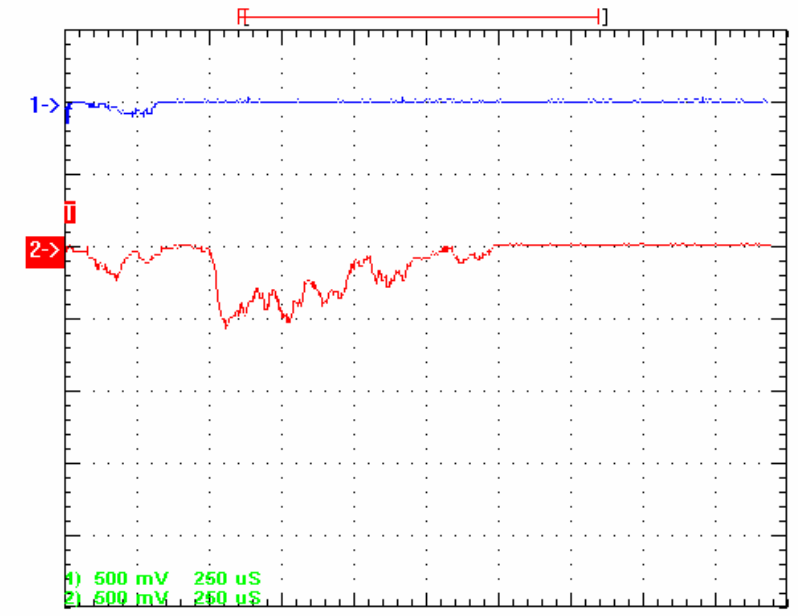

Fig. 7.9. Typical temporal behaviour of CH^* emission at ignition with use of stagnant zone by depth of $h=2$ *mm*. 1 (blue) – discharge in supersonic flow of air, 2 (red) – discharge in supersonic flow of propane-butane-air mixture.

7.4. Cavity as a flame stabilizing device

A cavity has allowed us to use a direct current power supply unit with output voltage of $U=2,5\text{-}4,5\ kV$ for creation of the surface discharge. With the help of this source it is impossible to create the discharge in free stream or the surface discharge in the channel without a stagnant zone, as its voltage is not enough for maintenance of the free discharge in supersonic flow. However the source allows to support the surface discharge in a cavity during time $t=1\text{-}2\ s$. The low-current high-voltage pulsed source, generating high-voltage pulses ($U=20\ kV$) by duration of $\tau=10\text{-}20\ \mu s$ and repetition frequency of $50\ Hz$ was used for breakdown of a discharge gap.

The discharge exists only in a cavity and is not flied out downwards on a stream at use of a stagnant zone by depth of $h>5\ mm$. These circumstances are promising from the point of view of a cavity use as a reservoir of the active particles promoting fast ignition and stable combustion of supersonic stream of gas mixture.

At small currents (*Fig. 7.10*) the discharge was unstable and ignition of a supersonic propane-air mixture occurred chaotically only in short time intervals with duration of $t=100\text{-}500\ \mu s$.

With increase in discharge current (*Fig. 7.11*) there is a time delay when the discharge exists in a propane-butane-air mixture without its ignition. The ignition of gas mixture takes place through $30\ ms$. Thus the discharge current reduces a little and the amplitude of its fluctuations increases. A voltage on electrodes and its fluctuations grow. Intensity of a luminescence of CH^* emission on an outlet of the aerodynamic channel sharply grows and a signal from the double probe located on an ending of the aerodynamic channel starts to be registered that confirms ignition and burning of a supersonic propane-air mixture.

At the further increase in discharge current (*Fig. 7.12*) the induction time decreases and the signal from a double probe grows. The received results show availability of a cavity use for flame stabilization of combustible supersonic mixtures.

The common view of a dielectric insert in a wide wall of the aerodynamic channel on which the discharge in a stagnant zone was formed is submitted in *Fig. 7.13*. The traces on a dielectric plate from the surface discharge in a supersonic gas flow are distinctly visible after several setting. One can see that the complex image, with formation of vortex reverse current, is left on a dielectric surface by discharge in cavity.

A boundary layer renders the big influence on structure of a stream in the narrow aerodynamic channel ($s=10x18\ mm^2$). It is possible to lock-out of the channel under ignition and

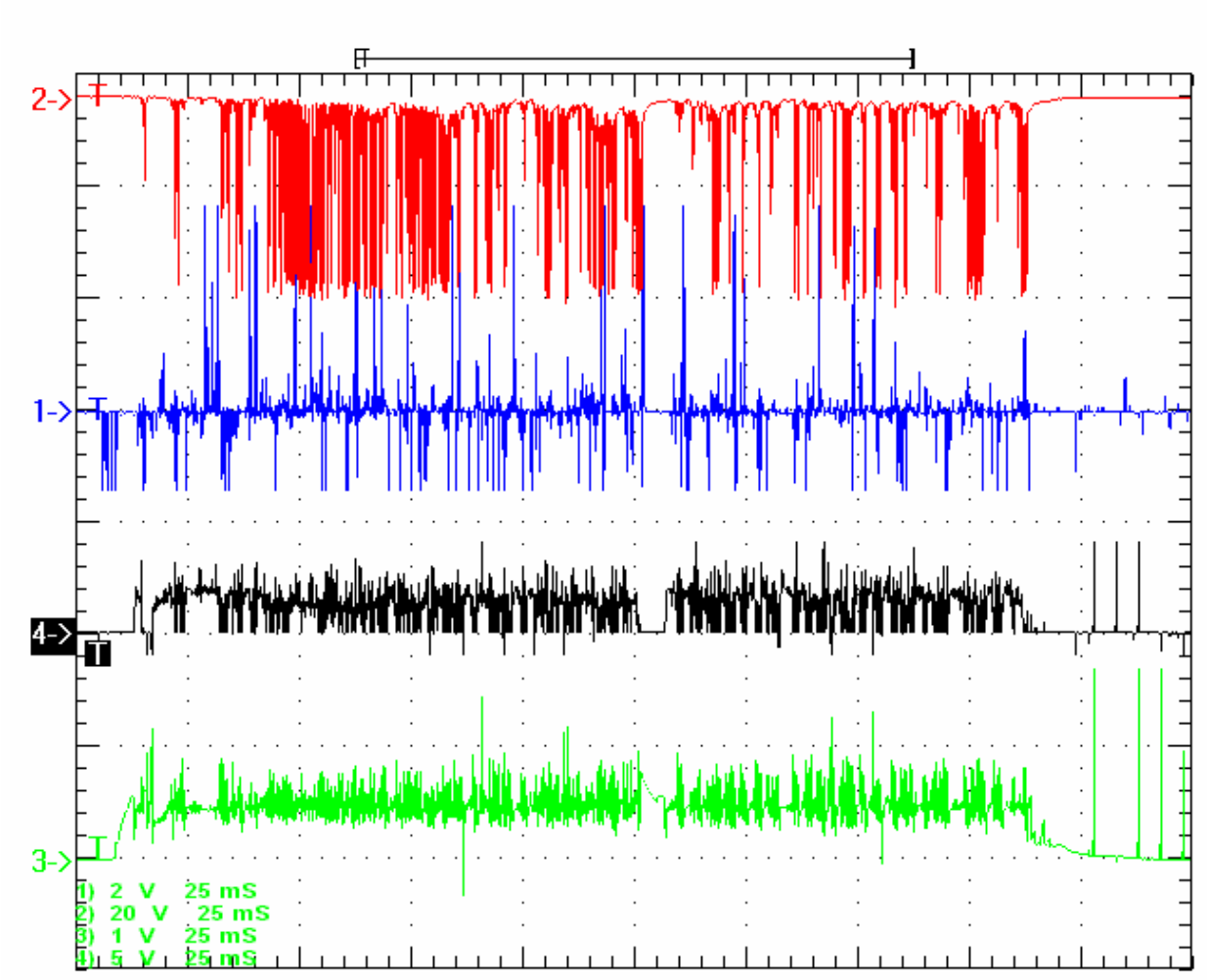

Fig. 7.10. Combustion of the supersonic propane-butane-air mixture in the aerodynamic channel. Transversal surface discharge in a stagnant zone of h=6 mm, p=150 torr, p_o=2 atm, p_g=5 atm, M=2, i=6 A, τ=200 ms. 1 (blue) - probe current z=20 cm; 2 (red) - typical temporal behaviour of CH^* emission z=20 cm (the transition A-X, the band (0,0), the wavelength λ=431,5 nm); 3 – (green) voltage; 4 (black) - discharge current.

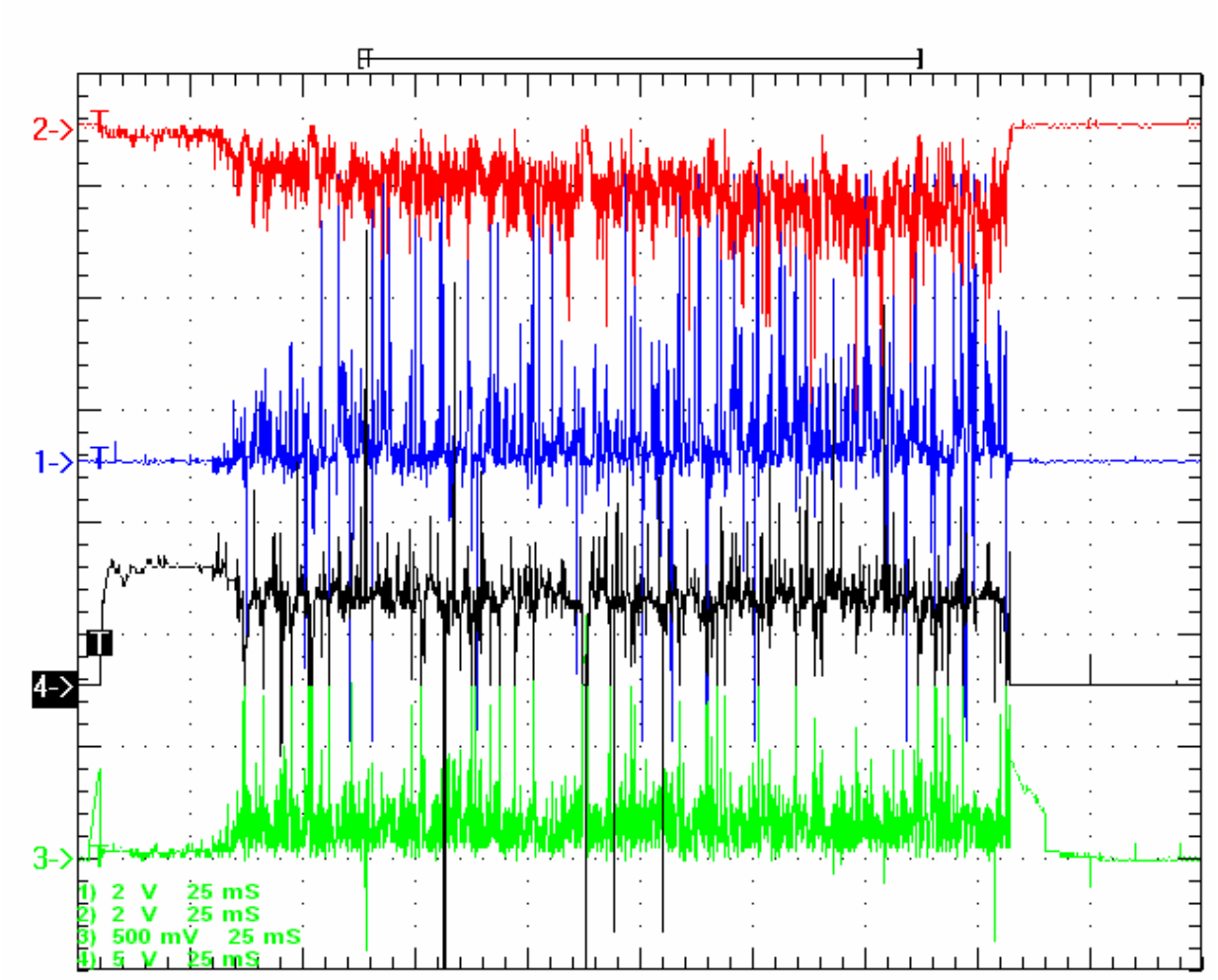

Fig. 7.11. The same, that *Fig. 7.10, i=17 A*.

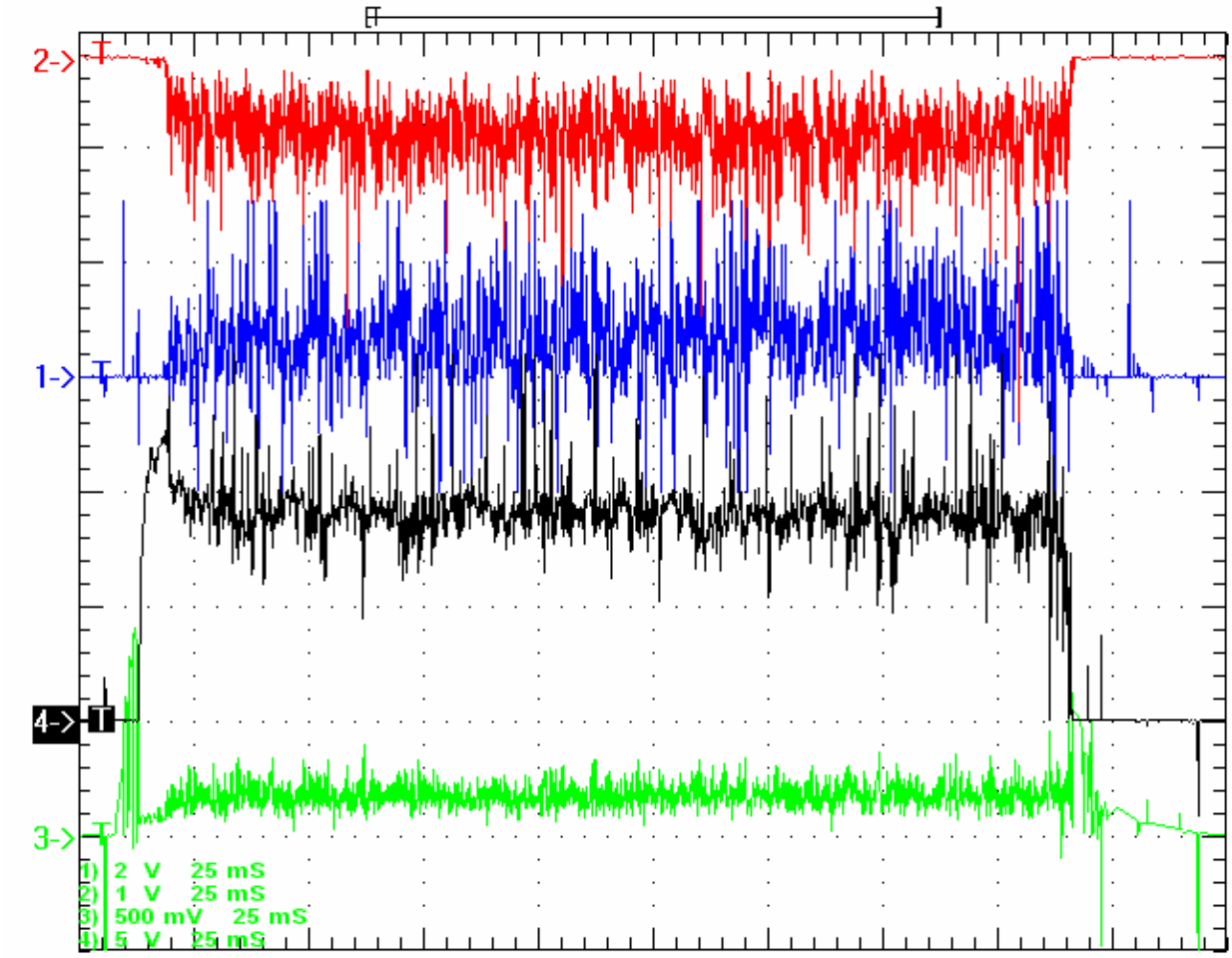

Fig. 7.12. The same, that *Fig. 7.10, i=40 A*.

Fig. 7.13. Common view of a cavity in a wide wall of the aerodynamic channel. The arrow shows a direction of supersonic flow.

burning of supersonic stream of gaseous fuels. Therefore for reduction of this effect the further experiments were carried out in the aerodynamic channel with section ($s=12,5x23\ mm^2$).

The typical temporal behavior of CH^* emission (the transition *A-X,* the band (0,0), the wavelength λ=431,5 nm), discharge current and voltage on discharge gap is represented in *Fig. 7.14* at use of transversal surface discharge in a stagnant zone in the aerodynamic channel for ignition and combustion of the supersonic propane-butane-air mixture. One can see that after breakdown the voltage on the discharge gap quickly reduces from *4,5 kV* till *250 V*. At the same time, there is a time delay of stationary combustion of propane-butane-air mixture achievement. Under experimental condition the time delay is about *400 ms*.

Time evolution of process of propane-butane-air mixtures burning was investigated at various values of discharge current and percentage of a mixture. In experiments the air consumption changed from *25* up to *100 g/s*, the gas consumption changed from *1* up to *8 g/s*, the discharge current was adjusted within the limits of *5-40 A*. Process of ignition of a supersonic stream of a combustible gas mixture was registered on sharp increase of a luminescence of the discharge in the region of spectrum *λ=431,5 nm*, on appearance of a signal from a double probe, on occurrence of a signal from the capacitor located on an exit of the aerodynamic channel, and on sharp change of acoustic noise.

Last circumstance is connected by that under our conditions the power of supersonic stream is equal of *22 kW*, the electric discharge power changes from *1* up to *5 kW*, whereas the thermal power at full combustion of propane-butane-air mixtures can be achieved up to *100 kW*.

Time dependences of intensity of radiation in spectral area near *λ=431,5 nm*, registered on an output of the aerodynamic channel at using of transversal surface discharge in a stagnant zone for ignition of the supersonic propane-butane-air mixture, are submitted in *Fig. 7.15* at various values of discharge current.

The time of beginning ignition (curve 1) and time of an achievement of stationary burning of a propane-butane-air mixture (curve 2) as a function of discharge current are submitted in *Fig. 7.16*.

From these figures it is visible, that rate of ignition increases with growth of discharge current, thus the stationary mode of burning is established faster. So at small discharge currents (*i<10 A*), that is at small put electric powers (*W<2 kW*) the burning begins only by the end of pulse duration *750 ms*, whereas at the big discharge currents (*i~30 A, W~6 kW*) the stationary mode of burning is achieved through *150-200 ms*.

Combustion of the supersonic propane-butane-air mixture in the aerodynamic channel

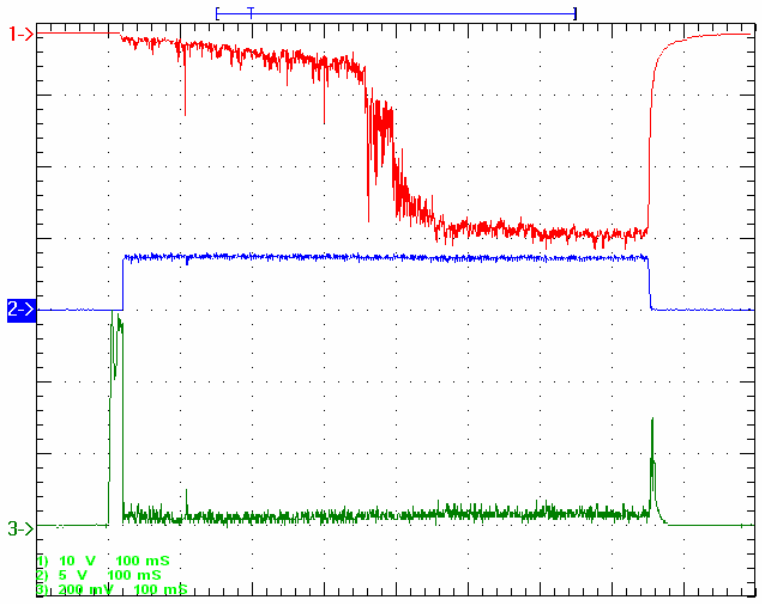

Fig. 7.14. Combustion of the supersonic propane-butane-air mixture in the aerodynamic channel. Transversal surface discharge in a stagnant zone $h=17$ mm, $L=70$ mm, $p=150$ torr, $p_o=2$ atm, $p_g=4$ atm, $M=2$, $i=12$ A, $U_d=250$ V, $\tau=750$ ms, $m_g=4,4$ g/s, $m_{air}=70$ g/s.
1 (red) - typical temporal behaviour of CH^* emission; 2 (blue) - discharge current; 3 (green) - voltage on discharge gap.

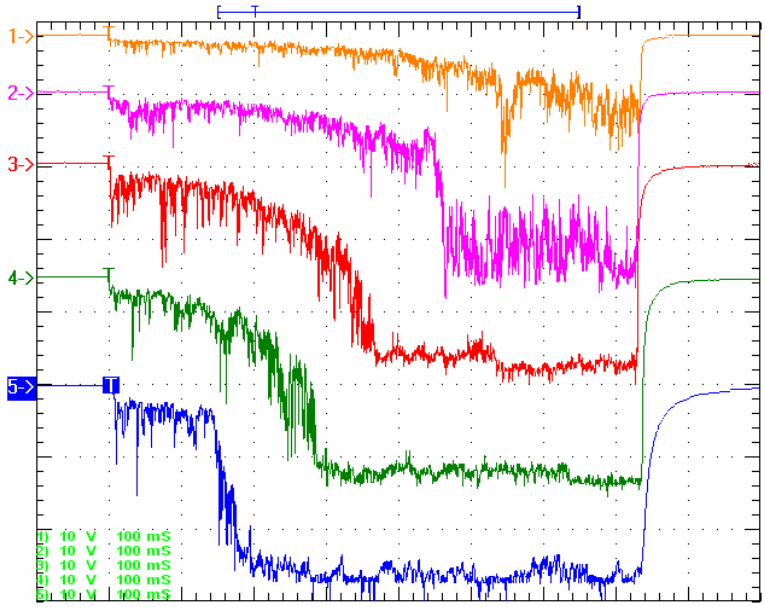

Fig. 7.15. Combustion of the supersonic propane-butane-air mixture.
i, A: 1-9, 2-11, 3-16, 4-19, 5-27. $M=2$, $\tau=750$ ms, $U_d=250$ V, $h=17$ mm, $L=70$ mm, $p=150$ torr, $p_o=2$ atm, $p_g=4,4$ atm, $m_g=5,4$ g/s, $m_{air}=70$ g/s.

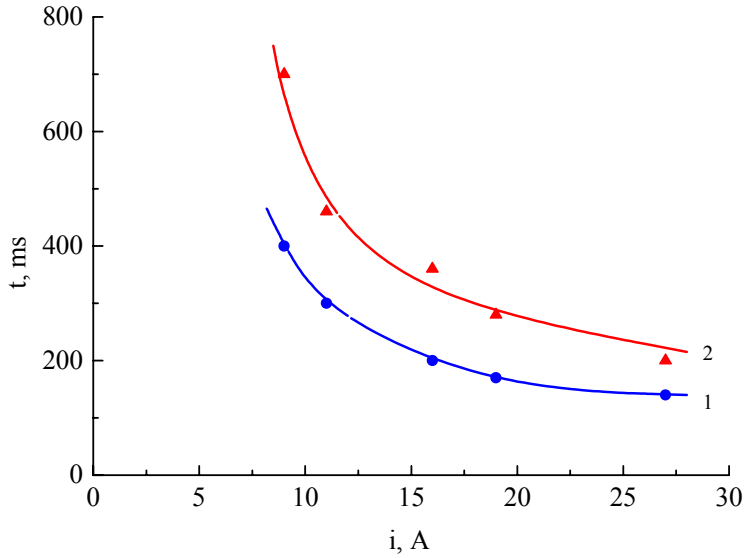

Fig. 7.16. The beginning ignition time (curve 1) and time of stationary burning achievement of a propane-butane-air mixture (curve 2) as a function of discharge current. $M=2$, $\tau=750$ *ms*, $U_d=250$ *V*, $h=17$ *mm*, $L=70$ *mm*, $p=150$ *torr*, $p_o=2$ *atm*, $p_g=4{,}4$ *atm*, $m_g=5{,}4$ *g/s*, $m_{air}=70$ *g/s*.

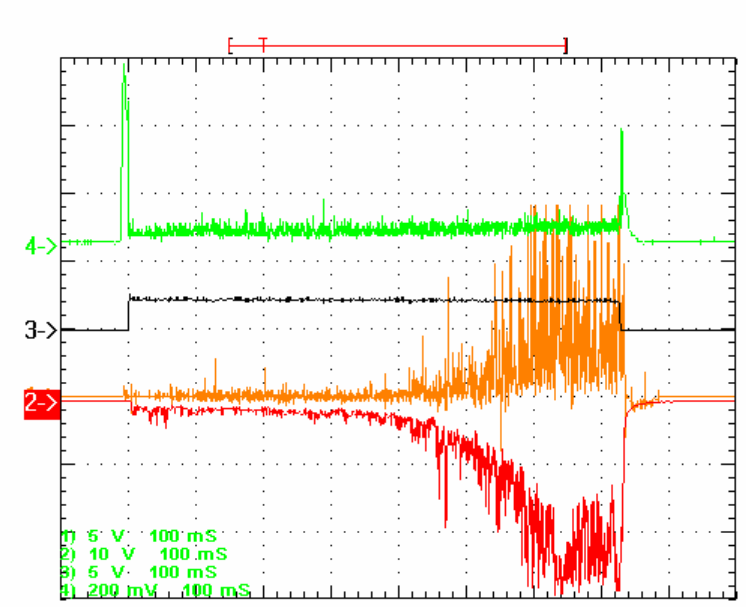

Fig. 7.17. Combustion of the supersonic propane-butane-air mixture in the aerodynamic channel. Transversal surface discharge in a stagnant zone $h=17$ *mm*, $L=70$ *mm*, at $p=150$ *torr*, $M=2$, $i=7$ *A*, $\tau=750$ *ms*. 1 - typical signal from the capacitor located on an exit of the aerodynamic channel; 2 - typical temporal behaviour of CH^* emission; 3 - discharge current; 4 - voltage on discharge gap.

with help of transversal surface discharge in a stagnant zone *h=17 mm, L=70 mm* at *p=150 torr, M=2, τ=750 ms* is given in *Fig. 7.17* at discharge current *i=7 A* and in *Fig. 7.18 at i=14 A*. From these figures one can see, that signal from the capacitor, located on an exit of the aerodynamic channel, as well as optical and probe method, can be used as a reliable way of diagnostic of process of combustion of a propane-butane-air mixture.

Process of fuel ignition strongly depends on structure of a combustible mixture. Time evolution of ignition of a supersonic combustible mixture at different percentage of gas in a mixture at constant amount of air is given *in Fig. 7.19*. Similar dependences have been received at the constant gas consumption and change of the air consumption. All measurements were carried out at discharge current *i=8 A*. Results of processing of the received data are submitted in *Fig. 7.20* and *Fig. 7.21*. One can see that both in case of a poor mixture, and in case of the enriched mixture, an achievement time of stationary mode of burning increases in comparison with stoichiometry of a mixture.

It is necessary to pay attention, that in our conditions in case of use for ignition of the powerful high-voltage pulsed power supply the induction time equals hundreds microseconds (look, for example, *Fig. 7.6-7.9*) whereas at use of low-voltage power supply for ignition of a gas mixture in the cavity the induction time sharply grows. This fact indirectly confirms our conclusion about strong influence of the charged and active particles, formed in the discharge at large values of reduced electric field, on process of ignition of supersonic gaseous fuels.

The bad quality of propane-butane-air gaseous mixture was used in last experiments. Under these conditions at burning of supersonic stream of propane-butane-air mixture plenty of soot was formed. Soot took root into a surface as the supersonic dielectric channel, and in a surface of the teflon plate placed on distance of 40 cm from an exhaust outlet of the channel on a window of the vacuum chamber as its protection against hot streams of products of combustion.

General view of the aerodynamic channel after about *20* starts of combustion of a supersonic stream of a propane-butane-air mixture is shown in *Fig. 7.22*. Duration of each start-up is *τ=750 ms*.

It is also necessary to note, that in experiments the optimum variant of a stagnant zone, stoichiometry of a propane-butane-air mixture, gas pressure and a mode of excitation of the surface discharge were not used. Optimization of these parameters should lead to more effective and full combustion of supersonic streams of gaseous fuels, ignited with the help of various types of the gas discharge.

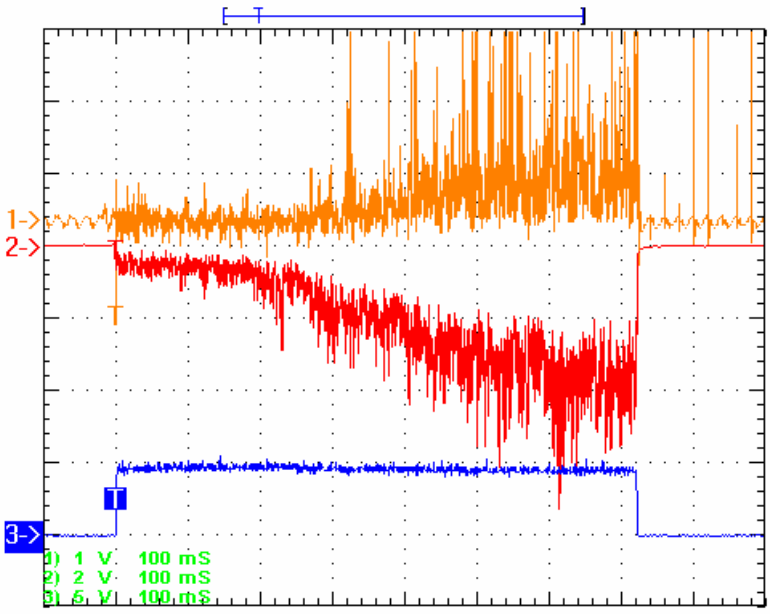

Fig. 7.18. Combustion of the supersonic propane-butane-air mixture in the aerodynamic channel. Transversal surface discharge in a stagnant zone *h=17 mm, L=70 mm* at *p=150 torr, M=2, i=14 A, τ=750 ms.* 1 - typical signal from the capacitor located on an exit of the aerodynamic channel; 2 - typical temporal behaviour of CH^* emission; 3 – discharge current.

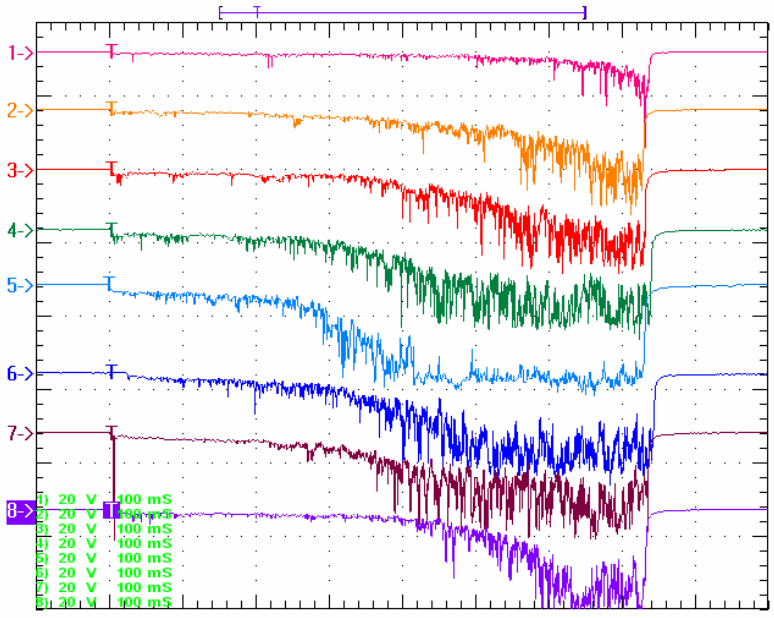

Fig. 7.19. Combustion of the supersonic propane-butane-air mixture. *M=2, τ=750 ms, i=8 A,* U_d*=250 V, h=17 mm, L=70 mm, p=150 torr,* p_o*=2 atm,* m_{air}*=70 g/s.* p_g*=(3,3-5,0) atm,* m_g*=(2,3-7,3) g/s*. In the figure the percentage of gas in a mixture increases from top to down (from a curve (1) up to a curve (2)).

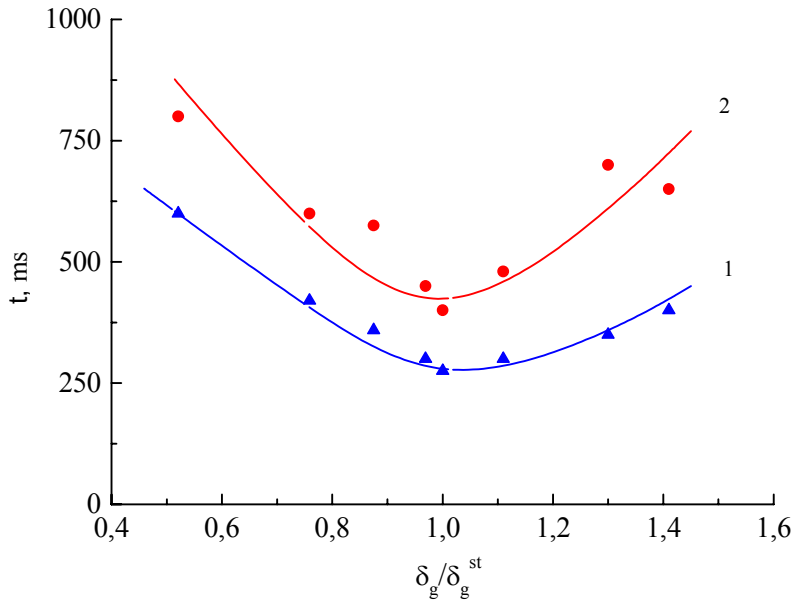

Fig. 7.20. The beginning ignition time (a curve 1) and time of stationary burning achievement of a propane-butane-air mixture (a curve 2) as a function of gas consumption. *M=2, h=17 mm, L=70 mm, τ=750 ms, p=150 torr, p_o=2 atm, m_{air}=70 g/s, i=8 A, U_d=250 V, p_g^{st}=4,1 atm, m_g^{st}=4,55g/s.*

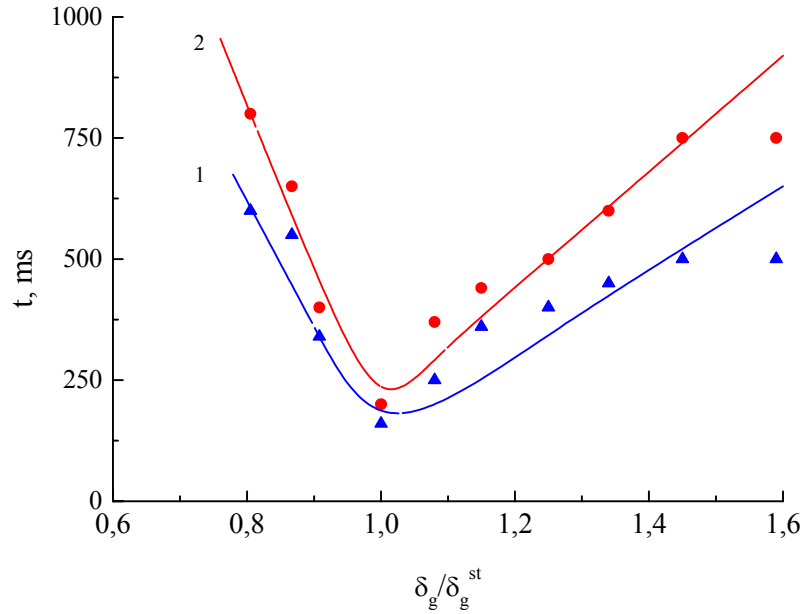

Fig. 7.21. Time of the beginning of occurrence of burning (a curve 1) and time of achievement of stationary burning of a propane-butane-air mixture (a curve 2) as a function of air consumption. *M=2, h=17 mm, L=70 mm, τ=750 ms, p=150 torr, U_d=250 V, i=8 A, p_g=4,05 atm, m_g=4,35g/s p_o^{st}=2 atm, m_{air}^{st}=70 g/s.*

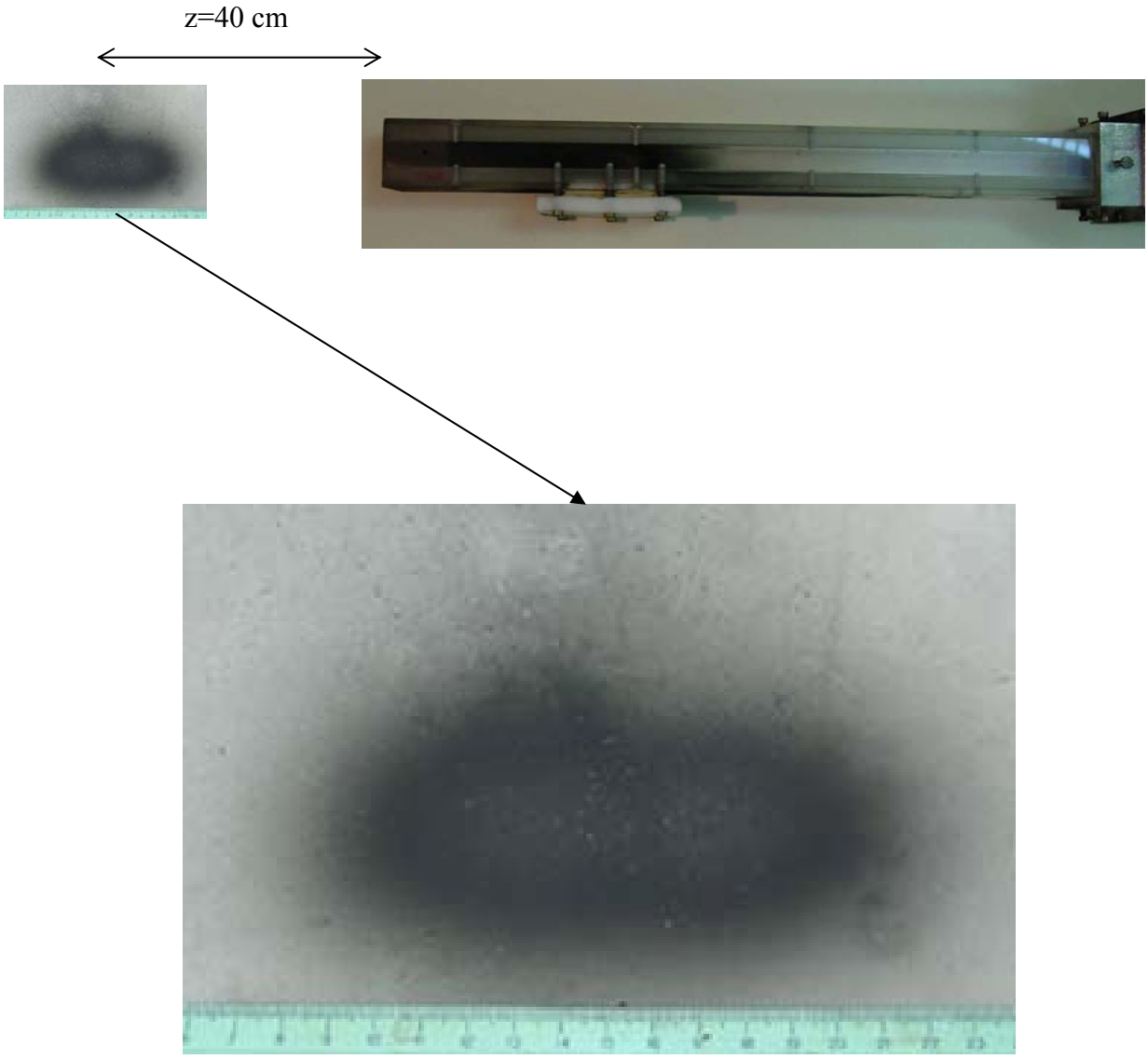

Fig. 7.22. General view of the aerodynamic channel after about 20 starts of combustion of a supersonic stream of a propane-butane-air mixture. Duration of each start-up is τ=750 ms

CHAPTER VIII
SUPERSONIC FLOW OVER CYLINDRICAL ANTENNA IN THE PRESENCE OF MICROWAVE DISCHARGE ON ITS SURFACE

8.1. Task formulation

Within the framework of non-viscous statement the analytical investigations of streamlining by supersonic flow of a cylindrical antenna, conjugate with conical tip are performed at organization of a microwave discharge on its surface. In experiments the discharge is propagated with finite velocity v_q from the end of the waveguide, delivering energy to the antenna, towards to a flow. In numerical calculations the energy input to gas in discharge is interpreted as energy source of the predetermined intensity, which one acts in wall boundary layer of depth δ. The geometry of a power-supplier is determined by a position of front of ionization z_q and depends on time. The purpose of calculations is the finding-out of main gas-dynamic features of streamlining by supersonic airflow of the antenna with a microwave discharge on its surface.

The set of the Euler equations for non-steady flow of gas with an axial symmetry looks like:

$$\frac{\partial}{\partial t}\begin{pmatrix}\rho\\ \rho u\\ \rho v\\ e\end{pmatrix}+\frac{\partial}{\partial r}\begin{pmatrix}\rho u\\ p+\rho u^2\\ \rho uv\\ (e+p)u\end{pmatrix}+\frac{\partial}{\partial z}\begin{pmatrix}\rho v\\ \rho uv\\ p+\rho v^2\\ (e+p)v\end{pmatrix}=\frac{1}{r}\begin{pmatrix}-\rho u\\ -\rho u^2\\ -\rho uv\\ -(e+p)u\end{pmatrix}+\begin{pmatrix}0\\ 0\\ 0\\ \rho\dot{Q}\end{pmatrix}, \tag{8.1}$$

where for ideal perfect gas

$$e=\frac{p}{\gamma-1}+\frac{\rho}{2}\left(u^2+v^2\right). \tag{8.2}$$

It is supposed, that power-supplier has Gaussian distribution on space in boundary area of depth δ. The power consumption W depends on density and can be determined during calculations.

$$\dot{Q}=Q_0\exp\left(-\left(\frac{r-r_s(z)}{\delta}\right)^2\right),\ z\ge z_q \tag{8.3}$$

and

$$\dot{Q} = Q_0 \exp\left(-\left(\frac{r - r_s(z_q)}{\delta} \right)^2 - \left(\frac{z - z_q}{\delta} \right)^2 \right), \; z < z_q . \tag{8.4}$$

The supersonic flow in real experiment was formed as a result of gas flow from open space into the chamber with low pressure through a profiled nozzle. In calculations the flow is considered boundless. The effects of real stream are neglected. The flow parameters on an output of a nozzle p_1 and T_1 are determined on known value of a Mach number M_1 and parameters in open space p_o and T_o.

$$\frac{p_0}{p_1} = \left(1 + \frac{\gamma - 1}{2} M_1^2 \right)^{\frac{\gamma}{\gamma - 1}}, \quad \frac{T_0}{T_1} = 1 + \frac{\gamma - 1}{2} M_1^2 . \tag{8.5}$$

The procedure of reduction to a dimensionless form on pressure p_1 and density ρ_1 of the formed supersonic flow, and also typical size l_1 is fulfilled. Calculations were carried out under the conditions corresponding to conditions of real experiment:

$$M_1 = 2, \; \gamma = 1.4, \; T_o = 300\,K , \; p_o = 760\,torr = 101325 N/m^2 , \; l_1 = 0{,}01\,m . \tag{8.6}$$

Density is determined from an equation of state:

$$\rho = p/RT , \tag{8.7}$$

where $R = R_o/\mu$, $R_o = 8314{,}32\,J/(K \cdot kmol)$-universal gas constant, $\mu = 28.964420\,kg/kmol$ - molecular weight of air.

The flow parameters:

$$p_1 = 97{,}13\,torr = 12950\,N/m^2 , \; T_1 = 166{,}7\,K , \; \rho_1 = 0{,}270\,kg/m^3 . \tag{8.8}$$

Thus, for recalculation of calculated value in physical one (the physical values are denoted by a tilde) the following scales can be used:

for pressure

$$\tilde{p} = p_1 p = 12950\,p \text{ N/m}^2 , \tag{8.9}$$

for density

$$\tilde{\rho} = \rho_1 \rho = 0.270\rho \text{ kg/m}^3 , \tag{8.10}$$

for temperature

$$\tilde{T} = T_1 T = 166.7\,T \text{ K} , \tag{8.11}$$

for velocity

$$\tilde{u} = \sqrt{p_1/\rho_1}\, u = 219\,u \text{ m/sec} , \tag{8.12}$$

for distance

$$\tilde{x} = l_1 x = 0.01x \text{ m}, \tag{8.13}$$

for time

$$\tilde{t} = tl_1 \Big/ \sqrt{p_1/\rho_1} = 45.6\times10^{-6} t \text{ sec}, \tag{8.14}$$

for power

$$\tilde{W} = W p_\infty l_1^2 \sqrt{p_1/\rho_1} = 284W \text{ Watt}. \tag{8.15}$$

It is supposed, that on a body surface $r = r_s(z)$ the condition of no flowing is realized. In accordance with experimental conditions diameter of a body is equal $d = 0{,}9$, a cone angle is equal 25^o. The total length of a body in calculations is chosen $L = 5$.

Calculations were carried out by a method of an establishment on time with use of MacCormac's finite-difference scheme of the second order of accuracy.

8.2. Dynamics of transitional processes at microwave discharge activation on the antenna surface

For experimental conditions the distribution speed of an ionization wave $\tilde{V}_q = 10^4$ m/sec that corresponds $V_q = 45{,}6$. The pulse duration $\tilde{\tau}_q = 100\ \mu s$ that corresponds $\tau = 2{,}19$. At such parameters the area of an energy supply covers so quickly whole antenna, that process can be considered as instantaneous one. This assumption is not necessary for carrying out of calculations as the program allows modeling the evolution of processes in time.

So, at first with the help of pseudoviscosity method, the streamline of the antenna calculates at absence of an energy supply. At $t = 0$ the instantaneous switching-on of energy source on full surface takes place. The thickness of a layer δ and intensity Q_o of energy source in calculations were varied. Further dynamics of transient processes up to the moment of stabilization was traced.

Such approach has allowed revealing the following basic stages of the physical phenomenon.

"Explosion" (*0<t<0,25*). The supply of energy originally results in practically instant increase of pressure. There is a cylindrical explosion on a surface and the shock wave is formed (look *Fig. 8.1*). At this stage a movement of gas can be neglected, as longitudinal gas velocity for considered time practically does not change. The gas-dynamical parameters change the same as in case of explosion in motionless gas. Pressure grows according to distribution of energy density on space and, hence, the temperature increases and the Mach number decreases.

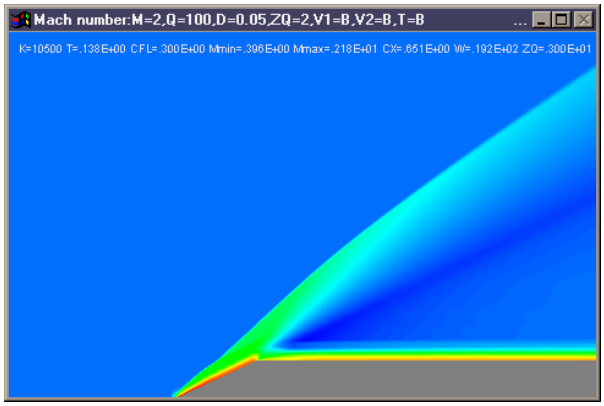

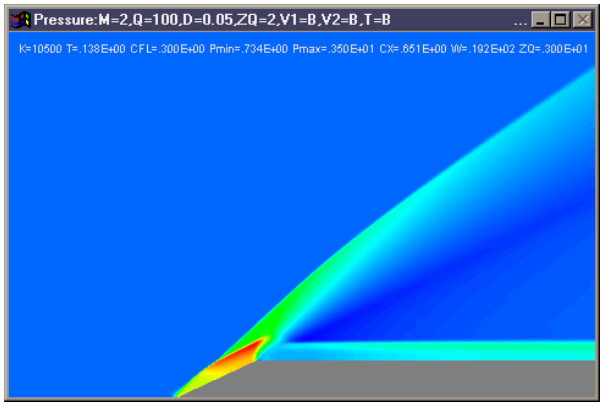

a) Mach number flow field b) static pressure flow field

Fig. 8.1. "Explosion" phase ($t = 0{,}138$) – $\delta = 0{,}05$, $Q_o = 100$.

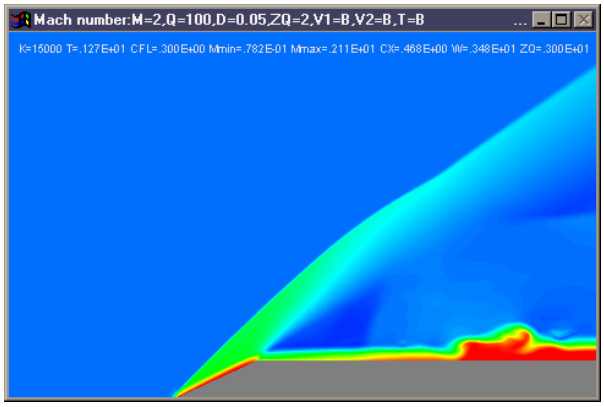

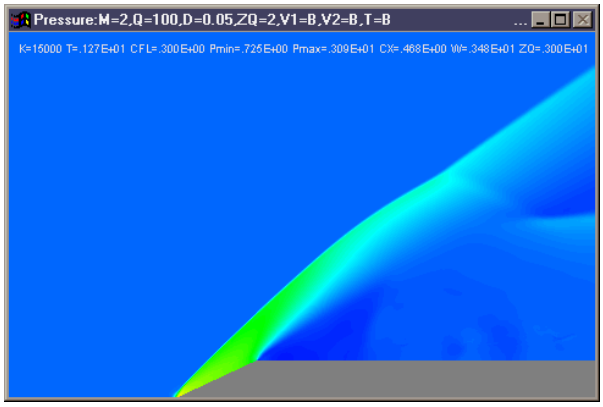

a) Mach number flow field b) static pressure flow field

Fig. 8.2. "Explosion products drifting" phase ($t = 2{,}27$) – $\delta = 0{,}05$, $Q_o = 100$.

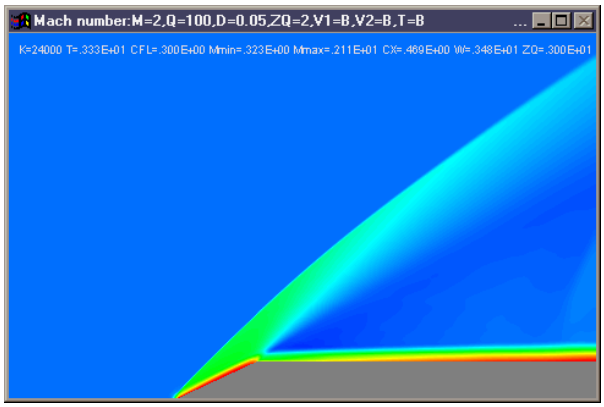

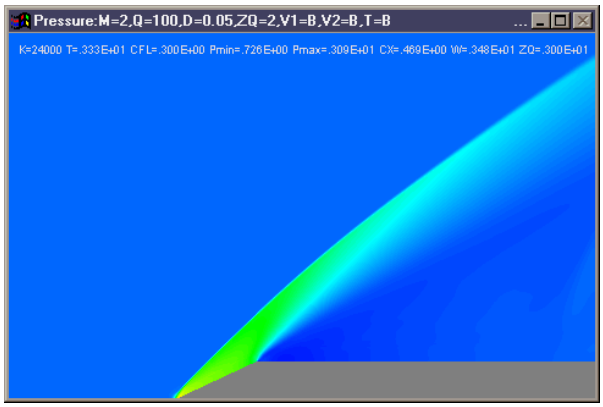

a) Mach number flow field b) static pressure flow field

Fig. 8.3. "Steady flow" ($t = 3{,}33$) – $\delta = 0{,}05$, $Q_o = 100$.

Drift of explosion products ($0,25<t<t_s$) and formation of a stationary picture of flow. The energy source continues to work, the explosive shock wave passes the limits of simulated area, however parameters of gas after explosion do not correspond to the stationary solution of a task on a flow of whole configuration by supersonic stream. The drift of explosion products by an oncoming stream begins. Thus because of instability of contact border the formation of vortexes is observed (look *Fig. 8.2*). As the explosion products are blown in area upstream the stationary flow pattern is formed around of the antenna. Therefore duration of the given stage depends on length of the antenna. For $L = 5$ the explosion products are basically blown for limits of computational area to a moment $t_s = 2,2$.

Steady flow ($t > t_s$). The stationary solution of a task corresponding to streamlining by a supersonic flow of the antenna and energy-supplyer is formed (look *Fig. 8.3*). The heating of gas takes place at its moving along whole external surface of antenna, that in absence of dissipation mechanisms results in continuous growth of gas temperature, increase of a sound velocity and decrease of Mach numbers. Therefore, the depth of area occupied by a subsonic flow is increased in the direction of the end of the antenna (see *Fig. 8.3a*). The pressure gradients in a transverse direction near to a lateral area absent and as a whole picture is similar to streamlining without an input of energy (see *Fig. 8.3b*).

Isolines of Mach number and static pressure are shown in *Fig. 8.4* for ″explosion″ phase ($t = 0,138$), in *Fig. 8.5* for ″explosion products drifting″ phase ($t = 1,27$) and in *Fig. 8.6* for ″steady flow″ ($t = 3,33$) at $\delta = 0,05$, $Q_o = 100$.

The distributions of some parameters (Mach numbers, static pressure, density and longitudinal component of velocity) on a lateral area of the antenna for different thicknesses of surface discharge ($\delta = 0,1$, $\delta = 0,05$) at identical intensity of energy-supplyer $Q_o = 100$ are given in *Fig. 8.7.* It is necessary to note, that these distributions practically coincide one another and essentially differ from a case of steady state flow without an input energy. Thus, relatively thin layers could be used to control of values of the gasdynamical parameters on the surface of relatively large bodies, for example, for the friction drag reduction. At an input of energy temperature is considerably increased, the longitudinal speed increases, but thus the Mach numbers decrease. Therefore it is necessary to keep care at the use of the term ″a flow is slow down up to subsonic speeds″ as thus the actual physical speed is increased. Let's mark also, that the stationary pressure profile along a lateral area of the antenna practically corresponds to streamlining without an energy input. The absence of gradients in a transverse direction was

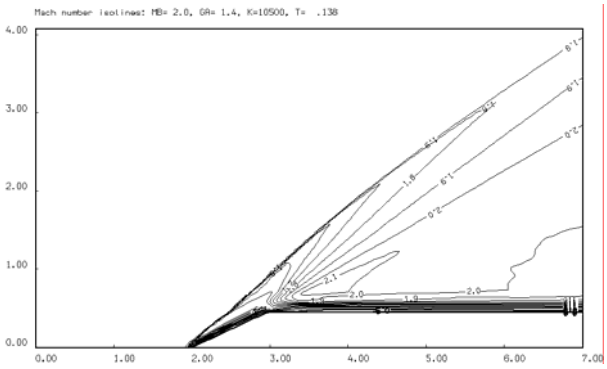

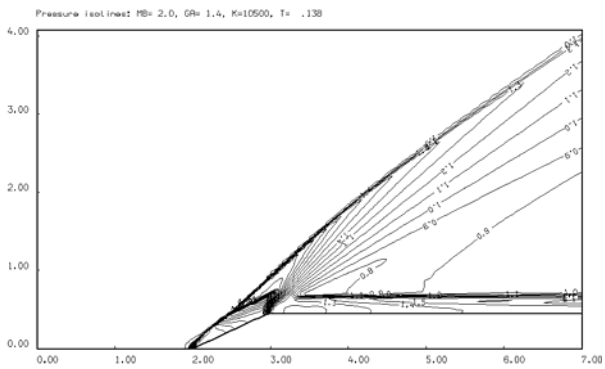

a) isolines of Mach number b) isolines of static pressure

Fig. 8.4. "Explosion" phase ($t = 0{,}138$) – $\delta = 0{,}05$, $Q_o = 100$.

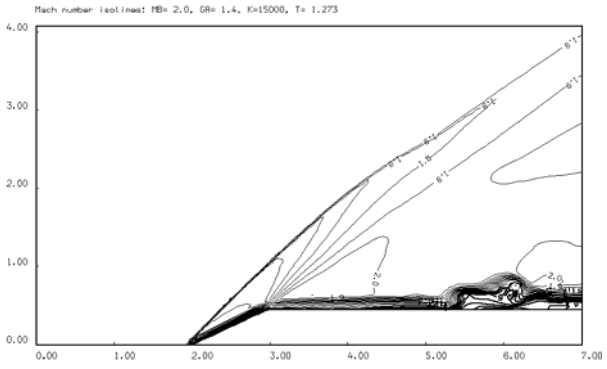

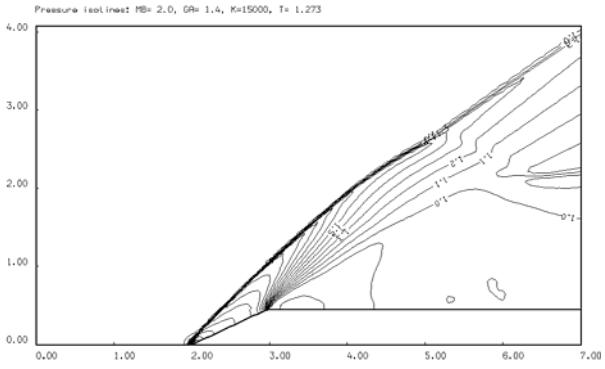

a) isolines of Mach number b) isolines of static pressure

Fig. 8.5. "Explosion products drifting" phase ($t = 2{,}27$) – $\delta = 0{,}05$, $Q_o = 100$.

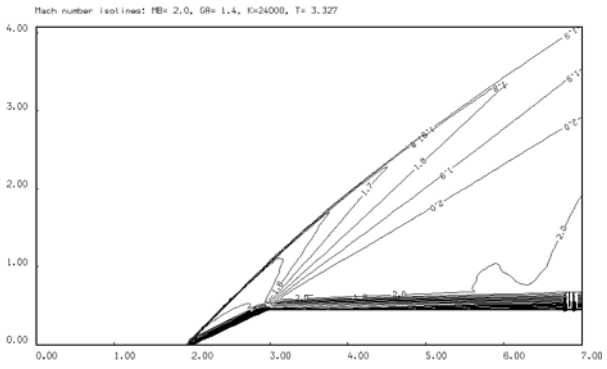

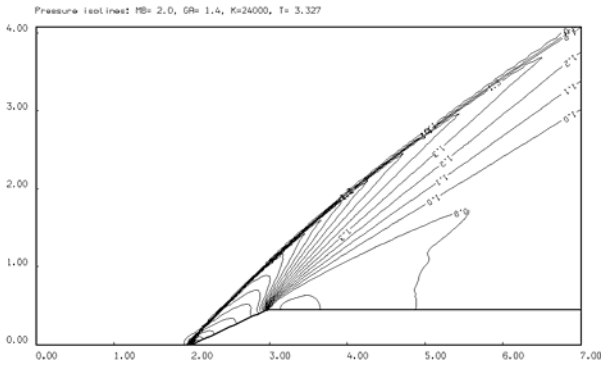

a) isolines of Mach number b) isolines of static pressure

Fig. 8.6. "Steady flow" ($t = 3{,}33$) – $\delta = 0{,}05$, $Q_o = 100$.

earlier marked. Therefore for definition of friction and heat transfer in steady conditions the simplified boundary layer theory can be used.

The interesting fact has turned out, that the input of energy results only in redistribution of static pressure on a surface, so that wave drag in steady conditions remains invariable. Dynamics of this process is submitted in *Fig. 8.8a*. At switching-on of microwave discharge at a phase of explosion is watched more than double increase of a wave drag, which is step-by-step reduced up to initial values. The given circumstance is necessary to take into account at planning of practical usage of surface microwave discharge for a decrease of friction drag.

The used model of ″mass″ energy-supplyer assumes that the dynamical decrease of power consumption is taken place at reduction of gas density in the field of gas discharge. In calculations a dynamical decrease of power consumption exceeded an order of magnitude. Calculations were carried out for parameters $\delta = 0{,}1$, $Q_o = 100$ and $\delta = 0{,}05$, $Q_o = 100$ or, accordingly, a steady-state values $W = 14{,}7$ and $W = 6{,}6$. Taking into account a rule of recalculation of powers in physical quantities is visible, that these values are less than energy spent in experiments (*20-100 kW*).

The performed calculations allow drawing the following conclusions.

1. The activation of energy source on the lateral surface is accompanied by complicated transitional gas-dynamical processes. The formation of a steady flow is preceded by an explosion processes because of instant pressure increasing and than explosion products drifting. On the stage of products drifting the appearance and evolution of vertex structures as a result of contact surface instability is possible. The stabilization time for the whole antenna length is larger than microwave pulse duration under experimental conditions.

2. Parameters distributions along the antenna surface for different energy layer thickness are almost identical. Thus, relatively thin layers could be used to control gas dynamic parameters on the surface of relatively large bodies.

3. For steady regimes the redistribution of static pressure on the antenna lateral surface does not produce the wave drag modification in comparison with the case of flow without energy input. However, on the explosion stage more than double short-time wave drag increasing was observed. This circumstance must be taking into account when planning the practical application of microwave discharge for the friction drag reduction.

4. The static pressure distribution on the antenna surface is practically the same as in the case of a flow over antenna without energy input. So, the simplified boundary layer model can be used to determine friction and heat transfer characteristics.

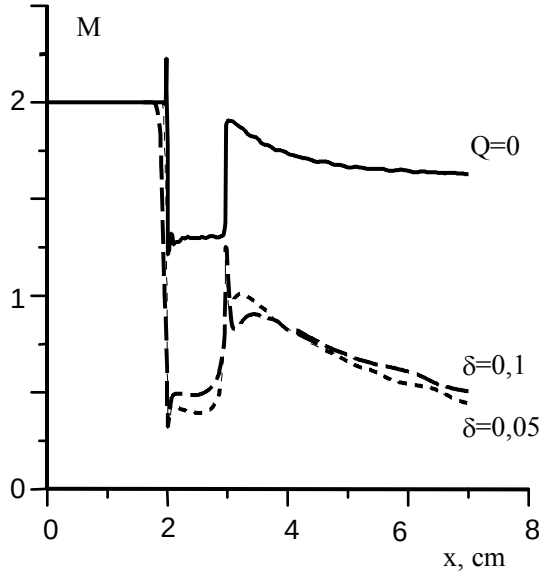

a) Mach numbers

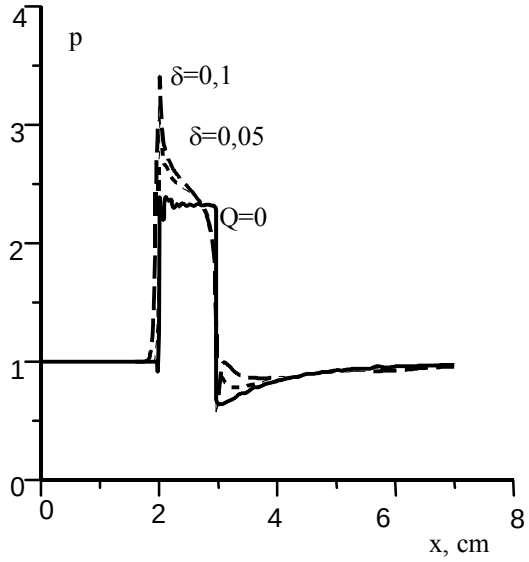

b) static pressure

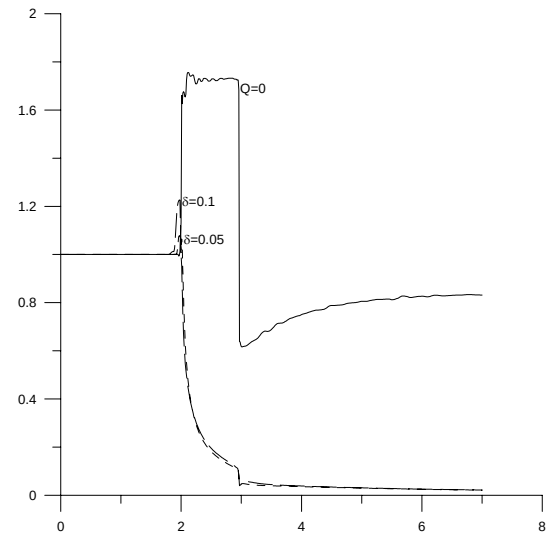

c) density

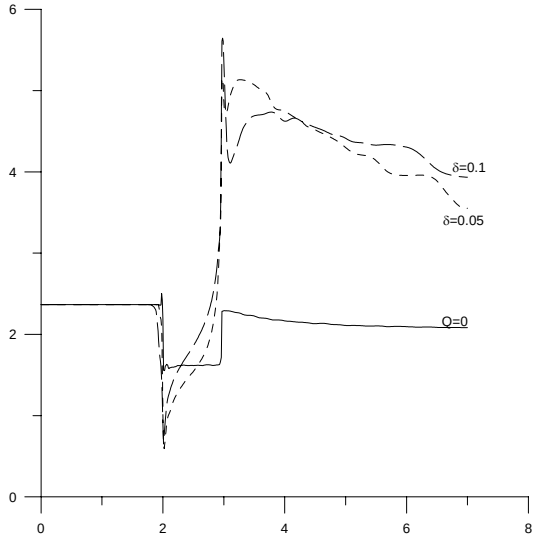

d) longitudinal component of velocity

Fig. 8.7. Parameters distributions on the symmetry axes and along the antenna external surface for different energy layer thickness in comparison with energy-input-free flow.

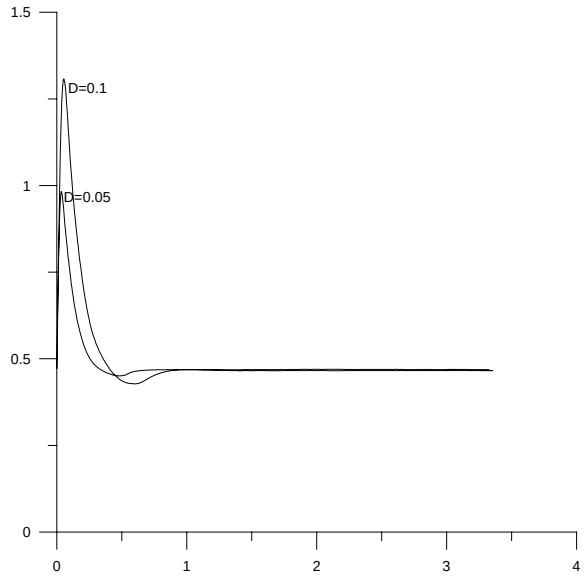

a) wave drag coefficient c_x

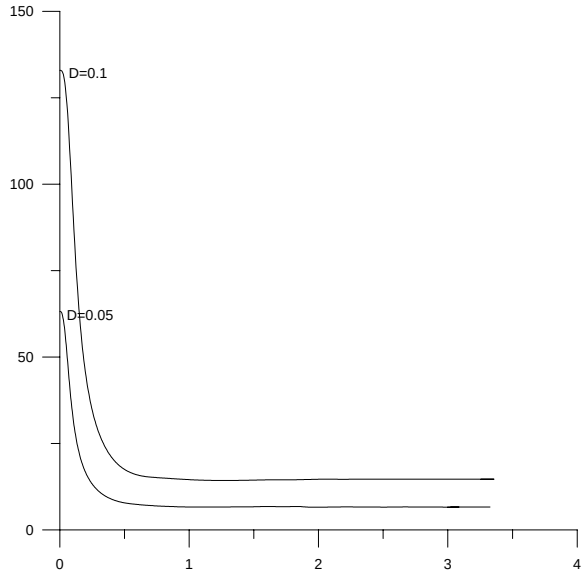

b) power input W

Fig. 8.8. Dynamics of integral parameters for microwave discharge activation for different energy layer thickness δ.

CHAPTER IX
NUMERICAL CALCULATION OF CHARACTERISTICS OF SUPERSONIC FLOW NEAR A FLAT PLATE WITH MICROWAVE DISCHARGE ON ITS SURFACE

9.1. Task formulation

The influence of heat deposition to gas in area of the turbulent supersonic boundary layer have been calculated in the presence of a rectangular thermal source in the turbulent boundary layer. Body geometry - flat plate; boundary conditions - heat-insulated surface. The system of averaged equations of turbulent motion of a perfect gas in the absence of external mass forces has been used:

$$\frac{\partial \rho u}{\partial x} + \frac{\partial \rho v_*}{\partial x} = 0,$$

$$\rho u \frac{\partial u}{\partial z} + \rho v_* \frac{\partial u}{\partial y} = \frac{\partial}{\partial y}\left(\mu_* \frac{\partial u}{\partial y} \right),$$

$$\rho u \frac{\partial I_o}{\partial z} + \rho v_* \frac{\partial I_o}{\partial y} = \frac{\partial}{\partial y}\left(\lambda_* \frac{\partial T}{\partial y} + \mu_* u \frac{\partial u}{\partial y} \right) + Q_v, \qquad (9.1)$$

$$\rho = \frac{pm}{RT},$$

$$\rho v_* = \rho v + \left\langle \rho' v' \right\rangle$$

$$I_o = I + \frac{u^2}{2}$$

$$\mu_* = \mu + \mu_t$$

$$\lambda_* = \left(\frac{\mu}{Pr} + \frac{\mu_t}{Pr_t} \right) c_p$$

where u and v - projections of a vector of speed to axes of orthogonal coordinates x (along a surface) and y (on a normal to it) accordingly; ρ - density; p - pressure; T - temperature; I - enthalpy; Q_v - the amount of heat brought in unit of time to the given point of gas from the outside; m - molecular weight of gas; R - universal gas constant; $<\rho' v'>$ - correlation of pulsations of density and normal component of flow speed; μ and μ_t – dynamic molecular and turbulent viscosity coefficients; c_p - specific thermal capacity of gas at constant pressure; Pr and

Pr_t - Prandtl number and its turbulent analogue (last three parameters are considered as constants).

In the calculations the coefficient of turbulent viscosity is determined on two-layer Cebeci and Smith model, describing heat exchange in a boundary layer at supersonic speeds of flow. Boundary conditions on a surface of streamlined body $y=0$ are $u=0$, $v=0$, $T=T_w$. Characteristics of a stream on external border of the boundary layer, marked by an index e, are considered known.

The problem is solved numerically by method of final differences. Preliminary the system (9.1) was transformed to a dimensionless kind. Thus the normal coordinate η is used.

$$\eta = \delta^{-1}(x)\int_0^y \rho dy \tag{9.2}$$

where $\delta(x)$ - normalizing function. The implicit stable difference scheme, providing approximation of the second order concerning steps Δx and $\Delta\eta$ of grid and stability of numerical calculation is used.

Calculations were carried out at flow Mach number $M_e=2$. Prandtl numbers $Pr=0,72$ and $Pr_t=0,9$, the relation of specific thermal capacities $\gamma=1,4$. For coefficient of molecular viscosity μ power temperature dependence $\mu \sim T^{\omega}$ with exponent $\omega=0,76$ is accepted.

The distributions of local coefficient of surface friction was calculated with help of formula

$$c_f = \frac{2\tau_w}{\rho_e u_e^2}, \tag{9.3}$$

where $\tau_w = \left(\mu \frac{\partial u}{\partial y} \right)\Big|_{y=0}$ is friction stress.

9.2. Heat deposition to gas in turbulent supersonic boundary layer

The influence of heat deposition to gas has been calculated in the presence of a rectangular thermal source in the turbulent supersonic boundary layer.

Three cases of external heat deposition to gas in area of the turbulent supersonic boundary layer near to a flat plate, streamlined by supersonic stream of air with flow Mach number $M=2$, were calculated at gas temperature in undisturbed flow $T_e=166,7\ K$. The geometry of an energy supply for these three cases is schematically submitted in *Fig. 9.1.* It was

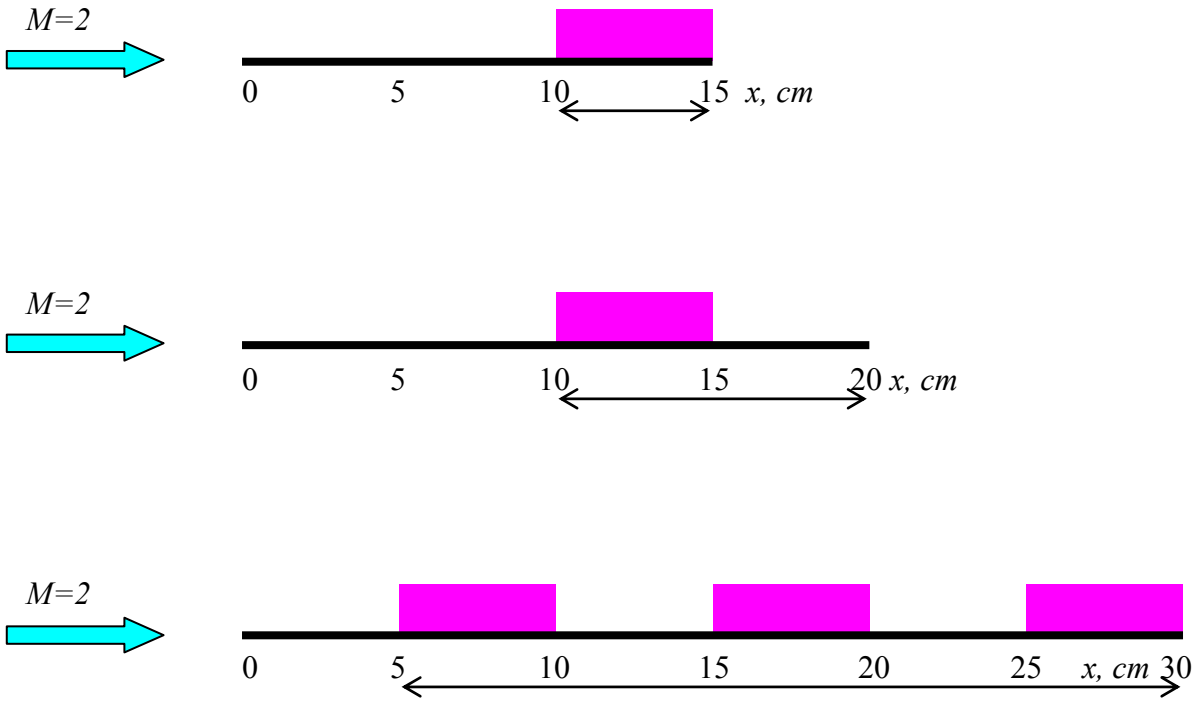

Fig. 9.1. Three cases of external heat deposition to gas in area of the turbulent supersonic boundary layer near to a flat plate, streamlined by supersonic stream of air.
The arrow ↔ allocates zones for which calculations were carried out.

considered, that thermal energy is deposited to a layer by thickness of $y=0,5\ mm$. Thus the heat area is completely located inside a boundary layer. $Y=0,0917\ mm.\ \delta=\delta^{*}\cdot Y$.

In the first case thermal energy was deposited to gas near plate of $L=15\ cm$ in length in rectangular area with coordinates ($x_1=10\ cm,\ x_2=15\ cm$). Calculation was made for area $10\ cm \le x \le 15\ cm$.

In the second case the heat was allocated near plate in length of $L=20\ cm$ in rectangular area with coordinates ($x_1=10\ cm,\ x_2=15\ cm$). Calculation was fulfilled for area $10\ cm \le x \le 20\ cm$.

In the third case thermal energy was deposited to plate of $L=30\ cm$ in length into three consecutive rectangular areas with coordinates of the first zone ($x_1=5\ cm,\ x_2=10\ cm$), the second zone ($x_3=15\ cm,\ x_4=20\ cm$) and the third zone ($x_5=25\ cm,\ x_6=30\ cm$). Calculation was made for area $5\ cm \le x \le 30\ cm$.

At first we shall consider results of calculations for the first case. The integral heat deposition to gas up-stream from section x and gas temperature longitudinal profile are given in *Fig. 9.2* and *Fig. 9.3*.

The influences of heat deposition to gas in turbulent supersonic boundary layer on radial profile of gas temperature and on displacement thickness of turbulent boundary layer are represented in *Fig. 9.4* and *Fig. 9.5*. The external heat deposition results in a pushing off of lines of a current from streamlined plate. Therefore the displacement thickness of turbulent boundary layer growths, when the heat deposition is increased. It has to lead to turbulent friction decrease.

Fig. 9.6 and *Fig. 9.7* testify this supposition. An input of energy in area of a turbulent boundary layer results in noticeable reduction of a local coefficient of turbulent friction at the expense of decreasing of a transverse gradient of longitudinal flow velocity and increase of a displacement thickness. As follows from *Fig. 9.6* the decrease in the local skin-friction coefficient is quite significant for the considered conditions.

The same results were received for the second case when the heat deposition to the gas takes place only on part of plate. Portion of gas heating has *5 cm* in length and calculations was also executed for a segment of a boundary layer of length *5 cm* downstream from a heated portion. It was supposed, that as well as in the first case energy was put in a surface layer by thickness $y=0,5\ mm$.

Integral heat supplied to gas up-stream from section x in the second case of heat deposition is shown in *Fig. 9.8*. The integrated energy remains a constant after section $x_2=15\ cm$ and does not depend on coordinate x, as energy is put into gas only in area from $x_1=10\ cm$ up to $x_2=15\ cm$.

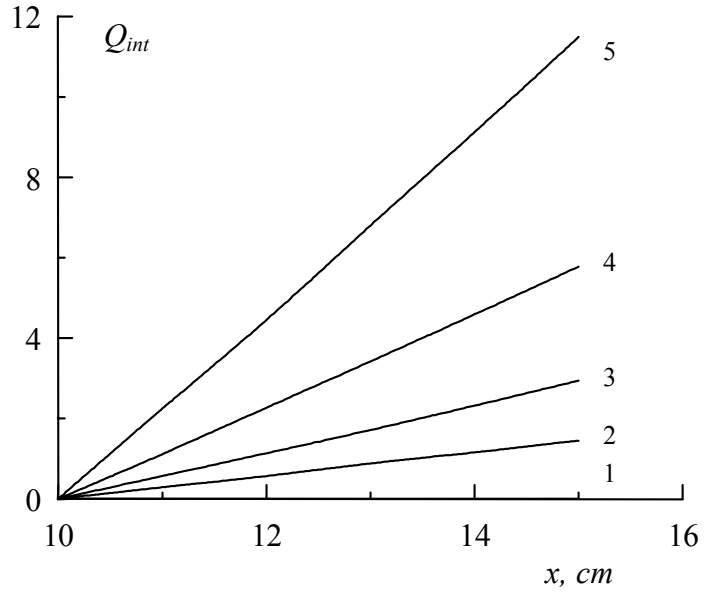

Fig. 9.2. Integral heat deposition to gas up-stream from section x in the first case.
M=2; x_1=10 cm; x_2=15 cm; y_2=0,5 mm; *A*: 1–0; 2–1; 3–2; 4–4; 5–8.

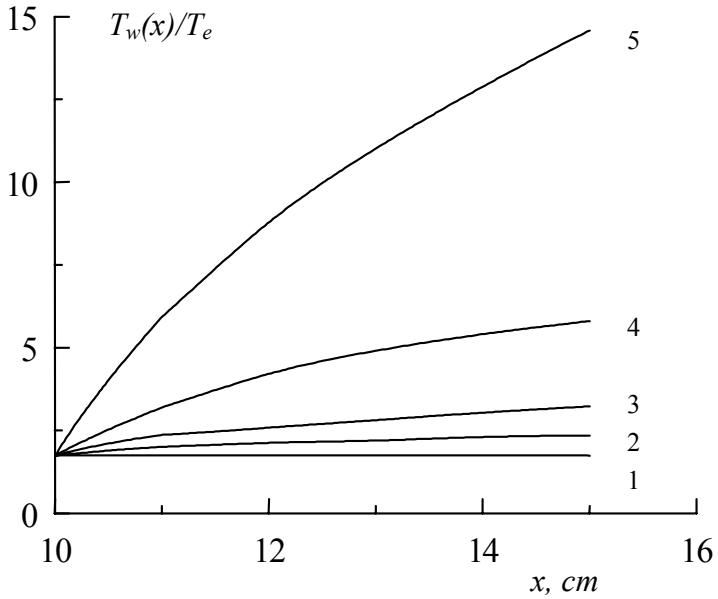

Fig. 9.3. Gas temperature longitudinal profile in the first case of heat deposition.
M=2; T_e=166,7 K; x_1=10 cm; x_2=15 cm; y_2=0,5 mm; *A*: 1–0; 2–1; 3–2; 4–4; 5–8.

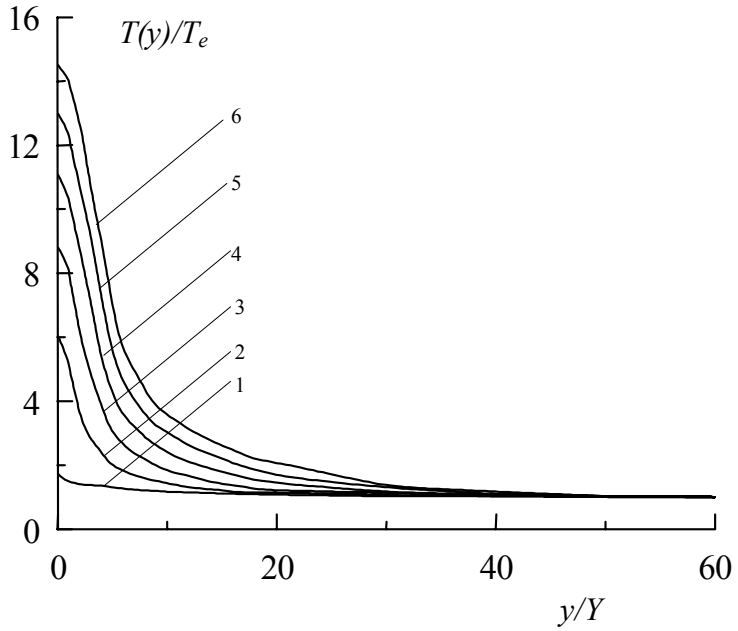

Fig. 9.4. Radial profile of gas temperature in the first case of heat deposition.
M=2; x_1=10 cm; x_2=15 cm; y_2=0,5 mm; Y=0.0917 mm; *A*: 1–0; 2–1; 3–2; 4–4; 5–8

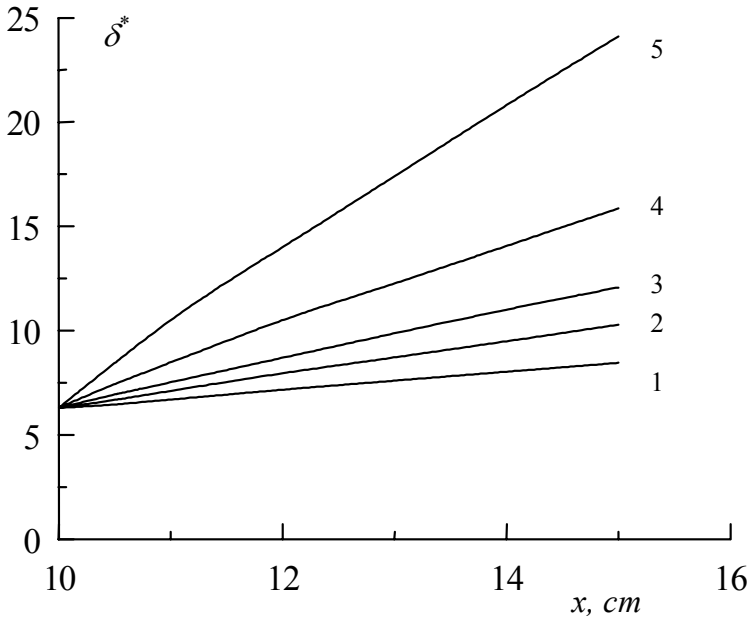

Fig. 9.5. Displacement thickness of boundary layer in the first case of heat deposition.
M=2; x_1=10 cm; x_2=15 cm; y_2=0,5 mm; Y=0.0917 mm; *A*: 1–0; 2–1; 3–2; 4–4; 5–8.

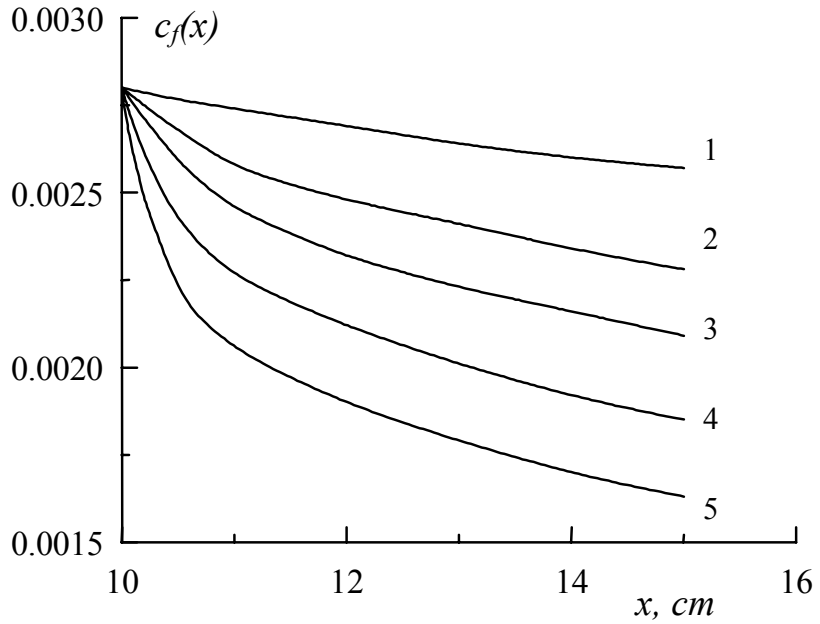

Fig. 9.6. Local friction coefficient in the first case of heat deposition.
M=2; x_1=10 cm; x_2=15 cm; y_2=0,5 mm; *A*: 1-0; 2-1; 3-2; 4-4; 5-8.

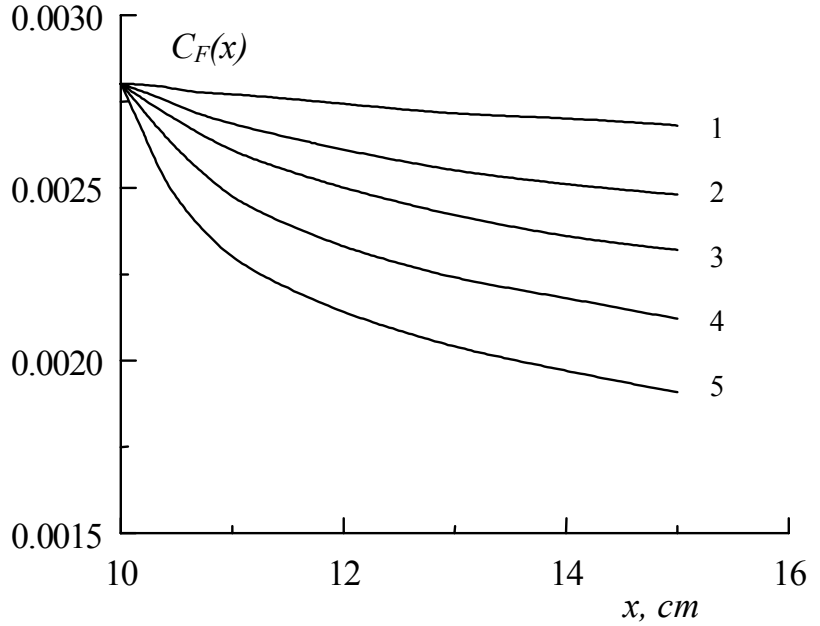

Fig. 9.7. Full friction coefficient in the first case of heat deposition.
M=2; x_1=10 cm; x_2=15 cm; y_2=0,5 mm; *A*: 1-0; 2-1; 3-2; 4-4; 5-8.

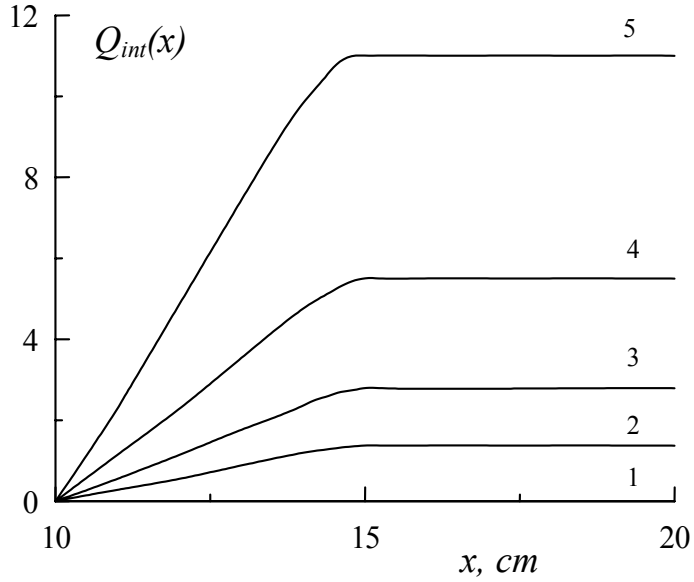

Fig. 9.8. Integral heat supplied to gas up-stream from section x in the second case of heat deposition. *M=2, x_1=10 cm, x_2=15 cm, x_3=20 cm, y_2=0,5 mm*, *A*: 1 – 0; 2 – 1; 3 – 2; 4 – 4; 5 –8.

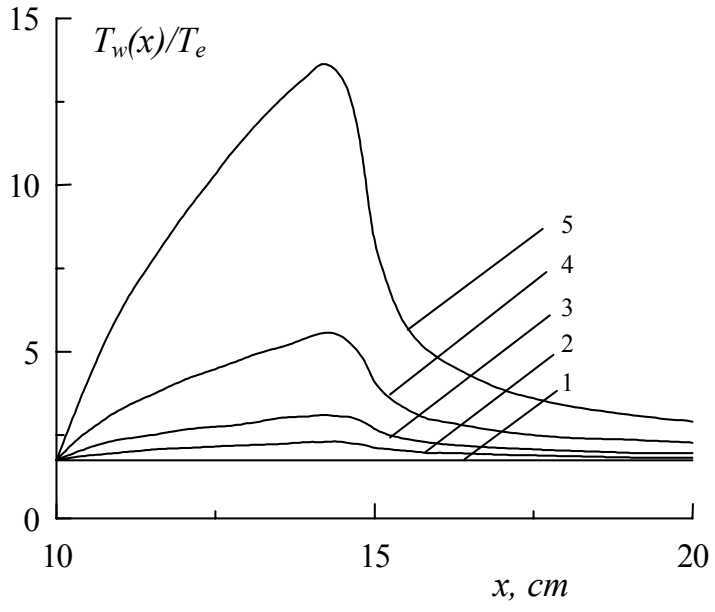

Fig. 9.9. Gas temperature longitudinal profile in the second case of heat deposition. *M=2; T_e=166,7 K; x_1=10 cm; x_2=15 cm; x_3=20 cm; y_2=0,5 mm*; *A*: 1–0; 2–1; 3–2; 4–4; 5–8.

Gas temperature longitudinal profile in the second case of heat deposition is submitted in *Fig. 9.9* at different values of energy deposition. It is visible, that the gas temperature monotonously rises in space downwards on a stream. Gas is heated up to the greater temperature by the end of area of the energy contribution with increase in input energy. Behind area of the contribution of energy the temperature of gas monotonously decreases downstream.

Boundary layer displacement thickness in the second case of heat deposition is pictured in *Fig. 9.10*. Dependences of local friction surface coefficient and full friction coefficient in the second case of heat deposition are given in *Fig. 9.11* and *Fig. 9.12*. It is visible, that reduction of coefficient of turbulent friction is spread to considerable distance downstream from a heated portion. Thus downstream from a thermal source the local friction coefficient and displacement thickness of a boundary layer are slowly reconstructed up to the values corresponding to undisturbed flow.

Results of calculation of displacement thickness and local friction coefficient for the third case when the same thermal energy was input or to one zone, or was distributed on three zones are presented in *Fig. 9.13* and *Fig. 9.14*. One can see that under considered conditions it is better to put energy into the local area in comparison with homogeneous distribution of the same energy on whole surface of a plate. Thus the significant friction reduction on whole streamlined surface is achieved at local gas heating due to effect of long-term memory of a turbulent boundary layer.

However if we shall consider the large surfaces and we shall change the distance between areas in which energy is input, number of such areas, the value of energy put in each such areas then it is possible to receive significant reduction in full surface friction in comparison with the local energy deposition because of accumulation of effect due to long-term memory of a turbulent boundary layer.

For check-up of this statement it is necessary to execute additional calculations, and also to carry out additional experiments.

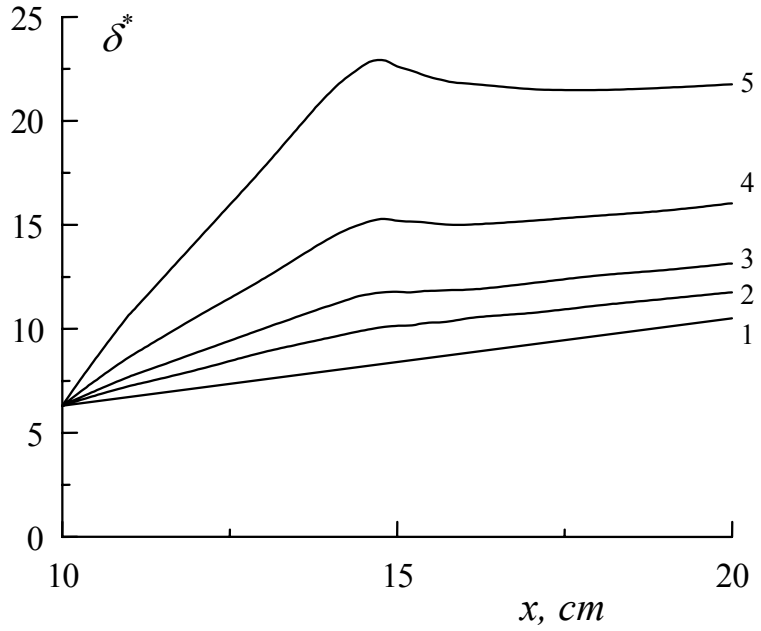

Fig. 9.10. Boundary layer displacement thickness in the second case of heat deposition. *M=2; T_e=166,7 K; x_1=10 cm; x_2=15 cm; x_3=20 cm; y_2=0,5 mm; Y=0.0917 mm*; *A*: 1–0; 2–1; 3–2; 4–4; 5–8.

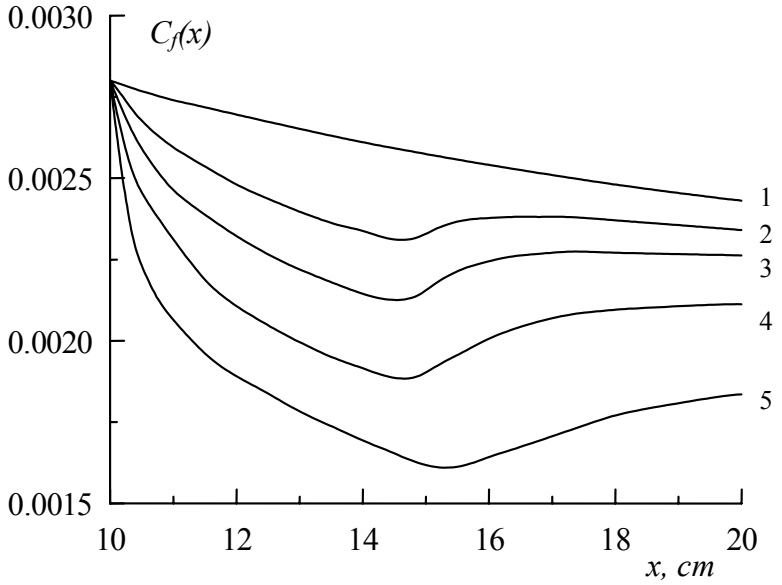

Fig. 9.11. Local friction surface coefficient in the second case of heat deposition.
M=2; x_1=10 cm; x_2=15 cm; x_3=20 cm; y_2=0,5 mm; *A*: 1 – 0; 2 – 1; 3 – 2; 4 – 4; 5 – 8.

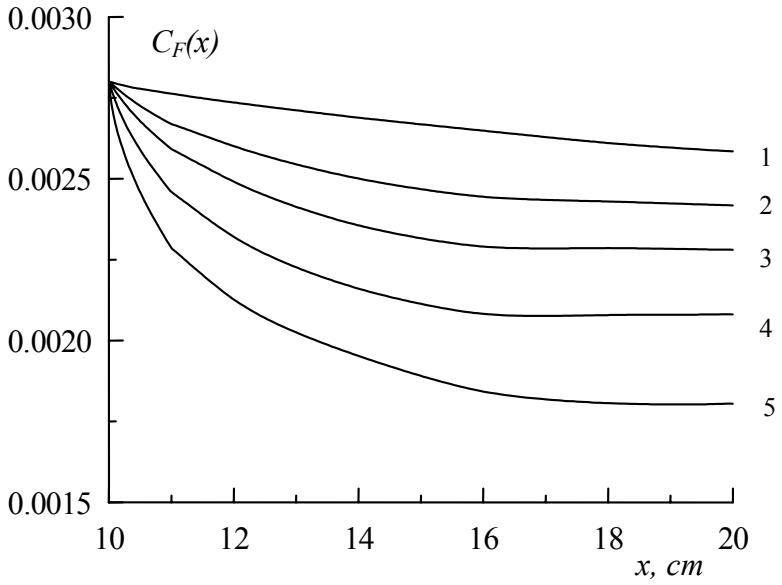

Fig. 9.12. Full friction coefficient in the second case of heat deposition.
M=2, x_1=10 cm, x_2=15 cm, x_3=20 cm, y_2=0,5 mm, *A*: 1 – 0; 2 – 1; 3 – 2; 4 – 4; 5 – 8

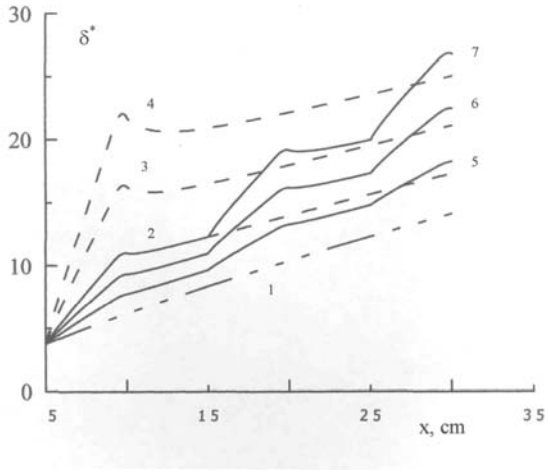

Fig. 9.13. Displacement thickness of boundary layer. Dash-dotted curve (1) - without energy supply. Dashed curves (2, 3 and 4) - at energy supply in rectangular area with coordinates (x_1=*5 cm,* x_2=*10 cm*); *A*: 2 - 3; 3 - 6; 4 - 9. Solid curves (5, 6 and 7) - at supply of the same energy in three consecutive rectangular areas with coordinates of the first zone (x_1=*5 cm,* x_2=*10 cm*), the second zone (x_3=*15 cm,* x_4=*20 cm*) and the third zone (x_5=*25 cm,* x_6=*30 cm*); *A*: 5 - 1; 6 - 2; 7 - 3.

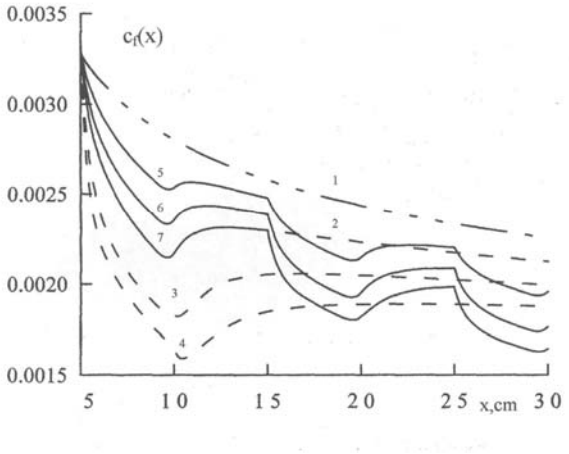

Fig. 9.14. Local friction surface coefficient. Dash-dotted curve (1) - without energy supply. Dashed curves (2, 3 and 4) - at energy supply in rectangular area with coordinates (x_1=*5 cm,* x_2=*10 cm*); *A*: 2 - 3; 3 - 6; 4 - 9. Solid curves (5, 6 and 7) - at supply of the same energy in three consecutive rectangular areas with coordinates of the first zone (x_1=*5 cm,* x_2=*10 cm*), the second zone (x_3=*15 cm,* x_4=*20 cm*) and the third zone (x_5=*25 cm,* x_6=*30 cm*); *A*: 5 - 1; 6 - 2; 7 - 3.

CHAPTER X
NUMERICAL MODELING OF SUPERSONIC FLOWS WITH ENERGY SUPPLY BY ELECTRICAL DISCHARGE. GAS-PHASE MODEL

10.1. Task formulation

Numerical model for studies of unsteady near wall discharge in supersonic flow have been developed too. The model was based on the Favre averaged Navier-Stokes equations for thermally equilibrium, chemically frozen air. For the description of turbulent transfer the algebraic Baldwin-Lomax model and two-parameter differential k-omega model were used. The pulse discharge influence on the gas flow was simulated by non-stationary near wall heat source with specified space and time distribution of intensity.

Basic assumptions

1. The gas is considered as an ideal one-temperature reacting mixture of perfect neutral gases;
2. Navier-Stokes approximation is employed to calculate molecular viscous fluxes;
3. Turbulent mean flow is described by Favre averaged [1] pressure *p,* velocity vector $\vec{u}$, mole fractions of species $X_i,\ i=1,\ldots,\nu,$ and temperature *T*;
4. Correlations of temperature and chemical composition fluctuations are neglected;
5. The Boussinesq approximation for the turbulent fluxes and Wilcox two-equations $k-\omega$ model [2] for calculation of turbulent transport coefficients are used;
6. Effect of electrical discharge on gas flow is modeled by local heat supply.

State equation

The gas state equation is given by

$$p = \rho R_u T / M ,$$

here ρ is density, R_u is a universal gas constant, and M is an average molecular weight of the mixture that is expressed through molecular weights of species M_i as

$$M = \sum_{i=1}^{\nu} M_i X_i . \qquad (10.1)$$

Thermodynamic properties

Molar enthalpy h_i and molar heat c_{pi} of species *i* are determined through partition function $Q_i(T)$ per unit volume:

$$h_i(T) = h_i^0 + R_u T^2 \frac{\partial \ln(Q_i V_m)}{\partial T}, \quad c_{pi}(T) = \frac{\partial h_i}{\partial T}, \tag{10.2}$$

where h_i^0 is a formation heat of species *i* and $V_m = R_u T / p$ is a mole volume.

In considered gas-phase model an evaluation of thermodynamic functions is based on the following approximation of dependence c_{pi} from temperature

$$c_{pi}(T) = \frac{a_{-2,i}}{T^2} + \sum_{k=0}^{5} a_{k,i} T^k \quad \text{for } T_{1,i} \le T \le T_{2,i}, \tag{10.3}$$

$$c_{pi}(T) = \mathrm{c}_{pi}(T_{1,i}) \quad \text{for } T_{1,i} \ge T, \tag{10.4}$$

$$c_{pi}(T) = c_{pi}(T_{2,i}) \quad \text{for } T_{2,i} \le T, \tag{10.5}$$

where coefficients $a_{k,i}$ are determined by an interpolation known tabular data in a range of temperatures $T_{1,i} \le T \le T_{2,i}$. The approximating formulas for $h_i(T)$ and $Q_i(T)$ are determined with a successive integration expressions for $c_{p,i}(T)$ on temperature with use as constants integration of tabular values of h_i and Q_i at some fixed temperature $T = T^*$.

Chemical reaction in gas phase

A molar rate of gas phase chemical reaction *j*

$$\sum_i \nu_{ji} [A_j] \Leftrightarrow \sum_i \nu'_{ji} [A_j], \tag{10.6}$$

where ν_{ji}, ν'_{ji} are stochiometric coefficients and $[A_i]$ is symbol of chemical species *i* is expressed as

$$\bar{\omega}_j = k_j^f \prod_{i=1}^{\nu} (\rho \gamma_i)^{\nu_{ji}} - k_j^r \prod_{i=1}^{\nu} (\rho \gamma_i)^{\nu'_{ji}}, \tag{10.7}$$

here k_j^f and k_j^r are forward and reverse rate constants of this reaction, γ_i is mass-mole fraction of *i*-th species defined as $\gamma_i = X_i / M$.

A molar production rate of species *i* per unit volume due to all chemical reactions is

$$\dot{\omega}_i = \sum_j (\nu'_{ji} - \nu_{ji}) \bar{\omega}_j. \tag{10.8}$$

Reverse rate constants of reactions are approximated by the generalized Arrhenius formula

$$k_j^r = a_j T_j^{b_j} \exp(-E_j / T_j). \tag{10.9}$$

The forward rate constants k_j^f are defined from detailed equilibrium condition

$$k_j^f / k_j^r = \prod_{i=1}^{\nu} (Q_i \exp(-h_i^0 / R_u T))^{(\nu'_{ji} - \nu_{ji})}. \tag{10.10}$$

Molecular transport properties

The molar diffusion fluxes $\vec{K}_{M,i}$ are determined from the Stefan-Maxwell relations [3] that are given by

$$\begin{gathered}\sum_{j=1}^{\nu} \bar{M} d_{ij} (\gamma_i \vec{K}_{M,j} - \gamma_j \vec{K}_{M,i}) = \frac{\partial \gamma_i M}{\partial \vec{r}}, \\ i = 1, 2, ..., \nu - 1 \\ \sum_{j=1}^{\nu} \vec{K}_{M,j} M_j = 0,\end{gathered} \tag{10.11}$$

where $d_{ij} = M / \rho \mathsf{D}_{ij}$, D_{ij} is a binary diffusion coefficient.

Molecular stress tensor $\hat{\tau}_M = (\vec{\tau}_{M,x}, \vec{\tau}_{M,y})^{\dagger}$ (momentum fluxes tensor with reversed sign) is given by

$$\hat{\tau}_M = 2\mu_M \hat{\varepsilon}, \quad \hat{\varepsilon} = \frac{1}{2}\left[\left(\frac{\partial \vec{u}}{\partial \vec{r}}\right) + \left(\frac{\partial \vec{u}}{\partial \vec{r}}\right)^{\dagger} - \frac{2}{3}\left(\frac{\partial}{\partial \vec{r}} \cdot \vec{u}\right)\hat{I}\right], \tag{10.12}$$

where $\hat{\varepsilon} = (\vec{\varepsilon}_x, \vec{\varepsilon}_y)^{\dagger}$ is tensor of deformation rates, $\hat{I}$ is unit tensor, μ_M is molecular viscosity.

The molecular heat flux $\vec{q}_M$ is given by following expression

$$\vec{q}_M = -\lambda_M \frac{\partial T}{\partial \vec{r}} + \sum_{i=1}^{\nu} \vec{K}_{M,i} h_i, \tag{10.13}$$

where λ_M is molecular thermal conductivity. For calculation of molecular viscosity and thermal conductivity the approximate formulas Wilke-Wassiljewa type [4] are used

$$\mu_M = \sum_{i=1}^{\nu} M_i \gamma_i Sc_i D_i, \qquad \lambda_M = \sum_{i=1}^{\nu} \gamma_i \left[c_{pi} + 2.5R_u(1.5Sc_i - 1)\right] D_i, \tag{10.14}$$

here $Sc_i(T) = \mu_i / \rho_i \mathsf{D}_{ii}$ is Schmidt number of species *i* calculated on molecular viscosity μ_i,

density ρ_i and a self-diffusion coefficient D_{ii} of this species in a pure form, D_i is coefficient defined by expression

$$D_i = \frac{1}{\sum_{j=1}^{\nu} \gamma_j d_{ij}}. \qquad (10.15)$$

Functions $d_{ij}(T)$ and $Sc_i(T)$ are determined by formulas

$$d_{ij}(T) = 3.12 \cdot 10^5 \frac{\bar{\Omega}_{ij}^{(1.1)}(T)\sqrt{2M_iM_j}}{\sqrt{T(M_i+M_j)}}, \qquad Sc_i(T) = \frac{5\bar{\Omega}_{ii}^{(1.1)}(T)}{6\bar{\Omega}_{ii}^{(2.2)}(T)}, \qquad (10.16)$$

$[d_{ij}] = \sec \cdot m/kmole, \quad [\Omega] = \text{Å}^2$, where $\bar{\Omega}_{ii}^{(1.1)}(T)$ and $\bar{\Omega}_{ii}^{(2.2)}(T)$ are collision integrals of diffusion and viscous types accordingly, $[d_{ij}]$ is sec/m·kmole, $[\Omega]$ is Å^2. The values of collision integrals are calculated through the potential of particles interaction at collision. In the present statement the simple interpolation dependence for calculation of collision integrals $\bar{\Omega}_{ii}^{(1.1)}(T)$ is used

$$\bar{\Omega}_{ii}^{(1.1)}(T) = (a_{ij} + b_{ij} \ln T)^2. \qquad (10.17)$$

Coefficients a_{ij} and b_{ij} are calculated on specified values of the collision integrals for $T_1 = 300K$ and $T_2 = 4000K$. Quantities of $\bar{\Omega}_{ii}^{(1.1)}(T_k)$ are determined on the Lennard-Jones potential. Values of potential parameters for identical particles pairs are taken from literature. Parameters of interaction potentials for the different particles are determined on combinatorial rules [3]. At an evaluation of the Schmidt number $Sc_i(T)$ for all components it is assumed to be $\bar{\Omega}_{ii}^{(2.2)}(T) = 1.1\bar{\Omega}_{ii}^{(1.1)}(T)$.

Turbulent transport model

Turbulent (Reynolds) stress tensor $\hat{\tau}_T$, turbulent heat flux $\vec{q}_T$, and turbulent diffusion fluxes $\vec{K}_{T,i}$ are expressed as

$$\hat{\tau}_T = 2\mu_T\hat{\varepsilon}, \qquad \vec{q}_T = -\lambda_T \frac{\partial T}{\partial \vec{r}} + \sum_{i=1}^{\nu} \vec{K}_{T,i} h_i, \ \vec{K}_{T,i} = -\rho D_T \frac{\partial \gamma_i}{\partial \vec{r}}. \qquad (10.18)$$

Eddy viscosity μ_T, turbulent thermal conductivity λ_T and turbulent diffusion coefficient D_T are determined through turbulent mixing energy k and specific dissipation rate ω

$$\mu_T = \rho\frac{k}{\omega},\ \ \lambda_T = \frac{\mu_T c_p}{\mathrm{Pr}_T},\ \ \rho D_T = \frac{\mu_T}{Sc_T}. \tag{10.19}$$

The values of turbulent energy k and specific dissipation rate ω are defined from two differential equations:

$$\frac{\partial \rho k}{\partial t} + \frac{\partial}{\partial \vec{r}}\cdot\left(\vec{u}k - (\mu_M + \sigma_T^*\mu_T)\frac{\partial k}{\partial \vec{r}}\right) = b_k, \tag{10.20}$$

$$\frac{\partial \rho \omega}{\partial t} + \frac{\partial}{\partial \vec{r}}\cdot\left(\vec{u}\omega - (\mu_M + \sigma_T\mu_T)\frac{\partial \omega}{\partial \vec{r}}\right) = b_\omega, \tag{10.21}$$

where

$$b_k = 2\mu_T\left(\vec{\varepsilon}_i\cdot\frac{\partial u_i}{\partial \vec{r}}\right) - \beta_T^*\rho\omega k, \quad b_\omega = 2\gamma_T\rho\left(\vec{\varepsilon}_i\cdot\frac{\partial u_i}{\partial \vec{r}}\right) - \beta_T\rho\omega^2, \tag{10.22}$$

$$\beta_T^* = 0.09, \quad \gamma_T = 0.56, \quad \beta_T = 0.075, \quad \sigma_T = 0.5, \quad \sigma_T^* = 0.5. \tag{10.23}$$

It is assumed that turbulent Prandtl and Schmidt numbers are $\mathrm{Pr}_T = 1$, $Sc_T = 1$.

10.2. Governing equations and numerical method

Governing equations

The integral form of two-dimensional governing equations in the Cartesian coordinates (*x,y*) for above gas-phase model is written as

$$\frac{d}{dt}\int_S \mathbf{U}dS + \int_{\delta S}\vec{n}\cdot\vec{\mathbf{F}}dl = \int_S \mathbf{\Omega}dS\ , \tag{10.24}$$

where S is a fixed control domain in a plane (x, y), δS is a boundary of domain , $\vec{n} = (n_x, n_y)$ is an unit outward normal to δS, $\mathbf{U}$ is a set of conserved variables per unit volume, $\vec{\mathbf{F}} = \vec{\mathbf{F}}^{inv} + \vec{\mathbf{F}}^{vis}$ represents a sum of the inviscid and viscous fluxes of $\mathbf{U}$ through the domain boundary and $\mathbf{\Omega}$ consists of the source terms. For considered gas-phase model these vectors are given by

$$\mathbf{U} = \{\rho\gamma_1, \ldots, \rho\gamma_\nu, \rho u, \rho v, \rho e_0, \rho k, \rho\omega\}^\dagger\ ; \tag{10.25}$$

$$\vec{\mathbf{F}} = \begin{Bmatrix} \rho\vec{u}\gamma_1 \\ \vdots \\ \rho\vec{u}\gamma_\nu \\ \rho\vec{u}u + p\vec{n}n_x \\ \rho\vec{u}v + p\vec{n}n_y \\ \rho\vec{u}h_0 \\ \rho\vec{u}k \\ \rho\vec{u}\omega \end{Bmatrix} + \begin{Bmatrix} \vec{K}_1 \\ \vdots \\ \vec{K}_\nu \\ -\vec{\tau}_x \\ -\vec{\tau}_y \\ \vec{q}_h - u\vec{\tau}_x - v\vec{\tau}_y \\ \vec{q}_k \\ \vec{q}_\omega \end{Bmatrix}; \tag{10.26}$$

$$\mathbf{\Omega} = \{\dot{\omega}_1, \ldots, \dot{\omega}_\nu, 0, 0, b_h, b_k, b_\omega\}^\dagger \,, \tag{10.27}$$

here u, v are the components of velocity vector $\vec{u}$, $e_0 = e + 0.5(\vec{u} \cdot \vec{u})$ is a total energy per unit mass, $h_0 = e_0 + p/\rho$ is a total enthalpy, b_h is heat source power,

$$\hat{\tau} = \hat{\tau}_M + \hat{\tau}_T = (\mu_M + \mu_T)\hat{\varepsilon} \,, \tag{10.28}$$

$$\vec{q}_h = \vec{q}_M + \vec{q}_T \,, \qquad \vec{K}_i = \vec{K}_{M,i} + \vec{K}_{T,i} \,, \tag{10.29}$$

$$\vec{q}_k = -(\mu_M + \sigma_T^* \mu_T)\frac{\partial k}{\partial \vec{r}} \,, \qquad \vec{q}_\omega = -(\mu_M + \sigma_T^* \mu_T)\frac{\partial \omega}{\partial \vec{r}} \,. \tag{10.30}$$

Numerical method

The governing equations are solved on the structured mesh through a finite volume approach. At this approach the finite difference equations system consists of numerical analogs of the conservation equations for the quadrilateral cells covering the computation domain and the difference approximation of the boundary conditions. This method yields an approximate solution $\mathbf{Z} = \{p, u, v, \gamma_1, \ldots, \gamma_\nu, T, k, \omega\}$ in a center of each cell and in a center of each cell side lying on the wall. The cells are built by intersection of the two discrete curve sets. The inviscid fluxes $\mathbf{F}_G^{inv}$ through cell sides are calculated from result of the exact Riemann problem solution $\mathbf{Z}_G = \Re(\mathbf{Z}_G^L, \mathbf{Z}_G^R)$ where $\Re$ is the Riemann problem solver. The left and right interfacial values $\mathbf{Z}_G^L$ and $\mathbf{Z}_G^R$ are defined by the limited one-dimensional extrapolation of $\mathbf{Z}$ from the cell-centers to the cell sides. The numerical viscous fluxes $\mathbf{F}_G^{vis}$ through cell sides are evaluated using the central and one-sided difference formulas of the second order accuracy. For time-marching integrating of governing equations the implicit Runge-Kutta scheme of second order accuracy is used. On every time step the flowfield parameters are computed due Gauss-Seidel line relaxation numerical technique.

10.3. Numerical analysis of near wall pulsed gas heating effect on skin-friction

First, the numerical modeling of process of streamlining of cylindrically blunted flat plate of finite thickness with length of *15 cm*, width of *2 cm*, and thickness of *0,2 mm* by supersonic airflow was carried out at various values of energy introduced into boundary layer.

Second, the calculations were performed for flow over blunted plate length of *50 cm* and thickness of *0,2 mm* for free stream Mach number M_∞=*2*, total pressure p_o=*1 atm,* and total

temperature T_o=300 K.

Chemically frozen gas phase model of heated air including two species (O_2, N_2) was used for calculations. Gas-wall thermal interaction was described by adiabatic model. Wall turbulence parameters were given by

$$k_w = 0, \quad \omega_w = \frac{6\mu_{M,w}}{\rho_w \beta_T \Delta_w n}, \tag{10.31}$$

where $2\Delta_w n$ is n-size of first near wall cell. Values of k and ω in free stream are specified by two conditions

$$k_\infty / 0.5u_\infty^2 = 10^{-7}, \quad (\mu_T / \mu_M)_\infty = 0.03. \tag{10.32}$$

Calculations have been carried out on mesh 400x200 adapted to flow peculiarities. The grid cells were condensed near plate surface, so that in a laminar sublayer region not less than 10 grid points were placed.

Fig. 10.1 shows the distributions along plate Reynolds number Re_θ calculated through momentum thickness θ for conditions at outer edge of the laminar boundary layer (for $P_d = 0$). The value $Re_\theta = 300$ often is used as criterion of laminar-to-turbulent transitions beginning. The *Fig. 10.1* indicates that transition (without heat supply) begins at $x \approx 2.6$ *cm* if this criterion to use. *Fig. 10.2* shows distributions of local skin-friction coefficient along plate for laminar and turbulent flow models without heat deposition. It is seen that used $k-\omega$ turbulence model also predicts laminar-to-turbulent transitions that location depends from specified free stream and wall values of turbulence parameters. For considered numerical boundary conditions for k and ω transition occurs some upstream in interval *1,0 cm*≤x≤*2,0 cm*.

In *Fig. 10.3* and *Fig. 10.4* the total power equals *1000 W* and in *Fig. 10.5* and *Fig. 10.6* the total power equals *2000 W*. One can see that effect of heat deposition leads to significant decreasing of the local turbulent friction coefficient. Moreover the effect exists during long time after the heat deposition to gas is switched off. During some hundreds microseconds the flow parameters slowly return in initial state. It indicates prospects of pulsed-periodical discharge usage.

Then three cases of the heat deposition have been considered (look *Fig. 10.7*): 1) only on section *10 cm*≤x≤*20 cm*; 2) on two sections *10 cm*≤x≤*20 cm* and *30 cm*≤x≤*40 cm*; 3) from x=*10 cm* to end of plate. Distance x is measured from plate heading. In all considered cases the heat was supplied during a time period of *100 μs* in the initial steady-state flow over plate. For this period the total heat supply was steady and it was uniformly distributed in the near wall

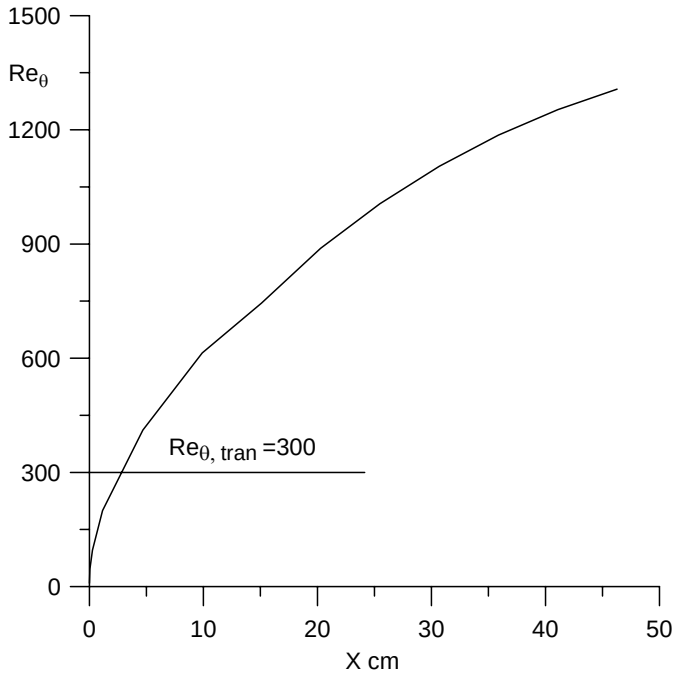

Fig. 10.1. Reynolds number calculated through momentum thickness and free stream parameters.

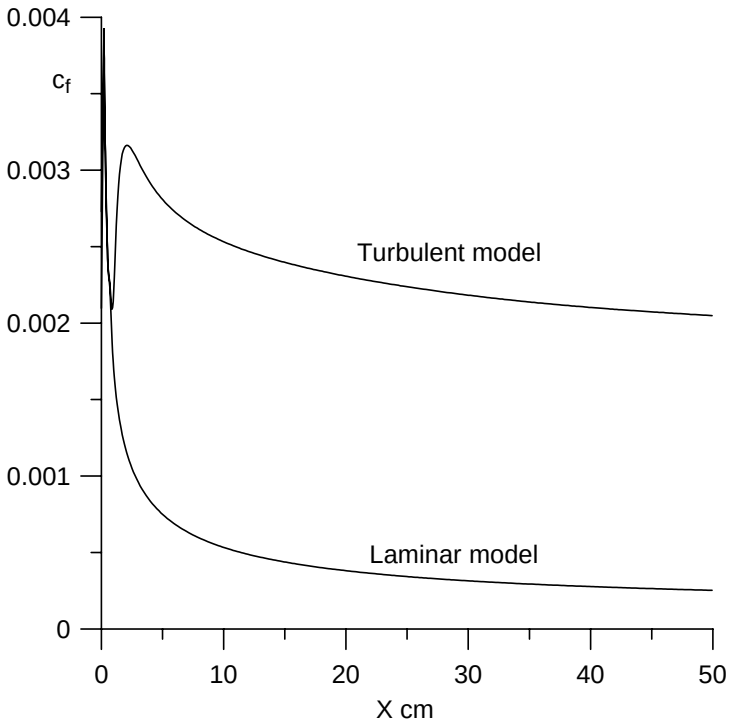

Fig. 10.2. Local skin-friction coefficients for laminar and turbulent flow models.

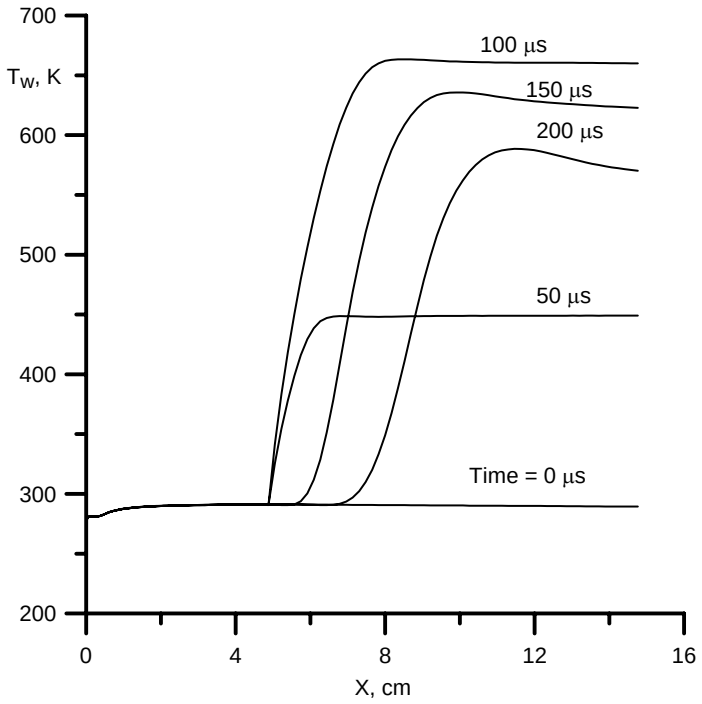

Fig. 10.3. The near wall heat deposition effect on the wall temperature distribution. *M=2; T_e=166,7 K; L=15 cm; x_h=5 cm; y_h=1 mm; z=2 cm; τ=100 μs; P_{total}=1000 W.*

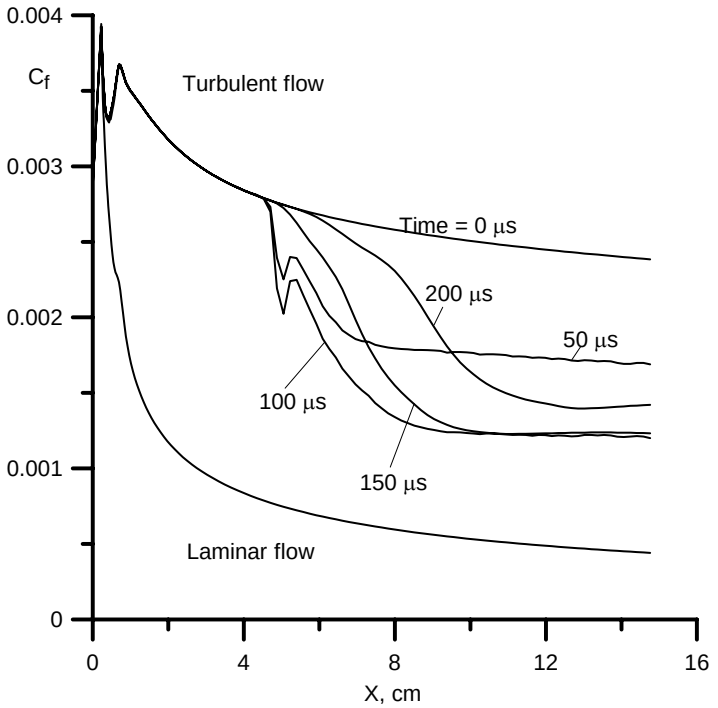

Fig. 10.4. The near wall heat deposition effect on the skin-friction coefficient distribution along plate.. *M=2; T_e=166,7 K; L=15 cm; x_h=5 cm; y_h=1 mm; z=2 cm; τ=100 μs; P_{total}=1000 W.*

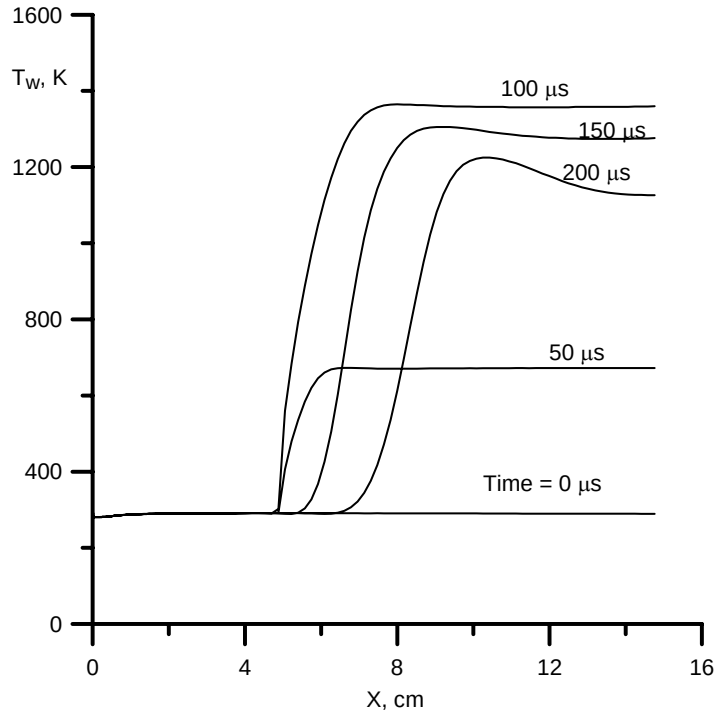

Fig. 10.5. The near wall heat deposition effect on the wall temperature distribution. *M=2; T_e=166,7 K; L=15 cm; x_h=5 cm; y_h=1 mm; z=2 cm; τ=100 μs; P_{total}=2000 W.*

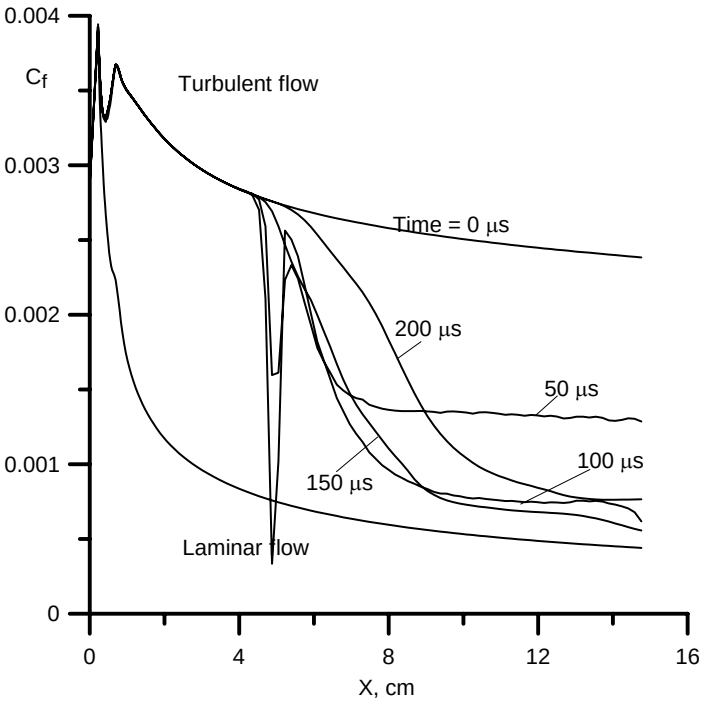

Fig. 10.6. The near wall heat deposition effect on the skin-friction coefficient distribution along plate. *M=2; T_e=166,7 K; L=15 cm; x_h=5 cm; y_h=1 mm; z=2 cm; τ=100 μs; P_{total}=1000 W.*

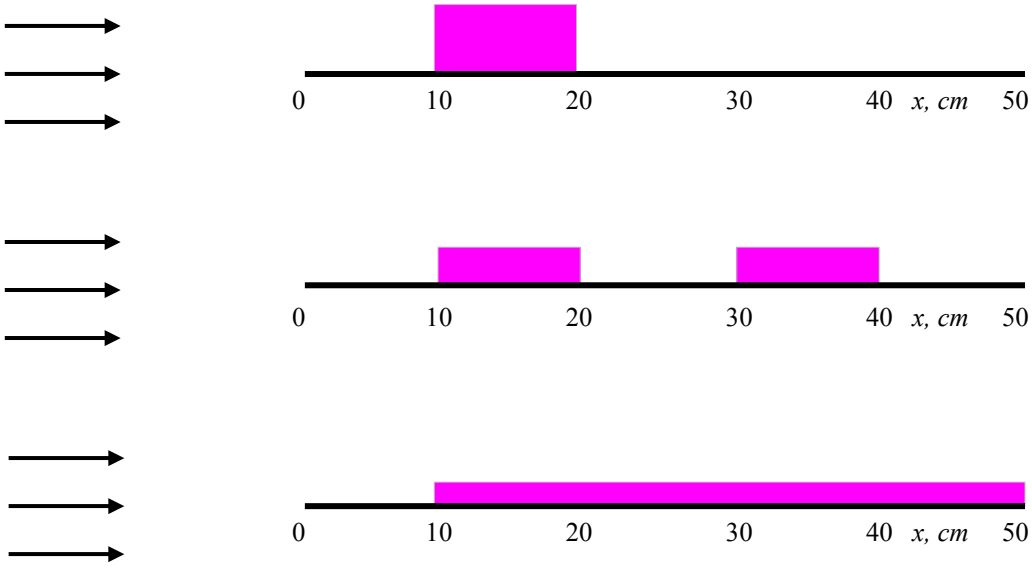

Fig. 10.7. Three cases of the heat deposition space distribution along plate surface. Case 1 (*10 cm<x<20 cm*); Case 2 (*10 cm<x<20 cm; 30 cm<x<40 cm*); Case 3 (*10 cm<x<50 cm*). *M=2, T_e=166,7 K, L=50 cm, y_h=1 mm, P_{total}=1000 W/cm, τ=100 μs.*

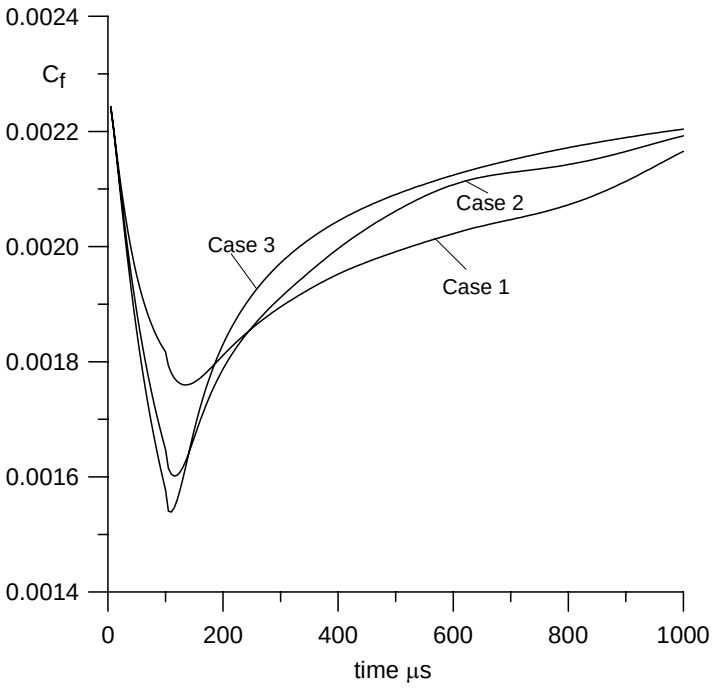

Fig. 10.8. Time dependence of the plate skin-friction coefficients for three heat deposition cases.

0,1 cm thick layer. Total heat supply power per unit plate width P_d was *1000 W/cm*.

In *Fig. 10.8* the time distributions of total skin-friction coefficient C_f for plate section *10 cm≤x≤50 cm* predicted in the three considered heat deposition cases are compared. The value of C_f is defined by expression

$$C_f = \int_{x_b}^{x_e} \tau_w dx / 0.5 \rho_\infty V_\infty^2 (x_e - x_b), \tag{10.33}$$

where τ_w is the skin-friction, ρ_∞ and V_∞ are the free stream density and velocity accordingly, $x_b = 10\,\text{cm}$, $x_e = 50\,\text{cm}$. *Fig. 10.8* indicates that the heat supply leads to decreasing of skin-friction. The time peak of a drag reduction is achieved at once after ending of heat deposition period. The most drug reduction about *31%* is for the third heat deposition case. The least one about *21%* is for the first gas heating case. After heat deposition ending the skin friction returns to initial value during some time. The relaxation time for considered conditions is about 1 ms.

In *Fig. 10.9-10.11* the predicted distributions of the local skin-friction coefficient c_f, wall temperature T_w, and wall pressure p_w along plate surface in some consecutive instants of time are compared. Presented on these Figures data are obtained for the first heat deposition case. During heat deposition perturbations of skin-friction and wall temperature distributions are located in region of gas heating. After termination of the heat supply these perturbations move downstream with average velocity about *350 m/s* and damp. The near wall heat deposition produces also appreciable perturbations of the wall pressure (*Fig. 10.11*) induced by streamlines derivation from the wall in the gas heating region.

Fig. 10.12 shows deformation of velocity profile in a wall boundary layer section x *=15 cm* during heat deposition time period and after one. These data are obtained also for the first gas heating case. Distance *n* on Figure is measured from the plate surface along normal to it. Heat deposition leads to the both boundary layer and laminar sublayer thickness increasing that causes decreasing of the skin-friction. The time history of turbulent energy profile in the boundary layer for same condition is shown in *Fig. 10.13*. It is seen that the gas heating pushes a peak turbulent energy off the wall and decreases its value. These Figures show also that the heat deposition region in considered conditions completely locates in the boundary layer.

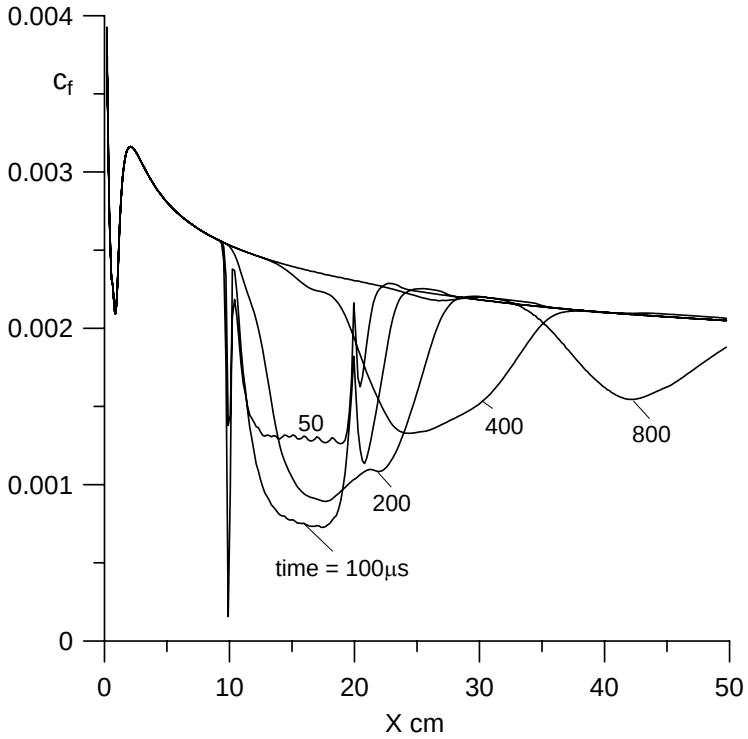

Fig. 10.9. Distributions of local skin-friction coefficients along plate surface in successive time instants for third case of heat deposition.

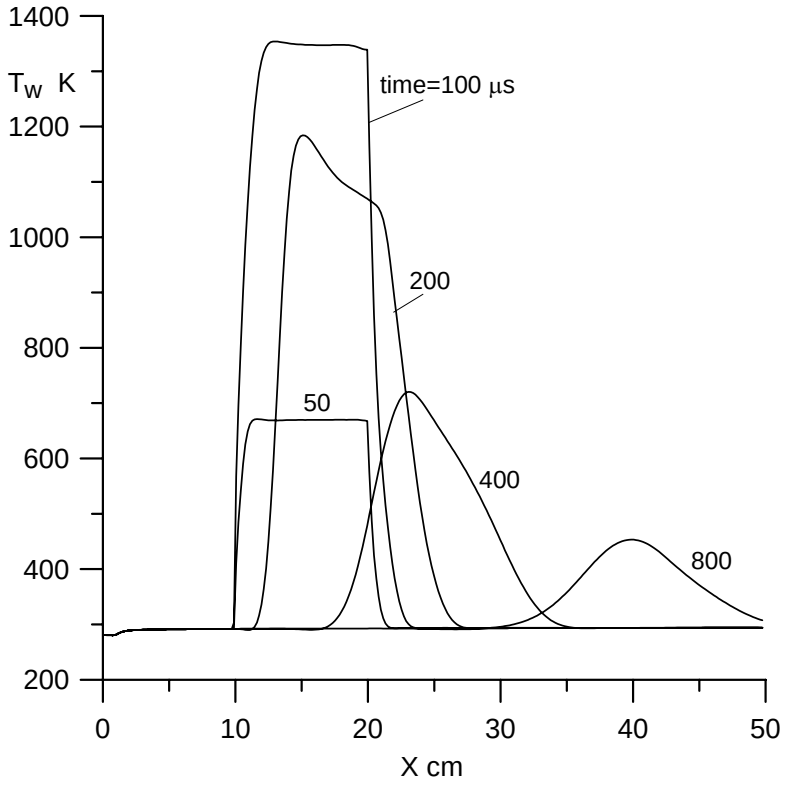

Fig. 10.10. Distributions of wall temperature along plate surface in successive time instants for third case of heat deposition.

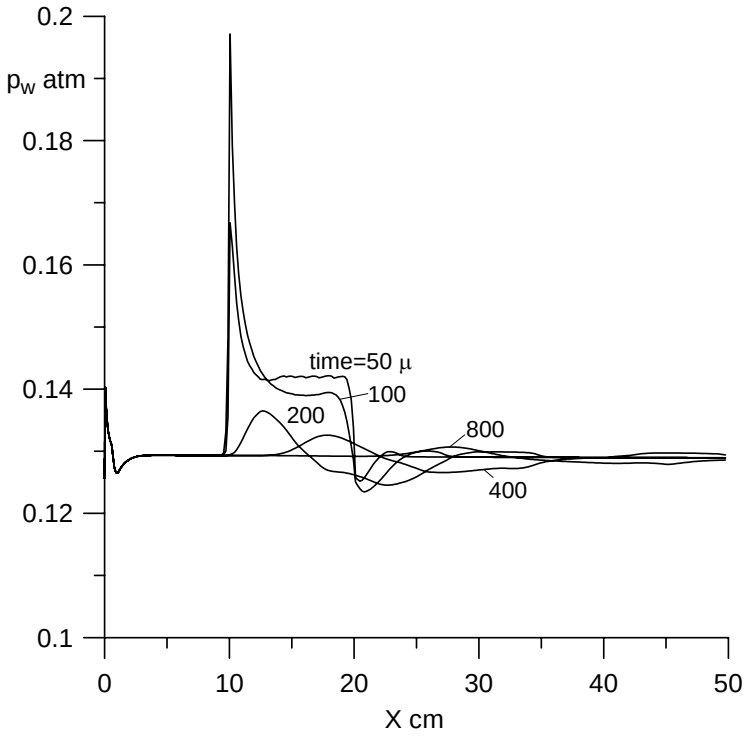

Fig. 10.11. Distributions of wall pressure along plate surface in successive time instants for third case of heat deposition.

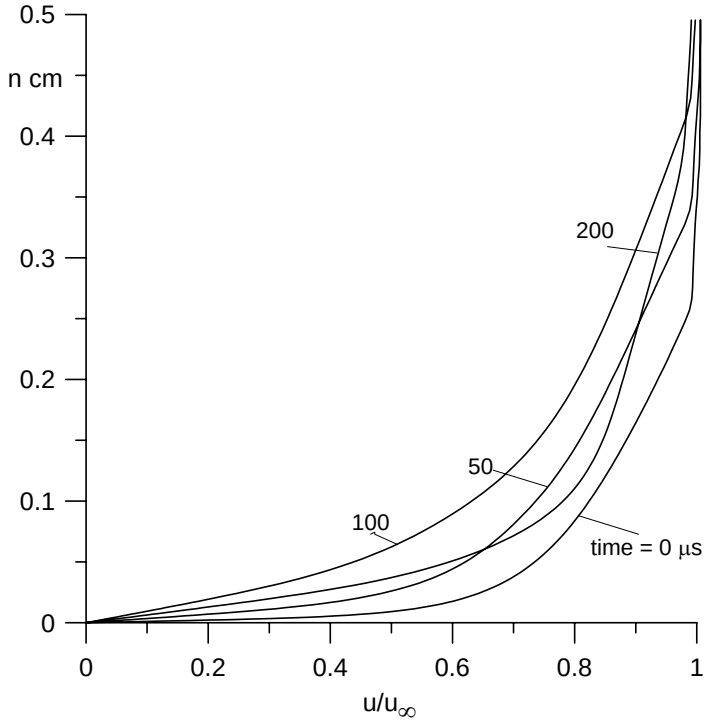

Fig. 10.12. Profiles of gas velocity in boundary layer section x = 15 cm for successive time instants.

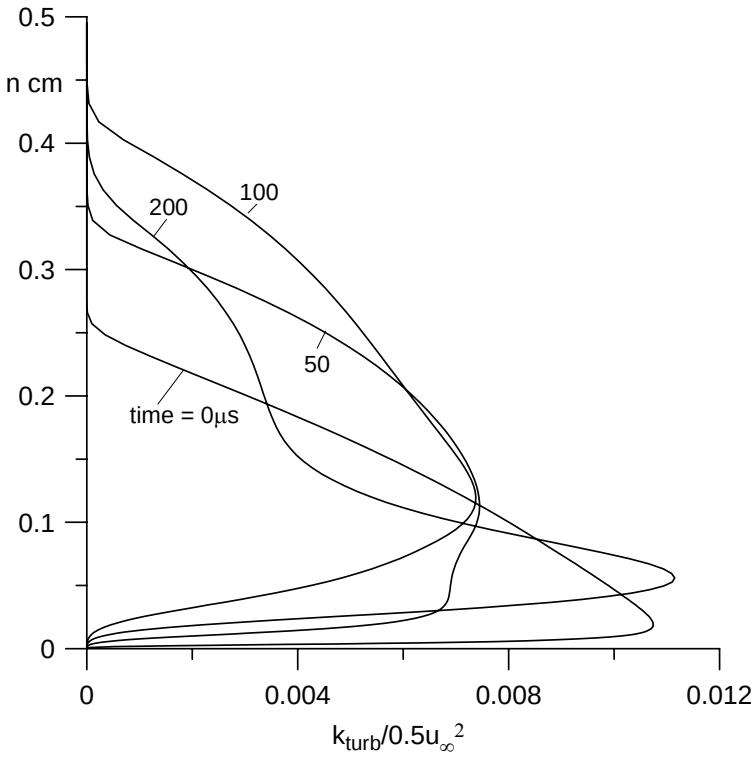

Fig. 10.13. Profiles of turbulent energy in boundary layer section *x=15 cm* for successive time instants.

CHAPTER XI
NUMERICAL MODELING OF GASEOUS FUEL IGNITION WITH HELP OF GAS DISCHARGE

11.1. Numerical modeling of ignition of supersonic air-propane mixture by near wall electrical discharge

Developed numerical technique (look Chapter X) has been employed to study C_3H_8/air ignition by near wall heat deposition. Computations have been performed for supersonic flow of stoichiometric propane-air mixture over blunted flat plate length of *15 cm* and thickness of *0,02 cm* for free stream velocity of *519 m/s*, pressure of *0,128 bar*, and temperature of *167 K*. Described above gas phase model involving *30* species (C_3H_8 ,*O, H,* O_2, N_2, H_2, *CO, OH,* H_2O, HO_2, H_2O_2, *HCO,* CO_2, *CH,* CH_2, CH_3, CH_4, C_2H, C_2H_2, C_2H_3, C_2H_4, C_2H_5, C_2H_6, C_3H_5, C_3H_6, *i-*C_3H_7, *n-*C_3H_7, CH_2O, CH_2OH, CH_3OH) and *70* chemical reactions (see Table 11.1, and Table 11.2) was employed to describe ignition process. Adiabatic, full non-catalytic model of gas-wall thermal and chemical interactions was used. Wall turbulence parameters were specified as in above item.

It was assumed that heat is deposed during time period of 100 μs with constant total power P_d*=2500 W/cm* uniformly into near wall region $0.5 \le x \le 15$ cm, $0 \le n \le 0.1$ cm . The heat supply is started into initially steady-state turbulent stream.

The time history of predicted gas temperature and some species mole fraction distributions along plate surface are shown in *Fig. 11.1-11.5*. *Fig. 11.6-11.7* demonstrate time behavior of temperature and propane mole fraction profiles in flow section x=15cm (plate end). Presented on Figures data indicate that for considered conditions ignition of fuel mixture occurs after ending of heat supply pulse on distance about *4 cm* from plate heading. To this time gas temperature near wall reaches *~3000 K*. Numerical analysis has shown that for more short heating pulse or lesser heating power when temperature does not amount to this level ignition does not occur. After ignition the burning front moves downstream with rate about *300 m/s*. Gas temperature decreases and completeness of combustion increases. In gas mixture behind burning front the fractions of final combustion products H_2O and CO_2 rise whereas the fractions of oxygen and the intermediate products of burning drop.

Table 2. Dissociation-recombination reactions [5]

$$k_r = AT^n \exp(-E/T),\ \mathrm{cm^6/mol^2\,s}$$

Reaction					E, K	A	n
O2	⇔	O	+	O	0	2.9e17	-1
H2O	⇔	OH	+	H	0	2.2e22	-2
H2	⇔	H	+	H	0	1.8e13	-1
OH	⇔	O	+	H	0	1.0e16	0
CO2	⇔	CO	+	O	2060	5.9e15	0
HO2	⇔	H	+	O2	0	2.3e18	-0.8
HO2	⇔	OH	+	O	0	1.0e17	0
H2O2	⇔	OH	+	OH	0	3.25e22	-2.0
HCO	⇔	CO	+	H	0	1.1e15	0
CH4	⇔	CH3	+	H	0	2.5e11	1.0
CH2O	⇔	HCO	+	H	0	4.7e15	0
C2H4	⇔	C2H2	+	H2	0	1.9e16	0
C2H5	⇔	C2H4	+	H	0	6.3e13	0
C2H6	⇔	CH3	+	CH3	0	3. 6e13	0
C3H6	⇔	C2H3	+	CH3	0	3.5e10	0
C3H7I	⇔	C2H4	+	CH3	0	1.0e11	0
C3H7N	⇔	C2H4	+	CH3	0	1.6e11	0
C3H7N	⇔	C3H6	+	H	0	2.9e14	0
C3H8	⇔	CH3	+	C2H5	0	2.0e17	-1.8
C3H8	⇔	C3H7n	+	H	0	3.6e13	0
C3H8	⇔	C3H7i	+	H	0	2.4e13	0
CH2OH	⇔	CH2O	+	H	0	1.4e14	0

Table 3. Exchange reactions [5]

$k_r = AT^n \exp(-E/T)$, cm³/mol·s

Reaction							A	n	E, K
OH	+	O	=	H	+	O2	2.00e14	0.0	8455
OH	+	H	=	O	+	H2	5.06e04	2.67	3160
H2O	+	H	=	H2	+	OH	1.00e08	1.60	1661
O	+	H2O	=	OH	+	OH	1.50e09	1.14	50
OH	+	OH	=	HO2	+	H	1.50e14	0.0	503
H2	+	O2	=	HO2	+	H	2.50e13	0.0	348
H2O	+	O2	=	HO2	+	OH	6.00e13	0.0	0.0
H2O	+	O	=	HO2	+	H	3.00e13	0.0	866
OH	+	O2	=	HO2	+	O	1.80e13	0.0	-204
H2O2	+	O2	=	HO2	+	HO2	2.50e11	0.0	-624
H2O	+	OH	=	H2O2	+	H	1.00e13	0.0	1802
H2O	+	HO2	=	H2O2	+	OH	5.40e12	0.0	503
CO2	+	H	=	CO	+	OH	4.40e06	1.5	-372
HCO	+	O	=	CH	+	O2	3.00e13	0.0	0
HCO	+	CO	=	CO2	+	CH	3.40e12	0.0	348
CO	+	H2	=	HCO	+	H	2.00e14	0.0	0
CO	+	H2O	=	HCO	+	OH	1.00e14	0.0	0
CO	+	HO2	=	HCO	+	O2	3.00e12	0.0	0
CH	+	H2	=	CH2	+	H	8.40e09	1.5	169
HCO	+	H2	=	CH2O	+	H	2.50e13	0.0	2008
HCO	+	OH	=	CH2O	+	O	3.50e13	0.0	2008
HCO	+	H2O	=	CH2O	+	OH	3.00e13	0.0	604
CH2	+	H2	=	CH3	+	H	1.80e14	0.0	7574
CH2O	+	H	=	CH3	+	O	7.00e13	0.0	0
CH2O	+	OH	=	CH3	+	O2	3.40e11	0.0	4499
CH3	+	H2	=	CH4	+	H	2.20e04	3.0	4399
CH3	+	OH	=	CH4	+	O	1.20e07	2.1	3835
CH3	+	H2O	=	CH4	+	OH	1.60e06	2.1	1238
C2H2	+	H	=	C2H	+	H2	1.10e13	0.0	1443
CH2	+	CO	=	C2H2	+	O	4.10e08	1.5	854
C2H	+	H2O	=	C2H2	+	OH	1.10e13	0.0	3522
C2H2	+	H2	=	C2H3	+	H	3.00e13	0.0	0
C2H2	+	HO2	=	C2H3	+	O2	5.40e11	0.0	0
C2H3	+	H2	=	C2H4	+	H	1.50e14	0.0	5133
C2H3	+	H2O	=	C2H4	+	OH	3.00e13	0.0	1515
CH3	+	CH3	=	C2H5	+	H	3.00e13	0.0	0
C2H4	+	HO2	=	C2H5	+	O2	2.00e12	0.0	2513
C2H5	+	H2	=	C2H6	+	H	5.40e02	3.5	2621
C2H5	+	OH	=	C2H6	+	O	3.00e07	2.0	2573
C2H5	+	H2O	=	C2H6	+	OH	6.30e06	2.0	325
C3H5	+	H2	=	C3H6	+	H	5.00e12	0.0	765
C3H6	+	HO2	=	C3H7I	+	O2	1.00e12	0.0	2513
C3H7n	+	H2	=	C3H8	+	H	1.30e14	0.0	4881
C3H7i	+	H2	=	C3H8	+	H	1.00e14	0.0	4196
C3H7n	+	OH	=	C3H8	+	O	3.00e13	0.0	2942
C3H7i	+	OH	=	C3H8	+	O	2.60e13	0.0	2248
C3H7n	+	H2O	=	C3H8	+	OH	3.70e12	0.0	829
C3H7i	+	H2O	=	C3H8	+	OH	2.80e12	0.0	433
CH2O	+	H2	=	CH2OH	+	H	3.00e13	0.0	0
CH2O	+	HO2	=	CH2OH	+	O2	1.00e13	0.0	3619
CH2OH	+	H2	=	CH3OH	+	H	4.00e13	0.0	3066
CH2OH	+	H2O	=	CH3OH	+	OH	1.00e13	0.0	853
C3H8	+	O2	=	C3H7n	+	HO2	5.50e05	1.5	0
C3H8	+	O2	=	C3H7i	+	HO2	3.00e09	0.5	0

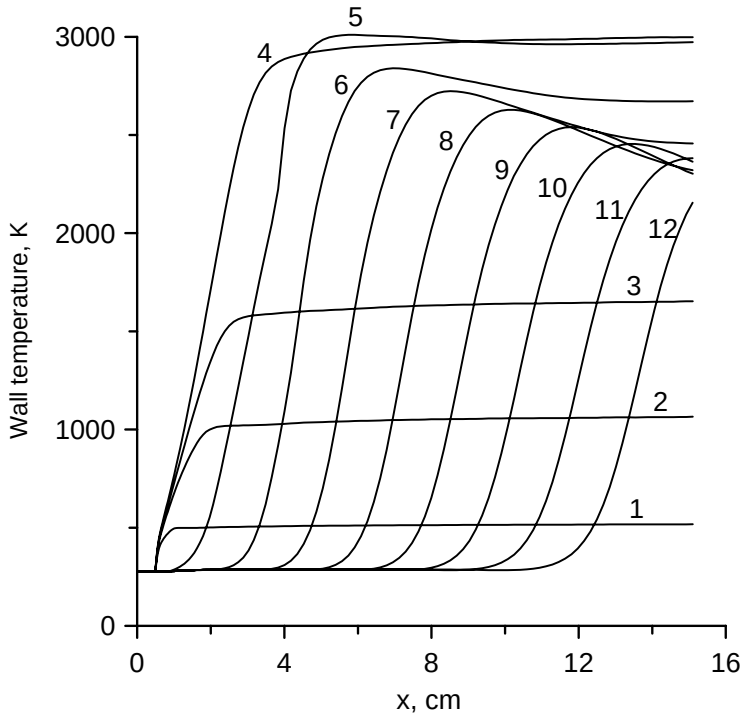

Fig. 11.1. Time history of wall temperature distribution. *t, μs*: 1 – 25; 2- 50; 3 – 75; 4 – 100; 5 – 150; 6 – 200; 7 – 250; 8 – 300; 9 – 350; 10 – 400; 11 – 450; 12 – 500.

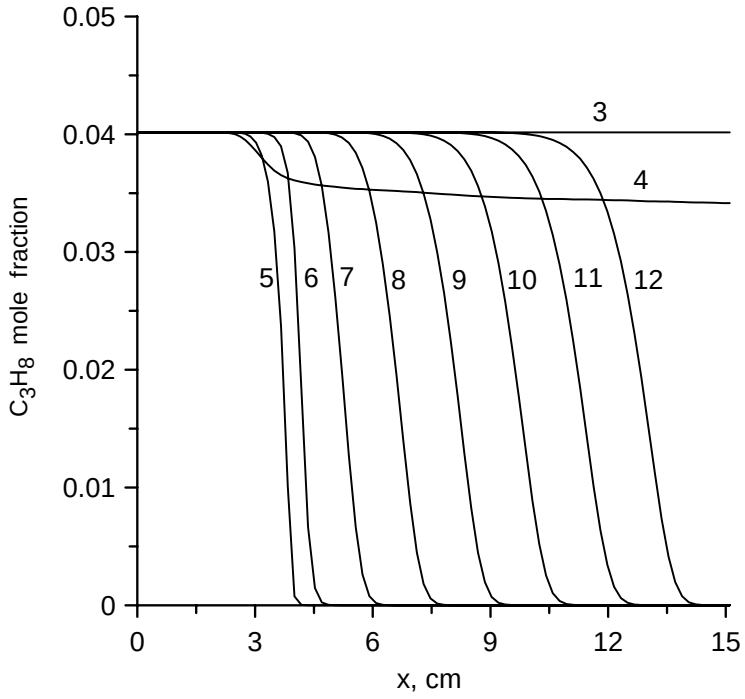

Fig. 11.2. Time history of wall C_3H_8 mole fraction distribution. Notations as in *Fig. 11.1.*

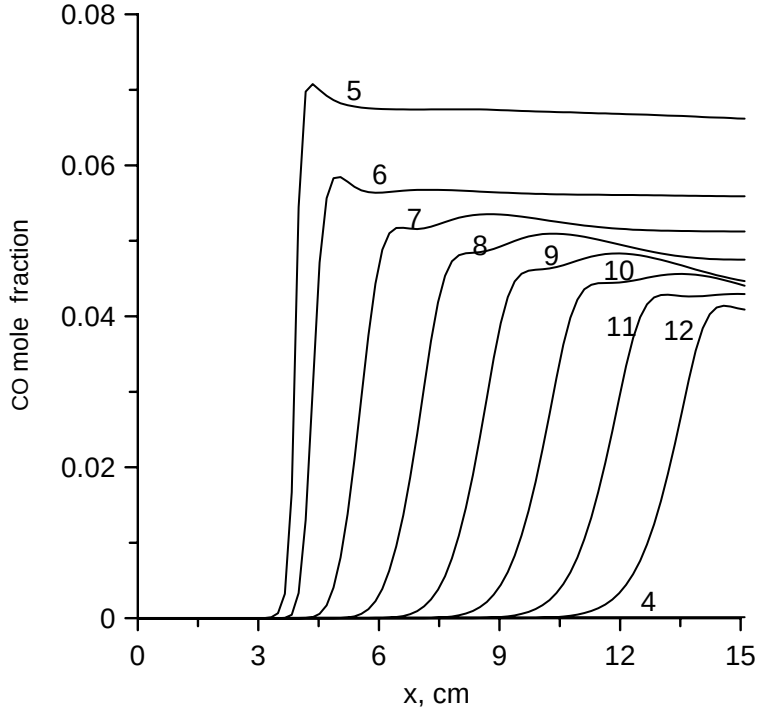

Fig. 11.3. Time history of wall CO mole fraction distribution. Notations as in *Fig. 11.1*.

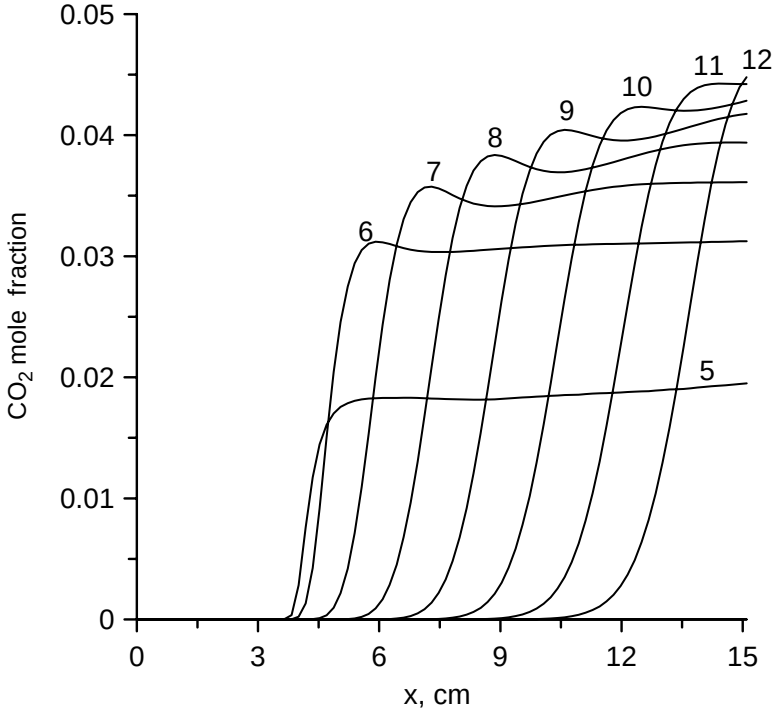

Fig. 11.4. Time history of wall CO_2 mole fraction distribution. Notations as in *Fig. 11.1*.

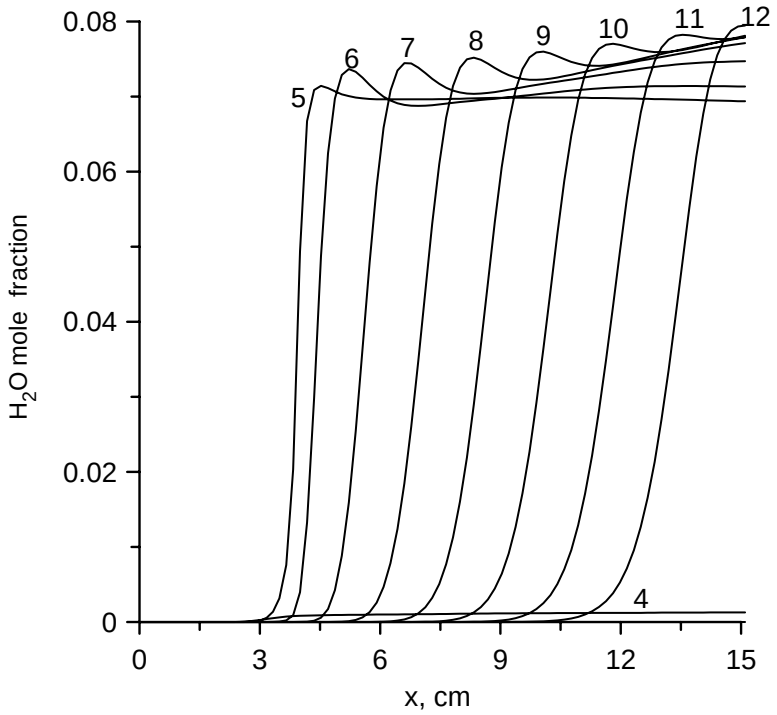

Fig. 11.5. Time history of wall H_2O mole fraction distribution. Notations as in *Fig. 11.1.*

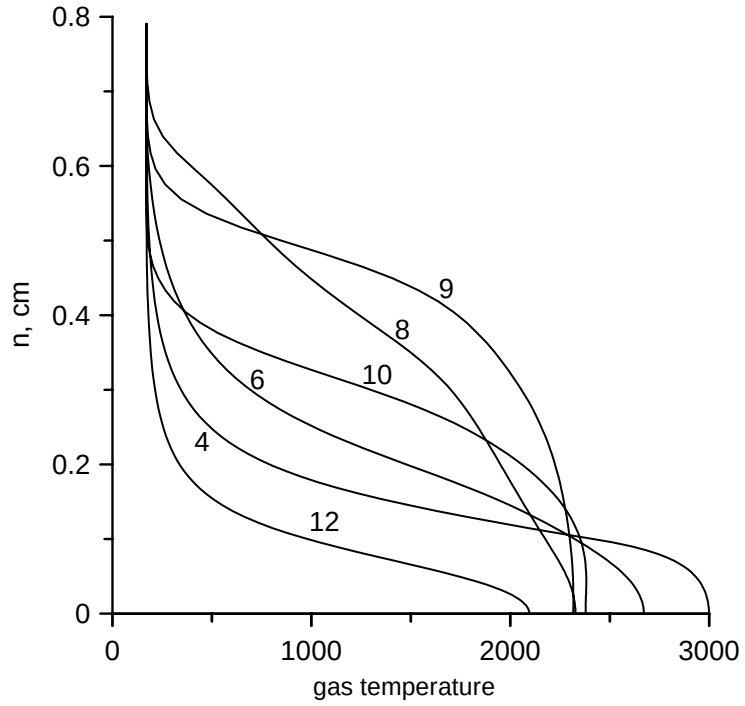

Fig. 11.6. Time history of temperature profile in section x = 15cm. Notations as in *Fig. 11.1.*

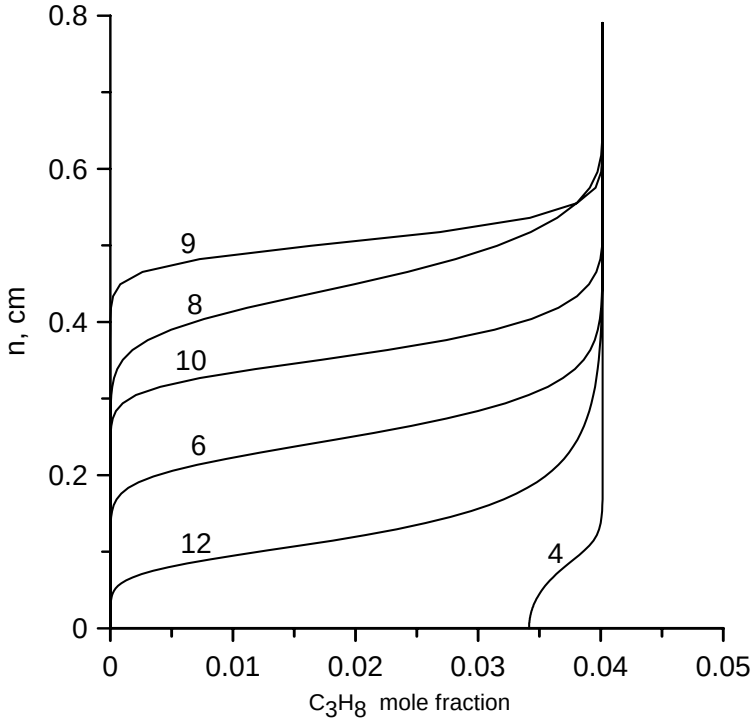

Fig. 11.7. Time history of C_3H_8 mole fraction profile for section *x=15 cm*.

Notations as in *Fig. 11.1.*

11.2. Mathematical model of kinetics of burning of gaseous fuels

It is known, that ignition of combustible gaseous mixtures can be realize or due to heating of gas to high temperature (thermal autoignition), or because of radicals and active particles. Finding-out of the mechanisms responsible for ignition at the presence of non-equilibrium low-temperature plasma of the gas discharge at high values of the reduced electric field, is one of the principal goals of the given project. The important problem is also the estimation of influence of parameters of the discharge on kinetics of ignition of gaseous fuels and modelling of process of their burning at the presence of the discharge.

In overwhelming majority of the executed experimental and theoretical researches, devoted to application of various types of gas discharges for ignition of fuels mixtures, the gas discharge was considered only as a source of thermal energy entered into system. But the various gas ionization degrees are achieved for different type of gas discharges at the same applied specific power. At this the electric energy input is differently distributed on internal degrees of freedom of molecular gas. This distribution is strongly dependent on the reduced electric field which, in turn, is determined by electrodynamics of the discharge. The opposite result can be received at the same power of energy source. For example, for an ignition of a supersonic flow of propane-air mixture we used freely localized volumetric microwave discharge, surface microwave discharge and volumetric pulse-periodic transversal discharge. All generators, creating plasma, were supplied from the same source of energy. However, the ignition of a propane-air mixture with the help of the microwave discharges took place already at pulse duration $\tau \approx 25\ \mu s$ whereas the pulse-periodic transversal discharge in the same conditions resulted in ignition only at $\tau \geq 150\text{-}200\ \mu s$. It testifies that in plasma of a microwave discharge there are more active particles than in plasma of the pulse-periodic discharge. Thus it is known that in a microwave discharge at high values of reduced electric field $E/n \geq 100\ Td$ the fast gas heating with rate of $dT_g/dt = 10^7\text{-}10^8\ K/s$ and high gas dissociation degree $\delta \sim 50\ \%$ are observed that also promotes of fuel ignition. Therefore from our point of view it is necessary to investigate in details the influence of the charged and active particles, which are very quickly formed in the discharge, on reduction of an ignition delay and on increasing of completeness of propane-air mixture combustion. The kinetical model was working out by us for finding-out of influence of different channels on ignition of combustible mixtures in supersonic flow.

For the analysis of kinetics of burning the mathematical model including more than 400 reactions and more than 100 components has been developed. Such components as H_z, N_z ($z=1,2$), O_x($x=1$-3), HO_z, H_2O_z, NO_x, HNO_y, ($y=1$-4), N_z0, N_xO_y, C_z, CO_z, C_yH_n ($n=1$-10), $C_xH_nO_z$, C_2N_2, HCN, NCO, and also other radicals and the charged particles are included in model.

The system of the equations describing processes of oxidation in such mixtures and including the equation for energy, the equation for concentration of particles, the equation of state have been put in a basis of model:

$$\dot{\gamma}_i = G_i - \gamma_i \sum_{k=1}^{M_1} G_k \,, \tag{11.1}$$

$$G_i = \sum_{q=1}^{M_2} \frac{\alpha_{iq}^- - \alpha_{iq}^+}{N} \left[R_q^+ - R_q^- \right], \tag{11.2}$$

$$R_q^{+(-)} = k_{+(-)q} \prod_{j=1}^{n_q} \left(N\gamma_{n_{jq}^{+(-)}} \right)^{\alpha_{jq}^{+(-)}} \,, \tag{11.3}$$

$$\dot{N} = N \sum_{k=1}^{M_1} G_k \,, \tag{11.4}$$

$$\dot{H} = 0 \tag{11.5}$$

$$H = N \cdot \sum_{i=1}^{M_1} \gamma_i \left(h_{0i}[T_0] + \int_{T_0}^{T} C_{Pi} dT \right). \tag{11.6}$$

Where

γ_i - mole fraction of corresponding component i,

N [mol/cm^{-3}] - total concentration,

c_{pi} - molar heat capacity of species i at p=const,

$h_{0i}[T_0]$ - molar enthalpy of formation of species i at $T_o = 298K$,

M_1 - full number of components,

$k_{+(-)q}$ - rate constants with participation of species i,

M_2 - full number of such reactions,

α_{iq}^+ and α_{iq}^- - stochiometric coefficients.

Decomposition

$$C_{Pi} = \sum_{a=1}^{6} C_{Pi}^{(a)} \left(\frac{T}{10^4} \right)^{a-1} \qquad (11.7)$$

has been used for calculation of a thermal capacity.

The rate constants for each of a component, including the charged particles and radicals, and also for each of reaction have been collected.

The database includes:

- enthalpy of formation for each component *i*;
- coefficients in decomposition of c_{pi} for each component *i*;
- stochiometric coefficients for each reaction;
- rate constants of reactions in a direct and reverse direction.

The database has been prepared and realized in the form of a computer database with the purpose of the further simplification of its use in calculations.

11.3. Mathematical modelling of autoignition of a hydrogen-oxygen mixture

The results of modelling of kinetics of burning of a hydrogen-oxygen mixture at various stochiometric ratios are resulted in *Fig. 11.8-11.10*. Modelling was fulfilled with use of the kinetical scheme including 9 component and 29 reactions.

From figures it is visible, that the creation of radicals takes place up to the moment of ignition. The ignition occurs at times *~1 ms*, that well coordinates to results of articles [1, 2].

Time dependence of typical temperature of a hydrogen-oxygen mixture is represented in *Fig. 11.11*. It is visible, that at the initial stage (*t=0-1 ms*) the gas temperature very slowly rises and then during the moment of ignition sudden changes from initial temperature *900 K* up to final *~3000 K*.

Dependences of ignition time of a hydrogen-oxygen mixture on hydrogen consumption are submitted in *Fig. 11.12* at various stochiometric ratios of components and at various initial gas temperatures. It is possible to see, that an induction time depends both on a ratio of mixture, and from initial gas temperature. At that with growth of temperature ignition time decreases at any ratio of components of a mixture. At the same time, at any gas temperature the ignition time of a mixture grows both at increase, and at reduction of a fraction of hydrogen in a mixture in comparison with a stochiometric ratio.

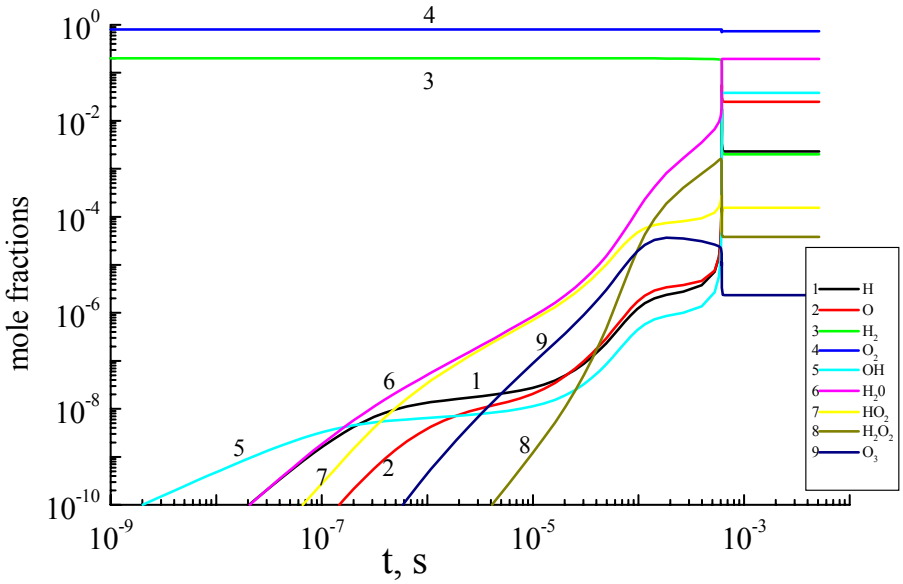

Fig. 11.8. Time dependence of mole fractions at ignition of hydrogen-oxygen mixture at initial gas temperature T_{in} =900 K, N_{in}=4,4·10^{-5} mol/cm^{-3} and stochiometric ratios H_2-O_2=0,8-0,2.

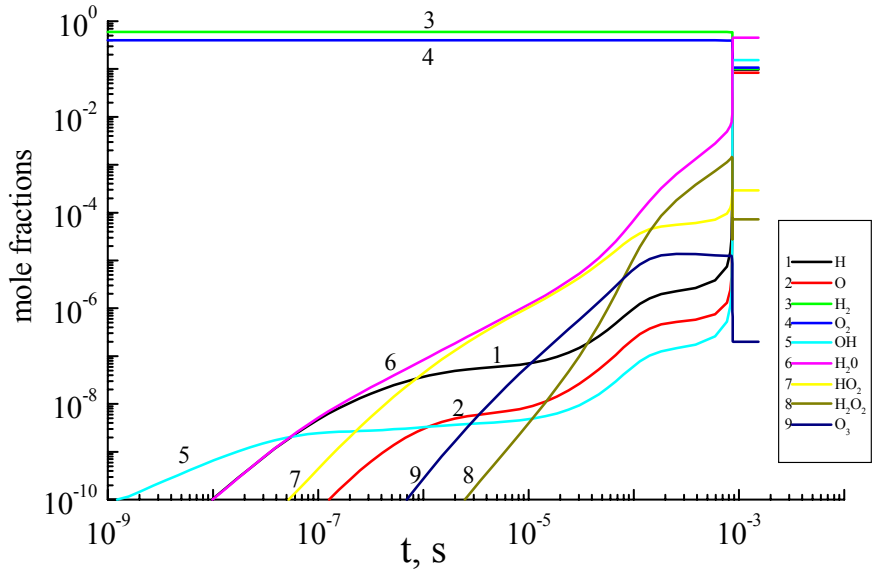

Fig. 11.9. Time dependence of mole fractions at ignition of hydrogen-oxygen mixture at initial gas temperature T_{in} =900 K, N_{in}=4,4·10^{-5} mol/cm^{-3} and stochiometric ratios H_2-O_2=0,6-0,4.

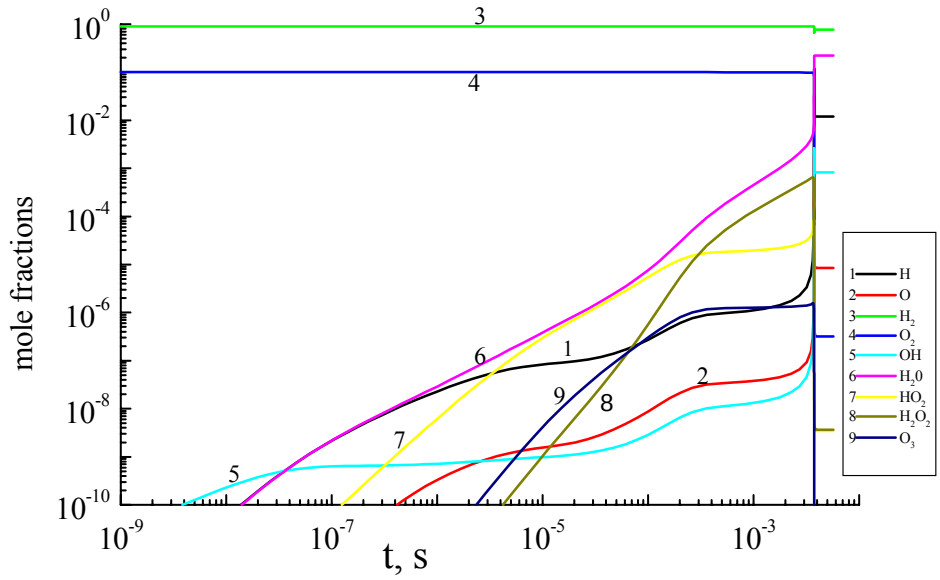

Fig. 11.10. Time dependence of mole fractions at ignition of hydrogen-oxygen mixture at initial gas temperature T_{in}=900 K, N_{in}=4,4·10^{-5} mol/cm^{-3} and stochiometric ratios H_2-O_2=0,9-0,1.

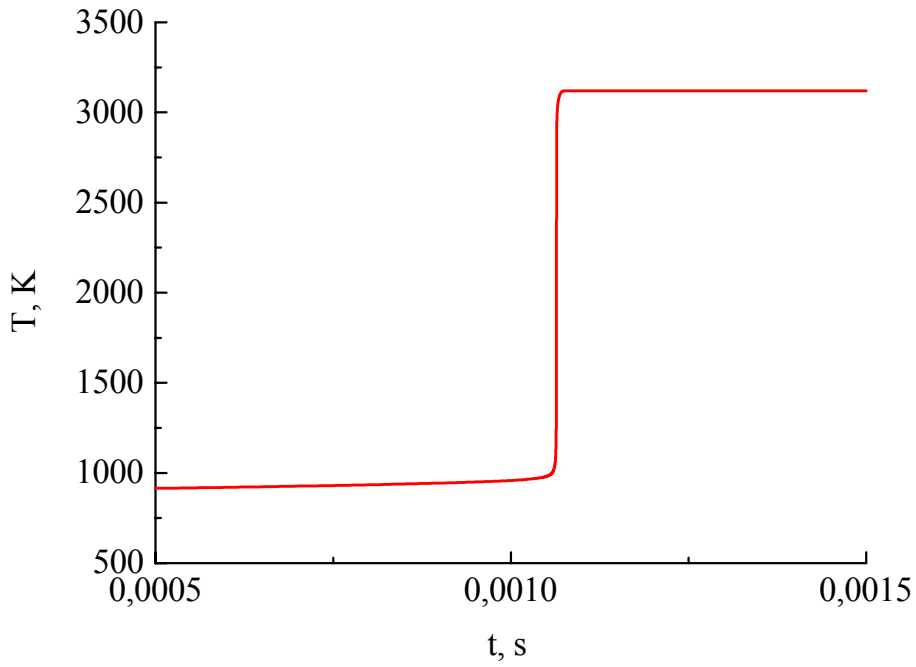

Fig. 11.11. Typical gas temperature vs time at burning of hydrogen-oxygen mixture at T_{in}=900 K and N_{in}=4,4·10^{-5} mol/cm^{-3}.

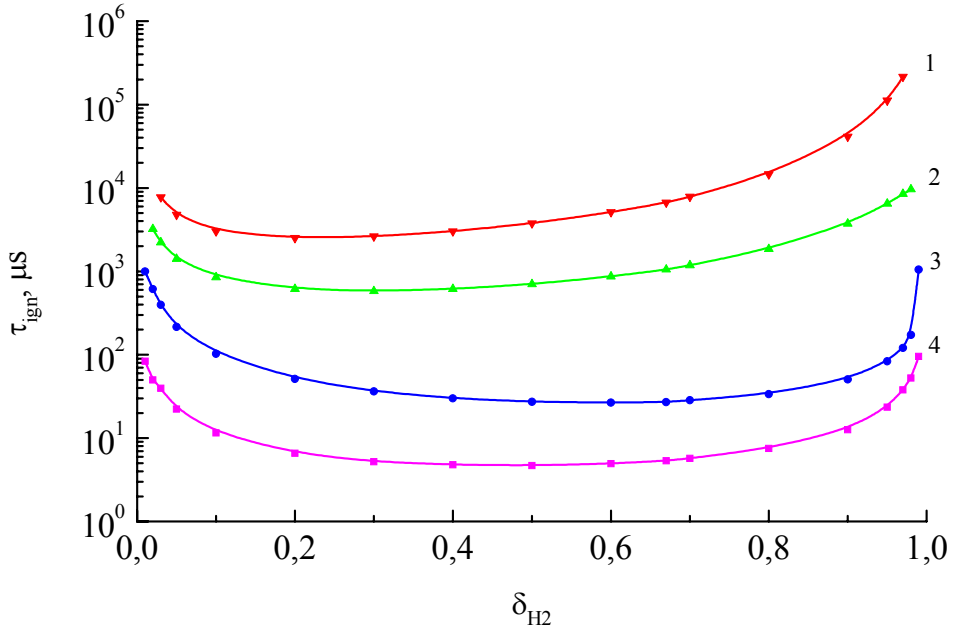

Fig. 11.12. Autoignition time vs hydrogen consumption in *H2-O2* mixture at *p=1 atm* and at instant gas heating up to initial gas temperatures T_{in}*=1000 K*.

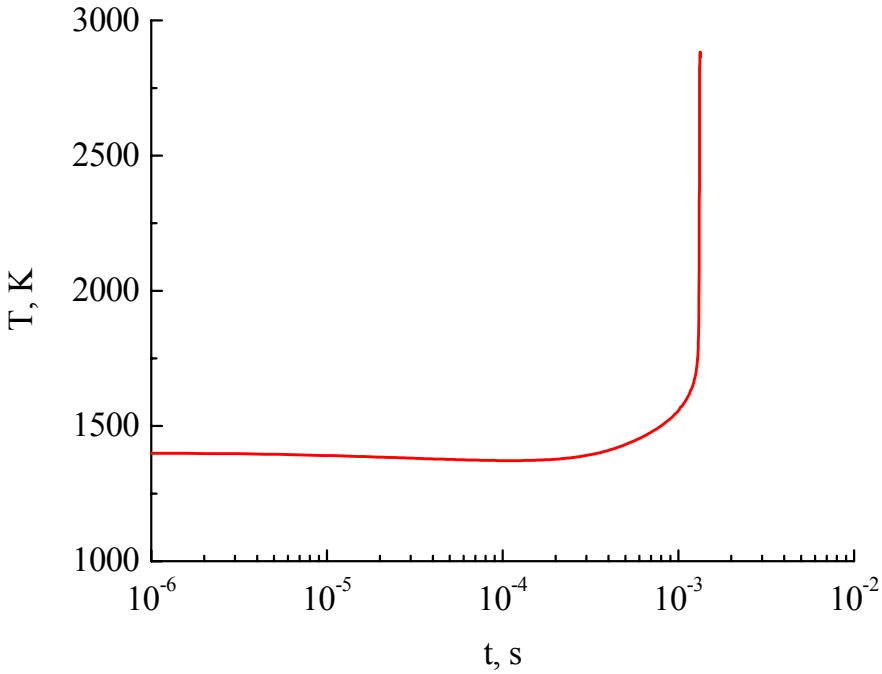

Fig. 11.13. Typical gas temperature vs time at burning of propane-air mixture at T_{in}*=1400 K and* N_{in}*=4,4·10*$^{-5}$ *mol/cm*$^{-3}$.

11.4. Mathematical modelling of autoignition of a propane-air mixture

The modelling of kinetics of burning of a propane-air mixture was fulfilled too. Calculations were made with use of the kinetic model including 102 components and 420 reactions.

Let's consider at first as preliminary destruction of individual hydrocarbons influences on dynamics of burning in atmosphere of oxygen. Result of calculation of time evolution of typical gas temperature at burning of C_3H_8 and its destruction products in a mixture with O_2 at initial gas temperature $T_{in}=1400\ K$ is submitted in *Fig. 11.13*.

It is visible, that at burning both C_3H_8, and products its thermal destruction there is extended enough time interval when the temperature of a mixture practically does not vary; then it sharply grows and reaches some stationary value. This time interval corresponds to the period of an induction (a delay of ignition). It is characterized by accumulation of active atoms and radicals (*H, O, OH,* HO_2, CH_3 and so on), determining dynamics of burning.

For the mixtures consisting of destruction products of saturated hydrocarbon C_3H_8 and O_2, the period of an induction in *1.5-2* times is less [3], than for mixtures C_3H_8 with O_2. Apparently, such reduction of the period of an induction is connected to distinction of mechanisms of formation of active atoms and radicals at oxidation of saturated hydrocarbons and their destruction products.

The temporal changes of concentrations of various components at burning of stochiometric $C_3H_8+O_2$ mixture are presented in *Fig. 11.14.*

Proceeding from consideration of the results, submitted in *Fig. 11.8-11.14*, it is possible to make the conclusion, that the basic mechanism of ignition in absence of the discharge is thermal ignition, as ignition occurs without participation of the charged particles and is defined by only chemical processes. In this case an ignition time is determined by time of formation of active atoms and radicals in conditions of absence of its creation connected with interaction with charged particles.

11.5. Numerical modelling of gas discharge influence on ignition of a hydrogen-oxygen mixture

The numerical computation of ignition of oxygen-hydrogen and propane-air mixtures at the presence of the discharge is based on the kinetical model of ignition and the burning, including additional in comparison with paragraphs *11.3* and *11.4* list of reactions.

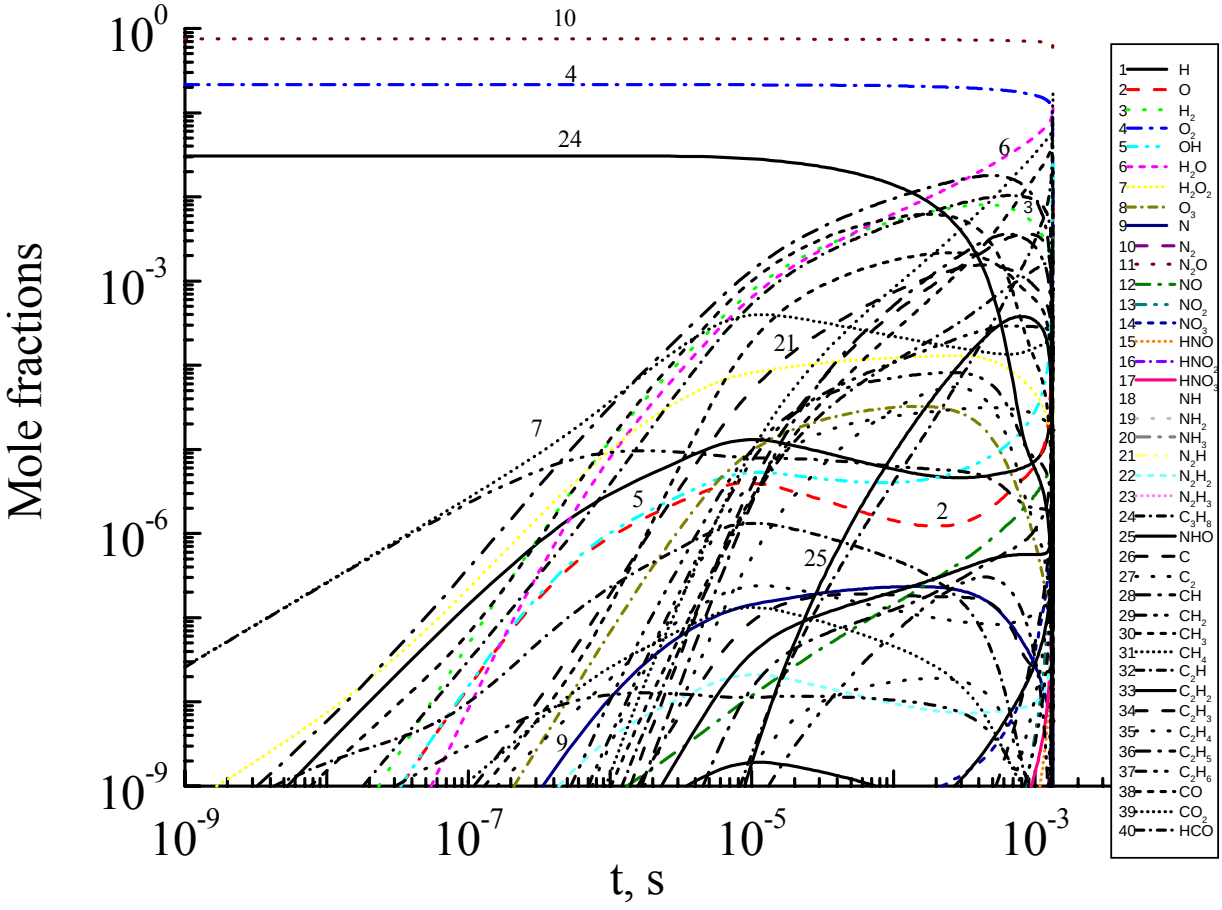

Fig. 11.14. Time dependence of mole fractions at ignition of propane-air mixture at initial gas temperature T_{in}=*1400 K,* N_{in}=*4,4·10*$^{-5}$ *mol/cm*$^{-3}$ and stochiometric ratio C_2H_8-*air=0,03-0,97.*

The ignition of the hydrogen-oxygen mixture calculated under the model with the account of molecules dissociation and creation of active radicals and charged particles at high values of reduced electric field is represented in *Fig. 11.15-11.18* at various values of electron temperature. It is visible, that the mechanism of ignition represented in *Fig. 11.15* is distinct from the mechanism of ignition of the hydrogen-oxygen mixture considered and simulated earlier in absence of the discharge (look *Fig. 11.8-11.10*). So, for example, process of creation of radicals and active particles is essentially accelerated at the presence of the discharge due to quantitative and qualitative changes from a simple formation of active radicals as a result of interaction of not charged particles to a creation of active radicals as a result of interaction with the charged particles. Thus rate of such reactions is more than rate of reactions with not charged particles. Obviously, it leads to reduction of time of creation of necessary for ignition amount of active particles and, accordingly, to earlier ignition.

As a consequence of this fact the mechanism of ignition varies also. In this case the creation of active components occurs generally due to the discharge. Besides, from *Fig. 11.15-11.18* follows that the rate of creation of radicals and the charged particles increases at growth of reduced electric field E/n that is electron temperature T_e. This circumstance results in essential reduction in an induction time.

Gas discharge influence on ignition time of H_2-O_2 stoichiometric (*67%-33%*) mixture is shown in *Fig. 11.19* at $p=1$ *atm* and at instant gas heating to various initial gas temperatures T_{go}. *Fig. 11.19* shows, that time of an ignition delay under condition of the gas discharge (that is at high value of reduced electric field) is decreased to some orders of values.

11.6. Numerical modelling of gas discharge influence on ignition of a propane-air mixture

In the given paragraph the preliminary results showing influence of an electric field on ignition of a propane-air mixture in conditions of the gas discharge are presented.

Typical gas temperature vs time at burning of propane-air mixture under condition of gas discharge is shown in *Fig. 11.20* at electron temperature $T_e=0,75$ *eV*, initial gas temperature $T_{in}=1400$ *K* and total concentration $N_{in}=4,4\cdot10^{-5}$ *mol/cm*$^{-3}$. It is visible, that at ignition of propane the temperature sharply grows from *1400 K* up to temperature of burning of propane *~2800 K* that well coordinates to experimental results.

Fig. 11.21 shows, as the concentration of various components changes in time at burning of stochiometric $C_3H_8+O_2$ mixture at the presence of the discharge. It is visible, that time of an

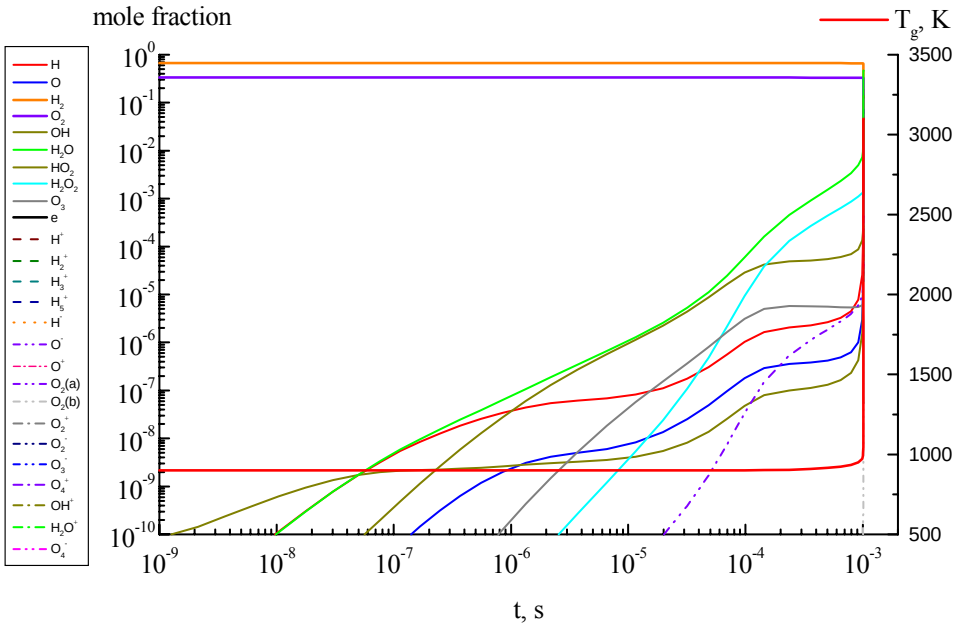

Fig. 11.15. Kinetics of H_2-O_2 stoichiometric mixture (*67%-33%*) ignition under condition of gas discharge at *p=1 atm*, instant gas heating to initial temperature T_{go}*=900 K and* T_e*=0 eV* (autoignition).

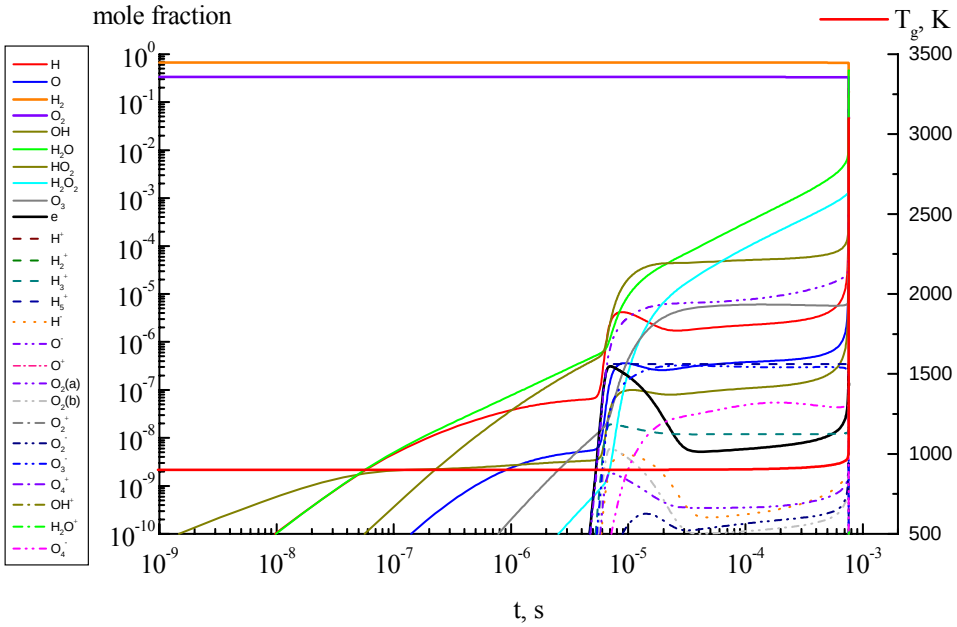

Fig. 11.16. Kinetics of H_2-O_2 stoichiometric mixture (*67%-33%*) ignition under condition of gas discharge at *p=1 atm*, instant gas heating to initial temperature T_{go}*=900 K and* T_e*=0,75 eV*.

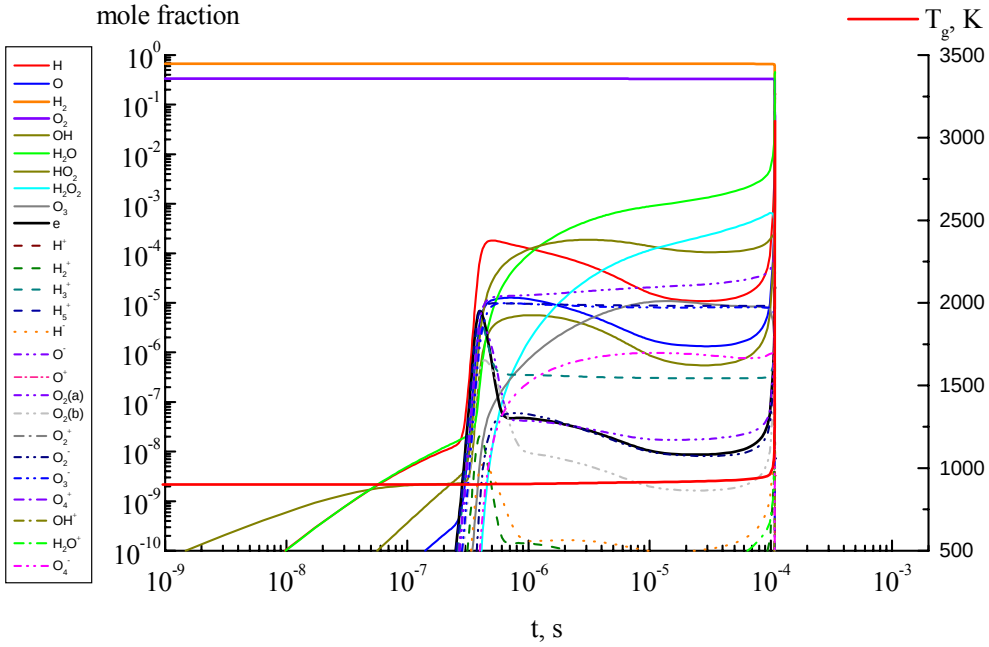

Fig. 11.17. Kinetics of H_2-O_2 stoichiometric mixture (*67%-33%*) ignition under condition of gas discharge at *p=1 atm*, instant gas heating to initial temperature T_{go}*=900 K and* T_e*=1,0 eV*.

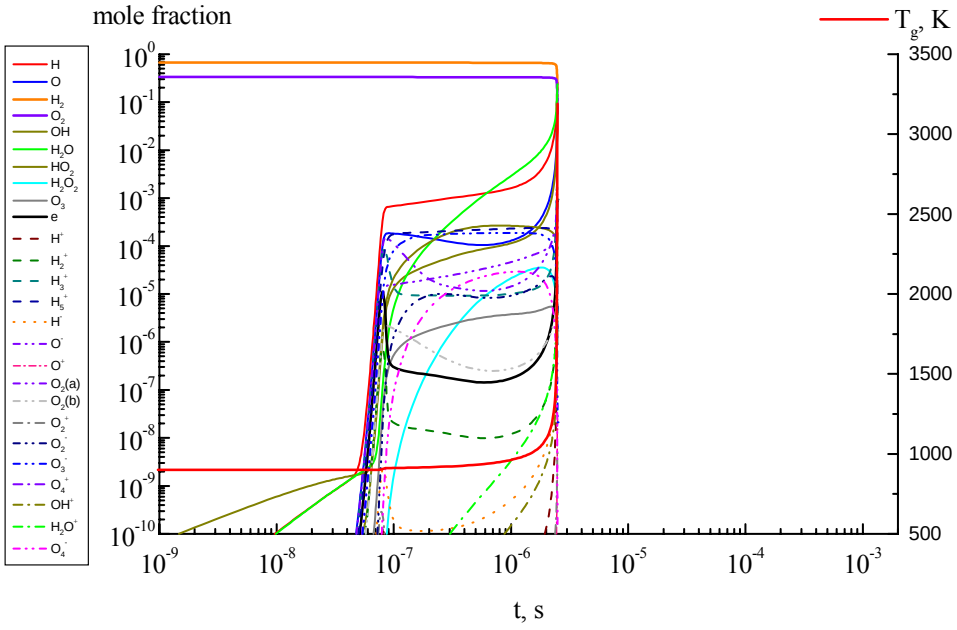

Fig. 11.18. Kinetics of H_2-O_2 stoichiometric mixture (*67%-33%*) ignition under condition of gas discharge at *p=1 atm*, instant gas heating to initial temperature T_{go}*=900 K and* T_e*=1,5 eV*.

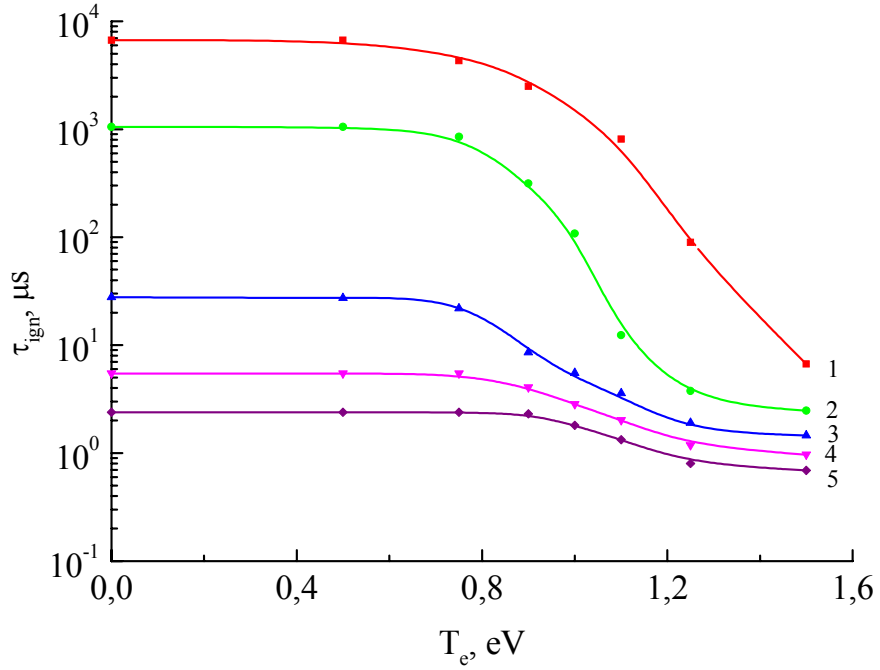

Fig. 11.19. Gas discharge influence on ignition time of H_2-O_2 stoichiometric (*67%-33%*) mixture at $p=1$ *atm* and at instant gas heating to various initial gas temperatures T_{go}, *K*: 1 - 800; 2 - 900; 3 - 1000; 4 - 1100; 5 – 1200.

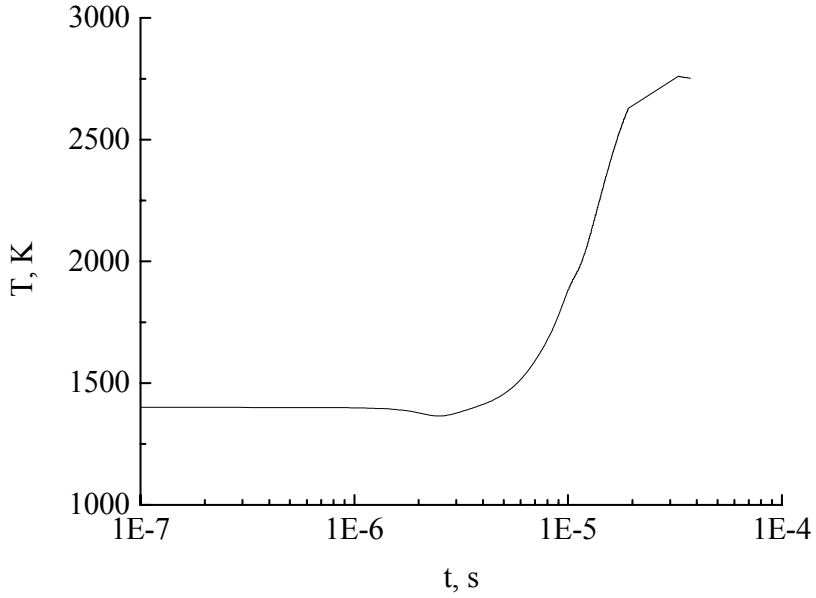

Fig. 11.20. Typical gas temperature vs time at burning of propane-air mixture under condition of gas discharge at $T_e=0,75$ *eV*, $T_{in}=1400$ *K* and $N_{in}=4,4\cdot10^{-5}$ *mol/cm*$^{-3}$.

ignition delay of a propane-air mixture under condition of gas discharge is reduced approximately in 36 times in comparison with autoignition (*Fig. 11.14*).

At oxidation of propane at the presence of the discharge concentration of atoms *H, O* and radicals *OH, HO_2, CH_3*, and so on at a stage of initiation of burning is essentially (in 100 and more times) more, than at oxidation without the discharge. It leads to that ignition of hydrocarbon fuel in presence of the discharge occurs essentially faster, than at thermal autoignition.

Thus, switching on of the discharge increases speed of formation of active atoms and radicals that results in earlier beginning of reactions of oxidation. The same acceleration occurs and to the subsequent reactions of interaction of destruction products of C_3H_8 and hydrogen and other reactions.

It is necessary to take into account that in the kinetic model of burning of a propane-air mixture the discharge action was determined only by the reactions taking place at burning of a hydrogen-oxygen mixture at the presence of high value of electric field. It is possible to assume, that addition of reactions with a birth of new active particles for the account of dissociation and ionization of propane and its destruction products should lead to essential increase in speed of ignition of a propane-air mixture.

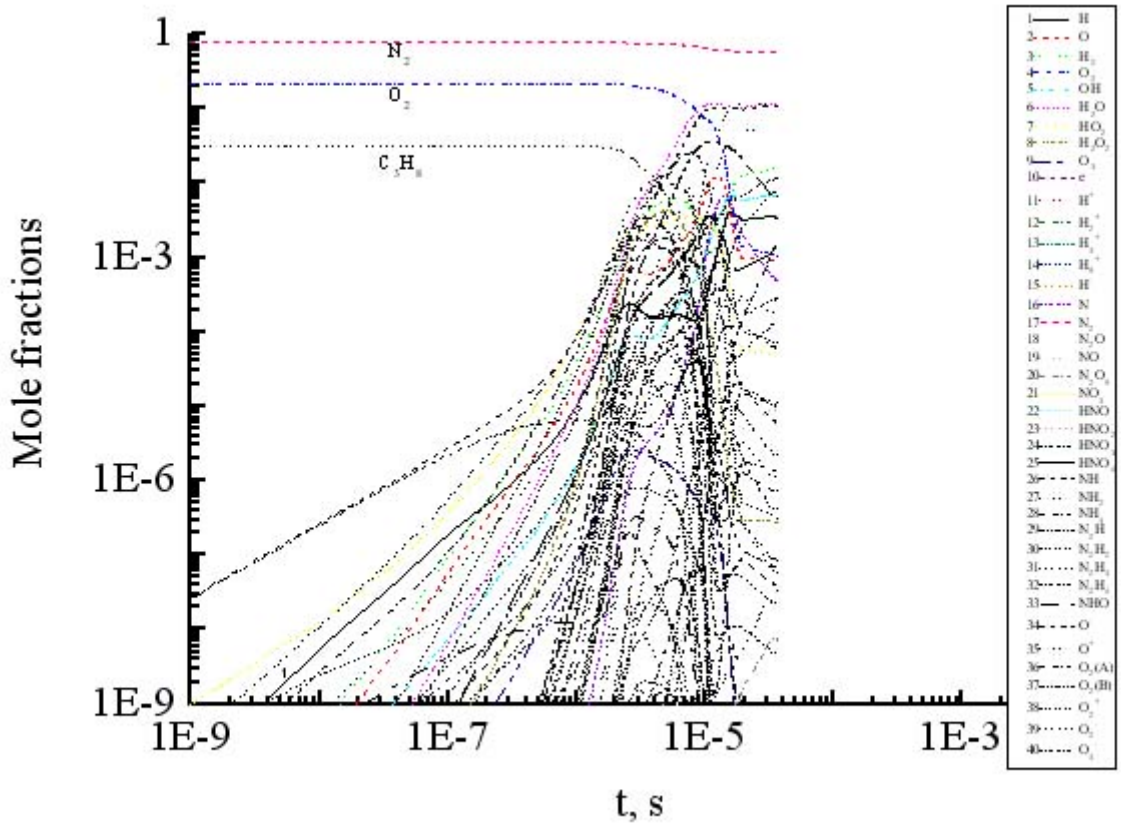

Fig. 11.21. Kinetics of propane-air stoichiometric mixture ignition under condition of gas discharge at *p=1 atm*, instant gas heating to initial temperature T_{go}*=1400 K and* T_e*=0,75 eV*.

CONCLUSIONS

1. The experimental installation used for studies of various types of microwave discharges in supersonic streams of air and propane-butane-air combustible mixtures is modernized. The pulsed magnetron generator was used as a source of microwave energy. The magnetron had following characteristics: wavelength $\lambda=2,4$ *cm*; mean microwave power $W_m<1$ *kW*; pulsed microwave power $W_p<300$ *kW*; microwave pulse duration $\tau=1\text{-}200$ μs; pulse repetition frequency $f=1–100$ *Hz*; pulse period-to-pulse duration ratio $Q=1000$. The discharge formed in a vacuum cylindrical chamber. The chamber inside diameter is *1 m*; its length is *3 m*. The vacuum system allowed to investigate the surface microwave discharge in diapason of pressures $p=10^{-3}\text{-}10^{3}$ *torr* (*Chapter II*).
2. The diagnostic facilities, allowing carrying out researches of the basic properties of microwave discharges in supersonic flow were developed, put together and approved. The complex includes: a set of spectroscopic equipment with digital and photographic registrations of plasma radiation with high spectral, spatial and temporal resolution; a set of electric probe equipment with digital registration of voltage-current characteristics; a high speed camera for registration of discharge dynamics with a high temporal resolution; a Schlieren diagnostic set up for digital registration of plasma dynamics; facility for measurement of flame conductivity, and so on (*Chapter III*).
3. The microwave discharge on external surface of dielectric body being flown of supersonic stream of air was investigated. The surface microwave discharges were formed on dielectric bodies of different geometry: on a flat plane; on an antenna of a rectangular section; on an antenna of a rectangular section with a wedge end part; on a cylindrical antenna with a spherical end part; on a cylindrical antenna with a conical end part; on an antenna of rectangular section with a smoothly transfer to the cylindrical antenna with a conical end part. It was experimentally shown (*Chapter IV*), that
   - for creation of surface microwave discharge at air pressure $p=1\text{-}300$ *torr* it is necessary the pulsed microwave power $W_p=20\text{-}300$ *kW*;
   - the surface microwave discharge propagation velocity equals 10^{7} *cm/s* at stage of discharge formation and decreases till 10^{4} *cm/s* to the ending of microwave pulse;
   - the breakdown wave defines a surface microwave discharge propagation at initial moment ($t=1\text{-}3$ μs). At a stage of the discharge existence ($t=3\text{-}100$ μs) the ambipolar diffusion is the main mechanism of discharge propagation, whereas the mechanism of slow burning is possible only at late stages ($t>100$ μs).

- the electric field near zone of discharge formation reaches value of *5 kV/cm*, and in zone of discharge stopping the electric field equals *300-500 V/cm*;
- the big value of reduced electric field *E/n=100-500 Td* leads to excitation, dissociation and ionization of molecules, that is to effective creation of active and charged particles;
- the electric field is located into thin boundary layer, that leads to effective energy contribution, that is to fast gas heating with rate of $dT_g/dt=10^7$-10^8 *K/s*. The gas are heating up to *2000-3000 K* during *20-30* μs;
- the electron density reaches 10^{13}-10^{14} cm^{-3} and the electron temperature changes from *4 eV* up to *6 eV* in an active phase of the discharge existence;
- the surface microwave discharge leads to significant changes of flow parameters near surface of body being flown around by supersonic air stream, that is, to essential reduction of turbulent skin friction;
- the inclination angle of a shock wave, arising on a leading edge of the antenna, accordingly, the Mach number of airflow changes at presence of a microwave discharge.

4. The freely localized microwave discharges created by focused beam of powerful electromagnetic radiation under conditions of free space, inside of aerodynamical channel, and also near body being flown of supersonic stream of air were studied. Their basic parameters were measured. It was shown (*Chapter V*), that
   - under conditions of low-temperature hydrogen plasma the fast gas heating with rate up to $\sim 10^2$ *K/*μs takes place in a stage of formation of the microwave discharge;
   - the gas temperatures achieves *3000 K*;
   - the electron density can reach 10^{15} cm^{-3} at atmospheric pressure;
   - the dissociation degree of hydrogen molecules reaches *20%*.
   - such parameters are encouraging from the point of view of use of freely localized microwave discharge for ignition of supersonic streams of hydrogen fuel;
   - there is an opportunity of creation of a microwave discharge before a body moving with supersonic velocity through the Earth's atmosphere;
   - the supersonic flow does not influence almost on a common view of microwave discharge, gas heating, and on a level of a microwave power required for maintenance of the freely localized microwave discharge;
   - the microwave discharge results in a reliable ignition of combustible fuel inside aerodynamical channel already at microwave pulse duration $\tau \sim 25$ μs;
   - the carried out experiments specify an opportunity of use of a freely localized microwave

discharge for supersonic aerodynamics.

5. The external ignition of a supersonic stream of a propane-air mixture was realized with the help of surface microwave discharges (*Chapter VI*). The non-equilibrium plasma of surface microwave discharge exists at high values of electric field and gas ionization degree. Due to these factors the fast gas heating and effective production of active particles takes place under conditions of surface microwave discharge. These facts are the important conditions for reliable and effective ignition of supersonic flows of combustible gaseous fuels (hydrogen-air and hydrocarbon-air mixtures).
6. The ignition of supersonic propane-butane-air flow with the help of the transversal surface discharge was obtained. The stabilizing action of a stagnant zone on process of propane-butane-air mixture combustion was investigated. It was shown (*Chapter VII*), that
   - the geometrical sizes of a cavity render very strong influence on general view of the transversal surface discharge, electric power level necessary for maintenance of the discharge in supersonic flow and ignition time of combustible mixtures;
   - the achievement time of stationary combustion of a propane-butane-air mixture in a cavity depends on discharge current, air and fuel consumption;
   - the cavity can use for stabilization of supersonic combustion;
   - the stationary burning of a supersonic propane-butane-air stream during $t=2$ *s* (maximal time of supersonic flow for used installation) was realized with help of the electrode transversal surface discharge created in a stagnant zone.
7. Within the framework of non-viscous statement the analytical investigations of streamlining by supersonic flow of a cylindrical antenna, conjugate with conical tip are performed at organization of a microwave discharge on its surface. It was shown (*Chapter VIII*), that
   - the activation of energy source on the lateral surface is accompanied by complicated transitional gas-dynamical processes;
   - the formation of a steady flow is preceded by an explosion processes because of instant pressure increasing and than explosion products drifting;
   - on the stage of products drifting the appearance and evolution of vertex structures as a result of contact surface instability is possible;
   - the relatively thin layers could be used to control gas dynamic parameters on the surface of relatively large bodies;
   - the static pressure distribution on the antenna surface is practically the same as in the case of a flow over antenna without energy input;

- the simplified boundary layer model can be used to determine friction and heat transfer characteristics.

8. The numerical modeling of process of streamlining of body by supersonic airflow was fulfilled at various values of energy introduced into the turbulent supersonic boundary layer. It was theoretically shown (*Chapter IX*) that
   - the surface microwave discharge influences on the characteristics of a supersonic flow;
   - the input of energy in area of a turbulent boundary layer results in noticeable reduction of a local coefficient of turbulent friction at the expense of decreasing of a transverse gradient of longitudinal flow velocity and increase of a displacement thickness;
   - the reduction of coefficient of turbulent friction is spread to considerable distance downstream from a heated portion;
   - the significant friction reduction on whole streamlined surface is achieved at local gas heating due to effect of long-term memory of a turbulent boundary layer.
9. Numerical model for studies of unsteady near wall discharge in supersonic flow have been developed too. The model was based on the Favre averaged Navier-Stokes equations for thermally equilibrium, chemically frozen air. For the description of turbulent transfer the algebraic Baldwin-Lomax model and two-parameter differential k-omega model were used. The pulsed discharge influence on the gas flow was simulated by non-stationary near wall heat source with specified space and time distribution of intensity. It was shown (*Chapter X*) that
   - the effect of heat deposition leads to significant decreasing of the local and full turbulent friction coefficient;
   - the effect exists during long time after the heat deposition to gas is switched off;
   - during some hundreds microseconds the flow parameters slowly return in initial state;
   - it indicates prospects of pulsed-periodical discharge usage.
10. The numerical technique was employed to study propane-air ignition by near wall heat deposition. Computations were performed for supersonic flow of stoichiometric propane-air mixture over blunted flat plate. Adiabatic, full non-catalytic model of gas-wall thermal and chemical interactions was used. Mathematical modelling of ignition of the premixed propane-butane-air flow revealed (*Chapter XI*) that supersonic fuel stream can be ignite on external surface of plate at deposited pulsed thermal power *80 W* per *1 cm*^{2}. Such value of pulsed power can be easily reached with the help of our experimental installation. Mathematical modeling of kinetics of stoichiometric combustion of hydrogen-oxygen (2:1) mixture at taking into account of molecules dissociation and creation of radicals and active

excited and charged particles under conditions of non-equilibrium gas discharge plasma revealed strong influence of value of reduced electric field (in other words, the electron temperature) on induction time. At this at initial gas temperature $T_g=900\ K$ and atmospheric pressure the ignition time changes from $\sim 1\ ms$ at electron temperature $T_e=0,1\ eV$ till $\sim 1\ \mu s$ at $T_e=1,5\ eV$.

11. Finally one can make the general conclusion that the microwave discharge is perspective way for application in such fields of supersonic aerodynamics as:
    - reduction of skin friction at moving of subsonic and supersonic vehicles in dense layers of atmosphere;
    - control of the characteristics of supersonic flow near a surface of flight vehicles and by that improvements of their aerodynamic properties;
    - fuel ignition in scramjets.

    However the additional researches directed on search of optimum modes of creation of microwave discharges in supersonic stream of gas is necessary to carry out.

REFERENCES

References to Introduction

1. ***V.M.Shibkov***. Investigation of Discharges Influence on Boundary Layer in Supersonic Airflow. //Final Technical Report under of ISTC Project 1866p, Physical Department of Moscow State University, October, 2001, Moscow.

References to Chapter I

1. ***A.V.Kazakov, M.N.Kogan, V.A.Kuparev***. Delay of laminar-turbulent transition by means of intensive localized heating of the surface in the vicinity of the leading edge of the plate. //High Temperature, 1996, v.34, No 1, p.42-47.
2. ***A.A.Pilipenko, G.K.Shapovalov***. Upravlenie sostoyaniem pogranichnogo sloya putem vvedeniya iskusstvennikh vozmushenii. //Uchenie zapiski TsAGI, 1986, v.17, No 4, p.73-78 (In Russian).
3. ***Yu.S.Kachanov, V.V.Kozlov, V.Ya.Levchenko***. Vozniknovenie turbulentnosti v pogranichnom sloe. //Novosibirsk, Nauka, 1982, 151p (In Russian).
4. ***A.V.Kazakov, M.N.Kogan, V.A.Kuparev***. Laminirizatsiya pogranichnogo sloya pri otritsatelnom gradiente davleniya i nagreve poverkhnosti. //Teplofizika visokikh temperatur, 1996, v.34, No 2, p.244-249 (In Russian).
5. **V.V.Kozlov**. Physics of flow structures. Flow separation. //Soros Education Journal, 1998, No 4, p.86-94. **V.V.Kozlov**. Otriv potoka ot perednej kromki i vliyanie na nego akusticheskikh vozmushenii. //Prikladnaya mekhanika i tekhnicheskaya fizika. 1985, No 2, p.112-115 (In Russian).
6. ***A.V.Kazakov, M.N.Kogan, V.A.Kuparev***. Ob ustojchivosti dozvukovogo pogranichnogo sloya pri nagreve poverkhnosti ploskoi plastini vblizi perednei kromki. //Izvestiya AN SSSR. Mekhanika zhidkosti i gasa, 1985, No 3, p.68 (In Russian).
7. ***A.V.Kazakov, M.N.Kogan, A.P.Kuryachii***. O vliyanii lokalnogo nagreva poverkhnosti na trenie v turbulentnom pogranichnom sloe na plastine. //Teplofizika visokikh temperatur, 1995, v.33, No 6, p.888-894 (In Russian).
8. ***A.V.Kazakov, A.P.Kuryachii***. The effect of viscous-nonviscous interaction on turbulent flow past a plate under conditions of local heating of its surface. //High Temperature, 1998, v.36, No 3, p.395-400.
9. ***Yu.V.Lapin.*** Turbulentnii pogranichnii sloi v sverkhzvukovikh potokakh gasa. //Moscow: Nauka, 1982. 312p. (In Russian).

10. ***C.Carvin, J.F.Debieve, A.J.Smits***. The Near-Wall Temperature Profile of Turbulent Boundary Layer. //AIAA Paper. 1988, No 136, 8 p.
11. ***A.V.Kazakov, M.N.Kogan, A.P.Kuryachii***. Vliyanie na trenie lokalnogo podvoda tepla v turbulentnii pogranichnii sloi. //Izvestiya RAN. Mekhanika zhidkosti i gasa, 1997, No 1, p.48 (In Russian).
12. ***A.V.Kazakov, M.N.Kogan, A.P.Kuryachii.*** The effect of the thermal properties of a body being flown about on friction and heat transfer under conditions of local heat input to a turbulent boundary layer. //High Temperature, 1997, v.35. No 1, p.61-66.
13. ***Chien K.Y.*** Prediction of Channel and Boundary-Layer Flows with a Low-Reynolds-Number Turbulence Model. //AIAA Journal, 1982, vol. 20, No 1, p.33.
14. ***V.M.Shibkov***. Investigation of Discharges Influence on Boundary Layer in Supersonic Airflow. //Final Technical Report under of ISTC Project 1866p, Physical Department of Moscow State University, October, 2001, Moscow.
15. ***S.Williams, S.Popovic, L.Vuskovic, C.Carter, L.Jacobson, S.Kuo, D.Bivolaru, S.Corera, M.Kahandawala, S.Sidhu***. Model and Igniter Development for Plasma Assisted Combustion. AIAA2004-1012.
16. ***N.H.Anikin, E.N.Kukaev, S.M.Starikovskaia, A.Yu.Starikovskii***. Ignition of hydrogen-air and methane-air mixtures at low temperatures by nanosecond high voltage discharge. AIAA 2004-83.
17. ***S.A.Bozhenkov, S.M.Starikovskaia, A.Yu.Starikovskii***. //Combust. Flame, 2003, v.133, p.133-146.
18. ***A.Ben-Yakar, R.K.Hanson***. Cavity Flameholders for Ignition and Flame Stabilization in Scramjets: Review and Experimental Study. AIAA 1998.
19. ***A.Ben-Yakar, M.R.Kamel, C.I.Morris, R.K.Hanson***. Experimental Investigation of H; Transverse Jet Combustion in Hypcrvelocity Flows. //AIAA Paper, 97-3019, 33rd Joint Propulsion Conference and Exhibit, Seattle, WA, July 6-9, 1997.
20. ***Vinogradov V., Kobigsky S.A., Petrov M.D***. Experimental Investigation of Kerosene Fuel Combustion in Supersonic Flow, //J. of Propulsion and Power, 1995, v.11, No.1, pp.130-134.
21. ***Ortwelli P., Mathur A., Vinogradov V., Grin V., Goldfeld M., Starov A***. Experimental and Numerical Investigation of Hydrogen and Ethylene Combustion in a Mach 3-5 Channel with a Single Injector. //AIAA Paper, 96-3245, 32nd Joint Propulsion Conference and Exhibit.

22. ***Segal C., Owens M.G., Teliranian S., Vinogradov V***. Flameholding Configurations for Kerosene Combustion in a Mach 1.8 Airflow. //AIAA Paper, 97-2888, 33rd Joint Propulsion Conference and Exhibit.
23. ***A.Ben-Yakar, A.Gany***. Experimental Study of a Solid Fuel Scramjet. //AIAA Paper 94-2815, 30th AIAA Joint Propulsion Conference, Indianapolis, IN, June 27-29, 1994.
24. ***V.A.Vinogradov, Yu.M.Shikhman, R.V.Albegovt, G.K.Vedeshkin***. About Possibility of Effective Methane Combustion in High Speed Subsonic Airflow. //11th AIAA/AAAF International Conference Space Planes and Hypersonic Systems and Technologies. 2002, Orleans, France, AIAA-2002-5206.
25. ***V.A.Vinogradov, Yu.M.Shikhman, R.V. Albegov, G.K.Vedeshkin***. Experimental research of methane combustion in high speed subsonic. //11th AIAA/AAAF International Conference Space Planes and Hypersonic Systems and Technologies. 2002, Orleans, France, AIAA-2002-5208.
26. ***D.J.Seery, C.T.Bowman***. An experimental and analytical study of methane oxidation behind shock waves. //Combustion and flame, 1970, v.14, p.37-48.
27. ***M.Frenklach, D.E.Bornside***. Shock-Initiated Ignition in Methane-Propane Mixtures. //Combustion and flame, 1984, v.56, p.1-27.
28. ***T.P.Coffee***. Kinetic mechanisms for premixed, laminar, steady state methane/air flames. //Combustion and flame, 1984, v.55, p.161-170.
29. ***N.G.Dautov, A.M.Starik***. On the problem of choosing a kinetic scheme for description of the volume reaction of methane with air. //Kinetics and Catalysis, 1997, v.38, No.2, p.207-230.
30. **A.M.Starik, N.S.Titova, L.S.Yanovskiy**. Peculiarity of kinetics of oxidation of destruction products of C_3H_8 and C_4H_{10} with air mixture. //Kinetics and Catalysis, 1999, v.40, No.1, p.11-26.

References to Chapter III

1. ***Herzberg G.*** Molecular spectra and molecular structura. 1. Spectra of diatomic molecules. N.Y.: D. van Nostrand, 1951,658p.
2. ***Ochkin V.N., Savinov S.Yu., Sobolev N.N.*** Mekhanizmi formirovaniya raspredelenij electronno-vozbuzhdennikh molekul po kolebatelno-vrashatelnim urovnyam v gazovom razryade. //Trudi FIAN USSR, 1985, v.157, p.6-85 (In Russian).

3. ***Budo A***. Uber die Triplett-Bandentermoformel fur den allgemeinen intermediaren Fall and Anwendung derselben auf die $B^3\pi$-, $C^3\pi$-Terme des N_2-Moleculs. //Ztschr.Phys., 1935, Bd. 96, p.219-229.
4. ***Dieke G***.H., Heath D.F. The first and second positive bands of N_2. //John Hopkins spectroscopic report No.17. Baltimore, (Md), 1959, 185p.
5. Plasma diagnostic. Edited by ***W.Lochte-Holtgreven***, North-Holland Publihing Company, Amsterdam, 1968.

References to Chapter IV

1. ***A.S.Zarin, A.A.Kuzovnikov, V.M.Shibkov***. Freely localized microwave discharge in air. - Moscow: Oil and gas, 1996, 204p (In Russian).
2. ***A.M.Devyatov, A.A.Kuzovnikov, V.V.Lodinev, V.M.Shibkov***. The mechanism of molecular gas heating in a pulsed free-localizing RF discharge. //Moscow University Physics Bulletin. Fizika, 1991, v.46, No 2, p.28-31.
3. ***A.A.Kuzovnikov, V.M.Shibkov, L.V.Shibkova.*** Free-localized pulse-periodic MW discharge in air. Kinetics of gas heating. //High Temperature, 1996, v.34, No 3, p.343-348.
4. ***V.M.Shibkov.*** Free-localized pulse-periodic MW discharge in air. Electric field strength in plasma. //High Temperature, 1996, vol.34, No 4, p.519-524.
5. ***A.A.Kuzovnikov, V.M.Shibkov, L.V.Shibkova.*** Kinetics of charged particles in a free-localized pulse-periodic MW discharge in air. //High Temperature, 1996, vol.34, No 5, p.651-655.
6. ***A.V.Kalinin, V.M.Shibkov, L.V.Shibkova***. //Vestnik Moskovskogo Universiteta. Seriya 3, Fizika, astronomiya, 1996, No 1, p.38-42 (In Russian).
7. ***V.V.Zlobin, A.A.Kuzovnikov, V.M.Shibkov***. Concentration of electrons in a stimulated MW discharge channel in nitrogen. //Moscow University Physics Bulletin. Fizika, 1988, v.43, No 1, p.98-100.
8. ***V.V.Lodinev, V.M.Shibkov, L.V.Shibkova***. Gas heating kinetics in pulse-periodic air discharge. //Moscow University Physics Bulletin. Fizika, 1996, v.51, No 2, p.26-31.
9. ***A.A.Kuzovnikov, V.M.Shibkov, L.V.Shibkova***. Kinetics of electrons in plasma of discharge, created in free space by focused microwave beam. //Zhurnal Tekhnicheskoi Fiziki, 1997, v.67, No 6, p.10-14 (In Russian).
10. ***A.F.Alexandrov, A.S.Zarin., A.A.Kuzovnikov, V.M.Shibkov, L.V.Shibkova***. Plasma parameters of non-consistent microwave discharge, created in programmable pulse. //Zhurnal Tekhnicheskoi Fiziki, 1997, v.67, No 7, p.19-23 (In Russian).

11. ***V.M.Shibkov***. Heating of gas under conditions of free-localized microwave discharge in air. Mathematical simulation. //High Temperature, 1997, v.35, No 5, p.681-689.
12. ***V.M.Shibkov***. Heating of gas under conditions of free-localized microwave discharge in air: Experiment. //High Temperature, 1997, v.35, No 6, p.858-862.
13. ***Yu.V.Zlobina, V.M.Shibkov, L.V.Shibkova***. Kinetics of heating and dissociation of molecules in pulsed discharge in hydrogen. //Fizika plasmi, 1998, v.24, No 7, p.667-671 (In Russian).
14. ***Shibkov V.M.*** Kinetics of gas heating in plasma created in supersonic airflow. //9th Intern. Space Planes and Hypersonic Systems and Technologies Conf. Norfolk, Virginia, USA, 1999, AIAA-99-4965.
15. ***V.M.Shibkov, A.F.Alexandrov, A.V. Chernikov, D.M.VanWie, et.al***. Freely localized microwave discharge in supersonic flow. //AIAA Paper, 2001, No.01-2946, p.1-8.
16. ***V.M.Shibkov, et.al.*** Surface microwave discharge in supersonic airflow. //Vestnik Moskovskogo Universiteta. Seriya 3. Fizika, astronomiya. 2000. v.41. No 6. p.64-66 (In Russian).
17. ***V.M.Shibkov, V.A.Chernikov, A.P.Ershov, L.V.Shibkova, et.al.*** Surface microwave discharge on dielectric body in a supersonic flow of air. //IV International workshop Microwave discharges: Fundamentals and applications. 18-22 September 2000, Zvenigorod, Russia, Yanus-K, Moscow. 2001. p.145-153
18. ***V.M.Shibkov, V.A.Chernikov, A.P.Ershov, L.V.Shibkova, et.al.*** Surface microwave discharge in supersonic airflow. //The 2nd Workshop on Magneto-plasma-aerodynamics in aerospace applications. 5-7 April 2000, Moscow, IHT of RAS, 2001 p.163-168.
19. ***V.M.Shibkov, V.A.Chernikov, Ch.N.Raffoul, D.M.VanWie, et.al.*** Surface microwave discharge in supersonic airflow. //32nd AIAA Plasmadynamics and Lasers Conference and 4th Weakly Ionized Gases Workshop, 11-44 June 2001. Anaheim, CA, USA. AIAA 2001-3087.
20. ***V.M.Shibkov, V.A.Chernikov, S.A.Dvinin, et.al***. Dense large-diameter uniform plasma of a surface microwave discharge. //15th International Symposium on Plasma Chemistry. Volume I. Oral Contributions. 9-10 July, 2001. France. p.179-184.
21. ***V.M.Shibkov, A.F.Alexandrov, V.A.Chernikov, et.al.*** Iinteraction of supersonic airflow with the combined microwave discharge, created on external surface of the wedge dielectric body. //V International Workshop Strong Microwave in Plasma. Nizhniy Novgorod, Russia, D26, D27 2002.
22. ***V.M.Shibkov, A.F.Alexandrov, V.A.Chernikov, A.P.Ershov, A.A.Kuzovnikov, L.V.Shibkova, I.B.Timofeev, A.V.Voskanyan, V.V.Zlobin.*** Interaction of supersonic airflow with the combined

microwave discharge, created on external surface of the wedge dielectric body. //The 5th International Workshop “STRONG MICROWAVES IN PLASMAS” August 1-9, 2002. Abstracts, p. D26.

23. ***V.M.Shibkov, S.A.Dvinin, A.P.Ershov, L.V.Shibkova, I.B.Timofeev.*** Surface microwave discharge in supersonic airflow. //The 5th International Workshop “STRONG MICROWAVES IN PLASMAS” August 1-9, 2002. Abstracts, p. D27.
24. ***V.M.Shibkov, A.F.Alexandrov, V.A.Chernikov, A.P.Ershov, P.Yu.Georgievskiy, V.G.Gromov, O.B.Larin, V.A.Levin, L.V.Shibkova, I.B.Timofeev, A.V.Voskanyan, V.V.Zlobin.*** Influence of the surface microwave discharge on the parameters of supersonic airflow near a dielectric body. //The 41st AIAA Aerospace Sciences Meeting and Exhibit and 5th Weakly Ionized Gas Workshop, 2003 , Reno, Nevada, USA, AIAA-2003-1192, p.1-7.
25. ***Shibkov V.M., Chernikov V.A., Ershov A.P., Karachev A.A., Shibkova L.V., Timofeev I.B., Voskanyan A.V., Zlobin V.V***. Ignition of the supersonic propane-air mixture with the help of the surface discharge. //The Fifth International Workshop on Magneto and Plasma Aerodynamics for Aerospace Applications, Moscow, 2004. Invited Reports, p.1-6.
26. ***Shibkov V.M., Chernikov V.A., Ershov A.P., Karachev A.A., Timofeev I.B., Voskanyan A.V., Zlobin V.V.*** Ignition of the supersonic propane-air mixture with the help of the surface discharge. //The Fifth International Workshop on Magneto and Plasma Aerodynamics for Aerospace Applications, Moscow, 2003. Abstract, p.52-53.
27. ***V.M.Shibkov, A.F.Alexandrov, V.A.Chernikov, A.P.Ershov, V.G.Gromov, I.V.Kuznetsov, O.B.Larin, V.A.Levin, L.V.Shibkova, I.B.Timofeev, A.V.Voskanyan.*** Surface microwave discharge. //International Conference on Physics of Low Temperature Plasma PLTP-03, Kiev, Ukraine, May 11–15, 2003. Invited Paper, p.1-6.
28. ***V.M.Shibkov, V.A.Chernikov, A.P.Ershov, A.A.Karachev, R.S.Konstantinovskij, L.V.Shibkova, I.B.Timofeev, A.V.Voskanyan, V.V.Zlobin.*** Propane-air mixture ignition with the help of the surface discharge. //International Conference on Physics of Low Temperature Plasma PLTP-03, Kiev, Ukraine, May 11–15, 2003. Invited Paper, p.1-6.
29. ***V.M.Shibkov, A.F.Alexandrov, V.A.Chernikov, A.P.Ershov, V.G.Gromov, I.V.Kuznetsov, O.B.Larin, V.A.Levin, L.V.Shibkova, I.B.Timofeev, A.V.Voskanyan.*** Surface microwave discharge. //International Conference on Physics of Low Temperature Plasma PLTP-03, Kiev, Ukraine, May 11–15, 2003. Abstracts, p.3-15-66.
30. ***V.M.Shibkov, V.A.Chernikov, A.P.Ershov, A.A.Karachev, R.S.Konstantinovskij, L.V.Shibkova, I.B.Timofeev, A.V.Voskanyan, V.V.Zlobin.*** Propane-air mixture ignition with

the help of the surface discharge. //International Conference on Physics of Low Temperature Plasma PLTP-03, Kiev, Ukraine, May 11–15, 2003. Abstracts, p. 3-16-66.

31. ***Karachev A.A., Shibkov V.M., Shibkova L.V.*** Izmerenie temperature gaza po nerazreshennoj structure molekulyarnikh spectrov. //The XXX Zvenigorodskaya konferentsiya po fizike plazmi I UTS, 2003., Moscow, Russia. p.222 (In Russian).
32. ***Aleksandrov A.F., Voskanyan A.V., Gromov V.G., Shibkov V.M., et.al.*** SVCh razryad na vneshnej poverkhnosti dielektricheskoj antenni. //The XXX Zvenigorodskaya konferentsiya po fizike plazmi I UTS, 2003, Moscow, Russia. p.191 (In Russian).
33. ***Shibkov V.M., Voskanyan A.V., Ershov A.P., Zlobin V.V., Karachev A.A., Konstantinovskij R.S., Chernikov V.A.*** Burning of the supersonic propane-air mixture in the aerodynamic channel with the stagnant zone. //The III International Symposium "Thermochemical processes in plasma aerodynamics", 2003, St-Petersburg, p.76-84.
34. ***V.M.Shibkov, V.A.Chernikov, V.G.Gromov, A.P.Ershov, L.V.Shibkova, I.B.Timofeev, A.V.Voskanyan.*** Freely localized and surface microwave discharges in supersonic airflow. //The III International Symposium "Thermochemical processes in plasma aerodynamics", 2003, St-Petersburg, p.240-251.
35. ***V.M.Shibkov, V.A.Chernikov, A.P.Ershov, L.V.Shibkova, I.B.Timofeev.*** Surface microwave discharge in supersonic airflow. In Book: "Strong Microwaves in Plasmas". Edited by A.G.Litvak, in two volumes. Institute of Applied Physics of the Russian Academy of Sciences, Nizhniy Novgorod, Russia, 2003, Volume 2, p.737-742.
36. ***V.M.Shibkov, V.A.Chernikov, V.G.Gromov, O.V.Larin, V.A.Levin, L.V.Shibkova.*** Interaction of supersonic airflow with the combined microwave discharge, created on external surface of the wedge dielectric body. In Book: "Strong Microwaves in Plasmas". Edited by A.G.Litvak, in two volumes. Institute of Applied Physics of the Russian Academy of Sciences, Nizhny Novgorod, Russia, 2003, Volume 2, p. 731-736.
37. ***V.M.Shibkov, A.P.Ershov, O.S.Surkont.*** Microwave discharge on external surface of quartz plate. International Conference "Micro- and nanoelectronics-2003" October 6-10, 2003, Moscow-Zvenigorod, Russia, Abstracts, p.O2-47.
38. ***Valery M. Shibkov, Vladimir A.Chernikov, Sergey A. Dvinin, Alexey P. Ershov, Andrey A.Karachev, Lidia V. Shibkova, Oleg S.Surkont, Anatoliy V.Voskanyan***. Microwave discharge on external surface of quartz plate. International Conference "Micro- and nanoelectronics-2003" October 6-10, 2003, Moscow-Zvenigorod, Russia, Invited Lectures, p.1-8.

39. ***V.M.Shibkov, A.D.Abramova, V.A.Chernikov, A.P.Ershov, V.G.Gromov, A.A.Karachev, R.S.Konstantinovskij, L.V.Shibkova, I.B.Timofeev, A.V.Voskanyan***. Microwave discharges in supersonic plasma aerodynamics. //The 42 AIAA Aerospace Sciences Meeting and Exhibit, 5-8 January 2004, Reno, Nevada, USA, 75-WIG-3, AIAA-2004-0513, p.1-11.
40. ***V.M.Shibkov, V.A.Chernikov, A.P.Ershov, R.S.Konstantinovskij, L.V.Shibkova, V.V.Zlobin.*** Propane-butane-air mixture ignition and combustion in the aerodynamic channel with the stagnant zone. //The 42 AIAA Aerospace Sciences Meeting and Exhibit, 5-8 January 2004, Reno, Nevada, USA, 123-WIG-5, AIAA-2004-0838, p.1-9.
41. ***Raizer Yu.P.*** Fizika gazovogo razryada, 1987, M. Nauka, p.591 (In Russian).
42. ***Gurevich A.V.*** Ionizatsiya nizhney ionosferi pod deistviem moshnikh radioimpulsov. – Geomagnetizm i aeronomiya, 1979, v.9, No4, p.633–640 (In Russian).
43. ***Mayhan J.T***. Comparison of various microwave breakdown prediction models. J.. Appl phys, 1971, vol. 42, № 13, p. 5362 – 5369.
44. ***Alekseev B.V., Kotelnikov V.A.*** Probe method of plasma diagnostic. Moscow, Energoatomizdat, 1988. 240 p. (In Russian).
45. ***Kagan Yu.M., Perel V.I.*** Probe methods of plasma investigation. //YFN, 1963, v.LXXXI, No.3, p.409-452 (In Russian).

References to Chapter V

1. ***A.S.Zarin, A.A.Kuzovnikov, V.M.Shibkov***. Freely localized microwave discharge in air. - Moscow: Oil and gas, 1996, 204p. (In Russian).
2. ***Zhou Qing, D.K.Otorbaev, G.J.H.Brussaard, M.C.M. van de Sanden, D.C.Schram***. //J.Appl.Phys. 1996, v.80(3), p.1312.
3. ***V.M.Shibkov***. Heating of gas under conditions of free-localized microwave discharge in air. Mathematical simulation. //High Temperature, 1997, v.35, No 5, p.681-689.
4. ***V.M.Shibkov***. Heating of gas under conditions of free-localized microwave discharge in air: Experiment. //High Temperature, 1997, v.35, No 6, p.858-862.
5. ***A.V.Kalinin, V.M.Shibkov, L.V.Shibkova***. //Vestnik Moskovskogo Universiteta. Seriya 3, Fizika, astronomiya, 1996, No 1, p.38-42 (In Russian).
6. ***V.V.Lodinev, V.M.Shibkov, L.V.Shibkova***. Gas heating kinetics in pulse-periodic air discharge. //Moscow University Physics Bulletin. Fizika, 1996, v.51, No 2, p.26-31.
7. ***A.A.Matveev,V.P. Silakov.*** Non-equilibrium kinetic processes in low-temperature hydrogen plasma. //Preprint N8. Russian Academy of Sciences General Physics Institute. M.: 1994, 30p.

8. ***G.M.Batanov, S.I.Gritsinin, I.A.Kossiy, et.al.*** SVCh razryadi visokogo davleniya. //Trudi FIAN USSR, 1985, v.160, p.174-203 (In Russian).
9. ***Yu.V.Zlobina, V.M.Shibkov, L.V.Shibkova***. Kinetics of heating and dissociation of molecules in pulsed discharge in hydrogen. //Fizika plasmi, 1998, v.24, No 7, p.667-671 (In Russian).
10. ***Devyatov A.M., Kalinin A.V., Mijovich S.P***. //Optika i Spektroskopiya. 1991, v. 71, ¹6, p.910 (In Russian).
11. ***Slovetskij D.I***. Dissotsiatsiya molekul electronnim udarom. //In book: Chimiya plasmi. M.: 1974, 156p (In Russian).

References to chapter IX

1. ***Favre A.*** Equations des gas turbulents compressibles, //Journal de Mecanique, v.4, 1965.
2. ***Coakley T.J.*** Development of Turbulence Models for Aerodynamic Applications, //AIAA Paper 97-2009, 1997.
3. ***Hirschfelder J.O., Curtiss C.F., Bird R.B.*** Molecular Theory of Gases and Liquids. John Wiley, New York, 1954.
4. ***Reid R.C., Prausnitz J.M., Sherwood T.K.*** The Properties of Gases and Liquids, McGraw-Hill Book Company, New York, 1977.
5. ***Katta V.R., Roquemore W.M.*** Simulation of Unsteady Flows in an Axisymmetric Research Combustor Using Detailed-Chemical Kinetics. AIAA/ASME/SAE/ASEE Joint Propulsion Conference & Exhibit, 34th, Cleveland, OH, July 13-15, 1998.

References to chapter XI

1. ***N.G.Dautov, A.M.Starik***. On the problem of choosing a kinetic scheme for description of the volume reaction of methane with air. //Kinetics and Catalysis, 1997, v.38, No.2, p.207-230.
2. ***I.S.Zaslonka, A.M.Tereza, O.N.Kulish, D.Yu.Zheldakov.*** //Khimicheskaya fizika, 1992, No 11, p.1491.
3. **A.M.Starik, N.S.Titova, L.S.Yanovskiy**. Peculiarity of kinetics of oxidation of destruction products of C_3H_8 and C_4H_{10} with air mixture. //Kinetics and Catalysis, 1999, v.40, No.1, p.11-26.